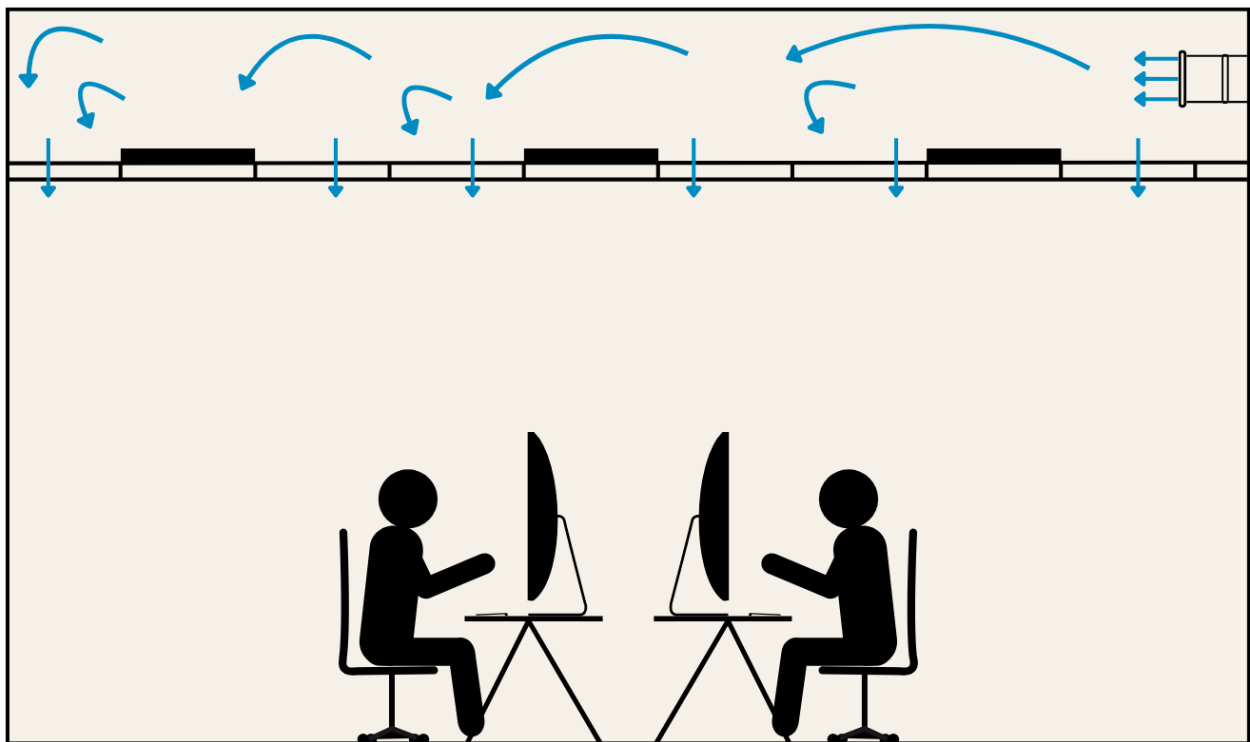


A configuration tool for diffuse ceiling ventilation

Master's Thesis

IE10-2





**AALBORG
UNIVERSITY**

STUDENT REPORT

The Faculty of Engineering and Science

BUILD, Department of the Built Environment

Thomas Manns Vej 23

DK-9220 Aalborg East

<https://www.build.aau.dk/>

Project title:

A configuration tool for diffuse ceiling ventilation

Project:

Master thesis

Project period:

September 2024 - June 2025

Project group:

IE10-2

Authors:

Anastasia Kjærland Hansen

Just Salling Buchhave

Sui Hoi

Supervisor:

Chen Zhang

Per Kvols Heiselberg

Number of pages main report: 81

Number of pages appendix: 61

Number of pages total: 146

Synopsis:

This thesis aims to lay the groundwork for developing a tool to optimise DCV by systematically examining the key factors influencing its cooling capacity. The primary objective is to understand how variations in specific parameters impact DCV system performance.

To achieve this, a comprehensive literature review will be conducted to gather existing knowledge and identify gaps that require further analysis. These gaps will be addressed through CFD simulations, which will form the basis for generating design charts that illustrate the relationship between parameter variations and the design curve.

Since no dedicated tool currently exists for DCV, this thesis aims to integrate existing knowledge, address data gaps through simulation-based analysis, and lay the groundwork for a practical DCV configuration tool. However, only a prototype for the tool has been developed in this thesis.

The content of this report is freely available, but publication with the source references should only be done in agreement with the authors.

An increased focus on energy optimisation in buildings, as well as improvements to the indoor climate, is placing new demands on modern ventilation solutions. In order to reduce heat loss, buildings are constructed with greater airtightness, which in turn leads to a higher cooling demand. Diffuse ceiling ventilation is a newer ventilation strategy in which supply air is introduced into the plenum above a suspended ceiling. The resulting overpressure causes the air to diffuse evenly through the porous ceiling panels. This method reduces the risk of draughts and large temperature gradients, even at high airflow rates.

Through a comprehensive literature review, a number of parameters influencing diffuse ceiling ventilation have been analysed. The results show that temperature gradients are generally not an issue with this type of ventilation. However, draughts may occur in specific cases, particularly in rooms with high ceiling height or low plenum height. The literature also reveals that certain critical aspects remain insufficiently investigated. Selected scenarios have therefore been examined in more detail through CFD simulations.

To address the identified gaps in the existing literature, CFD simulations have been carried out in this thesis to clarify various use cases. Based on the results of this work, design graphs have been developed to illustrate how changes in internal loads and room geometry affect the system's performance.

Since no dedicated calculation tool exists for diffuse ceiling ventilation, this thesis aims to use design graphs to develop such a configuration tool. However, due to the complexity of the various parameters and their interdependent effects on the system's performance, only a prototype of the tool has been developed in this thesis.

Et øget fokus på energioptimering af bygninger samt forbedring af det indendørs klima stiller nye krav til moderne ventilationsløsninger. For at reducere varmetab bliver bygninger konstrueret med større tæthed, hvilket medfører et øget behov for køling. Diffus loftindblæsning er en nyere ventilationsstrategi, hvor indblæsningsluften tilføres plenum over et nedhængt loft. Overtrykket i plenum medfører, at luften diffunderer jævnt gennem de porøse loftplader. Denne metode reducerer risikoen for træk og store temperaturgradienter, selv ved høje luftmængder.

Gennem et omfattende litteraturstudie er en række parametre, der påvirker diffus loftindblæsning, blevet analyseret. Resultaterne viser, at temperaturgradienter generelt ikke udgør et problem i denne ventilationsform. Træk kan dog opstå i særlige tilfælde, især i rum med enten stor loftshøjde eller lav plenumhøjde. Litteraturen afslører samtidig, at visse afgørende aspekter endnu ikke er tilstrækkeligt belyst. Udvalgte scenarier er derfor blevet undersøgt nærmere ved hjælp af CFD-simuleringer.

For at udfylde de identificerede huller i den eksisterende litteratur er der i dette speciale udført CFD-simuleringer, som belyser forskellige brugstilfælde. Ud fra resultaterne fra dette arbejde har det været muligt at opstille designgrafer som illustrer hvordan ændringer i den interne belastning og rumgeometri har indflydelse på systemets ydeevne.

Da der ikke findes et dedikeret beregningsværktøj til diffus loftindblæsning, har dette speciale til formål at anvende designgrafer til udviklingen af et sådant konfigurationsværktøj. På grund af kompleksiteten af de forskellige parametre og deres indbyrdes påvirkning af systemets ydeevne, er der dog kun udviklet en prototype af værktøjet i dette speciale.

Preface

This report is a Master's thesis, conducted as part of the Master of Science program in Indoor Environmental and Energy Engineering at the Department of BUILD, Aalborg University. The project was carried out from September 4, 2024, to June 4, 2025, corresponding to a total of 50 ECTS points.

This thesis explores key factors affecting DCV performance to support the development of a future configuration tool. A literature review and CFD simulations are used to generate design charts, illustrating how parameter changes impact cooling capacity. While no full tool is created, a prototype is presented as a first step.

We would like to express our sincere gratitude to our supervisors, Chen Zhang and Per Kvols Heiselberg. Their expertise and insights have greatly contributed to the progress of this project. We are especially thankful for the time and effort they dedicated to guiding us, and for their unwavering support, which has been crucial to the successful completion of this thesis.

We would also like to thank Olena Kalyanova Larsen and Peter V. Nielsen for their contribution. Especially Peter for his in-depth knowledge of design charts and his broad understanding of the theoretical field of ventilation.

Reading guide

The source references are made using the Harvard method [author, year]. The last revision of the page is indicated as the date. If this is not known, it is marked as *n.d.*. In case of the same author and year, a letter in [] indicates which specific source is meant. The bibliography is sorted in the following order: Name, title, and finally, the year.

The location of the source indicates what the source covers. In this report, the following applies:

- When the source is cited after a statement, it is the source for that particular statement.
- When the source is cited at the end of a sentence, within a period, it is the source for the entire sentence.
- When the source is cited after a period, it is for the entire preceding section.

All other references are indicated by numbers and, if applicable, page numbers. Figures are indicated by separate numbers, and "Figure" is written before the figure number. Similarly, tables are indicated with the table number, written as "Table." Figures and tables without source references have been created by the project group.

Formulas and symbols are presented and explained continuously throughout the report.

Nomenclature

Symbols

A	Area	[m ²]
Ar	Archimedes	[-]
b	Proportionality factor	[-]
g	Gravitational acceleration	[m/s ²]
h	Height	[cm]
M	Activity level	[met]
q	Air flow rate	[m ³ /s]
Q	Thermal heat load	[W/m ²]
Re	Reynolds	[-]
T	Temperature	[K]
Tu	Turbulence intensity	[%]
u	Velocity	[m/s]
μ	Dynamic viscosity	[kg/(m · s)]
ν	Kinematic viscosity	[m ² /s]
ρ	Fluid density	[kg/m ³]
Γ	Diffusion coefficient	[-]
ϕ	Transport variable	[-]

Sub- and superscripts

*	Dimensionless
l	Local
a	Average
draught	Velocity used for draught assessment
0	Supply
i	Supply
e	Exhaust
OCZ	Occupied Zone
01	Ankle level
11	Head height of a seated person

Abbreviations

ACH	Air Change Rate
BC	Boundary Conditions
CFD	Computational Fluid Dynamics
CRE	Contaminant Removal Effectiveness
DCV	Diffuse Ceiling Ventilation
DR	Draught Rate
IAQ	Indoor Air Quality
OCZ	Occupied Zone
PMV	Predicted Mean Vote
PPD	Predicted Percentage of Dissatisfied
RANS	Reynolds-averaged Navier–Stokes
TABS	Thermally Activated Building Systems

Table of Contents

	1
Chapter 1 Introduction	1
1.1 Traditional ventilation methods	1
1.2 Diffuse ceiling ventilation	3
1.3 Selection of design and performance parameters	5
1.4 Objective of thesis	8
Chapter 2 Methodology	10
2.1 Dimensionless numbers	10
2.2 Draught rate	12
2.3 Principle of developing design chart	13
2.4 CFD	16
2.5 Overall methodology used in the thesis	18
I Preliminary investigations	19
Chapter 3 Assessment of temperature gradient	20
3.1 Comparison with other ventilation strategies	20
3.2 Analysis of papers	22
Chapter 4 Assessment of velocity and draught	28
4.1 Analysis of papers	28
4.2 Draught rate	31
Chapter 5 Assessment of design parameters	33
5.1 Geometry	33
5.2 Diffuse ceiling panels	37
5.3 Heat sources	41
5.4 Inlet properties	43
5.5 Exhaust properties	43
5.6 Heating or cooling case	45
Chapter 6 Assessment of design charts	46
6.1 Existing design charts and graphs	46
Chapter 7 Conclusion of literature review	50

II Numerical investigations	51
Chapter 8 Numerical analysis	52
8.1 Selection of cases based on literature review	52
8.2 Heat load intensity analysis	53
8.2.1 Results	56
8.3 Geometry analysis	60
8.4 Setup	62
8.4.1 Results from one-sided heat load distribution	63
8.4.2 Results from increase in room height	66
8.5 Overall conclusion	72
Chapter 9 Design charts from numerical analysis	73
9.1 Evaluation of heat load intensity	73
9.2 Evaluation heat loads distribution	75
9.3 Evaluation of room geometry	76
Chapter 10 Configuration tool outline	77
III Recapitulation	78
Chapter 11 Discussion	79
Chapter 12 Conclusion	81
Bibliography	82
IV Appendix	85
Appendix A Electronic appendix	86
Appendix B Analysis of temperature in heating cases	87
Appendix C Average temperature	89
Appendix D Analysis of velocity in heating cases	92
Appendix E Selection of turbulence model	94
Appendix F Temperature sections	100
Appendix G Velocity sections	104
Appendix H Path lines	108
Appendix I Selection of reference points for design chart development	120

Appendix J	Investigation of residuals	123
Appendix K	Mesh independency of model 2	126
Appendix L	Mesh independency of model 3	130
Appendix M	Mesh independency of model 4	134
Appendix N	Design charts results	138
Appendix O	Design chart development	143
Appendix P	Configuration tool outline	146

Introduction 1

The enhanced focus on reducing emissions has increased attention on energy-consuming factors in building design, particularly HVAC systems, which are among the largest consumers of energy in our buildings. In Denmark, buildings account for approximately 40% of the total energy consumption, primarily for heating, ventilation, and lighting. [Energistyrelsen, 2025] In line with this, the new Danish Building Regulation for 2025 introduces stricter requirements for operational energy use in new buildings, further emphasising the need for more sustainable building solutions. [Byg & Bæredygtighed, 2024]

As part of this change, modern buildings are becoming more airtight to reduce heat loss. However, this increases the need for effective ventilation to maintain a healthy indoor climate and ensure no overheating. Particularly in offices and classrooms, where many occupants share a relatively small space. To meet this demand, energy consumption and operational costs often rise. Therefore, it is relevant to investigate the way buildings are ventilated to minimise this additional cost. While traditional systems such as mixing and displacement ventilation are commonly used today, a novel alternative, such as diffuse ceiling ventilation (DCV), could counteract some of the problems seen in these traditional systems. Therefore, DCV will be the focus of this paper. All the mentioned systems will be described to better understand the limitations and benefits of each system.

1.1 Traditional ventilation methods

The main focus of a ventilation system is to bring in fresh air into a room and remove stale or polluted air. The system should also help control temperature and humidity in a space. Mechanical systems usually supply filtered outdoor air, sometimes mixed with indoor air, and adjust the temperature depending on whether the space needs cooling, heating, or simply fresh air. [Nielsen, 1995]

One of the most commonly applied ventilation methods in practice is mixing ventilation, which is used in various spaces to provide fresh air and thermal comfort for occupants. Mixing ventilation relies on the supply of momentum flow from air terminal devices, where the air jet is delivered with high initial velocity. The air supply is positioned outside the occupied zone (OCZ) and ensures that the fresh air gets mixed with the polluted air in the room. This is done to achieve uniform temperature and pollutant distribution. The resulting velocity gradients generate strong turbulence, promoting effective air mixing and ensuring uniform distribution throughout the space. To remove the heat load generated by occupants and equipment, high velocities are needed, which can increase the draught risk compared to displacement ventilation. [Nielsen, 1995]

Displacement ventilation, on the other hand, delivers cool air at floor level, creating a stratified flow that relies on thermal buoyancy to displace polluted air. Heat sources cause warm, polluted air to rise to an upper zone, where it is extracted through the exhaust. The exhaust placement ensures the upward movement of warm air and pollutants, forming two distinct zones. The lower zone is colder and has cleaner air, and a warmer, polluted upper zone. Therefore, this ventilation type is also mainly recommended in rooms above 3 m. The movement of air within horizontal layers is key, with air moving easily within each layer, while the exhaust provides the force needed to move air between the layers. A potential drawback is the risk of draught at floor level and discomfort from temperature stratification. To prevent comfort issues, air should be supplied at low velocity and with minimal temperature difference compared to the room air. [Skistad et al., 2002] The principles of mixing and displacement ventilation are presented in Figure 1.1.

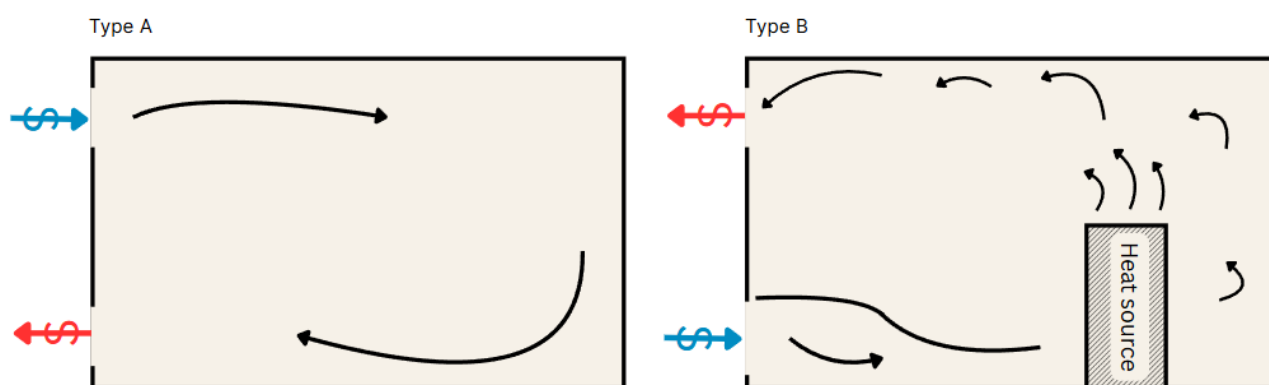


Figure 1.1. Different air distribution systems. Type A: Mixing ventilation and Type B: Displacement ventilation.

While traditional systems perform well in many cases, they can have limitations in specific situations. When cooling needs or heat loads are high, both mixing and displacement ventilation may cause draught for them to obtain the desired temperature. Displacement ventilation offers better air quality than mixing ventilation, but has its challenges. The low placement of the air supply can be an obstacle or lead to high velocities and low temperatures near the floor, which can cause poor thermal conditions in the room. These factors introduce limitations on the cooling capacity of the system for it to comply with proper thermal conditions. Mixing ventilation can lead to uneven air distribution and a poorer air quality, especially in spaces with high heat loads, as the air is mixed throughout the room rather than stratified. This occurs because mixing ventilation relies on turbulent airflows to dilute contaminants, which can create areas of stagnation or uneven temperature and contaminant concentrations, especially if supply airflows are not perfectly balanced. This can make it less efficient in providing thermal comfort and effective pollutant removal compared to displacement ventilation. [Nielsen, 1995; Skistad et al., 2002]

1.2 Diffuse ceiling ventilation

DCV is a new and innovative approach for ventilation. In this type of system, the space is divided into two zones by the suspended ceiling. The plenum is located at the top, and below is the ventilated room containing the occupied zone. The principle of DCV is illustrated in Figure 1.2, where the zones are indicated.

Unlike traditional ventilation systems, which supply air directly into the room through ducts, DCV introduces fresh air into the plenum above the suspended ceiling. This creates a positive pressure in the plenum, which drives low-velocity airflow evenly through the porous ceiling and into the room. The airflow inside the room is driven either by the momentum of the supplied air or by buoyancy effects generated by heat sources in the room. The ceiling panels can vary in function, with some being active panels, allowing airflow through perforations, while others can be passive panels, with insulated barriers that block airflow. The principle of DCV is shown in Figure 1.2.

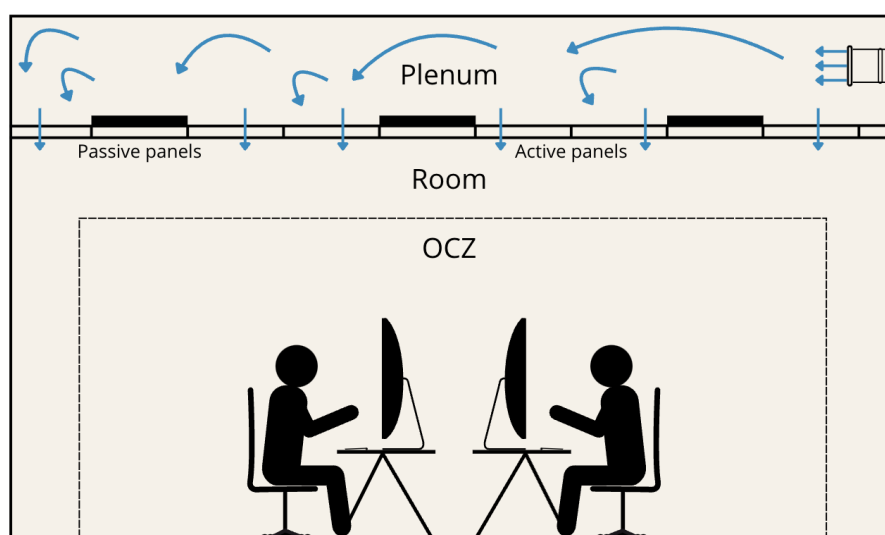


Figure 1.2. Idea of DCV principle. OCZ is marked with the dotted line.

The airflow pattern in a DCV system is illustrated in Figure 1.3. The figure shows how air enters the room through the perforated ceiling, and the cold downward airflow interacts with the upward thermal plumes generated by heat sources. The buoyant forces from these heat sources are typically strong enough to counteract the downward motion of the supply air, thereby promoting effective mixing within the space. This interaction dilutes the polluted air before it is extracted, resulting in a more uniform indoor environment.

The contaminant removal effectiveness (CRE) is used to evaluate how efficiently a ventilation system removes contaminants from a room. A high CRE indicates a better ability to remove contaminants. If the value of CRE is 1, the air is fully mixed. This is typically observed in a DCV setup due to its mixing ventilation behaviour. This leads to a relatively uniform contaminant distribution, even though the supply air is introduced at low velocity and diffuses across the entire ceiling. [Zhang and Heiselberg, 2019; Peng et al., 2021]

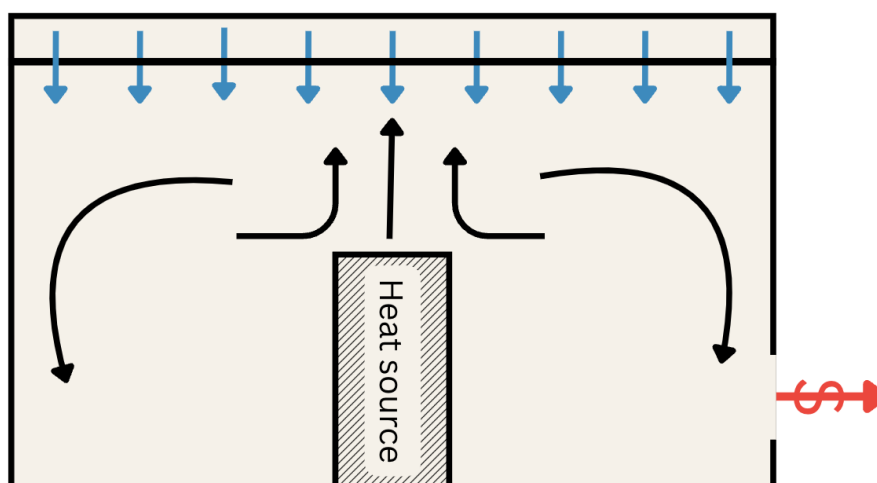


Figure 1.3. Air distribution principle of diffuse ceiling ventilation.

Benefits of DCV

The ceiling panels play a key role in DCV, replacing some of the traditional ductwork and diffusers. As the air is supplied across a large area, it enters the room at a low velocity and without a fixed direction. Although the air may initially enter the plenum from the ducts at a relatively high speed, its velocity is reduced as it passes through the porous ceiling into the room. This gentle and even air distribution helps minimise or even eliminate draughts in the OCZ, even when the supply air temperature is low.

As a result, the system can offer better thermal comfort for occupants. DCV also operates with much lower pressure drops compared to fully ducted systems, which means fans require less energy to run. This is not only reducing the operating costs but also makes it easier to combine DCV with natural ventilation strategies. [Hviid and Svendsen, 2012; Jacobs and Knoll, 2008] These benefits, along with the energy efficiency of the system and its ability to improve indoor climate, have made DCV an increasingly attractive solution for offices and other spaces with high ventilation needs and significant internal heat loads. These are also the types of spaces where draught problems are often seen with traditional ventilation systems. [Hviid and Svendsen, 2012]

DCV also demonstrates significant potential when integrated with thermally activated building systems (TABS). Full-scale experiments reveal that this integration can improve the thermal capacity of TABS by separating the thermal mass from the room, positively affecting energy efficiency. [Yu et al., 2015] However, this aspect is not explored further in the present study, as the focus remains on standalone DCV performance.

Because of the construction of a DCV system, the inlet air is naturally preheated in the plenum above the suspended ceiling. This preheating occurs due to heat transfer from the room below, thereby minimising, or maybe even removing, the need for additional mechanical preheating during the heating season. DCV also allows relatively high ventilation rates at low inlet velocities, making it an efficient solution for modern buildings with high cooling demands. [Zhang, 2016]

Limitations of DCV

As described, there are a number of limitations related to traditional ventilation methods. These limitations are partly solved by using DCV, which has a number of benefits regarding velocity and temperature supply and thereby achieving higher cooling capacity and reduced draught rate (DR). Although these benefits make DCV an attractive option, the method is still not widely adopted, which can be related to missing information in the field. Furthermore, it can be hard for a consulting engineer to determine if DCV is a suitable solution because standardised methods of calculation and execution are lacking in the field. This may be because there is still limited information and research available in the field. Without standardised methods for design, calculation, and installation, it can be difficult for consulting engineers to determine whether DCV is the right solution.

In addition to these challenges, DCV also presents some technical limitations. The low-pressure difference between the plenum and the room can sometimes lead to reverse airflow. This can cause hygiene issues and result in condensation forming on the ceiling panels or the concrete slabs due to the return of warm, humid air to the plenum, which can further result in office rain.

The air supply through the ceiling panels depends on the supply flow rate and the pressure drop in the panels. At lower flow rates, air is primarily delivered mainly through the ceiling panels, and increased airflow leads to a larger flow through cracks and gaps between the panels. [Zhang, 2016]

1.3 Selection of design and performance parameters

An analysis of Lindab's tool LindQST, was performed to identify key design and performance parameters. LindQST is the simulation tool developed for ventilation design. While multiple tools were considered during this process, LindQST stood out as the only relevant and capable option for this project, why it became the focus of the analysis of existing tools. The analysis of this tool has been made to understand which parameters are most important to include in the development of a new configuration tool for DCV.

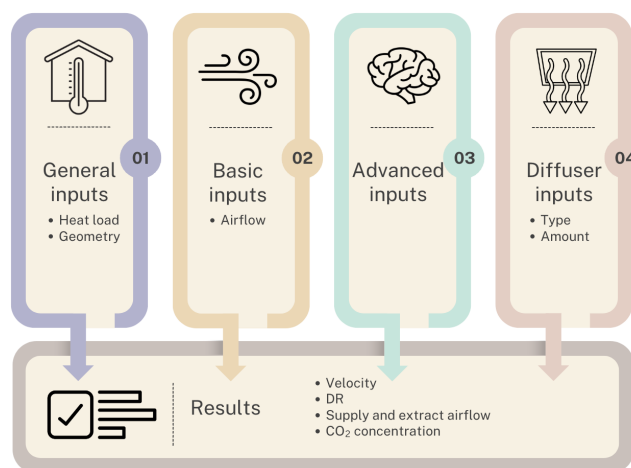


Figure 1.4. Structure of LindQST.

The structure and workflow of LindQST are shown in Figure 1.4. It starts with general inputs, where users enter basic room characteristics like heat load and geometry. This is followed by the basic inputs section, where airflow requirements for the space is handled. Next, users can fine-tune their setup using the advanced inputs, adjusting details such as the OCZ dimensions, sound reduction features, and any expected temperature gradients. Finally, the users define the diffuser inputs, where they choose the type and number of diffusers, with direct access to Lindab's product database. Once all inputs are filled in, the tool evaluates the system and returns results such as air velocity, DR, airflow rates, and CO₂ levels. The interactive 3D view makes it easy to visualise and improve air distribution, letting users adjust diffuser placement and settings to meet comfort and performance requirements. [Lindab AB, 2017]

Selection of design parameters

As presented in Figure 1.4, several inputs are needed to get a result from a tool. The structure of the DCV tool is shown in Figure 1.5. The tool is structured around three main categories of input: General inputs, Basic inputs, and Panel inputs. Each category plays an important role in ensuring that the tool can deliver accurate and reliable results for the performance of a DCV system. The General inputs define the overall context for the tool. These include fundamental parameters such as the geometry of the room, heat loads and room temperature. Together, these values describe the physical and thermal framework in which the ventilation system operates. The Basic inputs focus on inlet conditions. This is a crucial aspect, as airflow has a direct impact on how well the ventilation system can distribute fresh air and maintain thermal comfort. Ensuring that the airflow matches the requirements of the room is therefore vital for a meaningful assessment. The final input category, Panel inputs, relates to the diffuse ceiling elements themselves. Here, the number of perforated panels and their placement are specified. These details influence how air enters the space and how it spreads throughout the room.

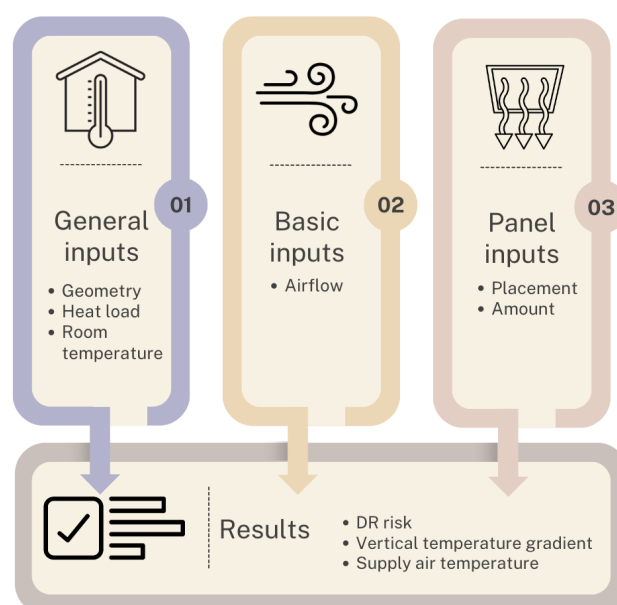


Figure 1.5. Idea of the structure for the DCV tool.

Once all inputs are provided, the tool can calculate results, such as DR, vertical temperature gradient and inlet temperature. These outputs offer valuable insights into occupant comfort, helping to identify areas where there may be discomfort from cold air movement or uneven temperature distribution.

Selection of performance parameters

To identify assessment parameters that may influence the performance of DCV, an analysis was conducted of how traditional ventilation strategies are typically evaluated. In LindQST, ventilation systems are evaluated based on sound pressure levels and air velocity in the OCZ. However, DCV does not face the same noise challenges as traditional systems, as it eliminates the need for diffusers and extensive ductwork, which are common sources of noise. Additionally, the suspended ceiling is often made from sound-absorptive materials, further reducing sound disturbances. [Jacobs and Knoll, 2008; Ogbuagu et al., 2023; Zhang et al., 2017]

Compared to traditional ventilation systems, DCV also operates at lower noise levels due to its minimal pressure drop and uniform air distribution, which prevents the formation of turbulent airflows [Mikeska and Fan, 2015; Nielsen and Jakubowska, 2009; Ogbuagu et al., 2023]. The low-pressure drop was confirmed in the study from Fan et al. [2013], and the study by Ogbuagu et al. [2023] found no noticeable noise issues in classrooms using DCV, as the even distribution of airflow prevents concentrated jets that could cause noise or draughts.

It should be noted that diffuse ceilings with fewer active panels exhibited higher sound absorption. The passive panels often have an insulation layer on the top side to prevent airflow through them. This insulation layer enhances the sound absorption of the panels. Different materials also have varying sound-insulating properties. [Kristensen and Jensen, 2015; Zhang et al., 2017]

Therefore, the primary performance criteria for evaluating DCV will be the temperature gradient within the room and the DR. These are also emphasised as important parameters when designing a room air distribution system [Nielsen et al., 2003]. The recommendations for these assessment parameters are based on Annex A about thermal environment in the International Standard [2006]. The values used can be found in Table 1.1.

Table 1.1. Thermal comfort categories and limits of local discomfort. [International Standard, 2006]

Category	Local discomfort			
	DR %	PD % vertical air temperature difference	PD % caused by warm or cool floor	PD % radiant asymmetry
A	< 10	< 3	< 10	< 5
B	< 20	< 5	< 10	< 5
C	< 30	< 10	< 15	< 10

These values are used in the further analysis to determine how well the system performs. It is wished to comply with Category B.

1.4 Objective of thesis

Overall, there is a need for standardised methods to ensure that DCV is applied when it is a suitable solution for a given project. Developing such a method would help engineers adopt this relatively new and unfamiliar ventilation system more widely. This led to the goal of creating a configuration tool to simplify the implementation of DCV in the building sector. To achieve this, it is necessary to identify the key design parameters that influence system performance and establish how they should be assessed.

To accomplish this objective, a thorough literature review will be conducted to compile existing knowledge regarding DCV, identifying potential gaps that require further investigation through CFD simulations. These simulations will make it possible to develop design charts that demonstrate the impact of parameter variations on the design graph.

This data collection can then be used to develop design charts that outline the operational area of a given system setup. Based on these design charts, a configuration tool can be developed. The tool is mainly meant to be used in the design phase of a construction project. The goal of the tool is to make it easy and simple to use, with inputs from the user and results that are easy to understand. The end user can thereby be engineers or architects designing a building. The architect can use the tool in the design process to make the aesthetics of individual rooms. If used by an engineer, the tool and thereby the implementation of DCV can solve problems with cooling needs and draught.

Outline of thesis

Since no dedicated tool currently exists for DCV, this thesis aims to integrate existing knowledge, address data gaps through simulation-based analysis, and lay the groundwork for a practical DCV configuration tool. The next section outlines the structure of the thesis, briefly describing what each chapter will cover.

Chapter 2: Introduces the fundamental theory used in this thesis. The chapter presents how results from different studies are made comparable, using dimensionless numbers. Design charts and how these are constructed are also presented, together with the numerical method used.

Part I: Preliminary investigations

Chapter 3: The dimensionless numbers are used to assess the temperature gradient and its relation to air change rate and room height, among other parameters. The investigation is based on different literature.

Chapter 4: The influence of velocity and draught on a DCV setup is investigated, based on cases from different literature.

Chapter 5: Analysis of design parameters and their influence on the system performance. The room geometry and heat sources are the main focus.

Chapter 6: Design charts are used to assess the system and compare what different design parameters influence are on a DCV system.

Chapter 7: To summarise the findings found in Part 1 of this thesis, this chapter is used as a partial conclusion.

Part II: Numerical investigations

Chapter 8: Presents the CFD cases and results. Multiple models are used in several simulations to fill out the gaps from the literature review.

Chapter 9: The CFD simulations form the basis of the design charts used in the configuration tool. This chapter presents the design charts developed based on the numerical analysis.

Chapter 10: Describes the outline for the configuration tool, and how the design charts should be implemented in the tool.

Part III: Recapitulation

Chapter 11: Provides a discussion of the tool, with proposals for further development and the limitations of the tool.

Chapter 12: Presents a general conclusion drawn from this study.

Methodology 2

This chapter presents the methodology used in this thesis. The methodology is a combination of theoretical analysis, physical quantities, design chart principle and numerical analysis. The overall methodology is described, and the theory and application of dimensionless numbers, DR, design charts, and CFD are presented. The theoretical framework is presented and discussed in relation to its relevance and contribution to the overall goal of the thesis.

2.1 Dimensionless numbers

The first method used is dimensionless numbers, which are essential for understanding the balance between buoyancy and inertial forces in ventilation systems. By using this methodology, it is possible to investigate whether the same approach as LindQST can be used.

Dimensionless numbers are quantities that have no physical units. They are formed by combining physical variables in such a way that all units cancel out. Dimensionless numbers make it possible to analyse similarities between different setups. In ventilation, this comparison makes it possible to compare different room sizes, air supply conditions, and thermal loads. The theory is based on the following source Nielsen [1999], unless otherwise indicated.

Archimedes number

The Ar number describes the ratio of buoyancy forces and inertial forces. It can therefore be used to characterise the balance between thermal buoyancy and momentum-driven airflow in ventilation systems. In a DCV setup, a low Ar number indicates a momentum-driven flow, while a high Ar number is present in cases with buoyancy-driven flow. The Ar number can be calculated from Equation 2.1.

$$Ar = \frac{H \cdot g \cdot (T_a - T_i)}{T_a \cdot u_i^2} \quad (2.1)$$

Where,

H	Room height	[m]
g	Gravitational acceleration	[m/s ²]
T_a	Average air temperature	[K]
T_i	Inlet air temperature to OCZ	[K]
u_i	Inlet air velocity	[m/s]

The inlet air velocity into a room with DCV can vary across the ceiling and is not easy to establish. Therefore, it is generalised and calculated based on the flow rate and the area of active panel area in the ceiling. The formula is shown in Equation 2.2.

$$u_i = \frac{q}{A_i} \quad (2.2)$$

Where,

q	Air flow rate	[m ³ /s]
A_i	Area of suspended ceiling	[m ²]

Reynolds number

The Re number is used to determine the balance between inertial and viscous forces in a fluid flow. In ventilation systems, it is commonly used to identify whether the airflow is laminar or turbulent. Therefore, this is tried on a DCV setup, where the Re number characterises the airflow through the porous or perforated ceiling, as well as the resulting flow in the room. The Re number can be calculated using Equation 2.3.

$$Re = \frac{\rho \cdot u \cdot L}{\mu} = \frac{u \cdot L}{\nu} \quad (2.3)$$

Where,

ρ	Fluid density	[kg/m ³]
u	Characteristic velocity of the fluid	[m/s]
L	Characteristic length	[m]
ν	Kinematic viscosity of the fluid	[m ² /s]

Dimensionless temperature and height

Throughout this paper, various studies are compared. To make this comparison, several parameters such as temperature and height are converted to dimensionless values, these differences are

normalised to ensure consistent comparisons across setups. The dimensionless temperature can be calculated from Equation 2.4.

$$T^* = \frac{T_l - T_i}{T_e - T_i} \quad (2.4)$$

Where,

T_l	Local temperature	[K]
T_i	Inlet temperature	[K]
T_e	Exhaust temperature	[K]

The dimensionless height can be calculated from Equation 2.5.

$$h^* = \frac{h_l}{h} \quad (2.5)$$

Where,

h_l	Local height	[m]
h	Total height	[m]

2.2 Draught rate

Draught rate (DR) is a parameter used in ventilation design to quantify the risks of thermal discomfort caused by air movement. The calculation of DR takes the air velocity, temperature, and turbulence intensity into account. The calculation for DR can be found in Equation 2.6. [Nielsen, 2007]

$$DR = (34 - T_{a,1}) \cdot (\overline{v_{a,1}} - 0.05)^{0.62} \cdot (0.37 \cdot \overline{v_{a,1}} \cdot T_u + 3.14) \quad (2.6)$$

Where,

DR	Draught rate	[%]
$T_{a,1}$	Air temperature	[°C]
$\overline{v_{a,1}}$	Mean air velocity	[m/s]
T_u	Turbulence intensity	[%]

The turbulence intensity is throughout this project set to 40% for the calculation.

2.3 Principle of developing design chart

The design chart is another approach, which primary function is to define the acceptable operational conditions for the DCV system. By developing design charts for various scenarios, these can be integrated into the configuration tool to serve as the foundation for calculations and performance assessments.

Many studies aim to identify the operating conditions where a ventilation system performs effectively. The findings from measurements and simulations are presented in design charts and can be used in the design of the system. Design charts simplify this process by representing established correlations between key parameters such as airflow rate, temperature difference, and comfort limits. The source used for the whole section is by Nielsen [2007].

Figure 2.1 shows a typical design area based on the supply airflow rate, q_0 , and the temperature difference, ΔT_0 , between supply and return. The white area represents the range of conditions where both indoor air quality and thermal comfort requirements are met. A minimum airflow is needed to maintain acceptable air quality, while the upper boundaries reflect limitations related to draught and vertical temperature gradients in the OCZ. In DCV, air movement is primarily driven by the room's heat load rather than the supply momentum. This means that draughts can occur due to buoyancy-driven flows rather than high inlet velocities. In the chart, the horizontal straight line represents the draught limit, while the curved line marks the threshold for acceptable temperature gradients and draught risk. These limits help define a design area where the system can operate effectively without compromising comfort or air quality.

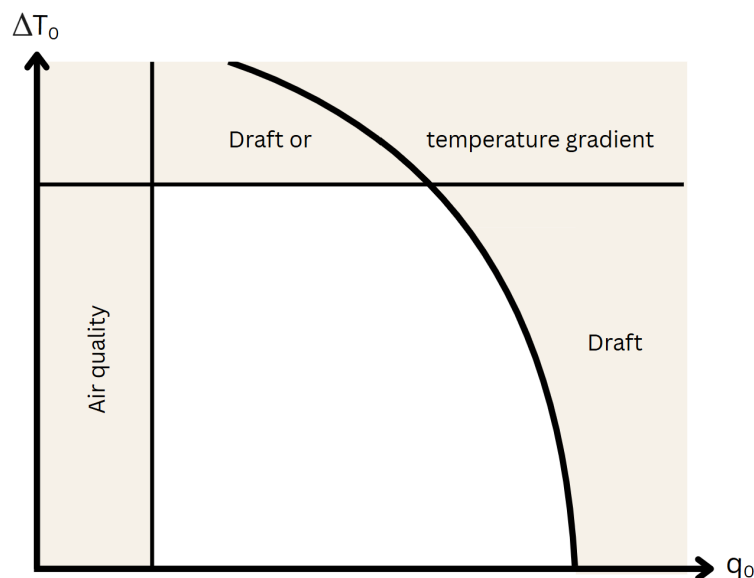


Figure 2.1. Design chart principle [Nielsen, 2007].

Additional system limitations can also be added, as shown in Figure 2.2. These include factors such as minimum supply temperature, maximum cooling capacity and flow rate limitations. The shaded areas in the figure indicate where the operational range is limited by these factors. The upper shaded area in the chart shows the limit for the minimum supply temperature, which can

be especially important in systems that use cold outdoor air for cooling. Just below, the curved boundary represents the system's maximum cooling capacity, indicating the point where the system may no longer be able to handle the cooling load. On the right side, vertical boundaries indicate restrictions due to maximum allowable airflow. These combined limits narrow down the usable design area by taking both technical performance and comfort considerations, ensuring the system can provide sufficient cooling without exceeding its operational limits.

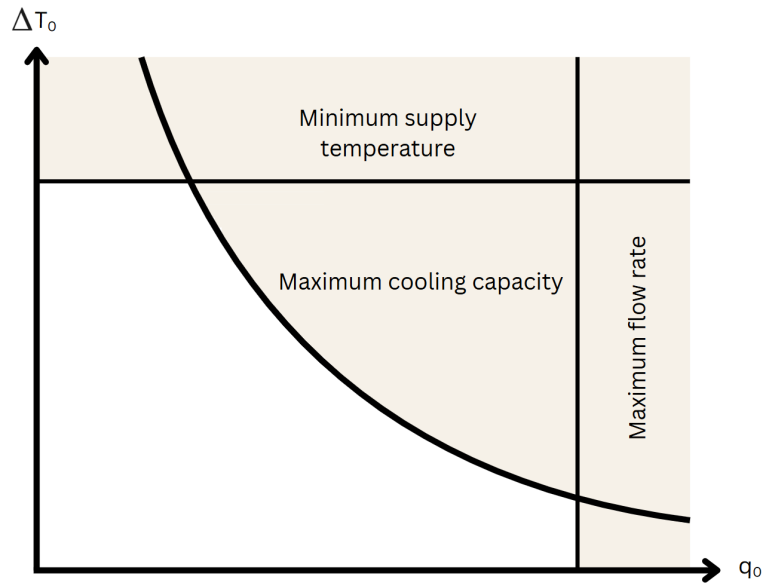


Figure 2.2. Design chart principle with maximum cooling capacity [Nielsen, 2007].

A widely used method for analysing air distribution systems is based on the similarity principle. This principle states that in fully developed turbulent flows, with high Re number, the non-dimensional air velocities within a room can be described as functions of the Ar number. The Ar number represents the ratio between buoyancy and inertial forces, and it is particularly important in scenarios where thermal stratification or temperature differences influence airflow patterns.

Using this principle, three key non-dimensional velocity ratios can be defined:

- The velocity at the upper boundary of the occupied zone u_{ocz} relative to the supply velocity u_0 .
- The velocity at ankle level of a person u_{01} relative to u_0 .
- The velocity at head height of a seated person u_{11} relative to u_0 .

These relationships are expressed as in Equation 2.7, 2.8 and 2.9.

$$\frac{u_{ocz}}{u_0} = func_1(Ar) \quad (2.7)$$

$$\frac{u_{01}}{u_0} = func_2(Ar) \quad (2.8)$$

$$\frac{u_{11}}{u_0} = func_3(Ar) \quad (2.9)$$

These equations make it possible to estimate results under different conditions, as long as the Ar number remains constant. This is especially helpful when using design charts, where curves with constant Ar number help identify limiting values for airflow rate, q_0 and temperature difference, ΔT , even if those exact conditions were not tested. Figure 2.3 shows a curve for constant Ar number that represents all combinations of q_0 and ΔT that result in the same airflow behaviour.

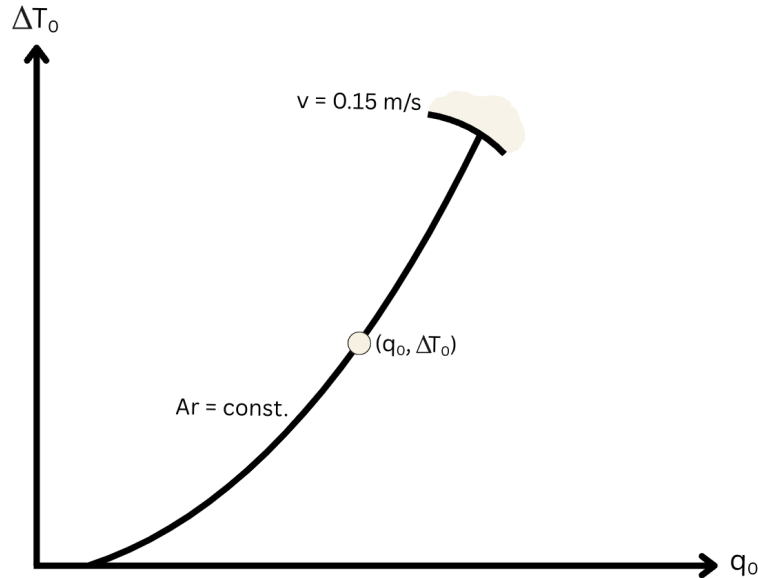


Figure 2.3. Design chart with limit based on an experiment at a given Ar number [Nielsen, 2007].

Along this curve, the velocity ratio remains constant, determined by the balance between inertial and buoyancy forces. The point $(q_0, \Delta T_0)$ on this curve represents the specific experiment, and by extending the curve, the draught limit, marked with the shaded area, can be identified. This indicates where the airflow would become uncomfortable due to excessive draught.

This method, expressed by Equation 2.10, makes it possible to determine the maximum airflow rate for a given temperature difference without testing every possible condition.

$$u = \frac{q_0}{a_0} \cdot \text{const} \quad (2.10)$$

Where,

q_0	Air flow rate	$[\text{m}^3/\text{s}]$
a_0	Supply opening area (ceiling)	$[\text{m}^2]$
const	Conditions along a line of constant Ar number	$[-]$

The formula can be used to determine the limiting air flow rate, q_0 for acceptable velocity levels in the OCZ. With this approach, it is possible to estimate airflow velocities under new operating conditions without running additional experiments, as long as the similarity conditions are still applicable. At the same time, it ensures reliable predictions of airflow and comfort limits.

In situations where the airflow pattern is strongly influenced by internal heat sources, such as occupants, equipment, or solar gains, the draught is not necessarily generated by the momentum

flow from the supply openings. Instead, it may be driven primarily by the thermal load within the room. This is the case for systems using DCV, where the supply velocity is low and buoyancy forces dominate the airflow pattern. In such systems, the similarity principle based on flow elements and the corresponding velocity functions Equation 2.7, 2.8, and 2.9 are no longer applicable. Instead, the design process relies on full-scale experiments or CFD predictions to capture the resulting airflow behaviour. The relationship between the thermal load, Q , and the resulting air velocity in the occupied zone can be described by an empirical function. This is expressed in Equation 2.11.

$$u = func_4(Q) \quad (2.11)$$

This expression makes it possible to determine the maximum allowable thermal load Q_{max} for a given reference velocity, such as 0.15 m/s, which is often used as a threshold to avoid draught discomfort.

2.4 CFD

For the numerical analysis, CFD is used as a tool. The software used in this thesis is Ansys 2019 R2. CFD is a powerful tool to simulate fluid flow, heat transfer, and mass transport. In a ventilation case, CFD can provide insights into airflow patterns and temperature distribution in a room without the need for a physical experiment. CFD provides a cost-effective and flexible way to test and optimise various design scenarios. A CFD model allows for numerical experiments under controlled conditions, making it easier to assess scenarios such as draught risks and temperature gradients. In this thesis, CFD is used to address the knowledge gaps identified through the literature review, with its main purpose being to provide data for the development of design charts in the configuration tool.

However, CFD presents some challenges. Accurate simulations require high-quality meshes, well-defined BC, and appropriate turbulence models. The reliability of CFD predictions depends on model validation and interpretation of results.

At the core of CFD is the general transport equation, which describes the conservation of mass, momentum, energy, and other scalar quantities in fluid flow. The general transport equation is shown in Equation 2.12.

$$\underbrace{\frac{\partial(\rho\phi)}{\partial t}}_{\text{Transient}} + \underbrace{\nabla \cdot (\rho\phi\mathbf{u})}_{\text{Convective}} = \underbrace{\nabla \cdot (\Gamma\nabla\phi)}_{\text{Diffusive}} + \underbrace{S_\phi}_{\text{Source term}} \quad (2.12)$$

Where,

ϕ	Velocity component	$[-]$
ρ	Fluid density	$[\text{kg}/\text{m}^3]$
\mathbf{u}	Velocity vector	$[\text{m}/\text{s}]$
Γ	Dynamic viscosity	$[\text{kg}/(\text{m} \cdot \text{s})]$
S_ϕ	Source term	$[\text{N}/\text{m}^3]$

This equation can represent different physical phenomena, such as a fluid problem, by specifying the variable ϕ , the diffusion coefficient Γ , and the source term S_ϕ . For a fluid problem, this will give the parameters. The application of the equation for the continuity and momentum equations is summarised in Table 2.1.

Table 2.1. Application of the transport equation to continuity and momentum equations.

	ϕ	Γ	S_ϕ
Continuity	1	0	0
x -momentum	u	μ	$-\frac{\partial p}{\partial x} + \rho_x g$
y -momentum	v	μ	$-\frac{\partial p}{\partial y} + \rho_y g$
z -momentum	w	μ	$-\frac{\partial p}{\partial z} + \rho_z g$

Here, μ is the dynamic viscosity, p is pressure, and g is the gravitational acceleration. The velocity components u , v , w represent the transport of momentum in the x , y , and z directions and can be made into the Navier-Stokes equations. For the continuity equation, since mass conservation is enforced, $\phi = 1$, and both diffusion and source terms vanish.

In turbulent flows, velocity and pressure can exhibit random fluctuations. To account for this behaviour, the Navier-Stokes equations are averaged using the Reynolds-averaged Navier–Stokes (RANS) approach. This introduces Reynolds stresses, which are unknown. The Reynolds stresses represent the effects of turbulence and must be modelled to close the system of equations. This is done by introducing turbulence models.

Several types of airflow can be observed in a room with DCV. In Figure 2.4, these different types of flows are illustrated.

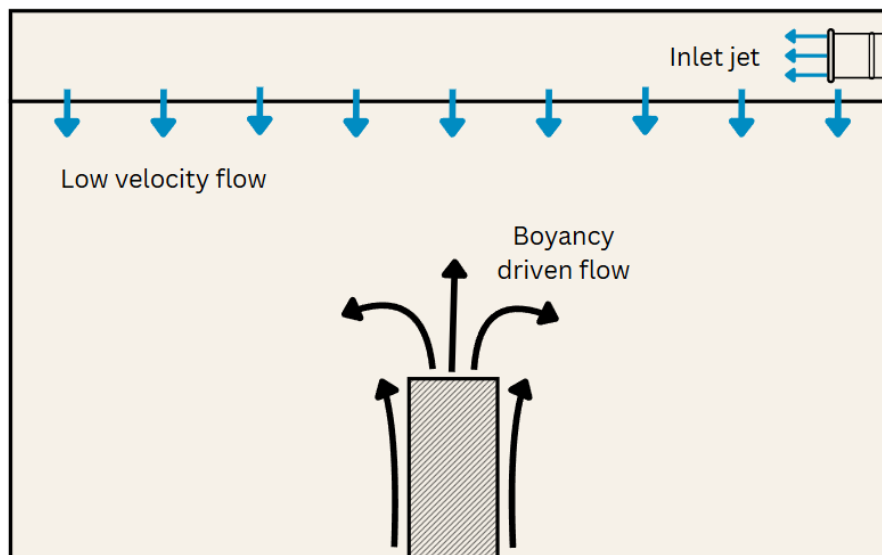


Figure 2.4. Flow types in a room with DCV.

From the inlet into the plenum, the airflow forms an air jet, characterised by high velocity and directional momentum. This flow is very different from the behaviour observed through the diffuse

ceiling itself, where the air gradually permeates into the room at a very low velocity, creating a nearly uniform and low-impulse supply.

Inside the OCZ of the room, buoyancy-driven flows dominate due to heat sources such as occupants, lighting, and equipment. These buoyancy flows are characterised by upward-moving thermal plumes.

2.5 Overall methodology used in the thesis

First, a comprehensive literature review is conducted to obtain knowledge of the important design and performance parameters affecting DCV. Dimensionless numbers are used to make different datasets comparable and also investigate whether the same approach used in other tools can be applied in a DCV configuration tool.

CFD simulations are used to fill out the gaps from the literature review and create cases that can be used for identifying how different parameters affect the system performance. Based on these simulations, design charts are developed. Design charts take into account the similarity principle and use the simulated results. The design charts are a great way of showing the acceptable operational condition for the system.

Part I

Preliminary investigations

This section presents preliminary investigations of temperature gradients, air velocity, and draught. It identifies key design parameters affecting the DCV system and analyses existing design charts.

Chapter 3	Assessment of temperature gradient	20
3.1	Comparison with other ventilation strategies	20
3.2	Analysis of papers	22
Chapter 4	Assessment of velocity and draught	28
4.1	Analysis of papers	28
4.2	Draught rate	31
Chapter 5	Assessment of design parameters	33
5.1	Geometry	33
5.2	Diffuse ceiling panels	37
5.3	Heat sources	41
5.4	Inlet properties	43
5.5	Exhaust properties	43
5.6	Heating or cooling case	45
Chapter 6	Assessment of design charts	46
6.1	Existing design charts and graphs	46
Chapter 7	Conclusion of literature review	50

Assessment of temperature gradient 3

When designing a room with DCV, it is crucial to examine the temperature distribution to ensure optimal thermal comfort. In other ventilation strategies, the temperature gradient is a limiting parameter for thermal comfort in a room due to the possibility of air stratification. In this chapter, this is investigated with dimensionless numbers to better understand the combination of momentum and buoyancy-driven air mixing within the room with DCV. This is done by looking at the temperature gradient from different studies and comparing them to investigate the correlations and differences.

3.1 Comparison with other ventilation strategies

The vertical temperature gradient in an indoor environment refers to the variations in the air temperature at different room heights. The gradient is typically illustrated in the full room height, but is most relevant in the OCZ. To ensure thermal comfort, the difference in temperature between the head level (1.1 m) and the ankle level (0.1 m) should not exceed 3°C, to comply with category B according to the International Standard [2006] standard.

In the study by Nielsen and Jakubowska [2009], they use an experimental setup of an office while varying the temperature difference between 3.5 and 12°C, without causing any discomfort in the OCZ. This is most likely due to the air being evenly distributed across the entire ceiling. Most other systems have limitations on ΔT , as excessive temperature differences can lead to stratification or uncomfortable draughts. However, a limitation in temperature is also found for DCV, where the surface temperature should not exceed the dew point of the air temperature to avoid condensation issues on the back side of the ceiling panels. [Fan et al., 2013; Zhang et al., 2017]

In the study by Zhang [2016], an experimental study representing an office room was conducted. In the study, the vertical temperature gradient from a DCV setup is compared to a setup with mixing ventilation. This comparison is shown at Figure 3.1.

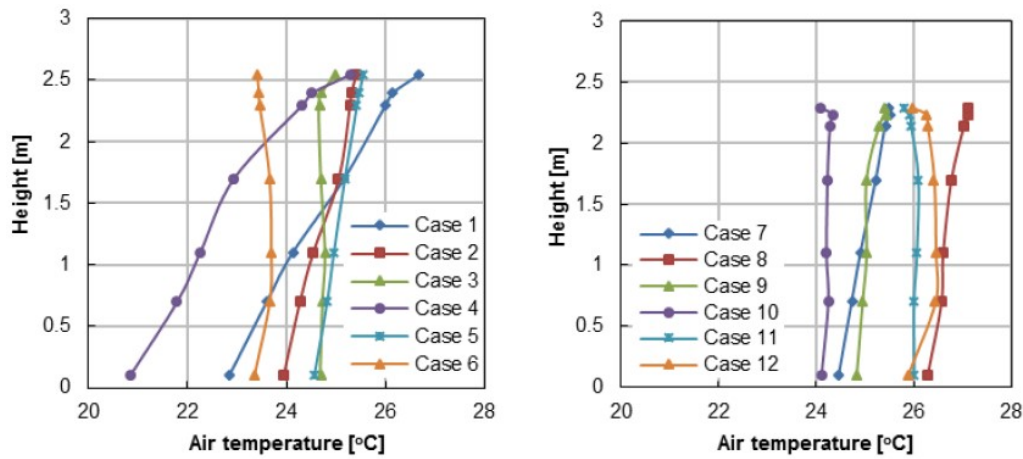


Figure 3.1. Vertical temperature difference. Mixing (left) and with DCV (right). [Zhang, 2016]

As can be seen from Figure 3.1, DCV minimises the temperature differences significantly within the room. With DCV, the airflow is evenly distributed across a large space, helping to decrease the temperature gradient. DCV is designed to keep the gradient within an acceptable range, contributing to enhanced thermal comfort.

Compared to traditional ventilation principles, DCV offers a higher cooling capacity. According to the design guide by Zhang et al. [2017] and the study by Nielsen and Jakubowska [2009], DCV achieves a cooling capacity of 72 W/m^2 , which surpasses the cooling capacities of mixing ventilation and displacement ventilation, which is respectively 53 W/m^2 and 40 W/m^2 . Additionally, Kristensen and Jensen [2015] reports that DCV can provide a cooling capacity exceeding 130 W/m^2 while still meeting the thermal comfort requirements of category B in the International Standard [2006].

3.2 Analysis of papers

The following sections will present a detailed analysis of the temperature gradient based on the various studies. Most of the studies focus on cooling scenarios. Only two studies examine heating cases, making it challenging to perform a comprehensive comparison. The results related to heating scenarios are provided in Appendix B.

Details about the papers used in the analysis are presented in Table 3.1.

Table 3.1. Summarised information about heating cases used in temperature assessment.

Paper	Case	Geometry [m]	ACH [h ⁻¹]	Temperatures [°C]			Heat load [W/m ²]	Placement of heat load
				Inlet	Exhaust	ΔT		
[Zhang, 2016]	[A1] 2h ⁻¹ 17°C	2.335 × 4.8 × 3.3	2.0	9.5	26.3	16.8	30	Centered
	[A2] 4h ⁻¹ 17°C	2.335 × 4.8 × 3.3	4.0	9.4	26.0	16.6	60	
[Nielsen et al., 2010]	[B1] 8h ⁻¹ 7°C	2.45 × 4.1 × 3.2	8.0	16	22.6	6.6	-	One sided
[Fan et al., 2013]	[C1] 4h ⁻¹ 7°C	2.9 × 6 × 3.6	3.5	16.7	24.0	7.3	31	One sided
	[C2] 5h ⁻¹ 9°C	2.9 × 6 × 3.6	5.1	17.2	26.0	8.8	53	
[Hviid and Svendsen, 2012]	[D1] 2h ⁻¹ 23°C	2.9 × 6 × 3.6	2.3	-3.1	19.8	22.9	50	Symmetrical
	[D2] 3h ⁻¹ 17°C	2.9 × 6 × 3.6	3.0	3.2	20.5	17.3	50	
	[D3] 6h ⁻¹ 9°C	2.9 × 6 × 3.6	6.0	11.2	20.5	9.3	50	
	[D4] 2.3h ⁻¹ 23°C	2.9 × 6 × 3.6	2.3	-3.2	19.9	23.1	50	
	[D5] 3h ⁻¹ 18°C	2.9 × 6 × 3.6	3.0	3.2	20.8	17.6	50	
	[D6] 6h ⁻¹ 9°C	2.9 × 6 × 3.6	6.0	11.2	20.4	9.2	50	
[Petersen et al., 2014]	[E1] 2h ⁻¹ 8°C	2.4×3.6×3.1	2.0	-	-	8.0	57	One sided
	[E2] 2h ⁻¹ 12°C	2.4×3.6×3.1	2.4	-	-	12.0	57	
	[E3] 3h ⁻¹ 3°C	2.4×3.6×3.1	2.6	-	-	3.0	57	
	[E4] 5h ⁻¹ 8°C	2.4×3.6×3.1	4.7	-	-	8.0	57	
	[E5] 6h ⁻¹ 12°C	2.4×3.6×3.1	5.5	-	-	12.0	57	
	[E6] 4h ⁻¹ 3°C	2.4×3.6×3.1	2.4	-	-	3.0	57	
	[E7] 7h ⁻¹ 8°C	2.4×3.6×3.1	2.6	-	-	8.0	57	
	[E8] 8h ⁻¹ 12°C	2.4×3.6×3.1	8.1	-	-	12.0	57	
	[E9] 6h ⁻¹ 3°C	2.4×3.6×3.1	6.1	-	-	3.0	57	
	[E10] 11h ⁻¹ 8°C	2.4×3.6×3.1	10.9	-	-	8.0	57	
	[E11] 13h ⁻¹ 12°C	2.4×3.6×3.1	13.4	-	-	12.0	57	

Known from the traditional ventilation systems, more parameters can affect the airflow in a room. This includes the geometry, where the room height typically has a significant impact on the efficiency of the system. A higher room height can lead to reduced air circulation and thereby create a greater vertical temperature gradient. In the papers presented in Table 3.1, it is seen that the room height between the different papers varies from 2.335 to 2.9 m without the plenum height. The width and length also vary, with the shortest length being 3.6 m and the longest 6 m. For the width of the room, this varies from 3.1 to 3.6 m. Although these differences are relatively small, they remain important factors to consider.

The ACH is a key parameter influencing the performance of any ventilation system. Generally, a low ACH results in insufficient mixing and vertical stratification, while a high ACH can increase the draught risk. Combined with the temperature difference between the inlet air and either the room or exhaust air, these factors are crucial for determining the effectiveness of any ventilation system. Therefore, analysing the temperature gradient in relation to ACH will be the first focus of the analysis.

Temperature difference vs. air change

The temperature difference between inlet and exhaust air has been plotted against the air volume for all the presented cases in Table 3.1. This has been done to get an overview of the existing cases. The plot is seen in Figure 3.2.

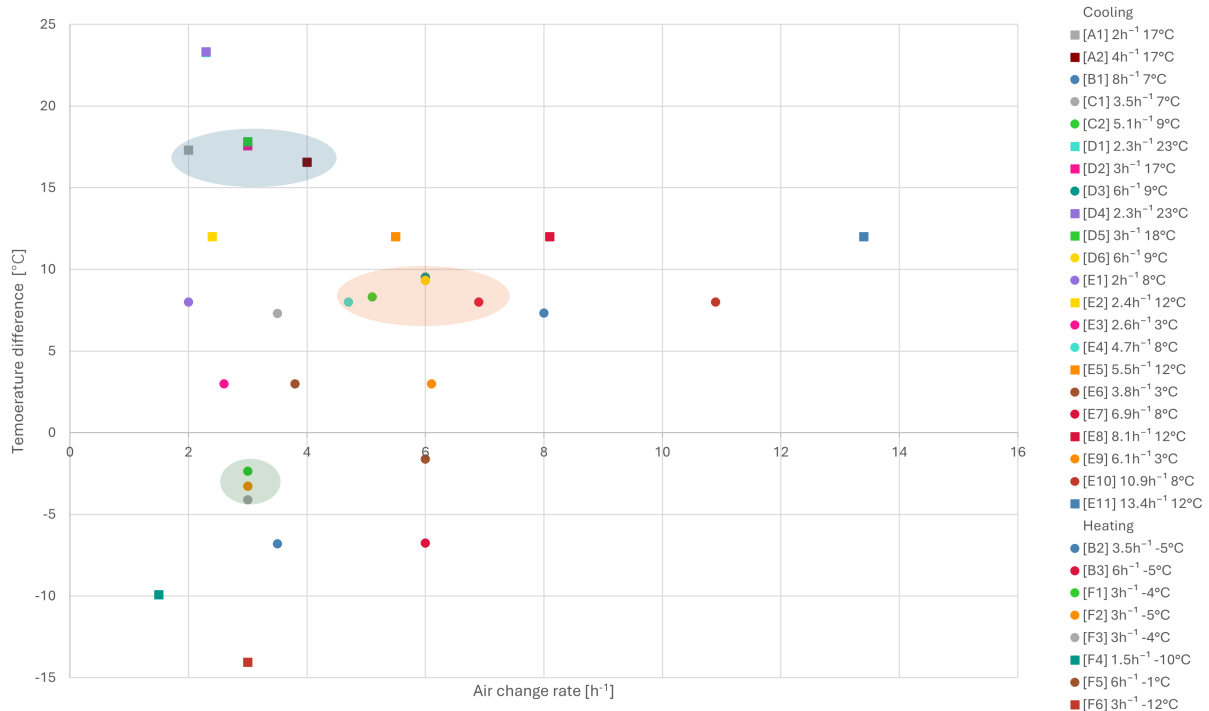


Figure 3.2. ACH vs. temperature difference.

The blue, orange, and green circles in the figures highlight cases with similar conditions regarding temperature difference and ACH. Therefore, it has been investigated if the vertical temperature difference is also comparable for these cases.

In some studies, the temperature gradient was specified for different parts of the room, while in others, only a single gradient representing the entire room was provided. To assess whether averaging the normalised temperature gradients could be a valid approach, an analysis was carried out, as detailed in Appendix C. The results showed that the average normalised temperature gradient is an acceptable representation of the room conditions.

Orange circle: C2, D3, D6, E4 and E7

For the orange cases, some variations in the temperature gradients were observed. The temperature gradients for these cases are presented in Figure 3.3.

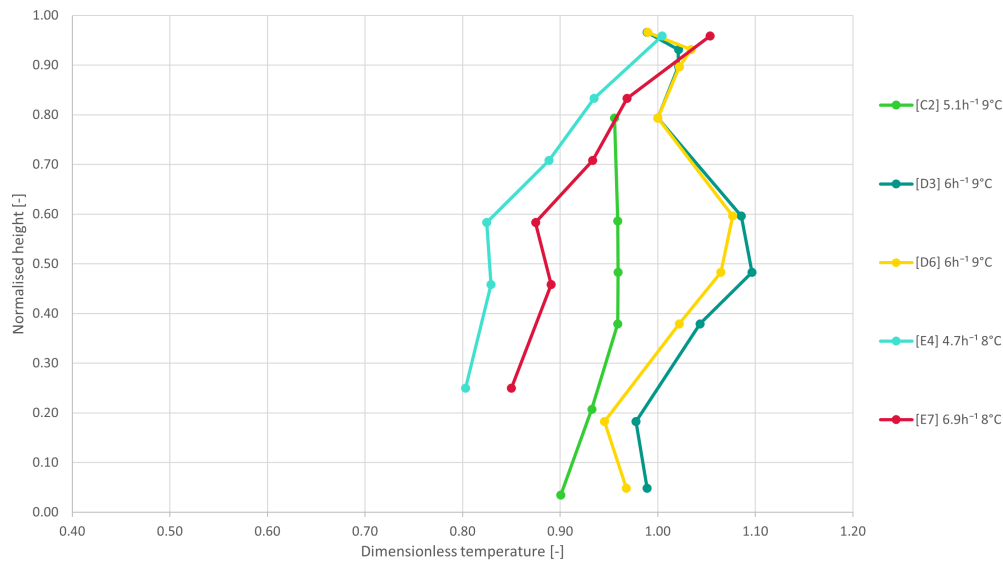


Figure 3.3. Temperature gradients for orange cases.

When comparing these cases based on heat load, it was noted that cases D3 and D6 have a heat load of 50 W/m^2 , case C2 has a heat load of 53 W/m^2 , and cases E4 and E7 have a heat load of 57 W/m^2 . The temperature gradients are arranged such that the cases with the highest heat loads are positioned on the left, while those with the lowest heat loads are on the right. Here, the cases with higher heat loads, E4 and E7, exhibit larger temperature gradients.

Blue circle: A1, A2, D2 and D5

In Figure 3.4, the temperature gradient for the blue cases can be seen.

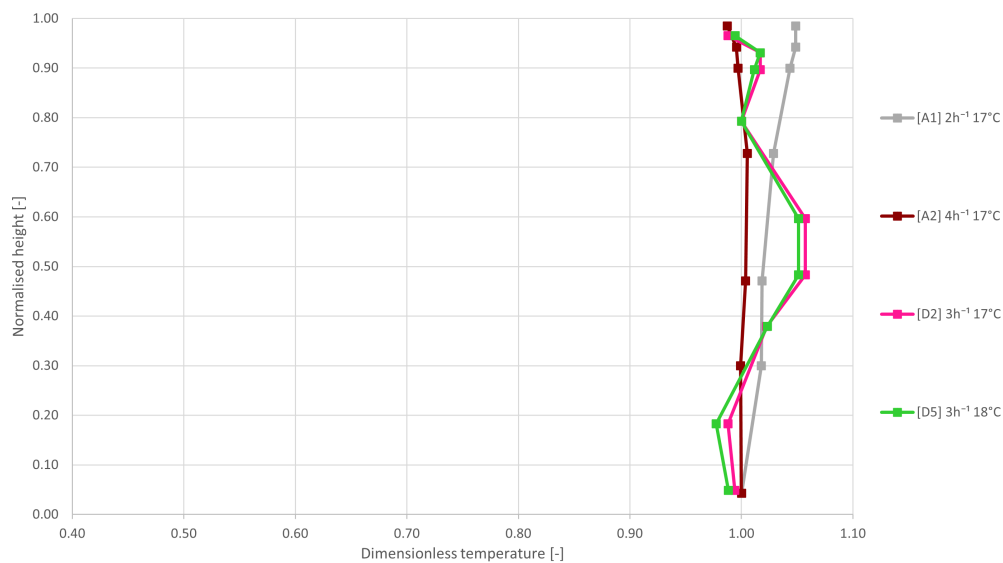


Figure 3.4. Temperature gradients for blue cases.

For these cases, similar tendencies were observed as for the orange cases. However, when analysing

the heat load for these cases, it was found that A1 had a heat load of 30 W/m^2 , A2 had a heat load of 60 W/m^2 , and both D2 and D5 had a heat load of 50 W/m^2 . Despite the greater variation in heat loads, the temperature gradients appeared more consistent, as shown in Figure 3.4. This observation suggests that at higher temperature differences, the impact of heat load on the gradient is reduced. It indicates that the air mixing in these cases is primarily momentum-driven rather than buoyancy-driven when temperature differences are high.

Green circle: B2, F1, F2 and F3

For the heating cases, the temperature gradients are seen in Figure 3.3

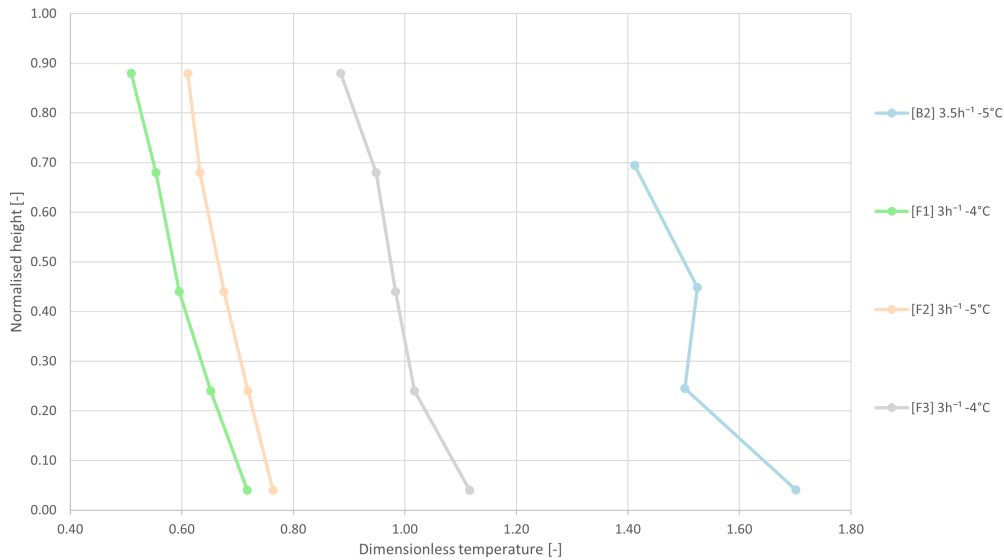


Figure 3.5. Temperature gradients for green cases.

These gradients appear similar, but they are offset along the x-axis. Although cases F1, F2, and F3 have the same heat load and room geometry, the supply temperature differs slightly, with F1 having the lowest temperature of 26.2°C and F3 having the highest of 27.7°C . In case B2, no heat load is present. This case has a supply temperature of 27.3°C and a higher ACH, which could explain the significant offset observed in Figure 3.5.

Archimedes number vs. air change rate

The following graphs present the Ar number for the cooling cases. The cases are grouped based on different ranges of the Ar number, as shown in Figure 3.6. The groups are organised from top to bottom, with the lowest Ar numbers displayed at the top and the highest at the bottom. The range for each group is specified at the top of each figure.

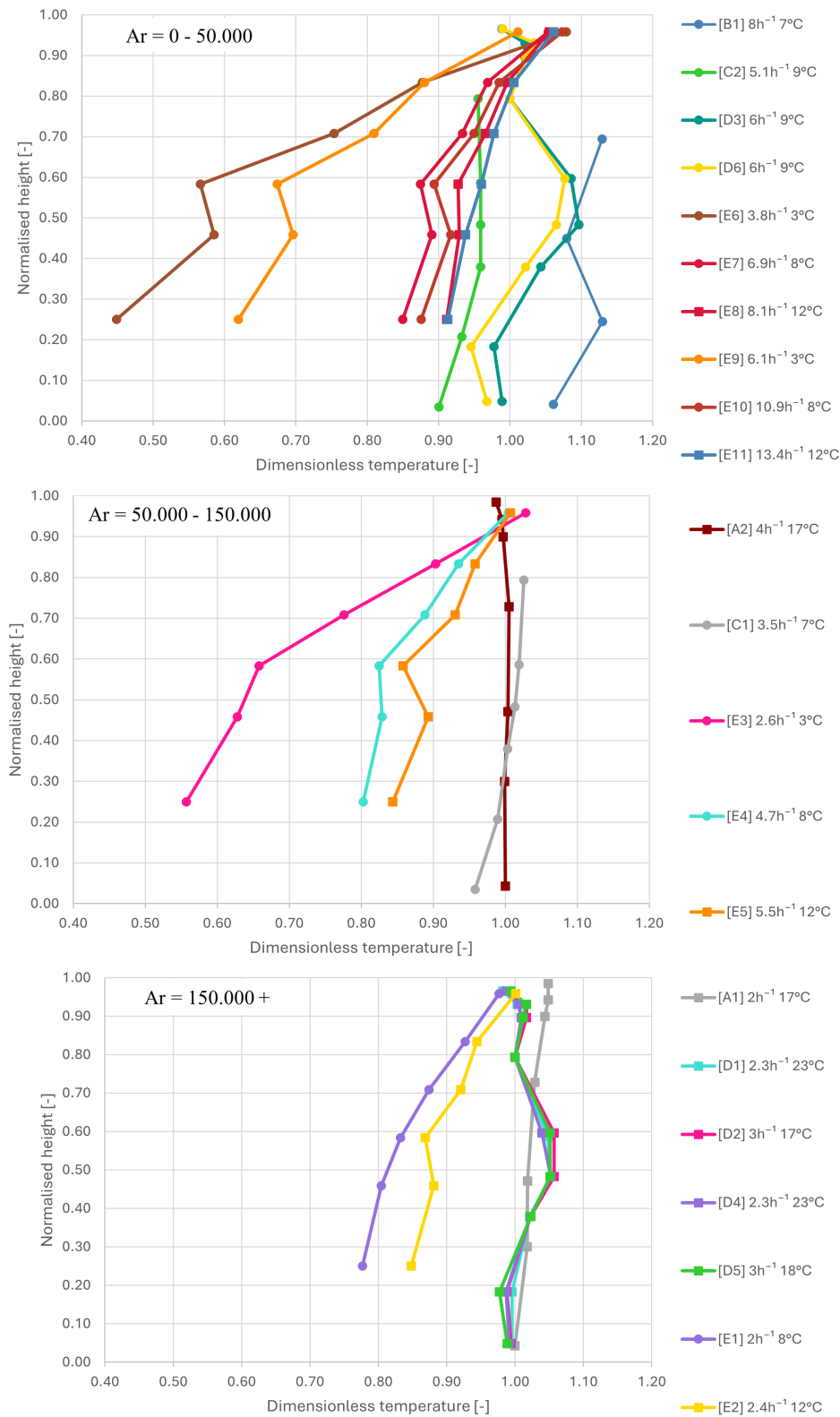


Figure 3.6. Comparison of Ar number for heating cases.

In general, it appears that the temperature gradient decreases as the Ar number increases. When the Ar number exceeds 600,000, the gradient is no longer observed. In cases with lower Ar numbers, the presence of a gradient seems to be influenced by the temperature difference between the inlet and exhaust air. Notably, the cases with the highest gradients also exhibit the smallest temperature differences. Additionally, the vertical temperature gradient does not appear to be influenced by the

ACH. Key values indicating when the gradient becomes minimal or disappears entirely can be found in Table 3.2.

Table 3.2. Ar number compared to the temperature difference.

Ar	ΔT
0 - 150,000	>3-8°C
150,000 - 600,000	>12°C

This analysis highlights that DCV effectively minimises temperature gradients compared to traditional ventilation strategies. The key to this lies in the way DCV combines momentum and buoyancy-driven air mixing, creating a more consistent temperature distribution throughout the room. A low Ar number combined with a small ΔT results in a low ACH, leading to the presence of temperature differences. This indicates that both momentum force and buoyancy force are low, and there is no strong driving force for mixing. A low Ar number combined with a high ΔT results in a high ACH and temperature differences. This indicates that both momentum and buoyancy forces are strong, promoting efficient air mixing. With high Ar, the temperature differences are high, and ACH is low. In this situation, no temperature gradients are observed.

Heat sources have also been shown to influence airflow in a room with DCV. The intensity of the heat source impacts DCV. According to Nielsen et al. [2010], to ensure sufficient air mixing, the system relies on internal heat sources to generate mixing, thereby reducing the temperature gradient.

However, the normalised temperature gradient is almost non-existent in all cases with temperature differences at 8°C or above. Case E6, which has the highest normalised temperature gradient, the maximum vertical temperature gradient found were 1.5°C [Petersen et al., 2014]. This fulfils category A, where the requirement is less than 2°C [International Standard, 2006]. Therefore, the temperature gradient when using DCV is shown not to be a limiting parameter. The findings therefore show that DCV can handle larger temperature differences without sacrificing thermal comfort. This is evident from various studies, which consistently demonstrate that DCV maintains temperature variations within the acceptable range set by the International Standard [2006].

Assessment of velocity and draught 4

Beside the thermal discomfort which can occur due to a temperature gradient, the air velocity also plays a crucial role. When designing a ventilation system, the air velocity can affect the occupants' comfort by causing draught, but it can also affect the air distribution. Ideally, airflow velocity is kept low to minimise this issue, but doing so can sometimes make it challenging to meet the ventilation requirements of the room. Unlike other systems that have airflow limits due to the risk of draught in the OCZ, DCV allows unrestricted airflow as long as it remains within traditional design constraints [Nielsen and Jakubowska, 2009]. A major advantage of DCV is its ability to maintain both low and high ventilation rates while minimising discomfort from draught, assuming the ceiling supply is sufficiently large [Kristensen and Jensen, 2015; Zhang et al., 2017]. International standards such as International Standard [2006] define comfort limits, with category B recommending a maximum air velocity of 0.2 m/s, though many studies adopt a more conservative limit of 0.15 m/s to reduce draught risk [Nielsen and Jakubowska, 2009].

4.1 Analysis of papers

The following section presents a detailed analysis of the findings from cases that have investigated air velocity. Most of the studies focus on cooling scenarios, which will be the primary focus of this analysis. Only a few studies examine heating cases, and due to the limited data available, it is not possible to conduct an extensive comparison. Therefore, these results are presented separately in Appendix D. In Table 4.1, the information about the papers included in the analysis is presented. The temperature difference represents the difference between supply and exhaust air temperatures

Table 4.1. Information about the cases with geometry, airflow, and temperature conditions.

Paper	Case	Geometry [m]	ACH [h ⁻¹]	Temperatures [°C]			Heat load [W/m ²]	Placement of heat load
				Inlet	Exhaust	ΔT		
[Fan et al., 2013]	[C1] 4h ⁻¹ 7°C	2.9×6×3.6	3.5	16.7	24.0	7.3	31	One sided
	[C2] 5h ⁻¹ 9°C	2.9×6×3.6	5.1	17.2	26.0	8.8	53	
[Petersen et al., 2014]	[E1] 2h ⁻¹ 8°C	2.4×3.6×3.1	2.0	-	-	8.0	57	One sided
	[E2] 2h ⁻¹ 12°C	2.4×3.6×3.1	2.4	-	-	12.0	57	
	[E3] 3h ⁻¹ 3°C	2.4×3.6×3.1	2.6	-	-	3.0	57	
	[E4] 5h ⁻¹ 8°C	2.4×3.6×3.1	4.7	-	-	8.0	57	
	[E5] 6h ⁻¹ 12°C	2.4×3.6×3.1	5.5	-	-	12.0	57	
	[E6] 4h ⁻¹ 3°C	2.4×3.6×3.1	2.4	-	-	3.0	57	
	[E7] 7h ⁻¹ 8°C	2.4×3.6×3.1	2.6	-	-	8.0	57	
	[E8] 8h ⁻¹ 12°C	2.4×3.6×3.1	8.1	-	-	12.0	57	
	[E9] 6h ⁻¹ 3°C	2.4×3.6×3.1	6.1	-	-	3.0	57	
	[E10] 11h ⁻¹ 8°C	2.4×3.6×3.1	10.9	-	-	8.0	57	
	[E11] 13h ⁻¹ 12°C	2.4×3.6×3.1	13.4	-	-	12.0	57	

The gradient is not important when looking at the velocity. Instead, it is the highest velocities, especially if placed close to the occupants. Therefore, the first part of this investigation will be to localise the placement of the highest velocity in each case.

Placement of highest velocity

Many papers investigate where the velocity is most critical, and the majority conclude that the highest velocities occur at ankle level. This is primarily due to the return flow at the floor level generated by thermal plumes and circulating airflow [Chodor and Taradajko, 2013; Kristensen and Jensen, 2015; Vilsbøll, 2014]. The velocities observed at this level range from 0.05 to 0.32 m/s [Seuntjens et al., 2022; Lestinen et al., 2018]. These velocity fluctuations are influenced by air movement patterns, air change rates, and heat loads. Higher air velocities are also recorded near the ceiling, driven by convective airflow patterns, which occur outside OCZ. The highest draught risk consistently occurs near the floor, particularly close to supply diffusers, where airflow acceleration is prominent. Despite the increased velocities at ankle level under DCV setups, they generally remain within comfort limits, ensuring compliance with comfort standards.

Figure 4.1 presents the analysed cases, illustrating the vertical position within the OCZ where the highest velocities are observed. The graph shows the correlation between the vertical placement and the ACH for each case.

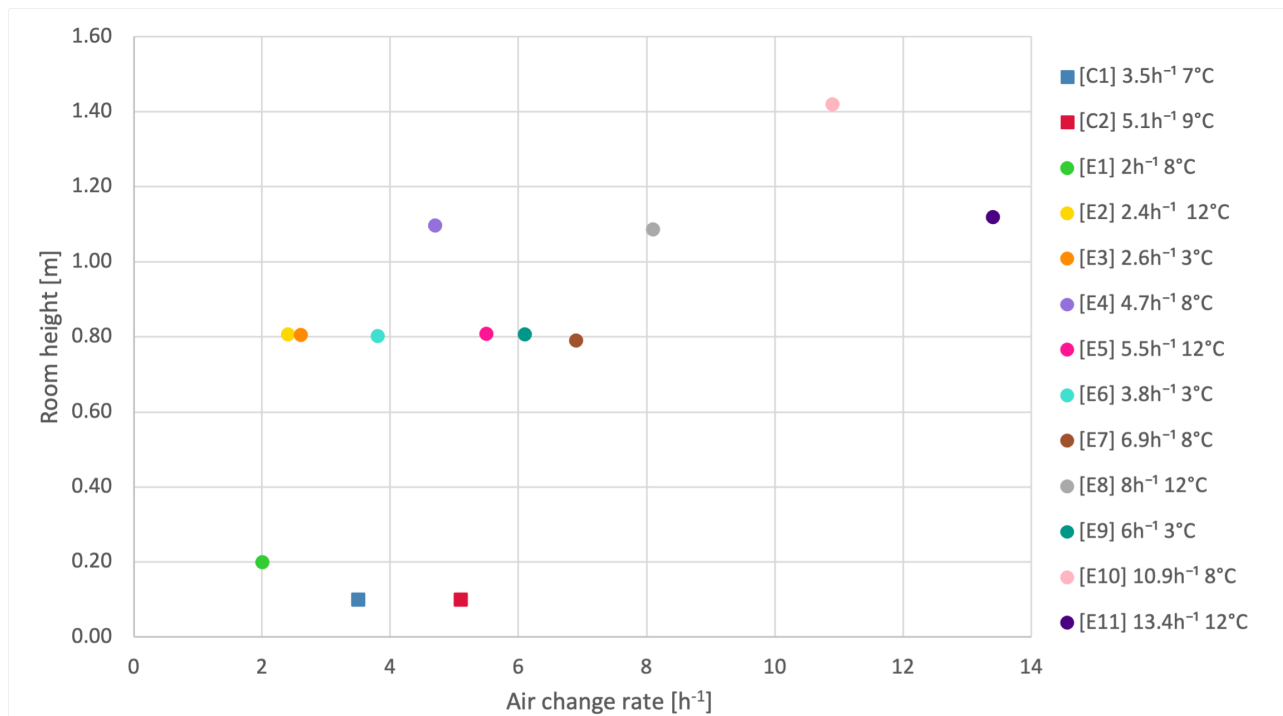


Figure 4.1. Vertical placement of highest velocity and corresponding ACH.

It is seen from Figure 4.1 that a higher ACH generally move the highest velocity point upward, meaning more air movement occurs at higher levels in the OCZ. Many of the data points from the paper by Petersen et al. [2014] regarding the vertical placement of high velocity are clustered around 0.8 meters. This finding differs from the majority of the existing literature, which typically reports

the highest velocities at ankle level. This discrepancy may be caused by various parameters such as room geometry, air change rates, heat loads, or the selected measurement points, which are limited when conducting experiments.

Max air velocities in correlation to ACH and ΔT

The relationship between maximum air velocity, ACH, and temperature difference is investigated to determine whether an increase in ACH or temperature difference correlates with higher airflow velocities within the OCZ. The graphs can be seen in Figure 4.2.

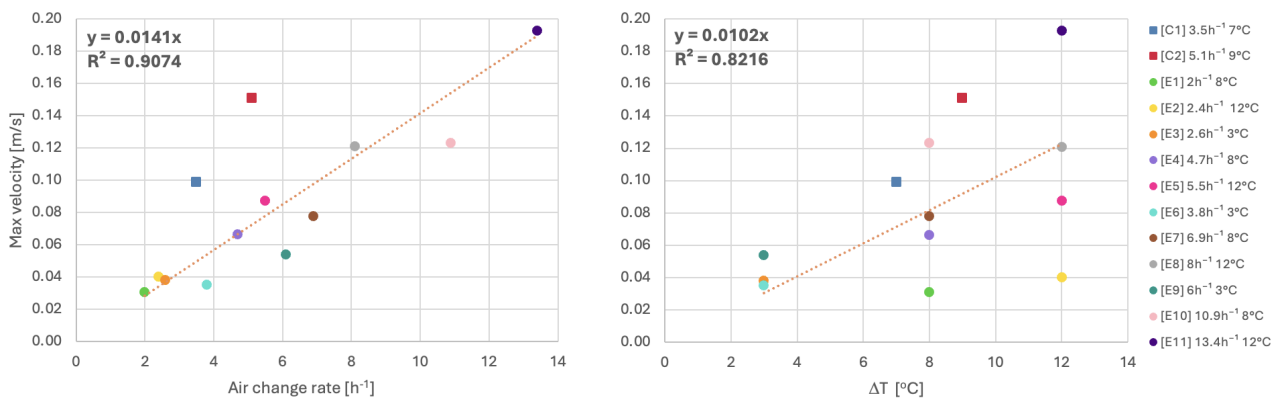


Figure 4.2. ACH and ΔT with corresponding max velocity.

The trendline for the graph with ACH and maximum air velocity has a R^2 value of 0.91, which indicates a strong correlation between the parameters. This means that the maximum velocity increases with an increase in ACH. Most cases align with this trend, with only a few deviating. Notably, cases C1 and C2 do not follow the trendline. These cases have a larger room volume than the others, which potentially contributes to the offset. Despite similar ACH values to other cases, their maximum velocities are higher, indicating that room geometry plays a crucial role in determining air velocity. It is also seen that the cases with a higher ΔT but similar ACH exhibit a greater maximum air velocity. This may be due to the enhanced airflow from buoyancy effects.

The correlation between max velocity and temperature difference was also investigated. It was found that the data is best represented by a linear correlation, with a R^2 value of 0.82. While this correlation is weaker compared to the relationship between ACH and maximum air velocity, it still suggests that ΔT influences the air velocity in a room, but to a smaller degree.

Correlation between max air velocities and Reynolds number

As described above, there seems to be a direct relation between ACH and ΔT with the max velocity. A direct correlation to the Re number is thereby expected, which leads to the next investigation. This will clarify whether there can be found a correlation between the maximum velocity and the Re number. The plot does not show any physical meaning, but can be used to visualise whether any correlation is present.

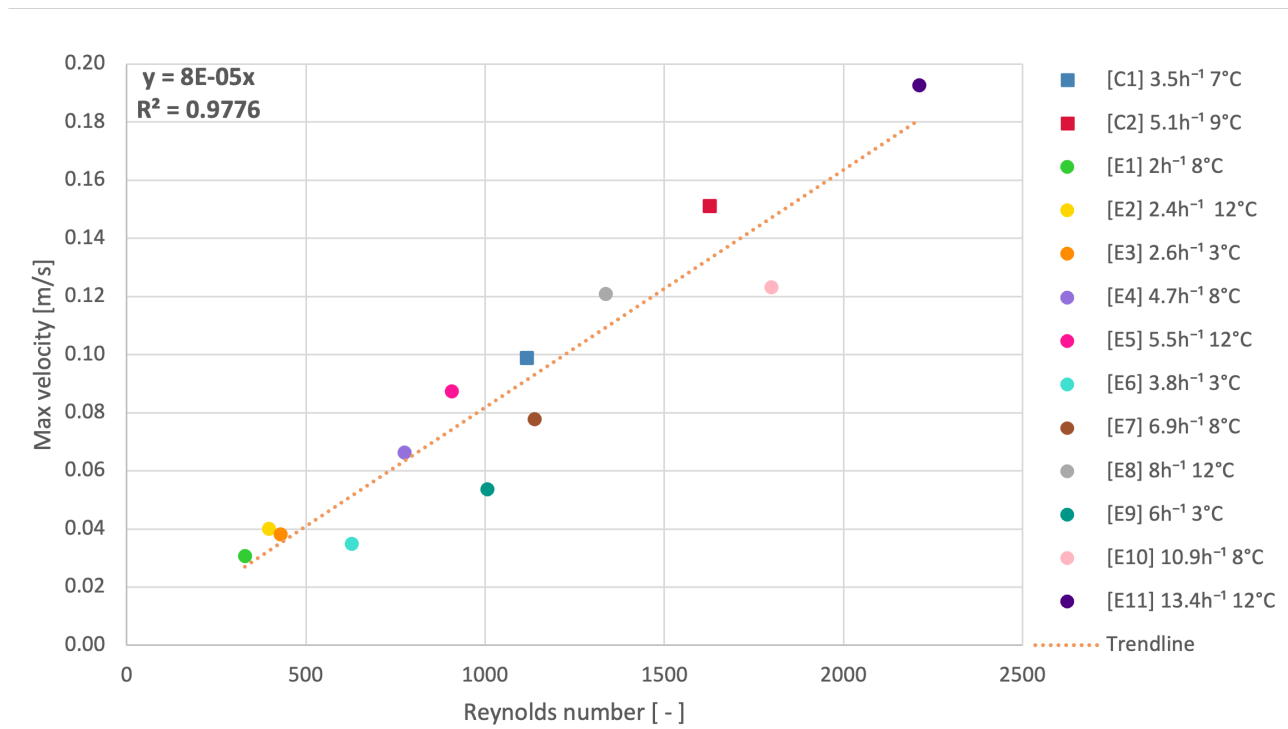


Figure 4.3. Re number vs. max velocity.

The trendline shows a linear tendency with minor deviations. The R^2 of 0.98 shows that it is a good predictor of max velocity. This indicates a direct correlation between the maximum velocity and the characteristic velocity determined based on the ACH divided by the inlet area. The correlation on the graph aligns with what was observed on the ACH vs. max velocity graph. Here, C1 and C2 did not follow the trendline because they exhibited higher maximum velocities, but these cases also had a larger room area.

4.2 Draught rate

One of the biggest indicators of whether the occupants are comfortable is the DR. Since a higher DR leads to dissatisfaction among occupants. In the following, the ACH and DR are compared and grouped by their height. This is done to get a better understanding of where the DR occurs and what the ACH is in the specific case. The height is illustrated with different shapes as shown in the legend. A square means the measurement is conducted at 0.1 m height, the circle is at 1.1 m, and the triangle is at a height of 1.7 m.

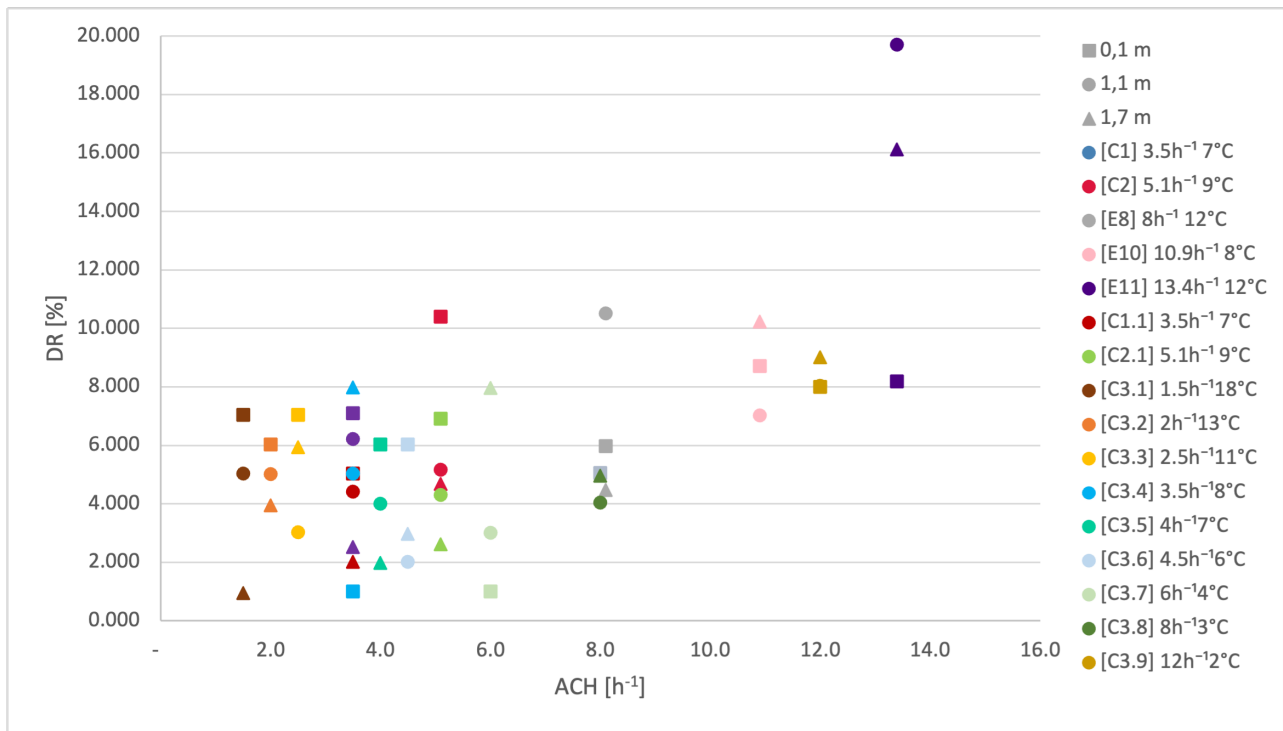


Figure 4.4. DR for all papers.

Based on the figure above, different conclusions can be made. It can be concluded that a low ACH results in a low DR in points at 1.7 m. If the ACH is increased, the DR at 1.7 m increases too. For experiments with lower ACH, it can be seen that the placement of the DR is at the lower part of the OZC. For higher ACHs, the DR placement shifts upwards and is either placed in 1.1 or 1.7 m.

It can also be noted that at lower ACH levels, DR remains low, confirming that minimal air movement reduces DR. At medium ACH, ranging from 4 to 6 h^{-1} , DR values start to vary more, with few cases being above 8-10%, this indicates that an increase in ventilation leads to a higher chance of discomfort. At high ACHs above 8 h^{-1} , DR is unpredictable, with some cases experiencing extreme draught discomfort, with DR above 15-20%, confirming that high airflow rates can lead to more air movement.

Air velocity is shown to be influenced by ACH, with higher ACH consistently leading to increased velocities. Temperature difference also impacts velocity, but to a smaller degree, as a greater temperature difference enhances buoyancy-driven airflow. Room geometry is also shown to influence airflow patterns, with larger volumes often exhibiting higher velocities despite similar ACH.

All these parameters are connected, and it is therefore difficult to simplify the system with dimensionless numbers. In the following, different design parameters will therefore be investigated thoroughly to better understand their influence on the system.

Assessment of design parameters 5

Based on the investigations of temperature gradient and velocity, it was observed that more parameters influence the system than those typically considered in traditional systems. Among other things, it was seen that the temperature gradient was affected by the heat load, and the velocity was affected by the room geometry, especially the room height. Therefore, this chapter will discuss different design parameters and describe them based on findings from several studies. This is done to understand the complexity of the system.

5.1 Geometry

Room geometry is a critical factor in any ventilation system design, as dimensions such as height, width, and length influence airflow patterns and the risk of draught. In a study by Zhang et al. [2016], it is recommended to use DCV in small office rooms, which, together with classrooms, are the most investigated room types with DCV. Several studies have examined the impact of geometric variations of rooms, including plenum height, room height, and room length.

Room height

Some studies have shown that room height affects the ventilation performance in a DCV setup. A numerical analysis conducted in a study by Zhang et al. [2015] examined room heights of 2.335, 3, and 4 m. In Figure 5.1, a clear connection between the room height and the DR can be seen. The room height of 2.335 meters has the lowest DR with a maximum of 13%, and the highest room of 4 m has a DR above 18%. It is not possible to comply with category A of thermal environment in any of the cases seen in Table 1.1. According to the standard, the maximum DR have to be below 10% to meet the requirements of this category. In category B, the maximum DR must be below 20%, which is met in all cases. However, for the case with a room height of 4 m, it is very close to this limit.

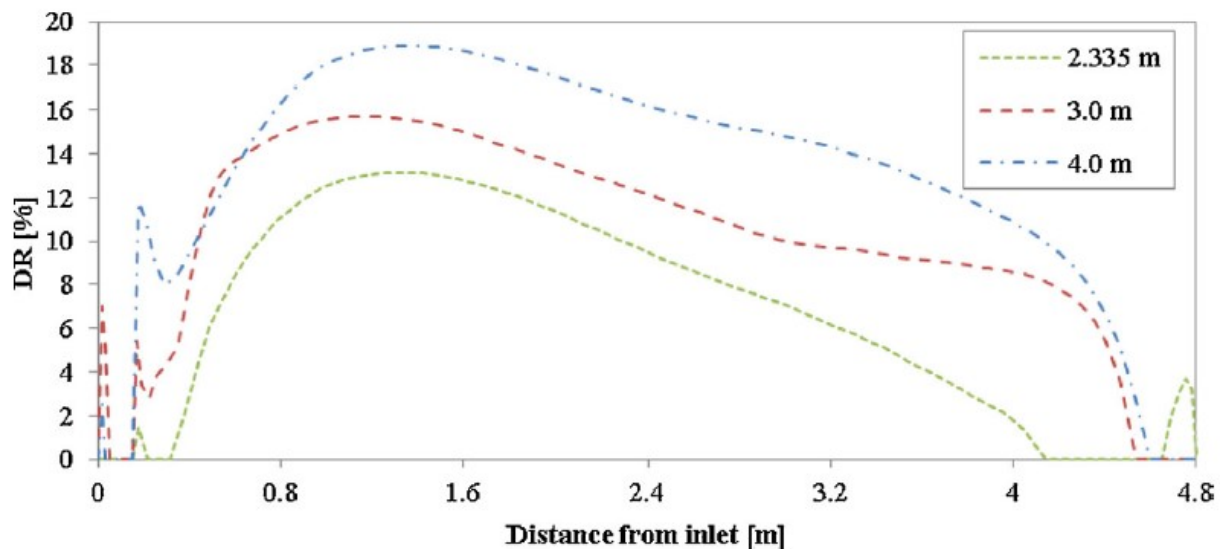


Figure 5.1. DR at different room heights [Zhang et al., 2015].

This increase in DR occurs because greater room height increases the recirculation intensity due to increased air entrainment. This accelerates air movement and enhances the risk of draught.

Similarly, in a study by Nielsen et al. [2015], a numerical comparison of two rooms with different heights were conducted. One room had a height of 2.5 m, and the other was 4.1 m. The comparison was based on cooling capacity, temperature gradient and velocity distribution. A design chart was made for different placements of heat sources in both rooms. The study showed that the cooling capacity decreased with the increase in room height. The acceptable operation area of the room with a height of 4.1 m was significantly smaller because the velocities were more significant in higher rooms. It was found that maintaining the same flow rate in both rooms resulted in higher velocities in the higher room. The increase in velocity may be due to the greater distance that the thermal plumes from the heat sources develop, allowing them to accelerate the surrounding air more. The reduction in cooling capacity could be due to the longer distance that the supply air must travel to reach the occupied zone, resulting in a loss of momentum. The upward movement of warm air from heat sources can counteract the downward movement of cooler air, which reduces the system's overall heat removal efficiency.

In a paper from Chodor and Taradajko [2013], two room heights of 3 and 4.4 m are compared. It is not clear whether ACH or airflow is maintained the same between the simulations. However, the study observes similar trends, with higher velocities in the higher room and greater cooling capacity in the shorter room, aligning with findings from other papers.

Based on these findings, a room height below 3 m is recommended for achieving efficient airflow distribution while minimising DR in the occupied zone [Zhang et al., 2017]. Lower ceilings help distribute air more effectively, as the low momentum airflow from the diffuse ceiling can reach the OCZ without causing unwanted turbulence [Nielsen et al., 2015]. In contrast, greater room heights negatively impact ventilation performance by disturbing the balance between buoyancy and momentum forces. This was also seen in Chapter 4, where the maximum air velocities were greater in rooms with a greater room height.

Length and width

In a study by Zhang et al. [2016], a numerical investigation of an office space with DCV was conducted. One of the parameters investigated was room length, comparing two configurations with lengths of 4.8 and 9.6 m. To ensure consistency between the cases, all other design parameters were kept constant. In the longer room, both the heat load and ventilation rate were doubled to maintain the same heat gain per square meter and ACH of 2 h^{-1} .

A winter scenario was analysed, revealing that local temperature and velocity differences decreased as the distance from the inlet increased. This outcome was expected, as the air had time to lose its momentum and become more uniform within the plenum before being distributed through the diffuse ceiling panels. Since the air lost more of its momentum before reaching the end of the room, this also reduced the convective heat transfer between the ceiling and the air. Consequently, the heat contribution from ventilation was not doubled when the area of the room was doubled. When the room length was doubled, the temperature in the plenum varied more, and was increased by 3°C . This happened because the supply air spent more time travelling through the plenum and had more interaction with the ceiling.

In a paper from Chodor and Taradajko [2013], experiments are made with the dimensions $4.40 \times 6.00 \times 4.65 \text{ m}$. The results are compared to the results from Jakubowska [2007], with the dimensions of $2.5 \times 4.2 \times 3.6 \text{ m}$ corresponding to one-third of the volume. To compare the results, they made the area independent by dividing the airflow by the area.

The results indicated that the smaller room had a higher cooling capacity. The report linked this difference primarily to the height of the room, and only this parameter was further investigated. However, when comparing these findings to the results from Zhang et al. [2016], it appears that the change in width and length might also have influenced the difference in cooling capacity.

In most of the investigated cases, the room length is shorter than 6 m. A common finding across many of these studies is that DCV tends to perform well. This could be due to the low supply velocity or low-momentum airflow that ensures an even and stable air and temperature distribution. The low impulse from the ceiling reduces the risk of turbulence and draught.

It is generally recommended that the room length does not exceed 10 m. If the room is longer than 10 m, the air distribution through the diffuse ceiling can become uneven because the low-momentum airflow has difficulty covering the entire space evenly. This can lead to temperature and air speed variations in different areas of the room. [Zhang et al., 2017] Consequently, some areas may experience heat buildup, while cooling may be insufficient in others [Zhang et al., 2016].

In such cases, it is recommended, according to the design guide by Zhang et al. [2017], to include extra air intake in the plenum or to use perforated ducts to ensure a more uniform air distribution. Alternatively, diffuse ceiling panels with a higher pressure drop can be used to improve uniformity [Nocente et al., 2020].

Plenum height

Study by Kristensen and Jensen [2015] emphasises that air passage through the plenum contributes to a certain degree of preheating, which can enhance comfort during colder periods. Achieving uniform air distribution within the plenum requires proper sizing of inlet areas and carefully managing pressure drops across the ceiling.

The effect of the plenum height was investigated in a numerical study by Zhang et al. [2016]. Here, the heights were varied from 5 to 35 cm, and it was discovered that a lower plenum height could cause draught but was also beneficial for energy efficiency. The convective heat transfer between the ceiling and the air was increased because the supply air was forced to interact with the warmer ceiling with a high momentum flow. This further resulted in an increase of approximately 3°C in the room.

However, it was also discovered that the lower plenum resulted in a nonuniform air distribution. With more air getting supplied closer to the plenum inlet and the air delivery decreases further away from the plenum inlet. In the plenum with a lower height, it was also discovered that the air did not mix properly within the space. As a result, the cold outdoor air was supplied with minimal preheating near the plenum inlet, leading to the temperature difference in the plenum exceeding 30°C. Despite this, the temperature distribution within the room was uniform. However, the non-uniform air distribution within the plenum impacted the airflow behaviour in the room and OCZ. From the CFD simulation, it was clear that the plenum height of 5 cm resulted in the highest velocities reaching up to 0.3 m/s, which could lead to draught.

No other study has investigated such small plenum heights. The study by Nielsen and Jakubowska [2009] examine the lowest plenum height found in the literature, apart from the investigation made by Zhang et al. [2016]. Here, an experimental investigation was made in a room with a plenum height of 0.15 m. This study generally reported low air velocities and found no issues related to either velocity or temperature during the operation of the DCV system.

In the design guide by Zhang et al. [2017], a minimum plenum height of 20 cm is recommended to ensure even air distribution and minimise the risk of draught. Lower plenum heights restrict air mixing in the plenum, leading to uneven distribution through diffuse ceiling panels and increasing the risk of draught in the room. Higher plenum heights lower the cooling capacity but do not seem to affect other performance parameters.

5.2 Diffuse ceiling panels

In DCV, the air can have different paths through the suspended ceiling. It can either be through slots and/or perforations in the ceiling slab. The different airflow paths can be seen in Figure 5.2. [Zhang and Heiselberg, 2019; Zhang et al., 2016]

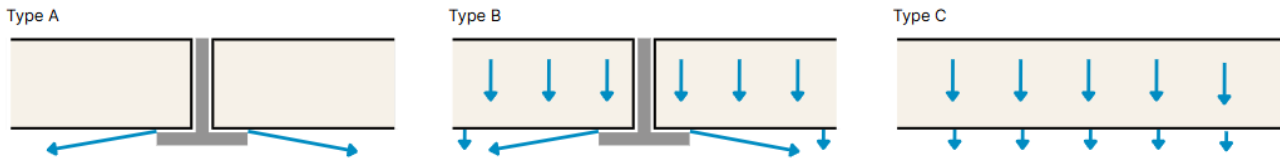


Figure 5.2. Types of airflow paths based on Zhang and Heiselberg [2019].

- Type A: The air is delivered through gaps between impenetrable ceiling panels.
- Type B: Perforated ceiling panels, where the air passes through both the panels and the gaps.
- Type C: Perforated ceiling panels, where air only passes through the panels.

In addition to the connections between panels and the perforation of the panels, the number of active panels and their placement are also parameters to take into account. This is investigated in the following sections.

Connection between the panels

The connections between the panels lead to crack flow, which refers to the unintended movement of air through small gaps or joints between ceiling panels, rather than through the designed porous surface. Crack flow is difficult to eliminate when the diffuse ceiling consists of multiple panels. This unintended leakage can alter the designed airflow distribution. In a study by Vilsbøll [2014], smoke experiments show how the air is supplied through the ceiling by passing through both panels and the t-profile joints, as shown in Figure 5.2 type B. In the study from Nielsen et al. [2010], the smoke experiment also conclude that air enters the room through narrow slots between the ceiling elements and their support structure. Smoke experiments indicate that microjets with high velocity and significant entrainment occur beneath the ceiling, extending up to 0.5 m into the room. Therefore, maintaining a minimum distance of 0.5 m between the occupied zone and the ceiling surface was recommended. From the various smoke experiments presented together with the smoke experiment presented in the study by Chodor and Taradajko [2013], the flow pattern in a room with DCV can be illustrated as seen in Figure 5.3.

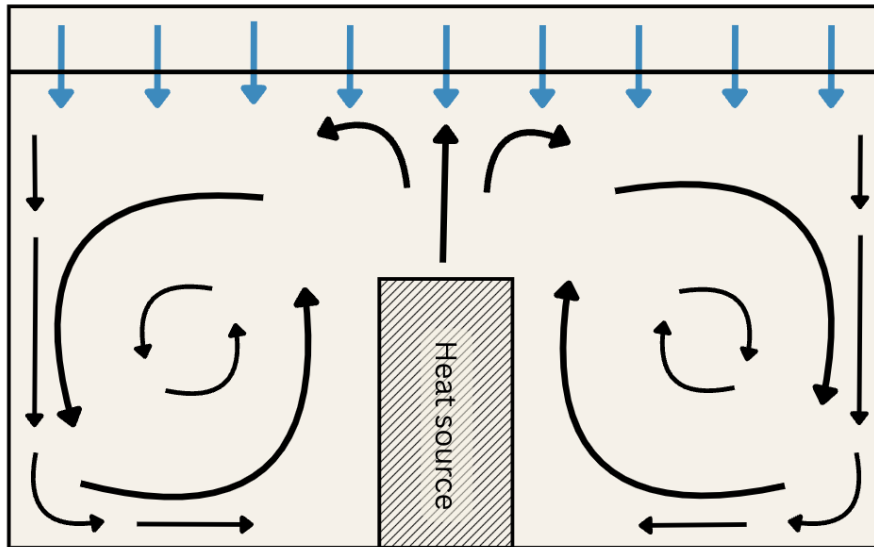


Figure 5.3. Flow in a room, based on smoke experiments.

In Figure 5.4, results from two studies have been compared. In the first study by [Jakubowska, 2007], the pressure drop through a mineral wool ceiling and a single panel of mineral wool is examined. It can be seen that the pressure loss through one single mineral wool panel is higher than through an entire mineral wool ceiling. This suggests that air bypasses the intended porous surface via joints between panels, supporting what was seen from the smoke experiments.

In a paper by Hviid and Svendsen [2012], gypsum tiles with an opening area of 17% (Gyp-17) and aluminium tiles with an opening area of 16.2% (Alu-16) were compared in an experimental setup resembling a classroom. A single panel and a whole ceiling were studied, and a crack flow of 64% was found for the gypsum ceiling and 17% for the aluminium ceiling.

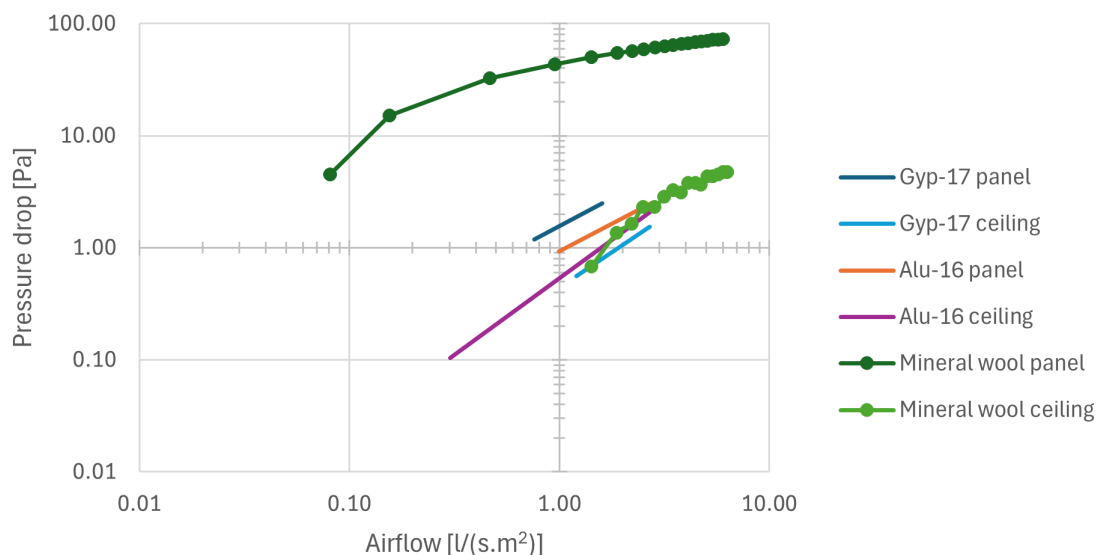


Figure 5.4. Pressure drop through different configurations [Zhang, 2016].

In Figure 5.4 it can be seen that the pressure drop across panel gaps is more than ten times lower than through the panels themselves, for the mineral wool panel. This leads to most airflow bypassing

the perforations and escaping through cracks.

The crackflow is very different between the three experiments. In a paper by Hviid and Svendsen [2012], thermovision pictures show that this difference could be due to the joints between panels. For the Gyp-17, these are placed on top of a reverse T-shaped joint, where the Alu-16 has an almost airtight connection. For the mineral wool, no information is found on the joint type. However, this one seems to be significantly less airtight.

The degree of resistance/permeability

Ceiling panels can be made from various materials, including perforated aluminium, gypsum, and mineral wool. These different materials have varying pressure resistances that affect the air distribution through the ceiling. In the study by Zhang et al. [2014], the pressure drop measurements from four different studies are compared. This comparison can be seen in Figure 5.5.

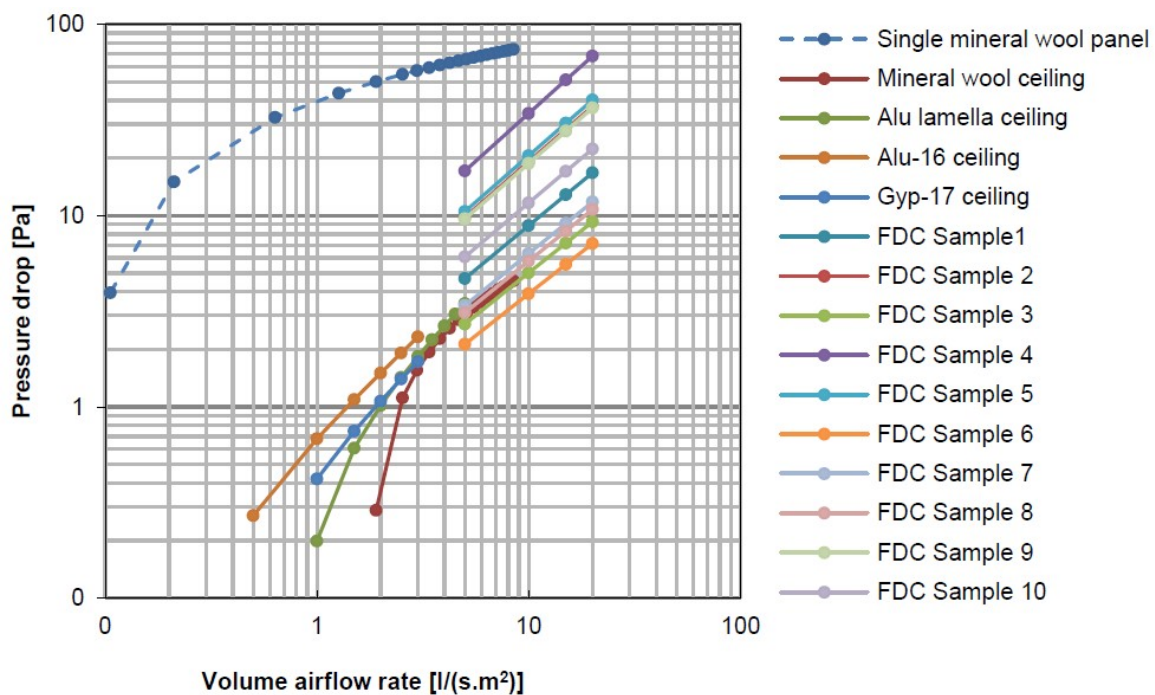


Figure 5.5. Pressure drop through different configurations [Zhang, 2016].

It is seen that the pressure drop through the different ceiling panels varies from 2 Pa to 20 Pa for airflow of 5 l/s per m² and from 7 Pa to 70 Pa for airflow of 20 l/s per m².

Compared to traditional ventilation types, this pressure drop can be 10 to 30 times lower than that observed in traditional mixing ventilation [Hviid and Svendsen, 2012; Jacobs and Knoll, 2008]. This significant reduction in pressure drop is one of the key factors contributing to the enhanced energy efficiency of DCV systems, particularly when integrated with natural ventilation.

Placement and number of active panels

Besides the air's path through the suspended ceiling, the number and placement of active panels significantly influence the cooling performance of DCV systems. An experimental study by Zhang et al. [2015] investigated the effect of varying the number of active panels in a classroom setup, comparing configurations with 100%, 50%, and 18% active panels. The results indicated that the system with 18% active panels handled the highest heat load. However, this effect was observed when the active panels were positioned directly above the heat sources. Therefore, the reason could be due to improved interaction between buoyant heat and cooler air. Similarly, Kozlowski et al. [2016] demonstrated that reducing the active panel area to 4.5% also enhanced cooling capacity compared to a 100% configuration.

In a study from Rahnama et al. [2019], an experimental study was conducted with active panels covering 100% and 2.4% of the ceiling. It was found that when heat sources were positioned on the opposite side of the 2.4% active panel configuration, cooling capacity remained higher than with 100% active panels. Yet, when the heat source was directly below the active panels, the increased air velocities indicated a lower capacity to maintain comfort. The study conducted a numerical analysis comparing compact and evenly distributed configurations, demonstrating that compact arrangements consistently provided better cooling performance, particularly at higher airflow rates. When heat loads were evenly distributed, compact panel placement also enhanced cooling. In contrast, positioning active panels directly above concentrated heat loads decreased cooling efficiency.

Another study by Sadeghian et al. [2022] explored three different room configurations an office, a meeting, and a waiting room. All room types have an active panel area of 30%, in both a centred and evenly distributed configuration. Centred placements proved most effective, particularly when occupants were seated along the walls, confirming that the centred panel configuration generally increases cooling efficiency.

The conclusions between the papers presented are not in total agreement. In general, DCV can handle the highest heat load if it is evenly distributed in the room. Most papers find an improvement in the cooling capacity if not the whole ceiling is used as an inlet, but the active panels are still placed together and not dispersed in the ceiling. More papers suggest that the better placement of the active panels is not just above the heat load but rather displaced from these. Studies consistently show that a smaller active panel area generally improves cooling efficiency, especially when panels are compactly arranged. However, the placement of heat sources relative to these active panels also plays a crucial role.

5.3 Heat sources

Based on the analysis above, it was found that heat sources affect many of the other design parameters while playing a crucial role in air mixing within a room. Due to the thermal buoyancy created by occupants, warm air rises and interacts with the cooler, fresh air supplied by the ventilation system [Zhang et al., 2015]. This buoyant movement generates natural convection currents, promoting effective air mixing throughout the space. The strength of this mixing process depends on factors such as the number of heat sources and their intensity, all of which impact the volume and temperature gradient of the rising air. Many of the studies which investigated the influence of active panels also examined the effect of the heat source placement. Generally, three types of heat source placement are used. In office rooms, either centred or one-sided heat sources are present, while classrooms may also feature evenly distributed heat sources. These three types of heat source distributions can be seen in Figure 5.6.

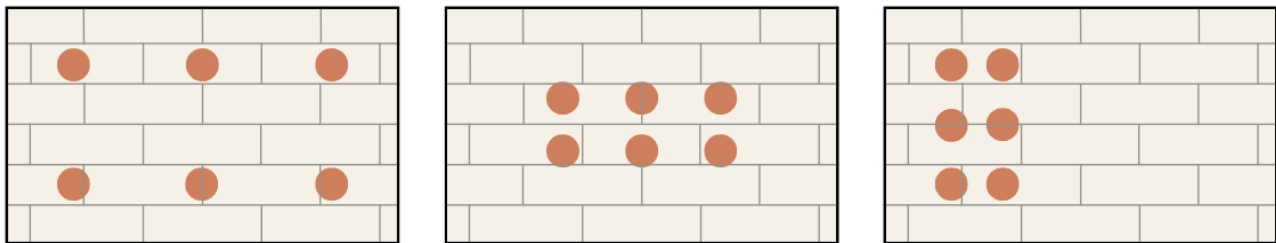


Figure 5.6. Different heat source placements.

In Zhang et al. [2015], various heat source placements are compared. Additionally, the one-sided heat source placement is tested on both the front and back sides of the room. It has been observed that evenly distributed heat sources do not cause air recirculation. In contrast, when the heat load is centred, air recirculation occurs on each side of the heat source. However, these recirculation patterns are not symmetrical. In cases where the heat load is located on one side of the room, one air recirculation occurs in the opposite direction of the heat sources. However, the recirculation differs when the heat sources are placed at the front and back of the room. Figure 5.7 shows the DR plotted against the distance from the inlet for the various heat distributions.

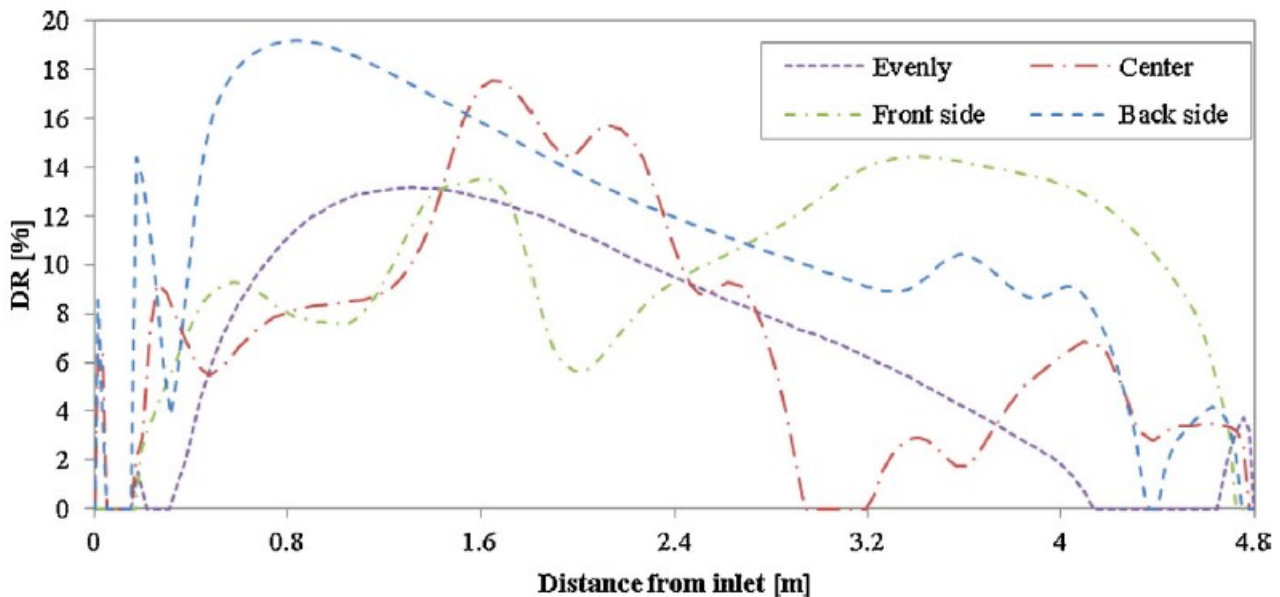


Figure 5.7. Draught risk vs. heat load locations. [Zhang, 2016]

It is concluded that an even distribution of heat sources results in the lowest DR. The difference in the results between front and back side placement indicates that the air is not evenly distributed throughout the plenum, and it seems like a larger amount of air is supplied in the front of the room. It is also seen that the highest DR is observed when the heat sources are placed on the back side of the room.

In the studies by Vilsbøll [2014] and Nielsen et al. [2015], the heat sources were arranged in three different ways, similar to the approach in Zhang et al. [2015], using an evenly distributed, centred, and one-sided distribution in their numerical analysis. The results showed that the evenly distributed heat load provided the highest cooling capacity.

The study by Rahnama et al. [2019] experimentally investigates the placement of the heat source concerning the active panels' area of 2.4%, as previously mentioned. Additionally, the impact of evenly distributed versus compact heat sources in a room with 100% active panels is examined. The findings concluded that the system can remove more heat when the heat load is evenly distributed throughout the room.

In a study by Chodor and Taradajko [2013], both the type and placement of heat sources were varied. The results showed that evenly distributed heat loads could result in both the highest and lowest cooling capacities, indicating that the vertical placement of the heat source also influenced system performance. Generally, it was observed that the higher the heat sources were positioned, the better the cooling capacity of the system.

Studies indicate that a well-distributed heat load leads to more stable airflow and improved thermal comfort. In contrast, concentrated heat sources can cause unstable airflow and uneven temperature distribution, increasing the risk of draught and localised overheating. Therefore, to reduce the risk of draught, heat sources should be evenly distributed within the room.

The vertical placement of heat sources plays a crucial role in air circulation within a space. Heat

sources located at higher positions, such as ceiling-mounted lights, can enhance buoyancy effects, stabilising airflow and leading to more consistent thermal comfort.

5.4 Inlet properties

The plenum inlet configuration has an impact on the air distribution in both the plenum and the occupied zone. The study by Zhang et al. [2016] presents a numerical analysis to examine the impact of different inlet configurations. The investigation includes a slot opening positioned just above the diffuse ceiling and a square opening located in the corner of the room. The paper analyses both temperature and velocity. A more significant temperature variation of the air was observed when the square inlet was used.

The design guide by Zhang et al. [2017] further analyses the plenum inlet, comparing a single air jet inlet with an inlet with vanes. These two types of inlets can be seen in Figure 5.8. In the vane inlet configuration, the air is divided into two jets before entering the plenum. The study shows that the inlet with vanes results in a more even air temperature distribution within the plenum. The results showed that the lowest temperature does not necessarily occur near the plenum inlet. It was concluded that the inlet location and configuration significantly influence the airflow pattern within the plenum and affect the variation of air temperature throughout the plenum.

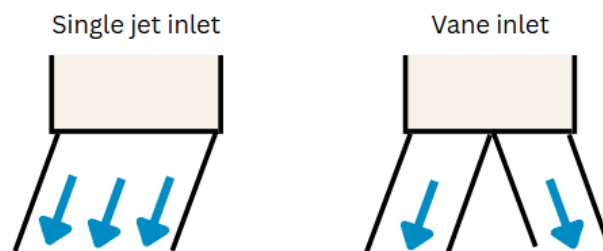


Figure 5.8. Principle of vane inlet [Zhang et al., 2017].

The paper suggests that uniform air distribution could be achieved by positioning the inlets on different edges of the plenum. However, this approach has not been investigated. Implementing such a configuration would likely require dampers in the plenum ductwork to balance the distribution, leading to additional investment in dampers and the need for electricity to operate the system.

5.5 Exhaust properties

For DCV, some studies have investigated the exhaust's effect on the system. In the paper by Nielsen et al. [2010], a movable exhaust opening is tested. This is done in an experimental setup where performance is analysed using a smoke experiment. The experiments with different exhaust placement locations indicate that the location is of minor importance to the air distribution pattern in the room.

In a study by Peng et al. [2021], three different exhaust placements are investigated, as illustrated in Figure 5.9. Two exhausts are positioned at the bottom of the room, one in the corner and the other in the middle of the wall, 0.25 m above the floor. The third exhaust is located at the top, centred 0.25 m below the suspended ceiling. The experimental results indicate that the top exhaust position can more efficiently remove contaminants, likely due to the airflow generated by the manikins and their heat release. Additionally, the results show that CO₂ is removed more rapidly when the exhaust is positioned at the top of the wall.

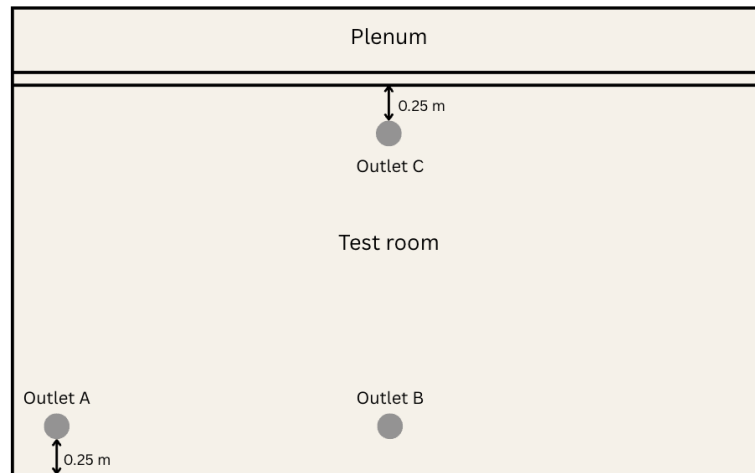


Figure 5.9. Exhaust positions in paper by Peng et al. [2021].

A similar study by Petersen et al. [2014] investigated two different exhaust configurations, both located on the wall next to the door. One exhaust was positioned just below the suspended ceiling, while the other was placed just above the floor. The exhaust configurations featured similar round duct openings. The experiment showed that placing the exhaust at the ceiling improved air change efficiency, while the local mean age of the air was higher when the exhaust was positioned at floor level. The exhaust placement also influenced the room temperature, resulting in slightly higher temperatures when the exhaust was located at floor level, while the vertical temperature difference pattern remained consistent.

The study by Peng et al. [2023] investigates three different exhaust positions, with two located in the centre of the facade wall, similar to the configuration described in Petersen et al. [2014], and one positioned at the lower centre of the opposite wall. A comparison of the lower exhaust positions on the two opposite walls shows minimal effect. However, consistent with findings from other studies, the vertical placement of the exhaust significantly influences performance. The study concludes that exhaust positioning has a greater impact on temperature effectiveness than on CRE, with this effect being more pronounced in heating scenarios. As a result, the study recommends a lower exhaust placement for both heating and cooling applications, which contrasts with the findings of Petersen et al. [2014], where a higher location is suggested to ensure effective contaminant removal.

The study by Nocente et al. [2020] conducted a numerical investigation using CFD simulations to examine different exhaust configurations. The first configuration models the exhaust as a square duct of 0.3 x 0.3 m located in the bottom corner next to the inlet wall. The second configuration uses a slot exhaust, with a height of 0.05 m and a width of 3.6 m, positioned at the bottom of the wall opposite to

the inlet wall. The analysis of the flow patterns revealed that the slot exhaust configuration produced a more uniform flow, with streamlines primarily perpendicular to the ceiling plane. In contrast, the square duct configuration generated vortices within the room.

The study concluded that the exhaust configuration has a greater impact on the system's pressure drop compared to the ceiling configuration. The slot exhaust maintained velocities throughout the room below the discomfort threshold, while the square duct configuration resulted in localised velocities exceeding 0.1 m/s near the exhaust.

The various studies indicate that the exhaust position significantly impacts ventilation performance in different systems. In systems with internal heat sources, higher exhaust positions are more effective for CO₂ removal due to buoyancy-driven airflow, whereas lower exhaust positions perform better when heat sources are absent. Overall, exhaust properties play a crucial role in air distribution and indoor air quality within DCV setups.

5.6 Heating or cooling case

The performance of a DCV system has been investigated for both heating and cooling configurations. In general, cooling cases are well documented and analysed through several studies. Heating configurations have not been studied as much, but some studies show different thermal behaviours in such setups. In the study by Nielsen et al. [2010], one cooling experiment and two different heating experiments are conducted. The results obtained from the experiments show a difference in how the DCV setup performs based on the situation. For heating cases, it is recommended to use a convector or floor heating to ensure sufficient operation.

Study by Peng et al. [2021] presents an experimental study which investigates the performance of a DCV setup in a heating configuration. In a heating setup, the buoyancy effect is opposite to the warm supply air and affects the heating performance of DCV. In heating cases, the setup is more dependent on heat sources in the room to ensure sufficient mixing of the air. This is not as crucial in a cooling scenario. This result fits with the findings from the study by Nielsen et al. [2010], where heat is needed to ensure sufficient operation, thereby making the implementation of floor heating necessary. As described by Peng et al. [2021], who analyses the exhaust positions in the two configurations. Here, it is found that using high-located exhausts in a heating situation can result in a short-circuit where the warm air is removed before it heats the OCZ.

Assessment of design charts 6

The previous chapters have highlighted the complex interplay between the many parameters that influence the performance of DCV. Because these factors are closely connected, describing the system's behaviour using dimensionless numbers alone becomes challenging. While tools like the Ar and Re numbers provide useful insights into flow regimes, they do not capture the nuanced performance of DCV across a wide range of conditions. A deeper understanding of how individual parameters affect system performance under different scenarios is needed to ensure sufficient design guidelines. This chapter examines existing design charts based on experimental data to explore key design parameters. By analysing variations in factors such as heat load distribution, room geometry, and other relevant design parameters, this chapter lays the foundation for a set of design charts that will help form the basis of the DCV configuration tool.

6.1 Existing design charts and graphs

The design chart illustrates the acceptable combinations of airflow rate and temperature difference, defining a zone that maintains good air quality, limits draught, and preserves comfortable vertical temperature gradients. Here, a higher temperature difference and airflow indicate a higher cooling capacity, without compromising the thermal comfort in the room.

Multiple papers have made design charts based on experimental data. These are presented in Table 6.1, where each paper has been assigned a letter, which is later used for reference in the figures. These studies investigate different parameters, and the design charts are a reflection of this.

Table 6.1. Names of the graphs and the corresponding papers.

Name	Paper	Investigation	Graph type
A	[Chodor and Taradajko, 2013]	Heat load placement and room height	Design graph
B	[Vilsbøll, 2014]	Heat load placement and room height	Design graph
C	[Rahnama et al., 2019]	Active panels amount	Design graph
D	[Kozłowski et al., 2016]	Active panels amount	Design chart
E	[Zhang, 2016]	Heat load placement and room height	Design chart

The table also indicates whether each study includes a design chart or only a design graph, clarifying which data can be used for direct comparison and which are limited to visual analysis. The design charts will be the foundation for the calculations in the configuration tool.

Investigation of heat load placement

The following graphs are a combination of the papers by Chodor and Taradajko [2013], Vilsbøll [2014] and Zhang [2016]. The design graphs in Figure 6.1 show a clear pattern when it comes to how the placement of heat loads affects DCV.

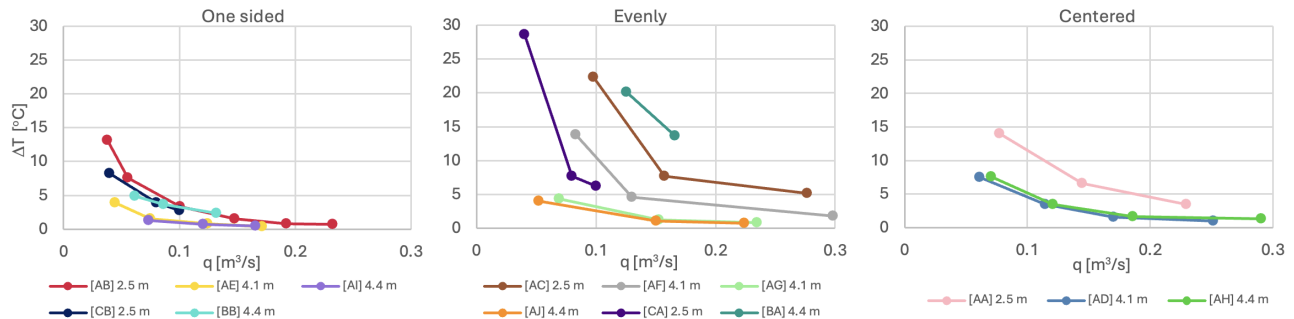


Figure 6.1. Design graphs with the different placement of heat sources in the room.

When heat loads are placed on one side of the room, the temperature differences are generally lower than in the other configurations. This indicates that less heat can be removed from the room while still complying with the thermal limits from International Standard [2006], resulting in a lower cooling capacity. However, this configuration tends to generate a more stable airflow, as seen in the graphs, which appear more concentrated, in contrast to the more scattered graphs observed for the evenly and centrally placed heat loads configurations. From Chapter 4, it was also seen that the one-sided heat load configuration tends to create a more predictable airflow pattern due to the concentration of the source. However, this can limit air mixing across the room, which may reduce the overall cooling effectiveness.

The evenly distributed heat load configuration delivers the highest cooling capacity among the three distributions. These results align with what was found in Section 5.3, where it was shown that evenly distributed heat sources promote more uniform interaction between supply and room air. However, this setup can lead to more uneven velocities due to multiple thermal plumes interacting across the room.

The centred configuration falls between the first two. Section 5.3 notes that centred heat loads can lead to symmetrical recirculation zones, which may improve airflow uniformity. However, this configuration does not achieve the same level of cooling capacity as the evenly distributed layout and may be less effective when dealing with high-intensity internal loads.

The results presented in the design graphs are in agreement with the findings from the previous chapters. The placement of heat loads has a direct influence on airflow structure, thermal stratification, and overall cooling capacity. These results reinforce the importance of considering internal load configuration when designing or evaluating DCV systems.

Investigation of room height

To examine if the room height has any impact on cooling efficiency, the same graphs from heat load distribution are sorted by different room heights. This can be seen in Figure 6.2, which compares data for room heights of 2.5, 4.1, and 4.4 m. In the figure, the distribution of heat load is also indicated by the different geometries. The circle indicates an evenly distributed heat load configuration, and a triangle and square indicate, respectively, a one-sided and centred heat load placement.

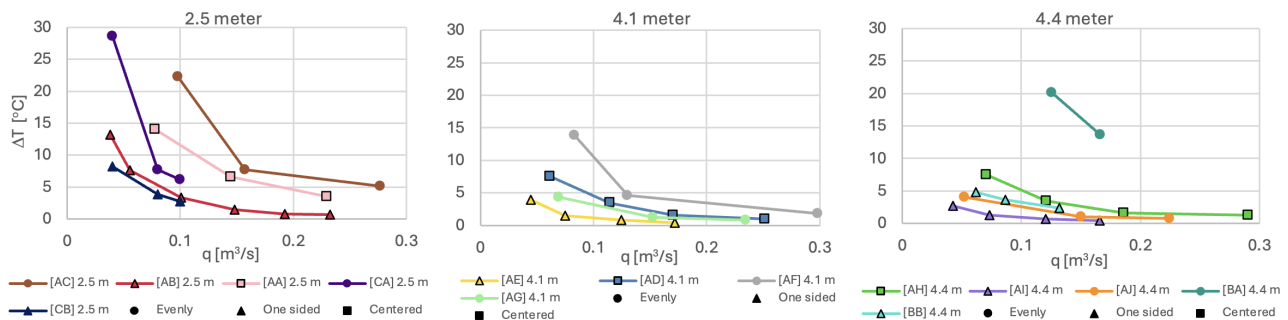


Figure 6.2. Design graphs with different room heights.

The graphs show that at a ceiling height of 2.5 m, the temperature differences and airflow rate are higher, which displaces the graph diagonally upwards. This suggests a higher cooling capacity in rooms with a lower ceiling height. This observation aligns with the findings in Section 5.1, which found that lower ceiling heights improve cooling efficiency by reducing the supply air's travel distance to OCZ, thereby minimising momentum loss.

In contrast, the graphs have a lower placement for the ceiling heights of 4.1 and 4.4 m, which indicates a reduced cooling capacity. As explained in Section 5.1, this is due to the longer distance the supply air must travel, which causes a loss of momentum before reaching OCZ. Studies such as Nielsen et al. [2015] show that taller rooms tend to have higher velocities and more recirculation, increasing draught risk. This supports the design chart findings, where taller ceilings result in lower temperature differences, even when airflow rates are higher.

These observations support the conclusion from Section 5.1, where it was suggested that ceiling heights above 3 meters are less suitable for DCV. In contrast, lower ceilings around 2.5 m improve cooling performance and airflow, highlighting ceiling height as a critical factor in DCV design.

Investigation of active panels

The influence of the area of active panels is examined in studies by Kozłowski et al. [2016] and Zhang [2016]. The design charts presented in Figure 6.3 combine experimental results from these studies and illustrate the effect of different perforation ratios.

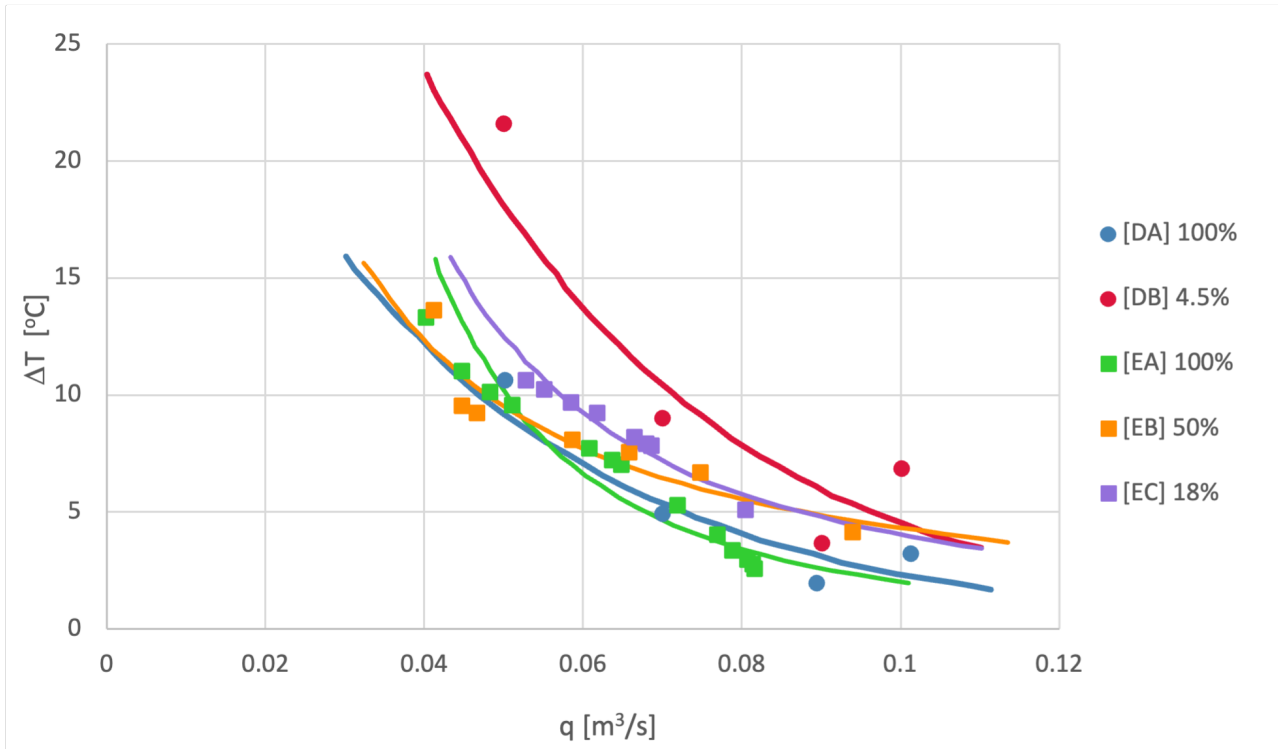


Figure 6.3. Design chart for diffuse ceiling ventilation with different opening area.

The data show that a smaller area of active panels results in a higher cooling capacity. This is because the supply air is delivered more directly and with greater intensity in specific zones, improving the interaction between the cooler supply air and the warmer room air.

These findings align with the results presented in Section 5.3, where smaller active areas, when compactly arranged and properly positioned in relation to the heat sources, were shown to improve the performance of DCV systems. In some cases, panel areas as small as 4.5% or even 2.4% outperformed fully perforated ceilings, not just due to reduced area, but due to better interaction with thermal plumes.

The results highlight the importance of selecting not only an appropriate panel size, but also a strategic placement relative to heat sources. Optimising both factors can significantly enhance cooling efficiency and thermal comfort in DCV system design.

Conclusion of literature review 7

Based on the conducted literature review and the initial analysis of key design and performance parameters for DCV, it is evident that multiple factors influence the system's performance. The reviewed studies highlight how geometry, plenum height, ceiling panel configuration, heat source distribution and intensity, as well as inlet and exhaust positioning, all play a role in ensuring comfort in a room. However, results vary across the studies, likely due to differences in BC such as room size, heat load, and panel layout. The investigation of dimensionless numbers, particularly the Ar and Re numbers, revealed no clear universal trends across systems, suggesting that DCV performance is highly scenario-specific. Therefore, dimensionless numbers were found to be unsuitable for evaluating DCV performance in a general sense. As a result, design charts were an alternative approach to support system evaluation and design. This approach is consistent with the rest of the literature review and provides a good representation of the interaction between different parameters.

Concerning temperature gradients, the findings indicate that DCV maintains acceptable thermal comfort conditions. Under such conditions, the vertical temperature gradient does not appear to be a limiting factor. In contrast, high air velocities and the associated risk of draught have been observed under certain configurations, especially in rooms with large ceiling heights or low plenums, emphasising the sensitivity of airflow behaviour to specific design conditions.

A key takeaway is that several aspects remain insufficiently addressed in the existing literature. These include the performance of DCV in heating scenarios, the effect of varying active panel patterns, and the interplay between heat load placement and ceiling configuration. Due to the extensive range of variables and the interactions between them, it is challenging to develop a standardised design guide, which may limit the broader adoption of DCV. Therefore, it is important to evaluate each parameter independently and its interactions with other parameters. This approach will be implemented in this thesis through CFD simulations. However, given time constraints, only a limited selection of parameters will be examined. The selection of CFD cases is aimed at fulfilling some knowledge gaps. The aim is to build a more robust and data-driven foundation for the configuration tool.

Part II

Numerical investigations

This section presents the numerical study, including the development and selection of CFD cases. These cases are selected based on the preliminary investigations from Part I. Design charts are developed based on the results from the CFD simulations. The outline for the configuration tool is presented, and further work on this tool is suggested.

Chapter 8 Numerical analysis	52
8.1 Selection of cases based on literature review	52
8.2 Heat load intensity analysis	53
8.2.1 Results	56
8.3 Geometry analysis	60
8.4 Setup	62
8.4.1 Results from one-sided heat load distribution	63
8.4.2 Results from increase in room height	66
8.5 Overall conclusion	72
Chapter 9 Design charts from numerical analysis	73
9.1 Evaluation of heat load intensity	73
9.2 Evaluation heat loads distribution	75
9.3 Evaluation of room geometry	76
Chapter 10 Configuration tool outline	77

Numerical analysis 8

The purpose of this chapter is to investigate some of the gaps found in the literature review. This is done with CFD simulations. The analysis consists of two parts, with the first investigating the effect of different heat load intensities. In this part, an already validated CFD model is used. The other investigation focused on different room geometries. For this analysis, new models are constructed. The CFD simulations will thereby provide some data which are needed to develop design charts for the configuration tool.

8.1 Selection of cases based on literature review

The literature review showed that a DCV system cannot be fully described using dimensionless numbers, as most design parameters influence the system. Design charts were proposed as a way to describe system performance, but this approach requires extensive data.

The analysis focuses on heat load intensity and room geometry, including heat load placement, each investigated individually. An overview of all simulated cases is provided in Table 8.1. Only cooling cases are taken into account, and the room temperature is aimed to be 23°C.

Table 8.1. CFD cases with BC.

Case	ACH [h ⁻¹]	Inlet velocity [m/s]	ΔT [K]	Inlet temp [°C]	Heat load [W]	Placement [-]	Geometry (HxLxW) [m]
Heat load intensity analysis							
1	4.8	0.62	3.36	19.64	200	Centered	2.335 x 4.8 x 3.3
2	6	0.78	2.69	20.31	200	Centered	2.335 x 4.8 x 3.3
3	10	1.30	1.61	21.39	200	Centered	2.335 x 4.8 x 3.3
4	4.8	0.62	7.23	15.77	430	Centered	2.335 x 4.8 x 3.3
5	6	0.78	5.78	17.22	430	Centered	2.335 x 4.8 x 3.3
6	10	1.30	3.47	19.53	430	Centered	2.335 x 4.8 x 3.3
7	4.8	0.62	17.15	5.85	1,020	Centered	2.335 x 4.8 x 3.3
8	6	0.78	13.72	9.28	1,020	Centered	2.335 x 4.8 x 3.3
9	10	1.30	8.23	14.77	1,020	Centered	2.335 x 4.8 x 3.3
10	4.8	0.62	24.04	-1.04	1,430	Centered	2.335 x 4.8 x 3.3
11	6	0.78	19.24	3.76	1,430	Centered	2.335 x 4.8 x 3.3
12	10	1.30	11.54	11.46	1,430	Centered	2.335 x 4.8 x 3.3
Geometry analysis							
13	4.8	0.62	7.23	15.77	430	One side	2.335 x 4.8 x 3.3
14	6	0.78	5.78	17.22	430	One side	2.335 x 4.8 x 3.3
15	10	1.30	3.47	19.53	430	One side	2.335 x 4.8 x 3.3
16	4.8	1.24	3.14	19.86	430	Centered	5.385 x 4.8 x 3.3
17	6	1.55	2.51	20.49	430	Centered	5.385 x 4.8 x 3.3
18	10	2.58	1.50	21.50	430	Centered	5.385 x 4.8 x 3.3
19	4.8	1.25	7.23	15.77	860	Centered	2.335 x 9.6 x 3.3
20	6	1.56	5.78	17.22	860	Centered	2.335 x 9.6 x 3.3
21	10	2.60	3.47	19.53	860	Centered	2.335 x 9.6 x 3.3

The geometry is kept mostly identical across all cases, with only a single dimension varying between each set of simulations. Each set consists of three simulations where the inlet velocity and temperature have been changed. The name of each case will consist of the ACH, ΔT and heat load. The name of case 1 will therefore be [1] 4.8 h⁻¹ 3.4°C 200 W.

8.2 Heat load intensity analysis

For cases 1 to 12, where the heat load intensity is investigated, the model is kept the same for all the simulations. Different heat load configurations are tested, where cases 1-3 contain people load, 4-6 people and equipment load. Case 7-12 is simulated with a solar heat gain. Thereby, only the heat load configuration and intensity are changed in this investigation.

Model layout

The model used for this investigation is called Model 1 and is the validated model from Zhang et al. [2016]. The model has the same dimensions as the "hot box" at the BUILD Institute at Aalborg University, and resembles a two-person office room with two manikins, a table with two computers and two work lamps. Every element is constructed as a square to simplify the geometry and make the mesh generation easier. This model is found in Figure 8.1

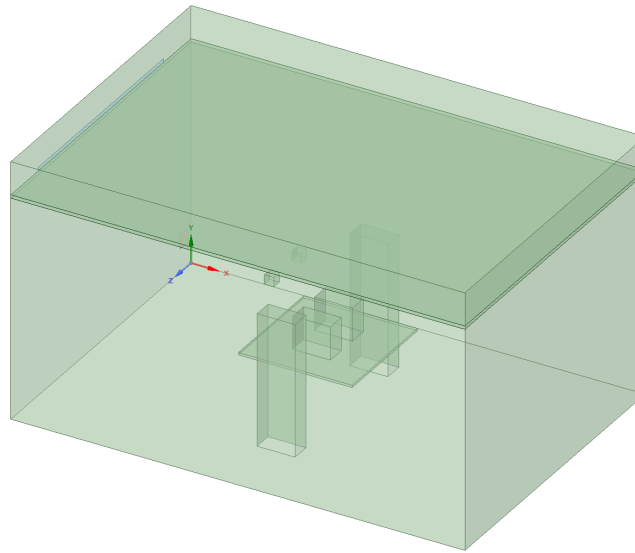


Figure 8.1. Geometry of model 1.

The simulation is conducted as a transient model. The reasoning behind this choice, along with details on the selected turbulence model and wall treatment, is provided in Appendix E. The turbulence model used is the standard $k-\epsilon$ model with non-equilibrium wall treatment.

Boundary conditions

The heat load analysis focuses on investigating different scenarios with varying heat sources. The heat sources used are occupants, equipment, and solar heat. The different combinations of these are presented in Table 8.2.

Table 8.2. Overview of cases in heat load investigation.

Case	Inlet velocity [m/s]	Inlet temperature [°C]	Heat Load [W]		
			Occupants	Equipment	Solar
[1] 4.8h ⁻¹ 3.7°C 200 W	0.62	19.64	100		
[2] 6h ⁻¹ 3.0°C 200 W	0.78	20.31	100		
[3] 10h ⁻¹ 1.8°C 200 W	1.30	21.39	100		
[4] 4.8h ⁻¹ 8.3°C 430 W	0.62	15.77	100	115	
[5] 6h ⁻¹ 6.7°C 430 W	0.78	17.22	100	115	
[6] 10h ⁻¹ 4.0°C 430 W	1.30	19.53	100	115	
[7] 4.8h ⁻¹ 19.7°C 1,020 W	0.62	5.85	100	60	700
[8] 6h ⁻¹ 15.8°C 1,020 W	0.78	9.28	100	60	700
[9] 10h ⁻¹ 9.5°C 1,020 W	1.30	14.77	100	60	700
[10] 4.8h ⁻¹ 27.5°C 1,430 W	0.62	-1.04	100	115	1,000
[11] 6h ⁻¹ 22.1°C 1,430 W	0.78	3.76	100	115	1,000
[12] 10h ⁻¹ 13.2°C 1,430 W	1.30	11.46	100	115	1,000

The heat load for occupants and equipment is based on values from Vorre et al. [2017]. The total heat load is divided into a convection and radiation part according to values found in ASHRAE [2016]. The solar heat values are derived from By og Byg [2002] and distributed based on manufacturer data from Pilkington [2025]. In Table 8.3, the calculation of the convective part of the heat load used in cases 10-12 can be found.

Table 8.3. Heat load distribution for cases 10-12.

	Heat load [W]	Convection [%]	Convection [W]	Surface area [m ²]	Heat flux [W/m ²]
Lamps	15	0.54	8.1	0.12	67.50
Occupants	100	0.40	40	1.92	20.83
PC's	100	0.90	90	0.50	180.00
Window (Abs.)	1,000	0.15	150	3.22	46.58
Carpet (Trans.)		0.67	670	2.64	253.79

The convective part of the heat load is applied directly to the heat source in the model, while the radiative part is distributed across the surfaces inside the room, excluding the ceiling. The heat flux value applied to the room surfaces can be found in Table 8.4.

Table 8.4. Heat flux on room surfaces.

Case	Surface heat flux [W/m ²]
1-3	2.24
4-6	2.87
7-9	5.47
10-12	6.98

Measurement positions in the room

To measure the temperature and velocity in the room, four different vertical lines are plotted. These lines make it possible to monitor the temperature and velocity at four different places in the room. The placement of the four measurement lines can be seen in Figure 8.2. To get an understanding of the flow direction and magnitude within the room, two planes are also examined. The first plane intersects the table positioned at the centre of the room, providing an overview of the overall airflow within the room. The second plane intersects the manikin, making it possible to analyse the thermal plume generated by the manikin. The two planes are shown in Figure 8.3.

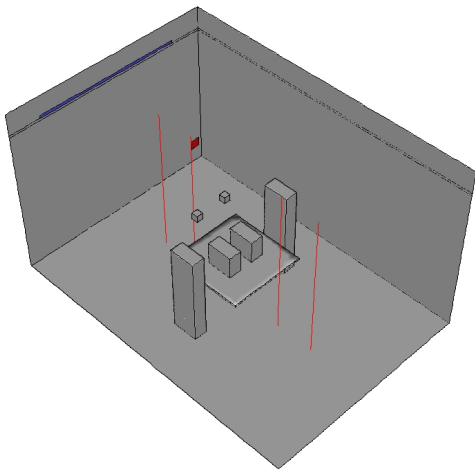


Figure 8.2. Placement of the measurement line, marked in red. The inlet and exhaust are located on the left.

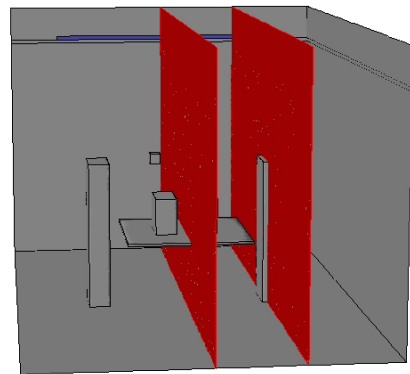


Figure 8.3. Placement of the section plane, marked in red. The inlet is located at the rear of the room.

These lines and planes should provide a comprehensive overview of the airflow in the room, which can be analysed based on the results.

8.2.1 Results

CFD analyses can produce a large amount of results and data. In this section, the most relevant results for understanding the airflow patterns in the room are analysed. These results include sections of the room displaying temperature and velocity results, and velocity path lines.

Temperature

The temperature distribution is compared between four cases. These cases have the same airflow rate but varying heat load and inlet temperature. The inlet temperature is calculated based on the heat load, ensuring the system theoretically has the right cooling capacity. The ACH is maintained at 6 h^{-1} throughout all cases. The analysis is conducted in the two presented section planes, and the

results can be seen in Figure 8.5. The results for the other cases can be seen in Appendix F. The focus is on the temperature distribution inside the room, and the plenum is not included in these pictures. The entire room and the results from the remaining simulations can be found in Appendix F.

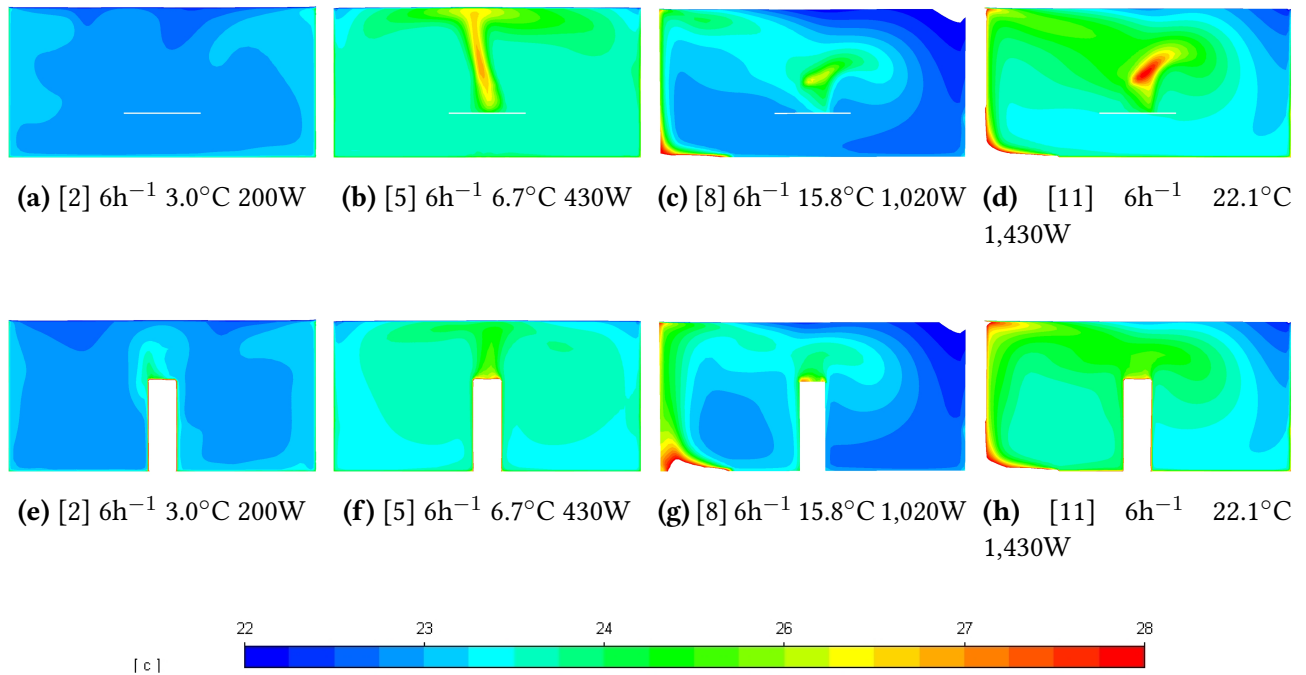


Figure 8.5. Temperature section. Top row: middle of the room. Bottom row: through the occupant.

From the figures, it is evident that the heat load is not very prominent in case 2, where only the occupants are present. In this case, warmer temperatures are also observed at the walls compared to the open space beside the occupant. In case 5, the plume from the heat sources is undisturbed and has the classical shape known from other literature. In cases 8 and 11, where the solar heat is added, the plume from the occupants and equipment gets disturbed by the airflow. To look further into this, the velocity and streamlines in the room are examined.

Velocity

The velocity is examined in the same way as the temperature, and based on the same cases and evaluation in the same two planes. For the other cases, the velocity sections can be seen in Appendix G.

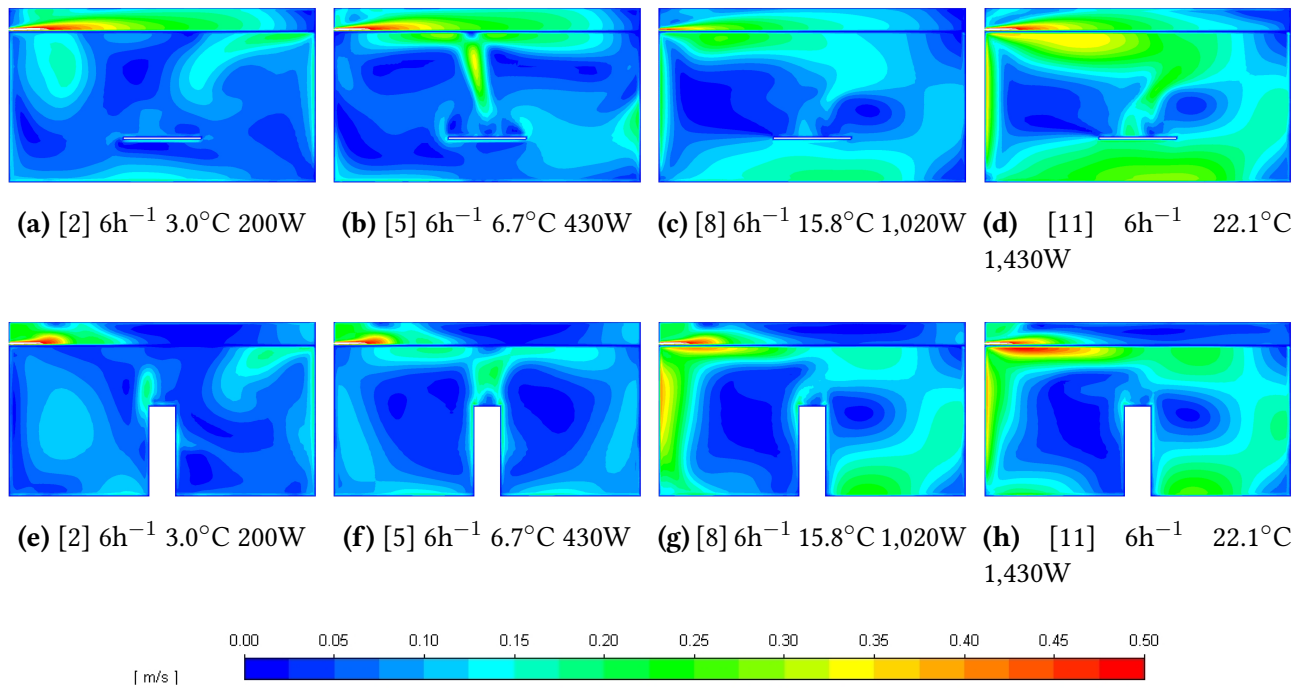


Figure 8.7. Velocity sections. Top row: middle of the room. Bottom row: through the occupant.

As seen in other literature, the velocities are higher near the edges of the room, this is especially seen in cases 8 and 11, where high velocities at floor level and near the wall are observed. This might be due to the increased heat load and higher surface temperatures. The facade with the window experiences high velocities in this region, which might be due to solar radiation. It is clear that this affects the movement of the air in the room. This can be further investigated by looking at the air's path lines in the room.

Pathlines

The path lines indicate the velocity and the direction of the movement of air. The focus has been on the plane through the occupant. The pathlines for all cases can be found in Appendix H. In Figure 8.8, the pathlines for case 2 are seen and in Figure 8.9, the pathlines for case 8 are seen. The limits are set from 0 to 0.5 m/s to get a wider range of colours on the arrows inside the room. In return, some of the arrows at the inlet are missing, since the inlet has a velocity of around 0.7 m/s.

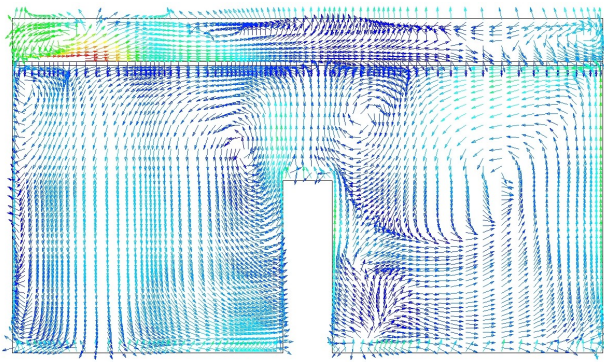


Figure 8.8. Path lines, [2] 6h^{-1} 3.0°C 200W.

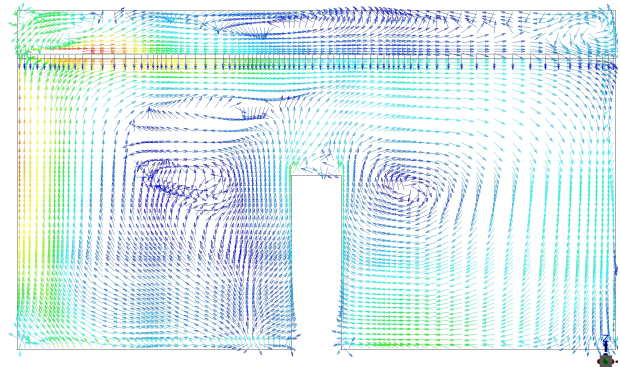


Figure 8.9. Path lines, [8] 6h^{-1} 15.8°C 1,020W.



From Figure 8.9, it can be seen that the air forms vortices on each side of the occupant, this is also the case for the other heat loads, except for the cases with the lowest heat load. The pathlines for this case can be seen in Figure 8.8, where it is the vortices are not as clear. It could seem like there is not enough buoyancy force to ensure mixing of the whole room, which could also be the reason for the warmer temperature at the walls observed on Figure 8.4e. In case 8, where solar radiation is included, the air is more turbulent and unpredictable, especially on the left side, where the solar radiation is inputted.

The path lines through the ceiling are also investigated. These can be found in Figure 8.10.

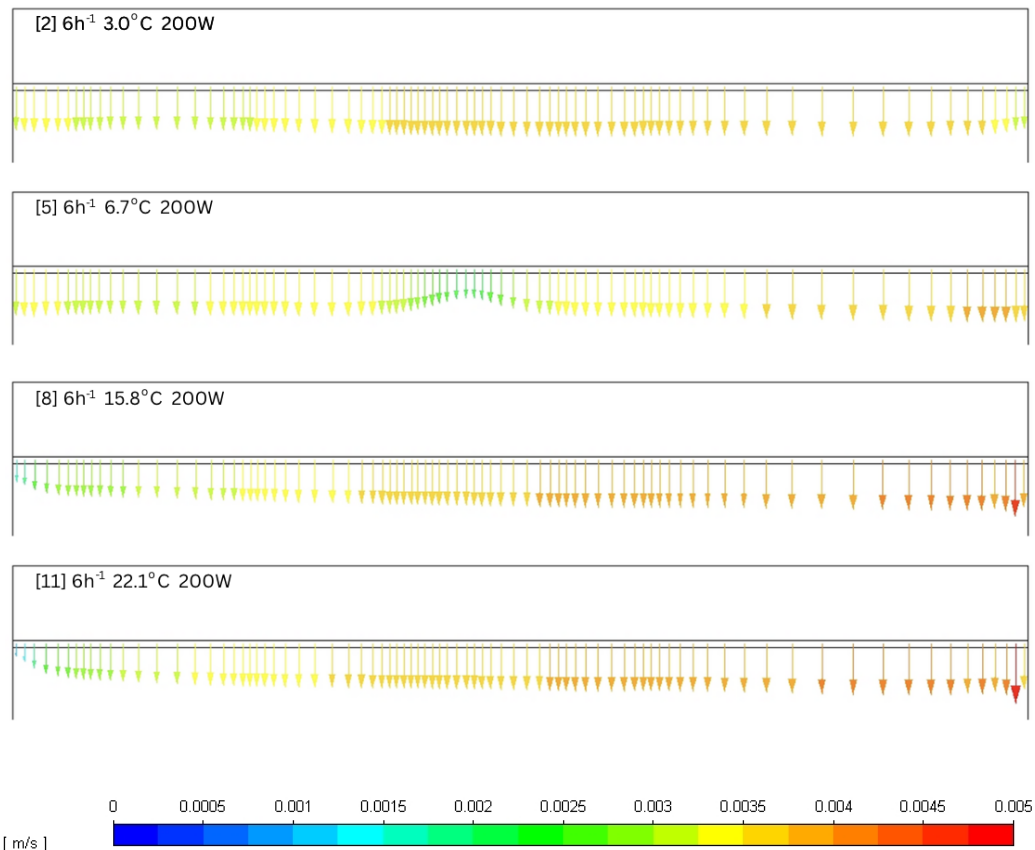


Figure 8.10. Air through ceiling panels in cases 2, 5, 8 and 11.

The velocities are generally low, and the air appears to be evenly distributed across most of the ceiling surface. In Case 5, however, a local dent in the airflow is observed above the occupant. This is caused by the thermal buoyancy from internal heat sources, which generates an upward plume. The resulting counteracting airflow disrupts the ceiling flow locally. Despite this disturbance, no reverse flow is observed in any of the cases.

Based on the pathline illustrations, Cases 8 and 11 show increased velocities toward the end of the room. This may be attributed to solar gains from the floor and wall surfaces, which accelerate the airflow. As seen in Figure 8.9, the streamlines indicate a clearer, ceiling-parallel flow in the presence of solar heating. This leads to the air being carried further into the room, enhancing the overall distribution.

8.3 Geometry analysis

The second analysis in this thesis aims to address some of the identified gaps in the literature concerning the influence of heat load placement, room height and room length.

Model layout

Several different geometries have been developed to test the influence of different parameters on a design chart. Model 1 is the one used and validated by Zhang [2016], and the rest have been made based on this model.

In the other models, one element is changed at a time. An overview of the different models constructed can be found in Table 8.5, with the naming of the model and what parameter is changed from the original Model 1. In Table 8.5, the file name in the external appendix can also be found.

Table 8.5. Overview of CFD models.

Model no	Parameter varied	New version	Model name
Model 1	-	-	Short_short_centered
Model 2	Heat load placement	One sided	Short_short_one_sided
Model 3	Room height	5 m	Short_high_centered
Model 4	Room length	9.6 m	Long_short_centered

Illustrations of the geometry of the different models constructed can be found in Figure 8.11 to 8.13.

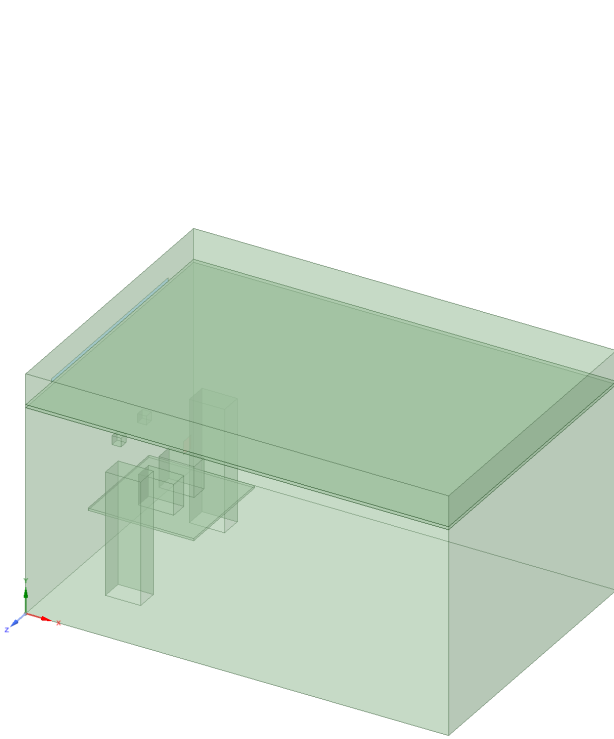


Figure 8.11. Geometry of Model 2.

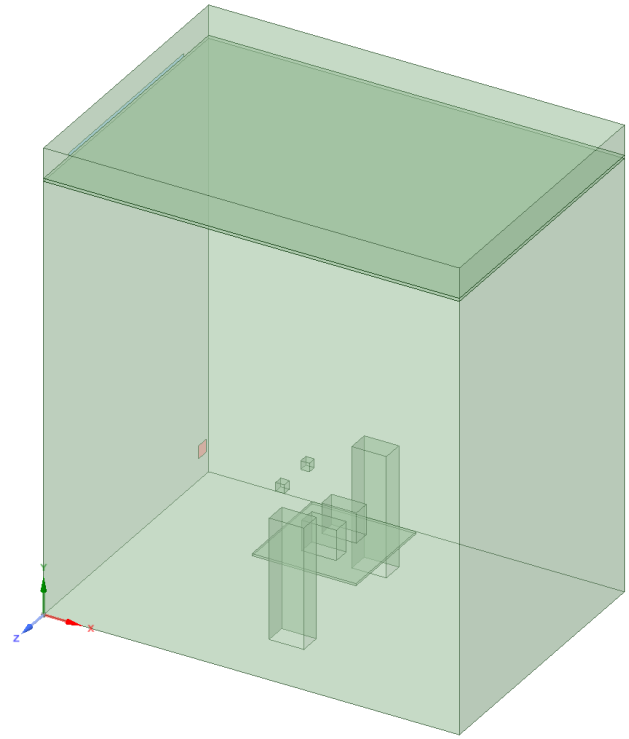


Figure 8.12. Geometry of Model 3.

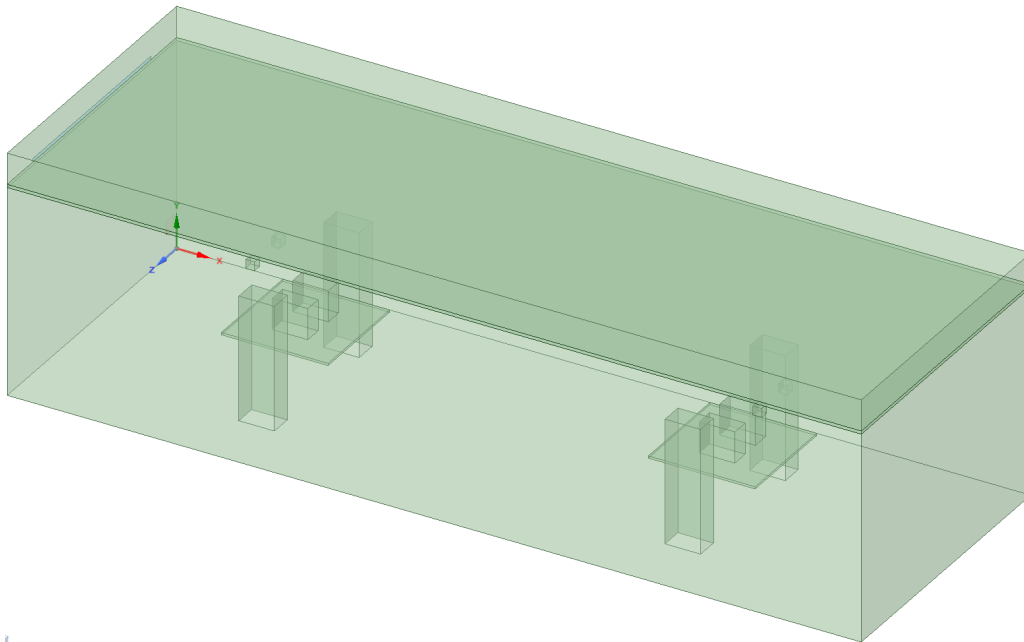


Figure 8.13. Geometry of Model 4.

As can be seen in the pictures, everything is kept the same between each model except for the varied parameter. In Figure 8.11, the placement of the heat sources is concentrated on one side of the room closest to the window/inlet. In Figure 8.12 and Figure 8.13 the heat load is placed in the same way or a similar way as in Figure 8.1, but the ceiling height and room length have respectively been increased. In Figure 8.13, a second set of heatloads has also been placed in the room.

In the three figures, it can also be seen that the inlet (blue) is made as a slot inlet, and the exhaust (red) is a square, both with the same orientation.

Because these models are developed for this thesis, some parameters which were not investigated for Model 1 have been examined for these models. In Appendix J, the influence of the monitored residuals has been investigated. It was found that these had a great impact on the model results and the convergence of the models. Mesh independence for model 2 has been conducted and can be seen in Appendix K. The monitored residuals were further refined for the finer mesh in this analysis to ensure that this model reached convergence. In Appendix L, the mesh independency test for Model 3, with a higher ceiling height, can be found. Lastly, the independence test for Model 4, which was a longer room, can be found in Appendix M. This model did not reach independence. However, the results from the first mesh are still included to obtain some indicative data. It should be noted that the results from this model should be interpreted with caution, as they cannot be considered fully reliable.

8.4 Setup

The models in this analysis use the same heat load as for cases 4-6 in the other investigation. This heatload is 430W, with occupants and equipment, but no solar heat. The values are chosen based on critical values in Vorre et al. [2017]. The value used in the models is found in Table 8.6

Table 8.6. Heat load, convection, and heat flux data.

Source	Heat Load [W]	Convection Fraction [%]	Convection Part [W]	Surface Area [m ²]	Heat Flux [W/m ²]
Lamp	15	54	8.1	0.12	67.5
Occupants	100	40	40	1.92	20.83
PC	100	90	90	0.5	180.0
Sum Model 1-3	430		276		
Sum Model 4	860		552		

The convective part of the heat load is placed directly on the heat load in the model, while the radiation part is divided by the surface area of the room and placed hereupon. This can be found in Table 8.7.

Table 8.7. Heat flux on room surfaces.

Case	Surface heat flux [W/m ²]
Model 2	2.87
Model 3	1.59
Model 4	3.35

Turbulence model

From the investigation in Appendix E, it was found that the turbulence model, Standard $k-\epsilon$, together with the equilibrium wall treatment, gave results similar to experiments with the same setup and heat load. Therefore, this turbulence model, which was also found to be the most frequently used in other literature, is also used in the following models.

The investigation also indicated that a transient approach is preferable when simulating DCV systems, particularly at high heat loads. Under such conditions, the large temperature difference between the inlet and the room air can lead to complex and unstable flow behaviour. However, since the heat load used in the geometry analysis is not critically high, and due to time constraints, a steady-state model was applied in this part of the study.

8.4.1 Results from one-sided heat load distribution

As examined earlier, the heat load distribution has a great impact on the system performance. In this section, the results of the investigation, where the heat load is concentrated on one side of the room, are presented.

Temperature sections

In Figure 8.15, the temperature section for the three simulations with one-sided heat load can be found. One section goes through the middle of the room, and the other goes through the occupants.

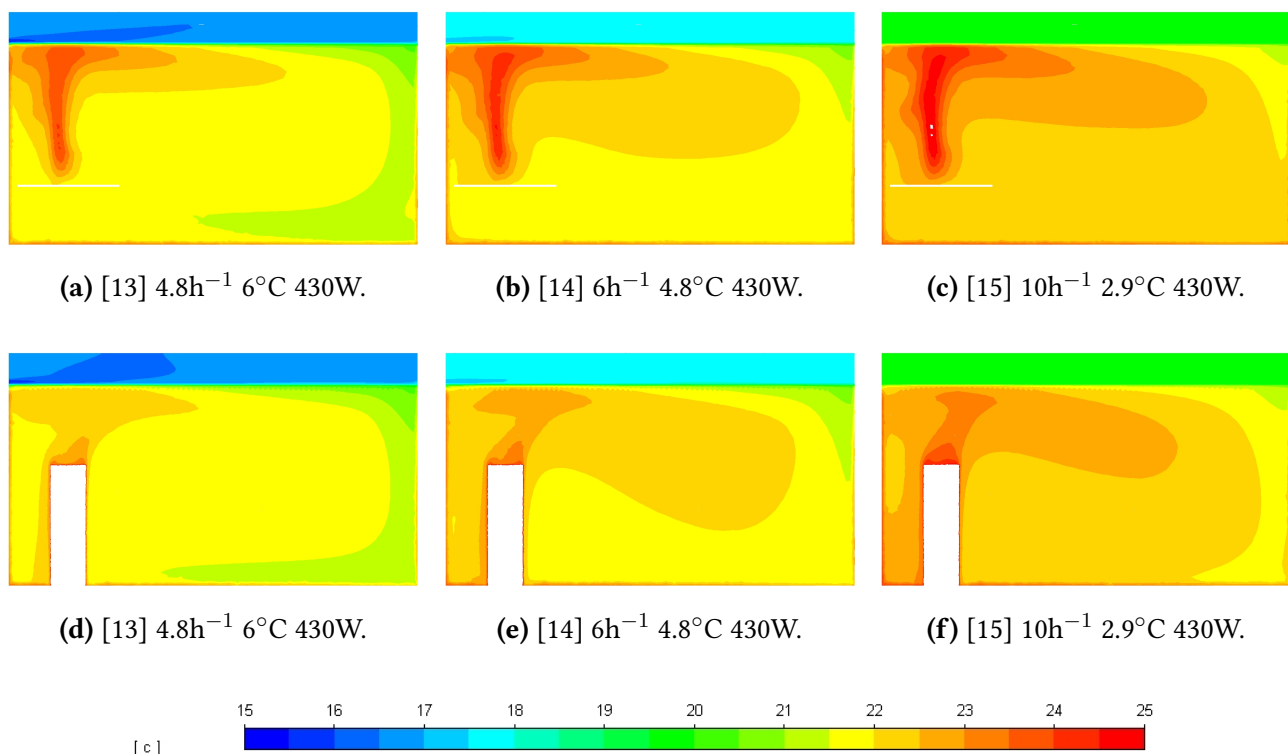


Figure 8.15. Temperature sections. Top row: middle of the room. Bottom row: through the occupant.

The plume from the different heat sources has the expected shape in all cases, but due to the placement close to a wall, the plume is not very symmetrical but skewed towards the opposite side.

Velocity sections

The velocity is also examined in the same two sections, These can be found in Figure 8.17.

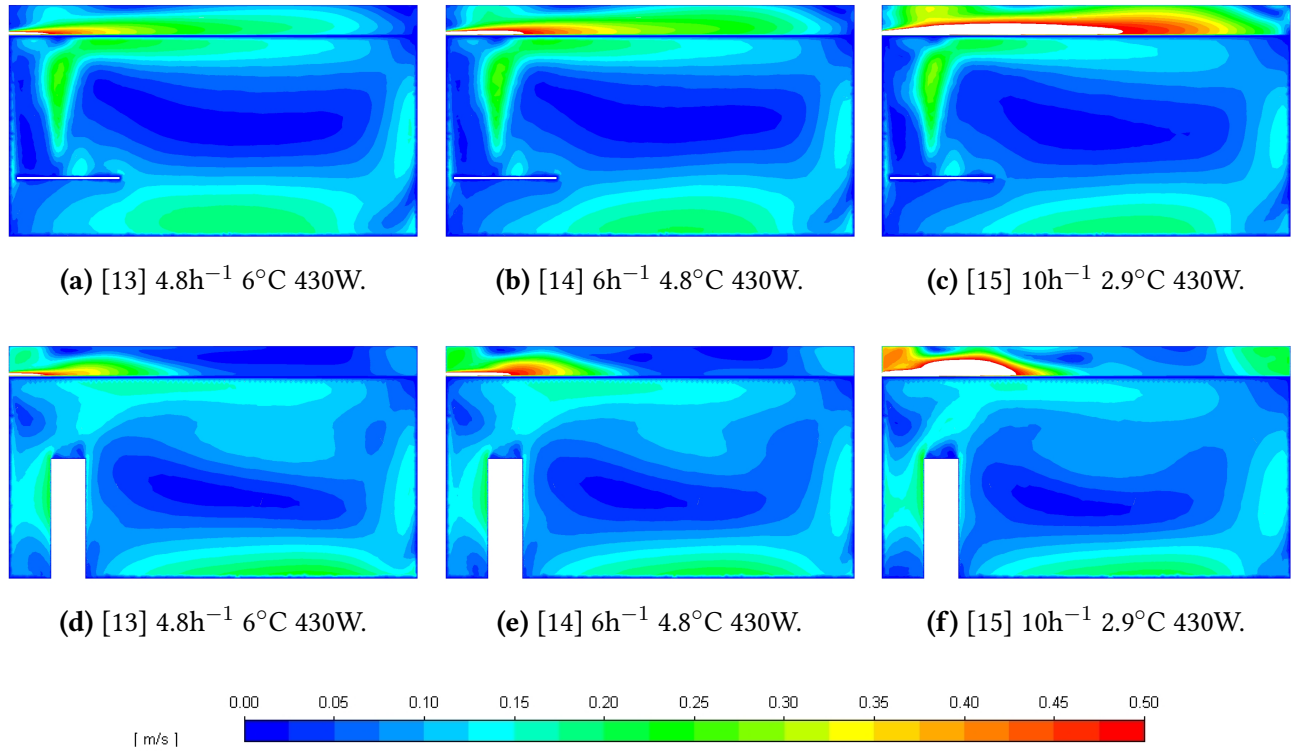


Figure 8.17. Velocity sections. Top row: middle of the room. Bottom row: through the occupant.

The velocity in the room is higher near the floor and walls, which is consistent with findings from other studies. Additionally, the velocity generated by buoyancy from the heat sources accelerates the air just below the ceiling. This behaviour is comparable to what was observed in the analysis with solar heat, where the window was also located just beneath the inlet. In that case, the airflow was carried further into the plenum before being distributed down into the room. To determine if the same is happening when the heat sources are concentrated below the inlet, the pathlines are observed.

Pathlines

The pathlines are also examined for the three cases. This is done through the occupant section, and can be seen in Figure 8.19.

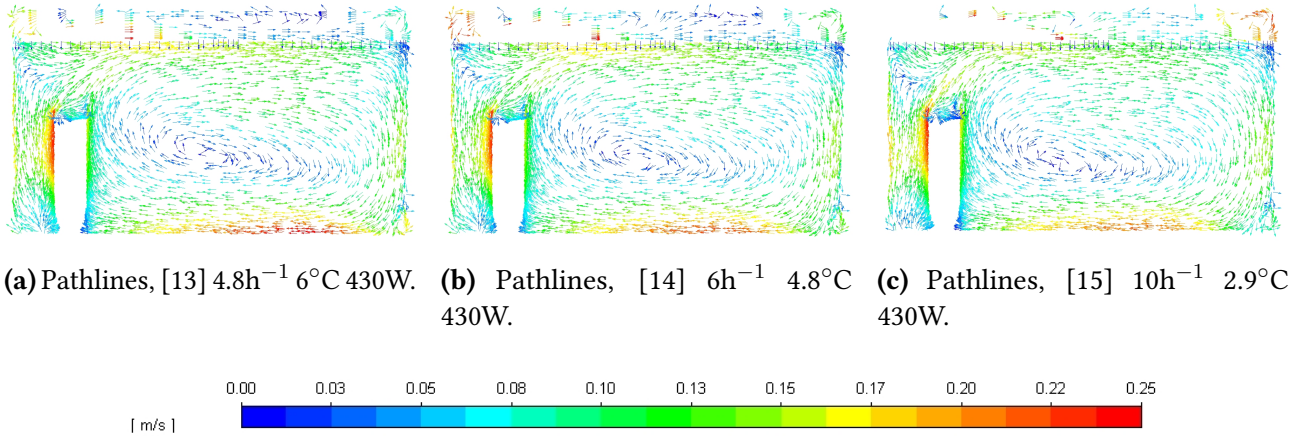


Figure 8.19. Pathlines through the occupant for cases 13, 14, and 15.

These figures illustrate the air movement within the room. As expected, a vortex forms on the right side of the occupant, and the velocity increases near the floor. Additionally, elevated velocities are observed at the head level of the occupant, particularly on the side facing the inlet and exhaust.

The pathlines through the ceiling can be seen in Figure 8.20. The arrows are placed in the middle of the suspended ceiling.

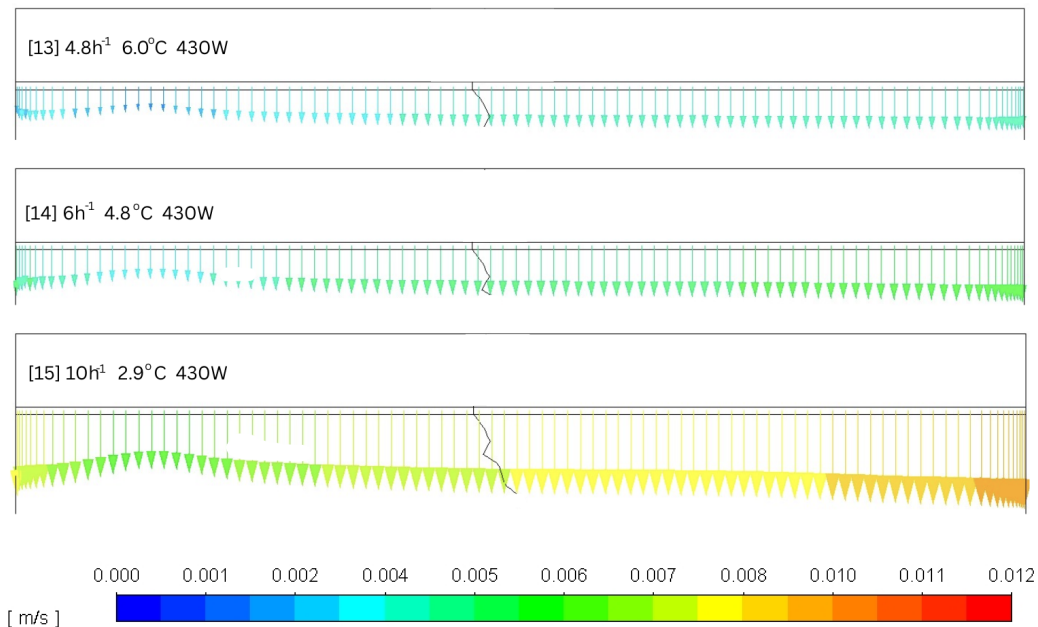


Figure 8.20. Air through ceiling panels in cases 13, 14 and 15.

The patterns are comparable to those seen for the same heat placed in the middle of the room. The air is evenly distributed throughout the ceiling with a dent above the heat load. For higher inlet velocities, the velocity through the ceiling also increases.

8.4.2 Results from increase in room height

The earlier presented literature review shows that room height has a great impact on the performance of the system. Therefore, a model with a room height of 5 m without the plenum has been constructed. The temperature and velocity results from this investigation will be presented in the following

Temperature

The temperature results from Cases 16 to 18 are shown in Figure 8.22. Certain areas of the room are not colored, which is due to local temperatures exceeding the upper limit of the colour map. Since these elevated temperatures occur between the PCs, the same colour map has been maintained across all cases to ensure consistency, and these outliers have been disregarded in the visual interpretation.

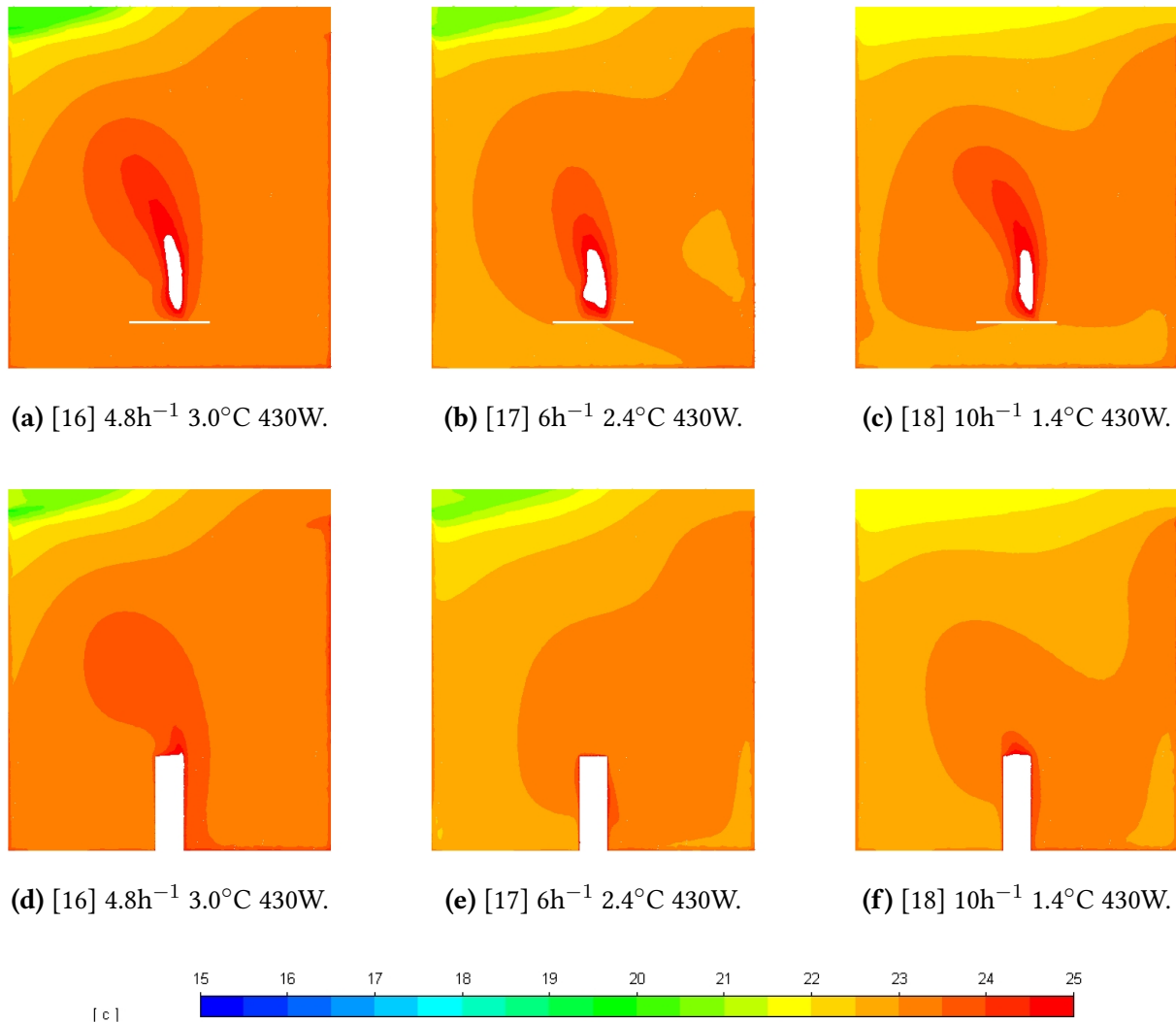


Figure 8.22. Temperature sections for Case 16, 17, and 18. Top row: middle of the room. Bottom row: through the occupant.

It can be observed that the supply air does not penetrate far into the space, which may negatively affect overall mixing in the room. In previous cases, the heat load was seen to accelerate the airflow

along the ceiling, helping to carry the air further into the plenum. In this case, however, the large distance between the heat sources and the ceiling prevents this effect, which could explain why the air does not reach the end of the plenum.

Velocity

The velocity section have also been investigated, these can be seen in Figure 8.24.

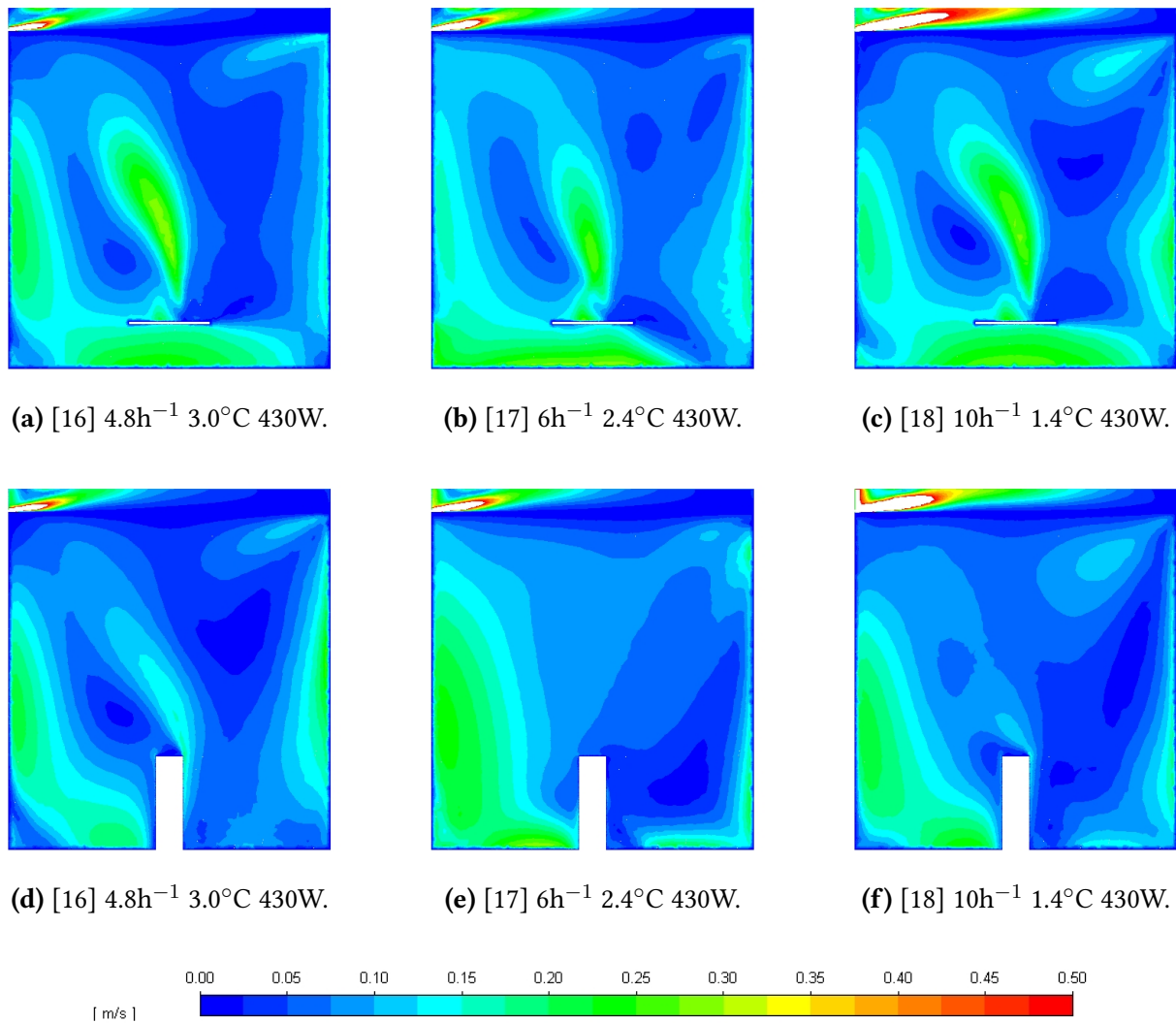


Figure 8.24. Velocity sections for cases 16, 17, and 18. Top row: middle of the room. Bottom row: through the occupant.

In contrast to the other cases, the air jet from the inlet appears to attach to the upper ceiling rather than the suspended ceiling. Additionally, the supply air does not seem to penetrate far into the plenum. Within the room, higher velocities are observed near the floor and walls, however, these zones of higher airflow extend further into the space than in previous cases. To gain a clearer understanding of the airflow patterns, pathlines are also examined.

Path lines

The velocity pathlines for cases 16 to 18 are seen in Figure 8.26.

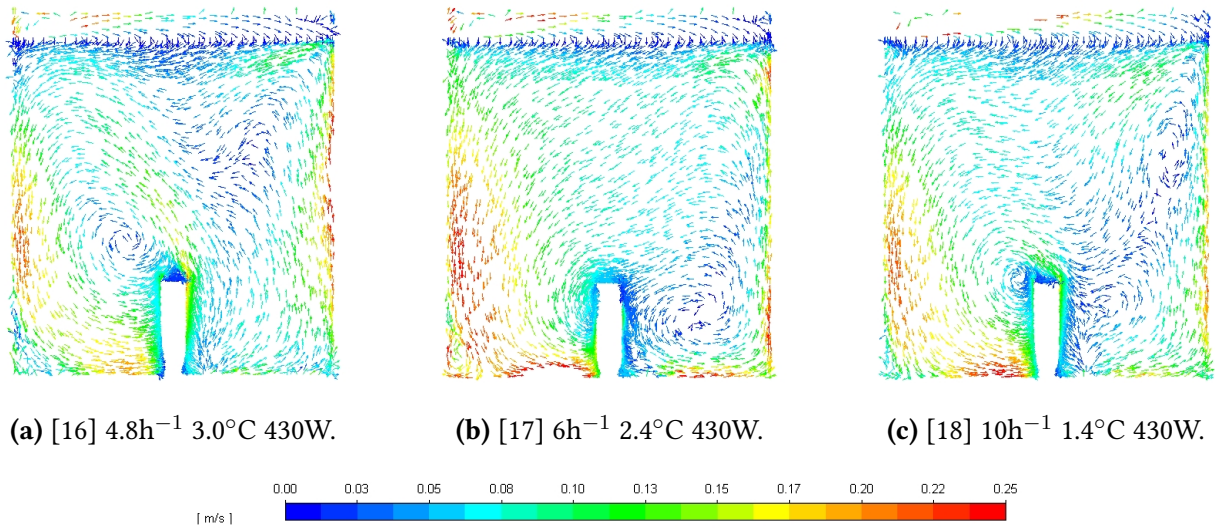


Figure 8.26. Pathlines through the occupant for cases 16, 17, and 18.

The images show some notable differences, but also certain similarities. In the area to the left of the occupant, beneath the inlet, the air is accelerated, resulting in higher velocities near the occupant's ankle on that side. In the rest of the room, however, the results appear quite different. This may be due to instability in the system. A similar observation was made in the study by Vilsbøll [2014], where increased plenum height led to unstable flow conditions.

Pathlines through the ceiling for cases 16 to 18 can be seen in Figure 8.27.

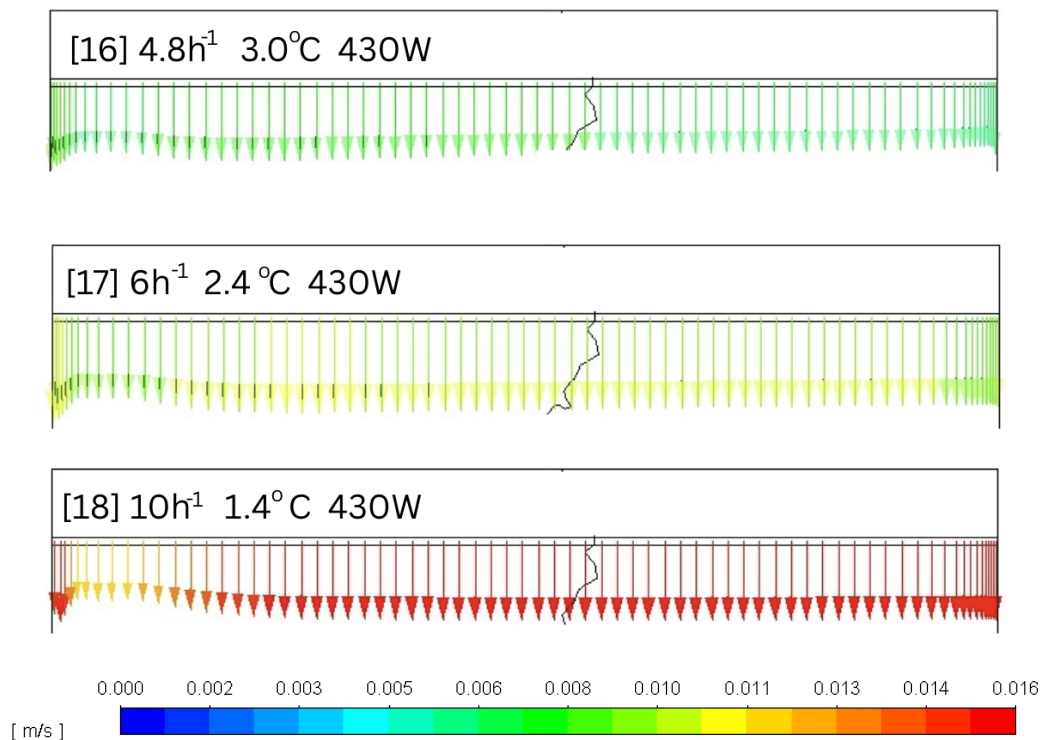


Figure 8.27. Air through ceiling panels in cases 16, 17 and 18.

A dent is observed at the inlet. Additionally, the air is evenly distributed across the entire ceiling. As seen in previous cases, the airflow through the ceiling increases as the inlet velocity increases.

Results from increase of room length

In the literature, room length was investigated in only one study, which found that the cooling capacity per square meter decreased as the room length increased. Concerns were also expressed regarding the ability of air to penetrate the entire plenum in longer rooms, and DCV was therefore primarily recommended for smaller spaces. In this study, DCV performance in a longer room is examined to gain a better understanding of these potential challenges.

The figures in this section are arranged in columns rather than rows, due to the different room dimensions compared to the other results.

Temperature

In Figure 8.29 a longer room has been constructed, and the temperature section in the middle of the room and through the occupant can be seen.

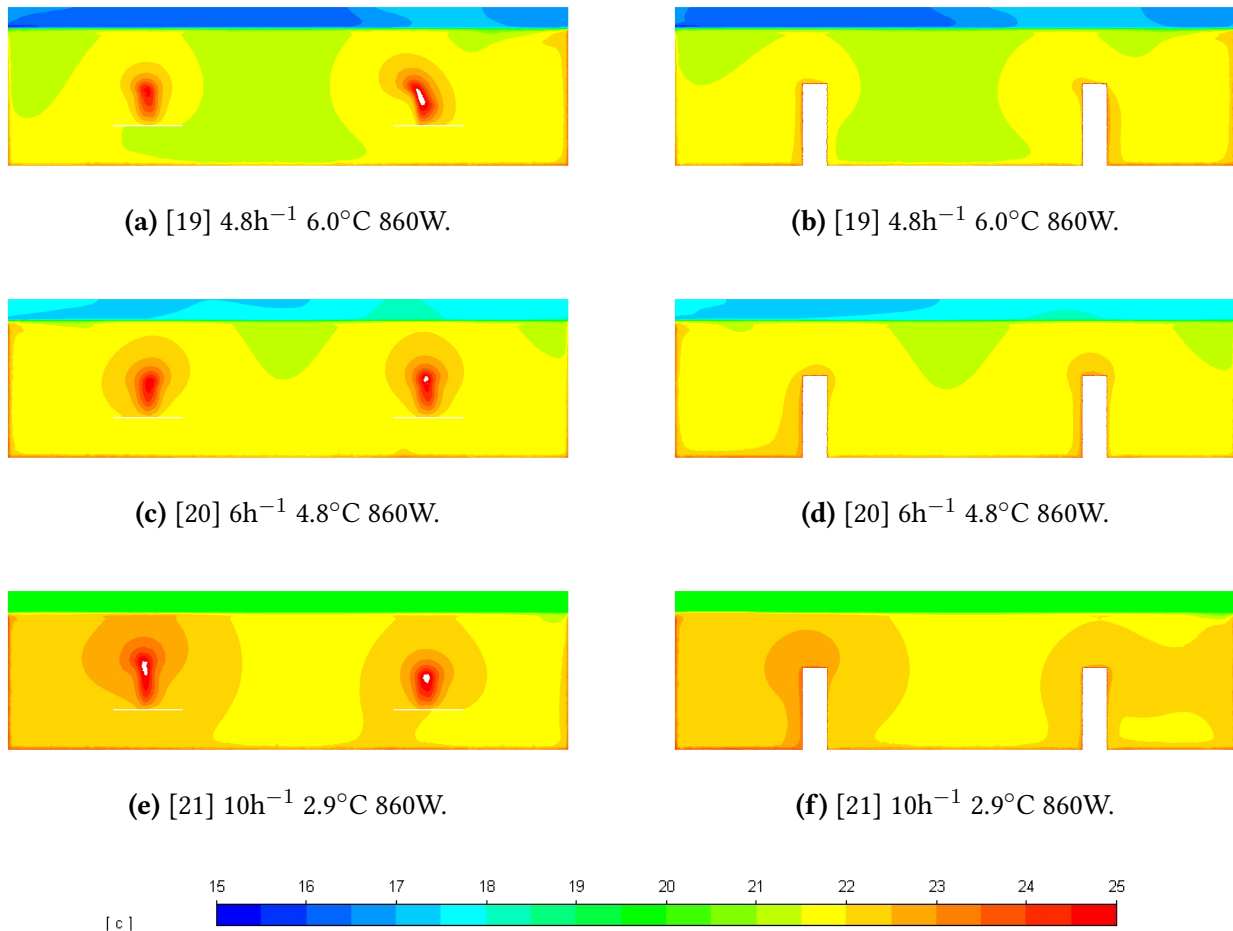


Figure 8.29. Temperature sections. Left column: middle of the room. Right column: through the occupant.

The plumes generated by the heat sources within the room are less pronounced compared to the other cases. In the plenum, the temperature appears more uniform than in the high-ceiling scenario, once again suggesting that the heat sources contribute to a more even distribution of air within the plenum. To better understand the airflow, the velocity and pathlines are investigated.

Velocity

The velocity in the sections through the middle of the room and the occupant are investigated. The velocity results for cases 19 to 21 are seen in Figure 8.31.

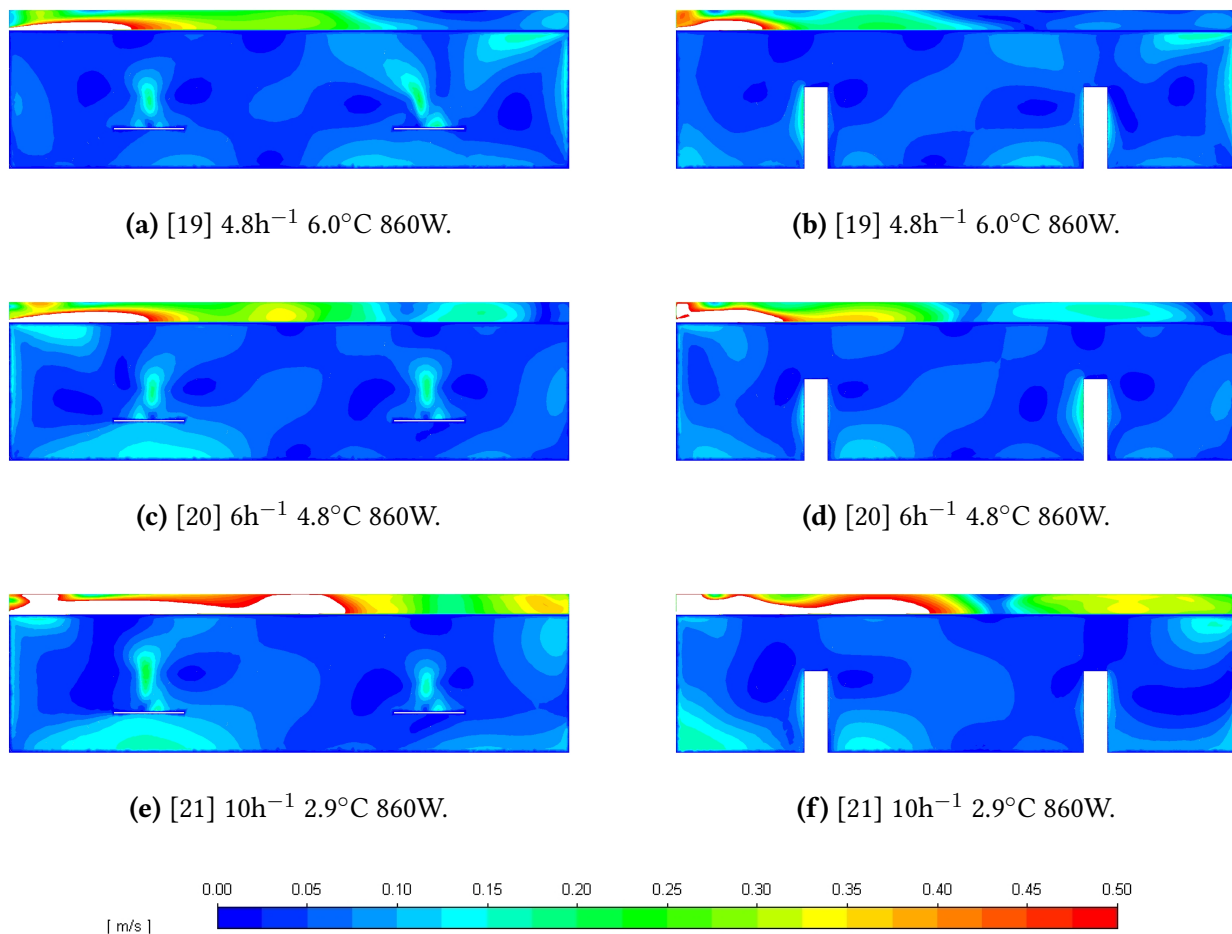


Figure 8.31. Velocity sections. Left column: middle of the room. Right column: through the occupant.

The velocity in the plenum is generally higher than previously observed, but only in the final case with the highest inlet velocity does the air appear to reach the far end of the plenum. Unlike earlier cases, elevated velocities near the floor and walls are less pronounced, and no critical zones are observed within the room.

Path lines

The pathlines for the different cases 19 to 21 can be seen in Figure 8.33.

Figure 8.32. Pathlines through the occupant for Case 19, 20, and 21. Displayed in a single column.

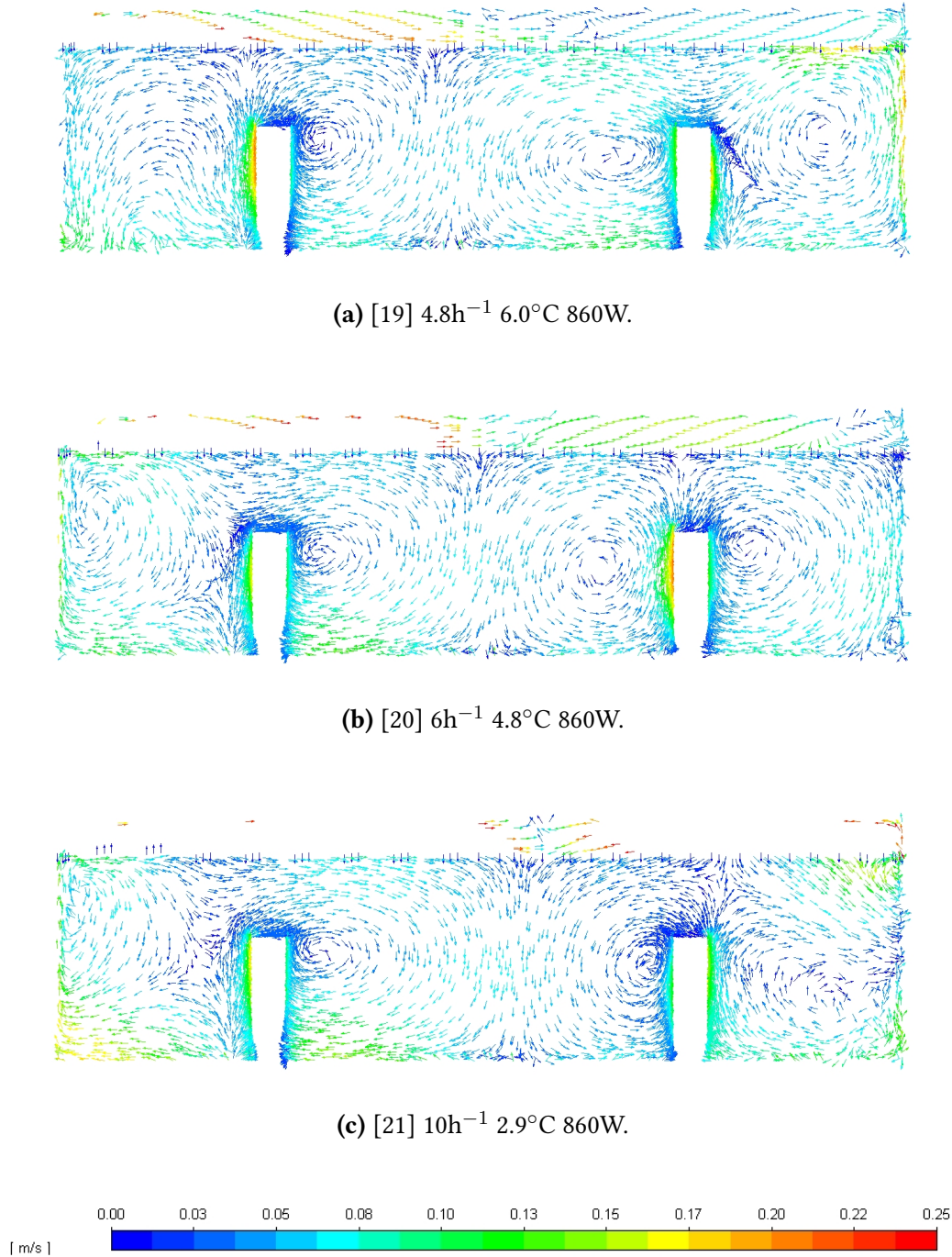


Figure 8.33. Pathlines through the occupant for cases 19, 20, and 21.

A clear trend is observed in all three cases: the airflow separates into two distinct recirculation zones, each centred around a heat source. These recirculation patterns divide the room into two separate airflow regions, which could seem to have limited mixing between them.

This flow separation could potentially impact thermal comfort and air quality, as it suggests that each occupant remains within a microenvironment, with minimal influence from the opposite side of the room. Since the exhaust is located on the left side, this may lead to a high age of air on the right side, potentially compromising ventilation effectiveness in that area.

The pathlines through the ceiling of the long room can be seen in Figure 8.34.

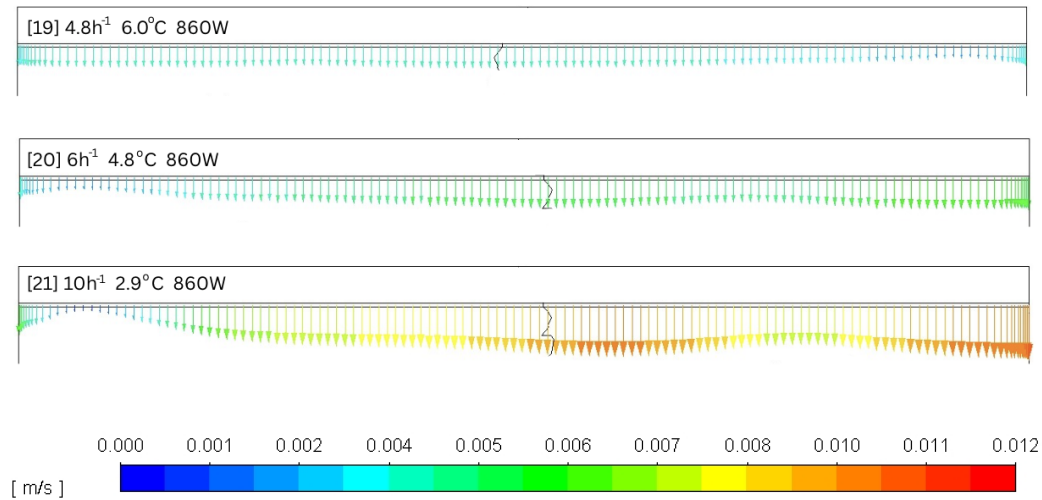


Figure 8.34. Air through ceiling panels in cases 19, 20 and 21.

From these images, dents can be observed above both sets of heat loads. The dent above the first set is more pronounced, and in case 21, it appears that reverse flow almost occurs.

8.5 Overall conclusion

The analysis has explored how varying heat load intensities and geometric room parameters influence the performance of a DCV system. Across the 21 CFD simulations, results confirm several tendencies reported in literature, such as the influence of thermal plumes, and they further highlight the importance of parameters like room height and heat load placement in shaping airflow patterns.

The simulations have provided valuable insight into the complex interplay between heat sources and ventilation flow. While some models, particularly the one with increased room height, exhibited signs of flow instability or limited mixing, however, the overall behaviour aligns well with expectations. The results are deemed sufficiently reliable to serve as the foundation for generating design charts in the following chapter.

Design charts from numerical analysis 9

In this chapter, the design chart from the heat load intensity and geometry analysis will be conducted. The design chart data is based on two reference points identified through a velocity analysis of the simulation, with the maximum velocity of the two being used as the basis.

9.1 Evaluation of heat load intensity

The two measurement points are placed on each side of the occupant at heights of 0.1 and 1.1 m. The point at 0.1 m is placed on the West side of the manikin, away from the exhaust and inlet and the point at 1.1 m is placed on the East side. A further description of the point selection can be found in Appendix I.

The velocity data for the two points are analysed to identify any relation between heat load and the placement of the maximum velocity. This must be analysed in combination with the case properties like ACH and temperature difference. These properties can be found in Table 9.1.

Table 9.1. Simplified overview of CFD cases with placement of maximum velocity.

Case	Point 0.1 m	Point 1.1 m
[1] 4.8h ⁻¹ 3.36°C 200 W		x
[2] 6h ⁻¹ 2.69°C 200 W		x
[3] 10h ⁻¹ 1.61°C 200 W	x	
[4] 4.8h ⁻¹ 7.23°C 430 W		x
[5] 6h ⁻¹ 5.78°C 430 W		x
[6] 10h ⁻¹ 3.47°C 430 W	x	
[7] 4.8h ⁻¹ 17.15°C 1,020 W	x	
[8] 6h ⁻¹ 13.72°C 1,020 W	x	
[9] 10h ⁻¹ 8.23°C 1,020 W	x	
[10] 4.8h ⁻¹ 24.04°C 1,430 W	x	
[11] 6h ⁻¹ 19.24°C 1,430 W	x	
[12] 10h ⁻¹ 11.54°C 1,430 W	x	

In cases 1-6, which have a heat load of 200 and 430 W, the max velocity is placed at a height of 1.1 m in the two cases with a lower ACH of respectively 4.8 and 6 h⁻¹. The case with an ACH of 10 h⁻¹ has the highest velocity at a height of 0.1 m. It should be considered that the cases with high ACH also have the lowest temperature difference between the inlet and exhaust. Both ACH and inlet temperature could therefore influence the system and where the maximum air velocity occurs. For

cases 7-12, all containing solar heat gain, the max velocities are placed at 0.1 m height. These cases have a high heat load of 1,020 W and 1,430 W.

Design charts

The graphs in this chapter show the average design graph for each set of simulations, the individual design charts can be found in Section N.1. The procedure for developing the design charts is described in Appendix O.

The idea of the analysis is to gain an understanding of the impact of different heat load amounts in the room. The two low heat loads contain respectively two occupants and two occupants in combination with equipment. The two high heat loads are with added solar gain. The design chart with different heat load amounts is shown in Figure 9.1. Each dot shows the simulated value from the CFD simulation. These are compared to the design chart developed by Nielsen and Jakubowska [2009]. This design chart is shown with the yellow line. In this case, an office room is simulated with a heat load resulting in a maximum of 1,060 W. This graph is named: [Nielsen et al, 2009] 1,060 W.

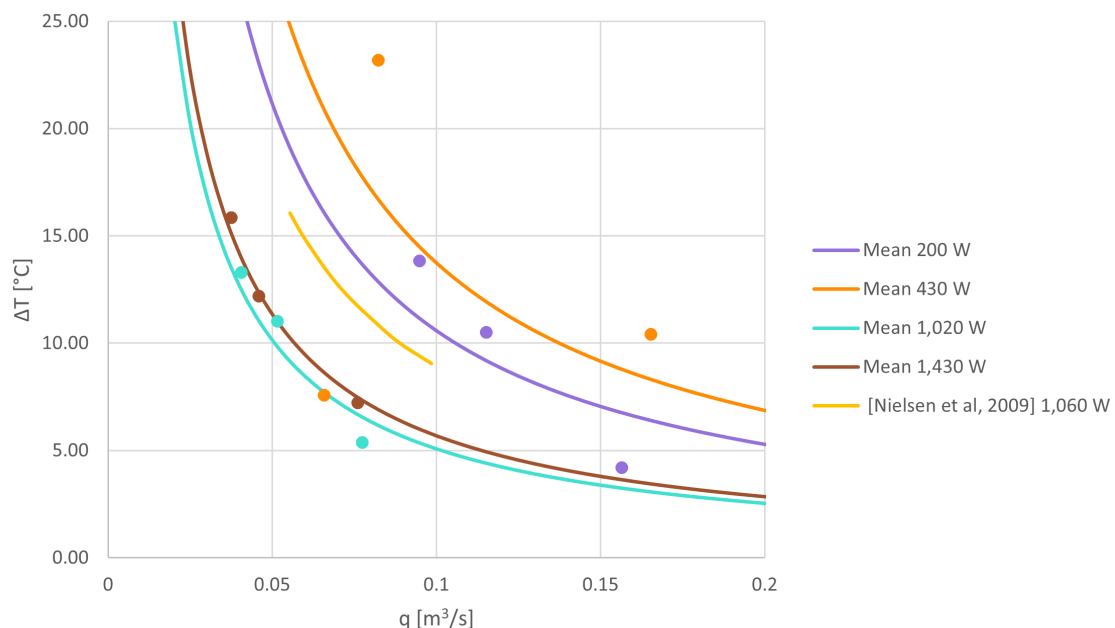


Figure 9.1. Average design chart for heat load intensity. Include data from Nielsen and Jakubowska [2009].

The figure illustrates the relationship between airflow rate and resulting temperature difference for various heat load intensities. When the heat source is vertically offset downward, which is seen in the cases containing solar heat, the cooling capacity of the system is reduced. This observation was also made by Chodor and Taradajko [2013] as mentioned in Chapter 5.

The case with 200 W exhibits a lower performance graph than the 430 W case, which aligns with the fact that a higher placement of the heat load provides better conditions for the system. The distance between the graphs could be explained by the fact that the low heat load in the 200 W scenario is insufficient to generate the buoyancy-driven mixing needed for efficient air distribution.

Additionally, the data points for the 430 W case are more scattered, which could indicate instability in the airflow pattern for that specific setup. The graphs for 1,020 W and 1,430 W are closely aligned, and the minor variations in their position are likely due to uncertainties in the simulations rather than significant performance differences.

Overall, the figure highlights how both heat load intensity and its vertical placement influence the effectiveness of the system, particularly in terms of airflow mixing and temperature stratification.

9.2 Evaluation heat loads distribution

To evaluate the impact of heat load distribution, cases with identical heat loads are compared. The comparison is made between a centred and a one-sided heat load configuration, each with a total of 430 W, where the reference model is the centred configuration. The centred heat load design chart is shown in the previous section. New simulations and corresponding design charts have been developed for the one-sided heat load cases. Three different cases at 430 W, each with varying ACH values and temperature differences, have been made, but only the mean is shown. The comparison between the mean heat load distributions is shown in Figure 9.2.

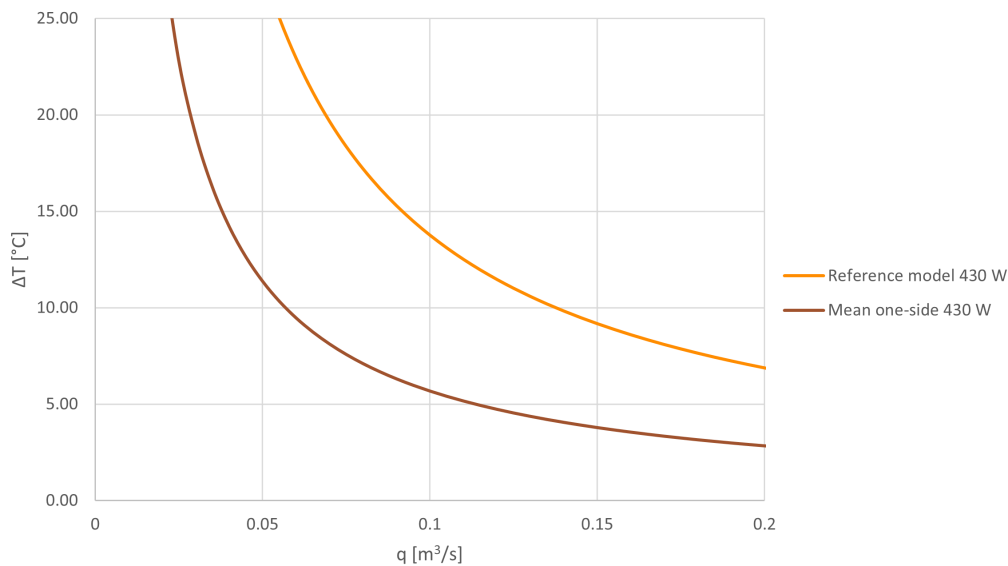


Figure 9.2. Centred vs. one-sided heat load distribution.

The design chart shows that the mean design graphs for the one-sided heat load distribution are displaced downward, indicating a lower cooling capacity compared to the centred heat load distribution. This observation aligns with the findings from the literature review.

9.3 Evaluation of room geometry

To compare different room geometries, three different models are made. One is the reference model in which no geometric or thermal parameters are altered, the second has an increased room height while maintaining the same heat load, and the third is a long room where both the room length and heat load are doubled. The design chart for this comparison is illustrated in Figure 9.3.

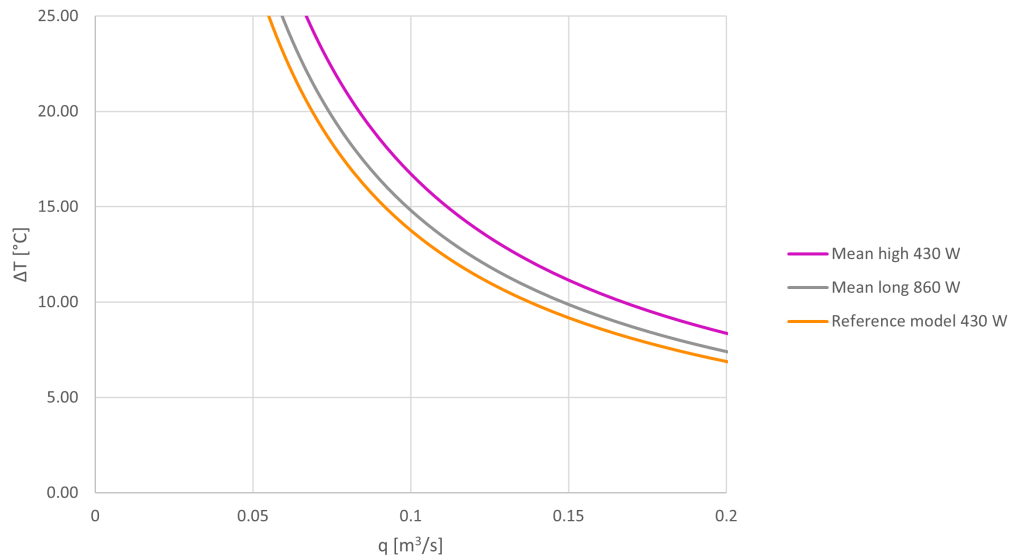


Figure 9.3. Design chart showing different room geometries.

The design chart shows that the three room models exhibit similar performance characteristics, with their graphs positioned close to each other. This suggests that these variations in room geometry do not influence the cooling capacity.

The graph for the high-ceiling room is positioned above the others, indicating a slightly higher cooling capacity. In contrast, the lowest capacity is observed in the reference model configuration. This outcome does not fully align with the literature, which generally finds that increased room height reduces cooling effectiveness due to longer air travel distances and greater recirculation. However, the differences between the cases are relatively small, and the results may be affected by uncertainties or limitations in the simulation models.

Configuration tool outline 10

Since it is not possible to define a general equation for DCV, it is necessary to create a specific design chart for each scenario. A large number of design charts must therefore be developed, as any change in a parameter requires a new design chart.

The tool is intended to function as a guideline to assess whether a specific system, given a set of user-defined input parameters, is compatible with DCV. An outline of the configuration tool is shown in Figure 10.1, a larger version can be found in Appendix P. The layout of the tool is structured into different steps, as illustrated in the figure. The first step covers general information, including room geometry, plenum geometry, placement of heat loads, and air supply. The next step is basic inputs, where information about the ventilation system is entered. Once the user provides all the required data, the tool will display a design chart that corresponds exactly to the specified input, ensuring that the output fully reflects the selected parameters. For the tool to function, a corresponding design chart must already exist for the given input. Otherwise, the configuration cannot be evaluated. This chart will indicate critical aspects such as draught risk and vertical temperature gradient, and help determine whether the proposed system configuration meets the performance criteria for DCV.

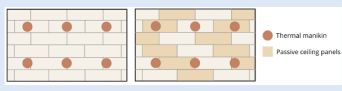
Diffuse ceiling ventilation calculation		
Room information Room type Room name Number of occupants Number of other heat load Placement of total heat load Geometry Length Width Height (without plenum) Plenum height Plenum depth Plenum inlet Placement (maybe not relevant) Size (to get the right air velocity)	Basic inputs Ventilation Supply airflow Extract airflow Room air temperature Requirements Max. velocity in occupied zone (V _{ai}) Needed cooling capacity Placement of perforated panels (room inlet) Percentage based on cooling demand input Placement from drop down menu 	Result Room Area Volume (V _r) Ventilation Supply air temperature Temperature difference (Δt _{ra}) Air change per hour, supply Cooling capacity Comfort Velocity in occupied zone (V _{ai}) Vertical temperature gradient Air velocity value used in comfort calculations (from Adv. In) Draught rate PMV PPD Temperature gradient (t _g) [K] Relative air velocity [m/s] Air temperature [°C] Mean radiant temperature [°C]

Figure 10.1. Outline of the configuration tool.

The parameters that have been identified and analysed so far in this thesis represent only a small fraction of all the factors that influence the performance of the DCV system. Therefore, many additional parameters still need to be investigated before the tool can be applied in practice. A potential future enhancement of the tool could include the integration of active and passive ceiling panels, panel permeability, and other relevant factors to improve its flexibility and applicability across a wider range of scenarios. To ensure the highest level of accuracy, future work should include both experimental studies and CFD simulations for all relevant parameter combinations, so that reliable and representative design charts can be developed for each case.

Part III

Recapitulation

This section summarises the key findings from the CFD analysis and configuration tool development. It includes a critical discussion of the results, comparing the outcomes with existing literature and identifying the implications for DCV systems. The section concludes with a comprehensive evaluation of the study's objectives and recommendations for future research.

Chapter 11 Discussion	79
Chapter 12 Conclusion	81
Bibliography	82

Literature review

The literature review formed the foundation of this thesis, but revealed some limitations. Most notably, DCV systems in heating scenarios are poorly represented, which creates a knowledge gap, as the thermal behaviour of DCV under heating conditions differs from cooling. This lack of data makes it difficult to establish robust design guidelines for year-round operation and highlights a clear need for further investigation.

Additionally, the combined effect of various design parameters is not fully addressed in most literature. Studies typically isolate a single variable, making it difficult to understand the complex interactions that occur in realistic setups. One of the central findings of this project is that many parameters in DCV design influence each other. Parameters such as room geometry, heat load, ceiling height, and distribution of active panels were analysed and found to have a significant impact on system performance.

Numerical models

The CFD simulations conducted in this thesis filled some of the knowledge gaps. Cases 1–12 were modelled as transient, whereas cases 13–21 were steady-state. Due to time constraints, it was not possible to test transient simulations for the steady-state models. This split introduces inconsistency in the numerical approach, which could influence the results, especially in geometries with unstable flow patterns. This was particularly evident in Models 3 and 4, where instabilities were observed, and it would have been valuable to investigate whether a transient approach could have resolved these issues.

Another limitation concerns the modelling of radiant heat, which was applied as wall-based BC rather than as occupant-specific heat sources. While this approach simplifies the simulation setup, it may affect airflow patterns and local thermal conditions, particularly airflow characteristics and plume behaviour. Ideally, these effects could have been evaluated through experimental validation, however, this was not feasible within the scope of this thesis. Although comparisons were made to findings in the literature, the lack of direct experimental verification introduces uncertainty in the interpretation of the CFD results.

Design chart development

The development of design charts resulted in several challenges. To enable comparison between simulations, it was necessary to select a specific measurement point in the room. This simplification risks ignoring other zones where draught or discomfort might occur, potentially underestimating local extremes.

The airflow in DCV systems is highly sensitive to changes in boundary conditions, room geometry, and the distribution or intensity of internal heat loads. Even relatively small adjustments in these parameters can lead to significant variations in flow patterns and draught behaviour. As a result, developing generalised design charts based on a limited number of discrete simulation cases poses a considerable challenge. There is a risk of overfitting the charts to specific configurations, which may not accurately reflect the performance of other, untested scenarios. It is also difficult to estimate results between the simulated cases because the relationship between input parameters and system performance is not always linear. This makes it hard to predict how the system will behave in new situations. To improve this, a more detailed study covering a wider range of parameters is needed, or a smarter, data-driven method could be used to help fill in the gaps more accurately.

Configuration tool

The configuration tool developed in this thesis is a concept, but it is limited in scope. It is based only on a subset of the parameter space investigated in the literature and simulations. Consequently, it cannot yet support arbitrary room configurations or automatically generate interpolated charts for intermediate cases.

The configuration tool developed in this thesis presents a prototype rather than a final version. While it was intended to include the simulated cases generated as part of this study, this has not yet been fully implemented. Furthermore, the tool would still be limited to the specific scenarios that have been simulated and cannot account for conditions beyond those cases. To improve its applicability, the tool should be expanded with additional simulations to cover a broader range of design scenarios. In addition to the parameters already investigated, other critical factors, such as ceiling panel configurations in combination with the spatial distribution of heat sources, also play a significant role in DCV performance. Similarly, the vertical placement of heat sources and varying occupant densities affect thermal plumes and mixing efficiency. Therefore, a more comprehensive parametric study that includes these aspects is recommended for future work. Such investigations could provide deeper insights into how these design parameters interact with airflow patterns and impact local comfort conditions in the occupied zone.

Conclusion 12

This thesis aims to get a broader implementation of DCV by developing a prototype configuration tool based on both literature and numerical analysis. The literature review confirmed that DCV can maintain acceptable thermal comfort conditions, with vertical temperature gradients generally remaining within acceptable limits. However, high air velocities and thereby the risk of draught were found to occur under specific configurations, particularly in rooms with high ceiling heights or low plenum heights. These findings suggest that while DCV has distinct benefits, its performance is sensitive to certain design conditions.

The investigation also examined dimensionless numbers such as the Ar and Re numbers in characterising DCV performance. It was found that these parameters offered limited value for general evaluation, as no consistent trends could be identified across different systems. This confirms the idea that DCV cannot be fully described by simplified models and requires a more nuanced approach.

To explore this complexity further, CFD simulations were carried out to fill knowledge gaps identified in the literature. The selection of CFD cases focused on varying heat load intensity, heat load distribution, and room geometry. The simulations confirmed that DCV performance is highly scenario-specific and influenced by multiple interdependent parameters. Notably, higher heat loads were found to reduce the cooling capacity of the system, while centred or evenly distributed heat loads improved system performance. One-sided heat loads, by contrast, led to lower cooling capacity and greater instability in the airflow.

The development of design charts based on CFD results enabled the visual representation of performance limits for specific design configurations. These charts were used as the basis for a configuration tool prototype. However, the charts depend on a limited number of discrete simulation cases and cannot yet accommodate interpolation or extrapolation to new scenarios.

The CFD modelling process itself highlighted the importance of carefully selecting turbulence models and boundary conditions. Nonetheless, results from some simulations, particularly those involving high ceilings, showed flow instability, which could be resolved with transient simulations.

Overall, the thesis shows that DCV has some benefits that traditional ventilation systems lack, however, a successful implementation requires detailed, case-specific analysis. The many interacting factors involved make it difficult to develop a fully generalised configuration tool. However, the approach presented here lays a solid foundation. Future work should focus on expanding the database of simulated cases and validating results experimentally. These steps will be essential for turning the current prototype into a robust, reliable, and user-friendly design tool.

Bibliography

- ANSYS [2023], *How to select appropriate wall function for turbulence modeling and what is the requirement for y plus?*, <https://innovationspace.ansys.com/knowledge/forums/topic/how-to-select-appropriate-wall-function-for-turbulence-modeling-and-what-is-the-requirement-for-y-plus/>.
- ANSYS [2025], *Workbench User's Guide*, https://ansyshelp.ansys.com/account/secured?returnurl=/Views/Secured/corp/v194/wb2_help/wb2_help.html.
- ASHRAE [2016], *ASHRAE Handbook - Fundamentals*, American Society of Heating, Refrigerating and Air-Conditioning Engineers.
- By og Byg [2002], *Naturlig ventilation i erhvervsbygninger*, <https://edu.anvisninger.dk/anvisninger/p-anv202-naturlig-ventilation-i-erhvervsbygninger>.
- Byg & Bæredygtighed [2024], *Nye klimakrav til byggeriet fra 2025: Hvad skal vi forberede os på i byggebranchen?*, <https://bygogbaeredygtighed.dk/nye-klimakrav-til-byggeriet-fra-2025-hvad-skal-vi-forberede-os-paa-i-byggebranchen/>.
- Chodor, A. D. and Taradajko, P. P. [2013], 'Experimental and numerical analysis of diffuse ceiling ventilation'.
- Energistyrelsen [2025], *Byggeri og renovering, Energibesparende tiltag for nybyggeri og renovering af eksisterende byggeri.*, <https://ens.dk/forsyning-og-forbrug/byggeri-og-renovering>.
- Fan, J., Hviid, C. A. and Yang, H. [2013], 'Performance analysis of a new design of office diffuse ceiling ventilation system'.
- Hviid, C. A. and Svendsen, S. [2012], 'Experimental study of perforated suspended ceilings as diffuse ventilation air inlets'.
- International Standard [2006], 'Iso 7730:2005 ergonomics of the thermal environment - analytical determination and interpretation of thermal comfort using calculation of the PMV and ppd indices and local thermal comfort criteria'.
- Jacobs, P. and Knoll, B. [2008], 'Diffuse ceiling ventilation, a new concept for healthy and productive classrooms'.
- Jakubowska, E. [2007], 'Air distribution in rooms with diffuse ceiling inlet'.
- Kozlowski, B. M., Silkjær, M. H., Vasilevskis, S. and Myhre, S. H. [2016], 'Diffuse ceiling ventilation - full scale experiment and numerical predictions of diffuse ceiling ventilation'.
- Kristensen, M. H. and Jensen, J. S. [2015], 'Impact of diffuse ceiling ventilation systems on indoor environmental quality in classrooms'.

- Lestinen, S., Kilpeläinen, S., Kosonen, R., Jokisalo, J. and Koskela, H. [2018], 'Experimental study on airflow characteristics with asymmetrical heat load distribution and low-momentum diffuse ceiling ventilation'.
- Lindab AB [2017], *LindQST 5.1 User manual*, https://www.lindqst.com/lindQST_5_User_Manual.pdf.
- Mikeska, T. and Fan, J. [2015], 'Full scale measurements and CFD simulations of diffuse ceiling inlet for ventilation and cooling of densely occupied rooms'.
- Nielsen, P. V. [1995], 'Lecture notes on mixing ventilation'.
- Nielsen, P. V. [1999], 'Lecture notes on scale-model experiments'.
- Nielsen, P. V. [2007], 'Analysis and design of room air distribution systems'.
- Nielsen, P. V. and Jakubowska, E. [2009], 'The performance of diffuse ceiling inlet and other room air distribution systems'.
- Nielsen, P. V., Jensen, R. L. and Rong, L. [2010], 'Diffuse ceiling inlet systems and the room air distribution'.
- Nielsen, P. V., Larsen, T. S. and Topp, C. [2003], 'Design methods for air distribution systems and comparison between mixing ventilation and displacement ventilation'.
- Nielsen, P. V., Liu, L. and Jensen, R. L. [2015], 'Diffuse ceiling ventilation and the influence of room height and heat load distribution'.
- Nocente, A., Arslan, T., Grynning, S. and Goia, F. [2020], 'CFD study of diffuse ceiling ventilation through perforated ceiling panels'.
- Ogbuagu, T.-C. C., Linden, E., MacCutcheon, D., Nilsson, E., Persson, T. and Kabanshi, A. [2023], 'On the performance of diffuse ceiling ventilation in classrooms: A pre-occupancy study at a school in southern sweden'.
- Peng, P., Pomianowski, M., Zhang, C., Guo, R., Jensen, R. L., Jønsson, K. T. and Gong, G. [2021], 'Experimental investigation on the ventilation performance of diffuse ceiling ventilation in heating conditions'.
- Peng, P., Zhang, C., Li, W., Pomianowski, M., Gong, G., Fang, X., Chun, L. and Guo, R. [2023], 'Investigation on indoor airflow and contaminant dispersion of diffuse ceiling ventilation in heating and cooling modes'.
- Petersen, S., Christensen, N. U., Heinsen, C. and Hansen, A. S. [2014], 'Investigation of the displacement effect of a diffuse ceilingventilation system'.
- Pilkington [2025], *Spectrum*, <https://www.pilkington.com/da/dk>.
- Rahnama, S., Nielsen, P. V., Afshari, A., Bergsøe, N. C., Johra, H. and Jensen, R. L. [2019], 'Evaluating the cooling capacity of diffuse ceiling ventilation system - full-scale experimental study'.

- Sadeghian, P., Rahnama, S., Afshari, A. and Sadrizadeh, S. [2022], 'The role of design parameters on the performance of diffuse ceiling ventilation systems – thermal comfort analyses for indoor environment'.
- Seuntjens, O., Belmans, B., Buyle, M. and Audenaert, A. [2022], 'A critical review on the adaptability of ventilation systems: Current problems, solutions and opportunities'.
- Skistad, H., Mundt, E., Nielsen, P. V., Hagström, K. and Railio, J. [2002], 'Displacement ventilation in non-industrial premises'.
- Vilbøll, R. W. [2014], 'Diffuse ceiling ventilation - experimental and numerical analysis based on variation of room geometry and heat load distribution'.
- Vorre, M. H., Wagner, M. H., Maagaard, S. E., Noyé, P., Lyng, N. L. and Mortensen, L. [2017], 'Branchevejledning for indeklimaberegninger'.
- Wirowski, A., Kubacka, E., Kaszubska, P. and Walisiak, W. [2024], 'Numerical analysis of the dynamic properties of bionic raster ceilings'.
- Yu, T., Heiselberg, P., Lei, B., Pomianowski, M., Zhang, C. and Jensen, R. [2015], 'Experimental investigation of cooling performance of a novel hvac system combining natural ventilation with diffuse ceiling inlet and TABS'.
- Zhang, C. [2016], 'Diffuse ceiling ventilation air distribution and thermal comfort'.
- Zhang, C. and Heiselberg, P. [2019], 'Diffuse ceiling ventilation'.
- Zhang, C., Heiselberg, P. K., Chen, Q. and Pomianowski, M. [2016], 'Numerical analysis of diffuse ceiling ventilation and its integration with a radiant ceiling system'.
- Zhang, C., Heiselberg, P. and Nielsen, P. V. [2014], 'Diffuse ceiling ventilation: A review'.
- Zhang, C., Kristensen, M. H., Jensen, J. S., Heiselberg, P. K., Jensen, R. L. and Pomianowski, M. [2015], 'Parametrical analysis on the diffuse ceiling ventilation by experimental and numerical studies'.
- Zhang, C., Yu, T., Heiselberg, P. K., Pomianowski, M. Z. and Nielsen, P. V. [2017], 'Diffuse ceiling ventilation - design guide for wood wool cement panel'.
- Zhang, W., Zhang, W., Bai, Y. and Wen, S. [2023], 'Enhancing indoor environmental quality: Personalized recommendation method for demand-oriented indoor ventilation strategy'.
- Zhang, W., Zhang, W., Mizutani, K. and Zhang, H. [2021], 'Decision-making analysis of ventilation strategies under complex situations: A numerical study'.
- Zhang, W., Zhang, W., Zhang, H., Xuan, Y. and Liu, X. [2023], 'Effective improvement of a local thermal environment using multi-vent module-based adaptive ventilation'.

Part IV

Appendix

Appendix A	Electronic appendix	86
Appendix B	Analysis of temperature in heating cases	87
Appendix C	Average temperature	89
Appendix D	Analysis of velocity in heating cases	92
Appendix E	Selection of turbulence model	94
Appendix F	Temperature sections	100
Appendix G	Velocity sections	104
Appendix H	Path lines	108
Appendix I	Selection of reference points for design chart development	120
Appendix J	Investigation of residuals	123
Appendix K	Mesh independency of model 2	126
Appendix L	Mesh independency of model 3	130
Appendix M	Mesh independency of model 4	134
Appendix N	Design charts results	138
Appendix O	Design chart development	143
Appendix P	Configuration tool outline	146

A.1 Analysis

Analysis of existing data.xlsx

File used to analyse existing studies comparing velocity, temperature, draught, and dimensionless numbers.

A.2 CFD models

Four models have been used throughout this thesis. The naming of these models can be found in Table A.1.

Table A.1. Overview of CFD models.

Model no	Parameter varied	New version	Folder name
Model 1	-	-	Short_short_centered
Model 2	Heat load placement	One sided	Short_short_one_sided
Model 3	Room height	5 m	Short_high_centered
Model 4	Room length	9.6 m	Long_short_centered

A.3 Design chart developement

Design chart heat load intensity.xlsx

File used to create design chart for heat load intensity.

Design chart distribution and geometry.xlsx

File used to create design chart for heat load distribution and geometry.

A.4 Configuration tool outline

Configuration tool outline.xlsm

Draft file outlining the configuration tool concept, including an illustrative example of how the tool might be developed.

Analysis of temperature in heating cases B

The purpose of this chapter is to present the analysis of the temperature conditions in heating cases. An overview of the relevant cases, including geometry, ACH, inlet and exhaust temperatures, heat loads, and heat load placements, can be found in Table B.1.

Table B.1. Information about the cases with geometry, airflow, and temperature conditions for heating cases.

Paper	Case	Geometry [m]	ACH [h ⁻¹]	Temperatures [°C]		Heat load [W/m ²]	Placement of heat load
				Inlet	Exhaust		
[Nielsen et al., 2010]	[B2] 3.5h ⁻¹ -5°C	2.45 × 4.1 × 3.2	3.5	27.3	22.6	0	-
	[B3] 6h ⁻¹ -5°C	2.45 × 4.1 × 3.2	6.0	27.2	22	0	
[Peng et al., 2021]	[F1] 3h ⁻¹ -4°C	2.5 × 4.2 × 3.6	3.0	26.17	22.27	13	Centered
	[F2] 3h ⁻¹ -5°C	2.5 × 4.2 × 3.6	3.0	26.75	21.93	13	
	[F3] 3h ⁻¹ -4°C	2.5 × 4.2 × 3.6	3.0	27.71	23.57	13	
	[F4] 1.5h ⁻¹ -10°C	2.5 × 4.2 × 3.6	1.5	33.25	23.58	13	
	[F5] 6h ⁻¹ -1°C	2.5 × 4.2 × 3.6	6.0	25.25	23.92	13	
	[F6] 3h ⁻¹ -12°C	2.5 × 4.2 × 3.6	3.0	37.2	24.85	13	

The Ar number for the heating cases is found below.

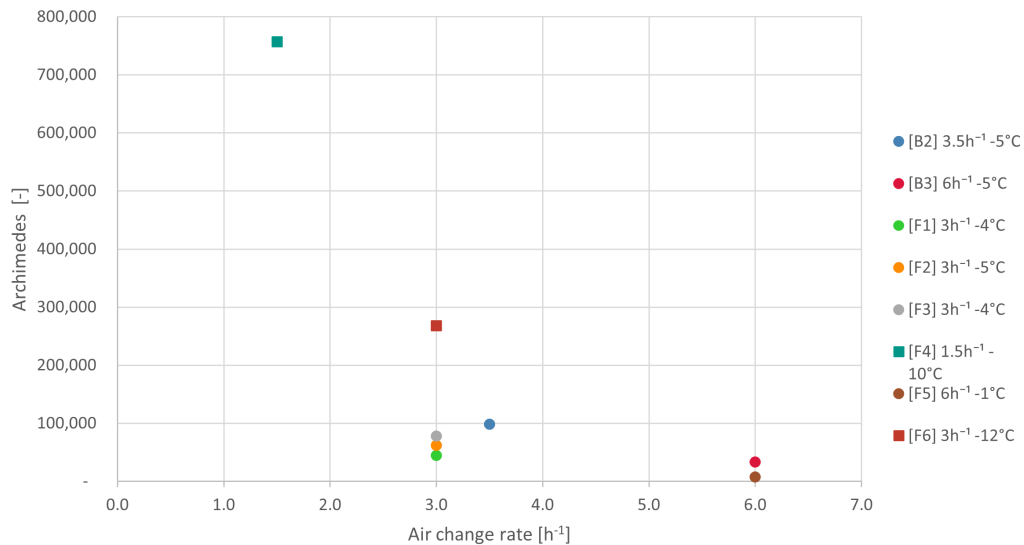


Figure B.1. ACH vs. Ar number for heating cases.

The temperature gradient for the heating cases has been sorted based on their Ar number. This grouping can be found on Figure B.2

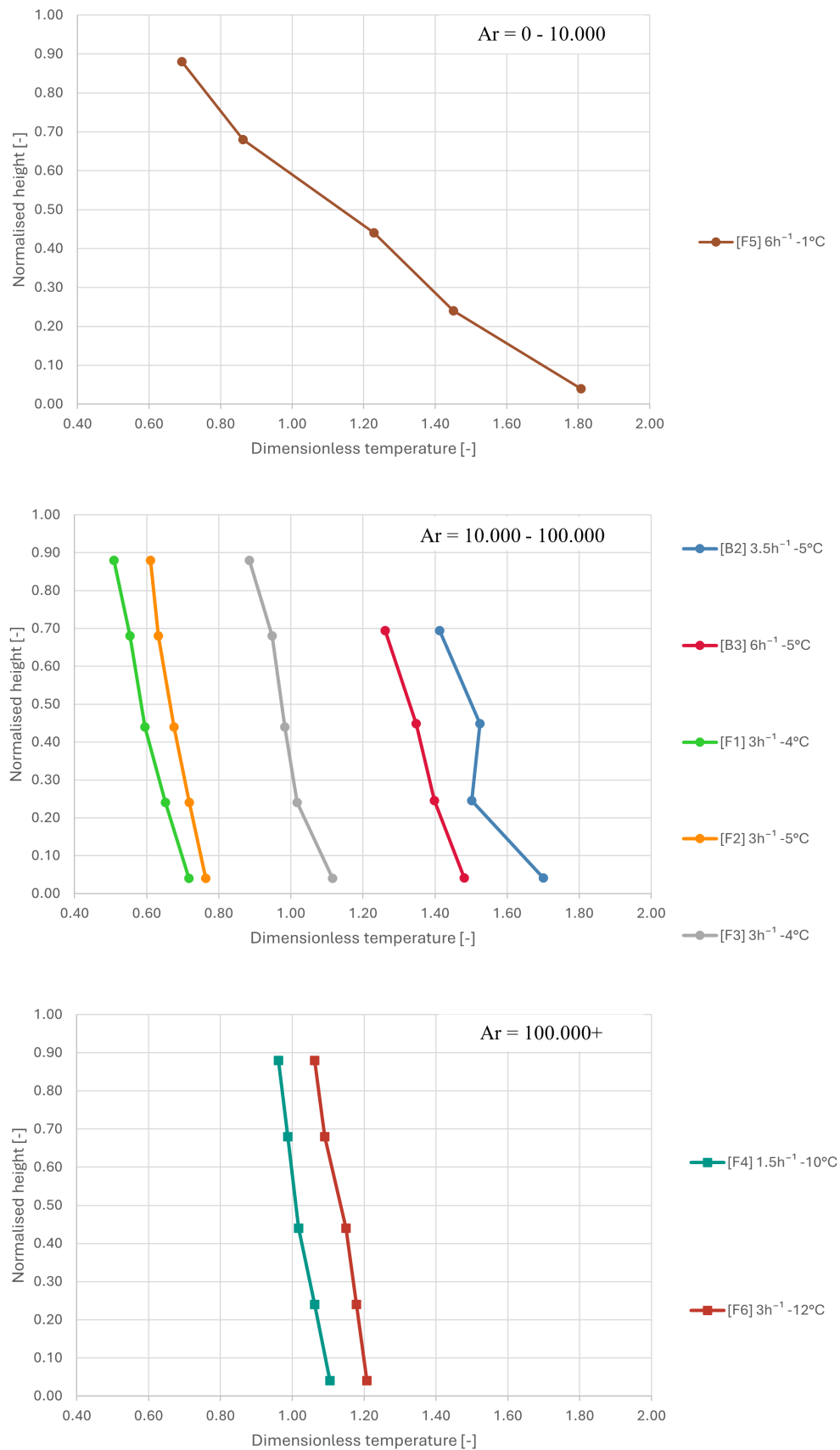


Figure B.2. Temperature distribution for different heating cases grouped by Ar number.

It can be seen from the figures that the gradients are very similar for Archimedes numbers above 10,000, however, an offset on the x-axis is observed.

Average temperature C

In some studies, the temperature gradient in different parts of the room was specified, while in others, only a single gradient for the entire room was specified. It was therefore decided to investigate whether it was an acceptable assumption to take an average of the normalised temperature gradients in the various cases and proceed with one gradient per case. The dotted lines on the following figures represent the temperature gradient at different locations in the experiment, while the solid lines indicate the average.

From paper by Nielsen et al. [2010]:

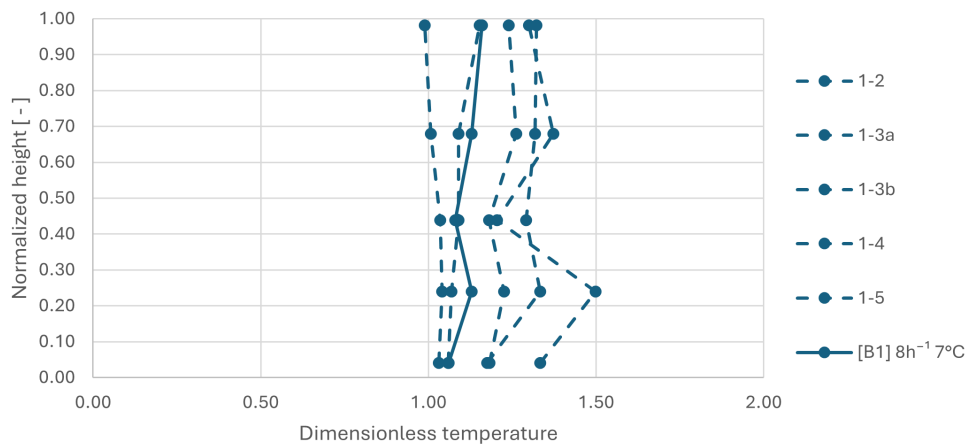


Figure C.1. Average temperature analysis for case B1.

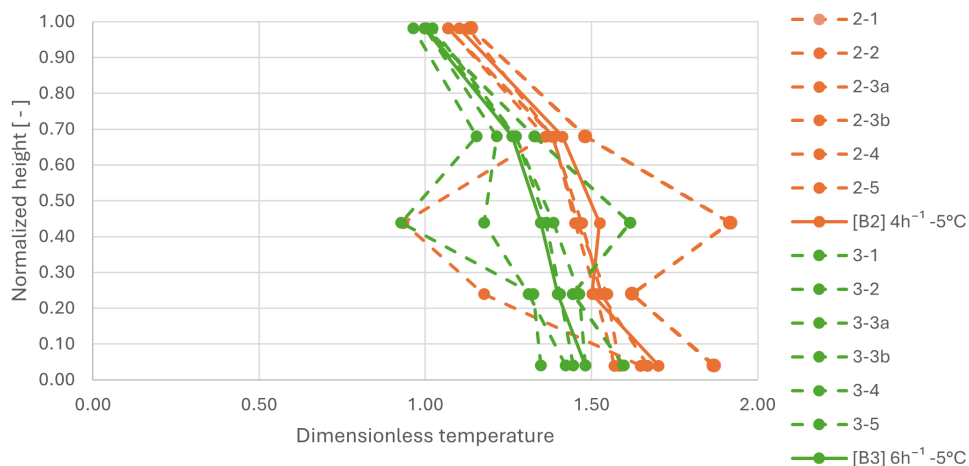


Figure C.2. Average temperature analysis for case B2 and B3.

From paper by Fan et al. [2013]:

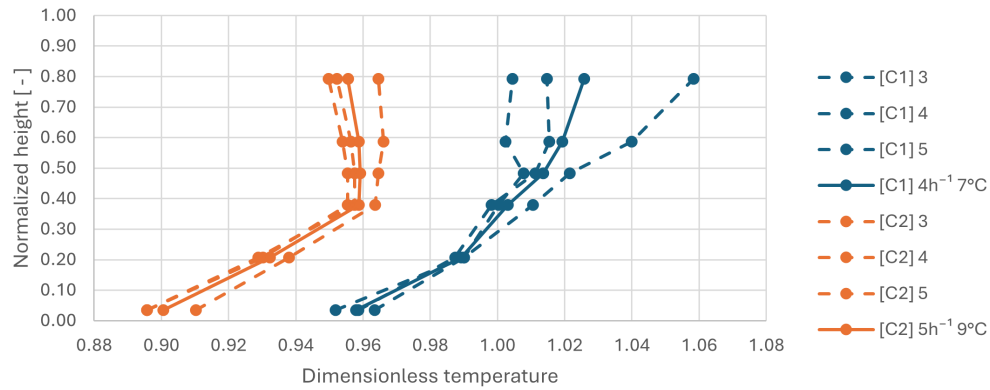


Figure C.3. Average temperature analysis for case C1 and C2.

From paper by Petersen et al. [2014]:

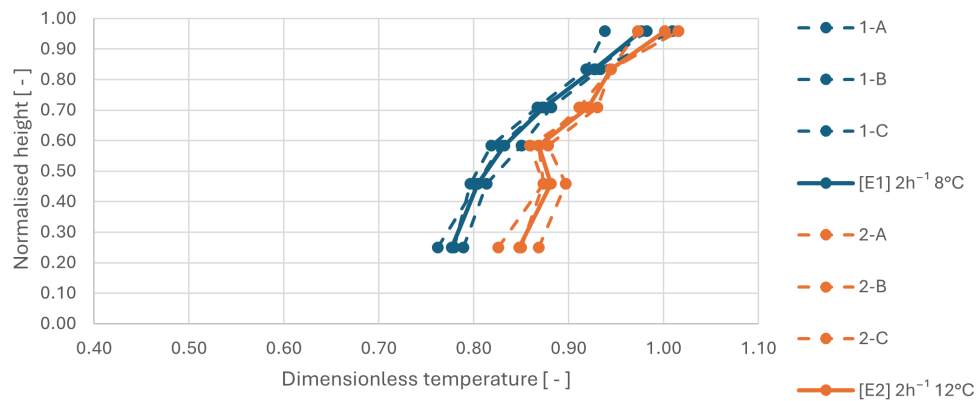


Figure C.4. Average temperature analysis for case E1 and E2.

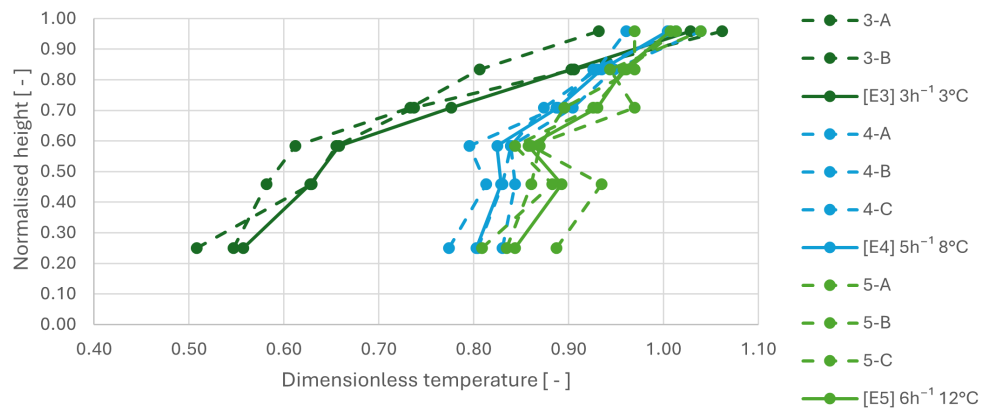


Figure C.5. Average temperature analysis for case E3, E4 and E5.

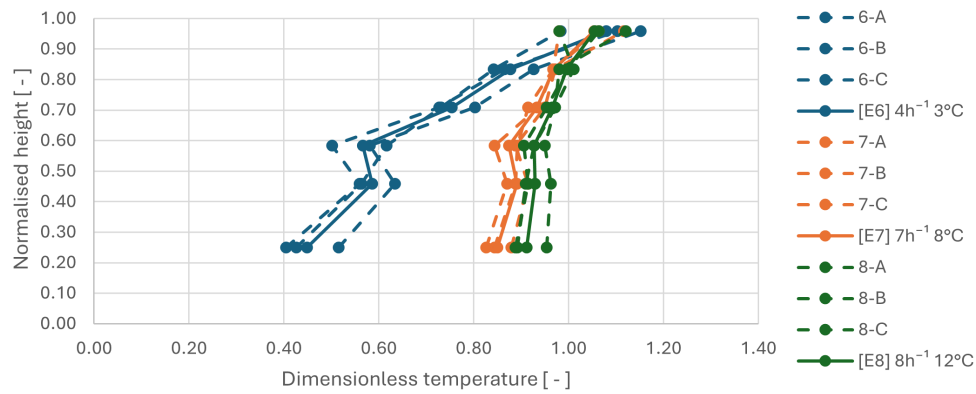


Figure C.6. Average temperature analysis for case E6, E7 and E8.

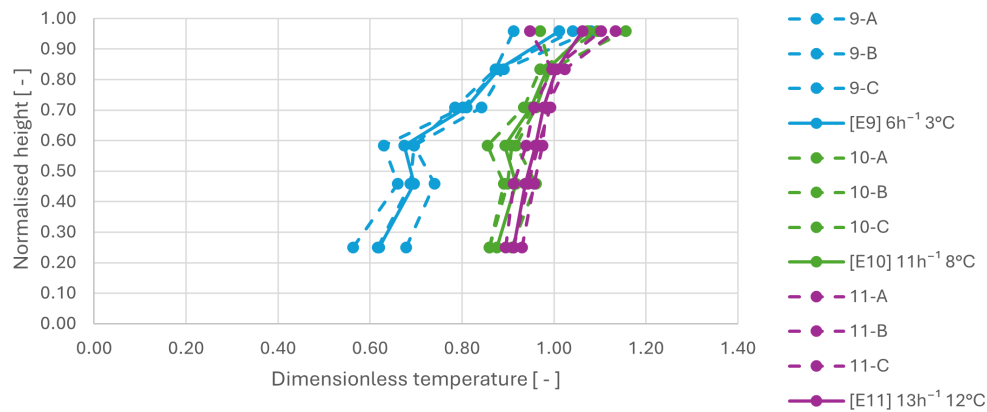


Figure C.7. Average temperature analysis for case E9, E10 and E11.

From paper by Peng et al. [2023]:

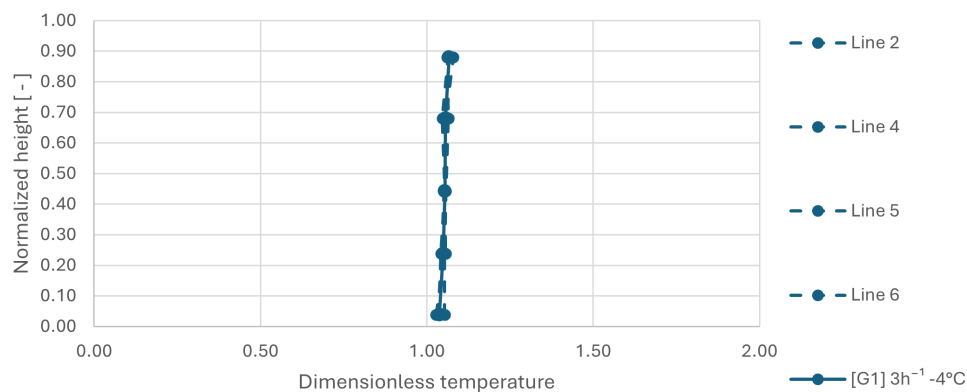


Figure C.8. Average temperature analysis for case G1.

For each study, an average temperature gradient is found to be representative of the conditions in the room when looking at the normalised temperatures. Therefore, these have been used further in the analysis.

Analysis of velocity in heating cases D

This chapter presents the analysis of the velocity in heating cases. An overview of the relevant cases, including geometry, ACH, inlet and exhaust temperatures, heat loads, and heat load placements, can be found in Table D.1.

Table D.1. Information about the cases with geometry, airflow, and temperature conditions for heating cases.

Paper	Case	Geometry [m]	ACH [h ⁻¹]	Temperatures [°C]			Heat load [W/m ²]	Placement of heat load
				Inlet	Exhaust	ΔT		
[Peng et al., 2021]	[F1] 3h ⁻¹ -4°C	2.5×4.2×3.6	3.0	26.2	22.3	-4	13	Centered
	[F2] 3h ⁻¹ -5°C	2.5×4.2×3.6	3.0	26.8	21.9	-5	13	
	[F3] 3h ⁻¹ -4°C	2.5×4.2×3.6	3.0	27.7	23.6	-4	13	
	[F4] 1.5h ⁻¹ -10°C	2.5×4.2×3.6	1.5	33.3	23.6	-10	13	
	[F5] 6h ⁻¹ -1°C	2.5×4.2×3.6	6.0	25.3	23.9	-1	13	
	[F6] 3h ⁻¹ -9°C	2.5×4.2×3.6	3.0	37.2	24.9	-9	13	
	[F7] 3h ⁻¹ -4°C	2.5×4.2×3.6	3.0	28.6	24.1	-9	0	
	[F8] 3h ⁻¹ -4°C	2.5×4.2×3.6	3.0	28.04	24	-9	7	

Placement of highest velocity

Firstly, the placement of the highest velocity has been investigated. This investigation is illustrated in Figure D.1.

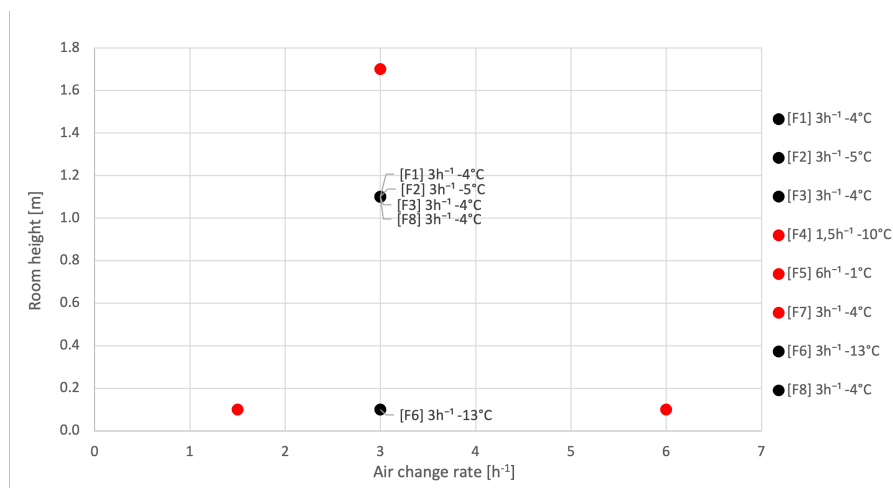


Figure D.1. Vertical placement of highest velocity vs. ACH for heating cases.

The graph with heating cases does not exhibit clear trends, as the vertical placement of the highest velocity varies depending on the ACH. There appears to be no correlation between vertical placement and temperature difference.

Correlation between max air velocities and ACH or ΔT

For the heating cases, the ACH does not vary much between the few available cases. This can be seen in Figure D.2 where the maximum velocity is plotted against the ACH. In Figure D.3, the maximum velocity against the temperature difference has been plotted.

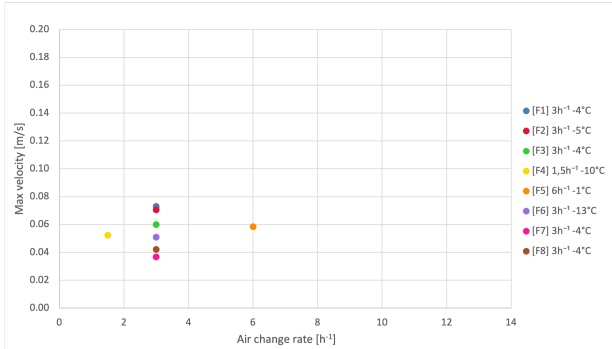


Figure D.2. ACH vs. max velocity for heating cases.

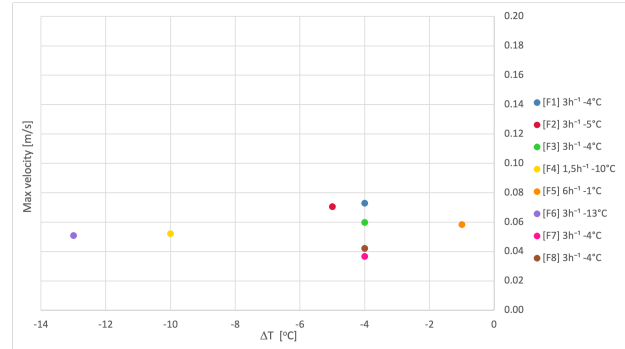


Figure D.3. Temperature difference vs. max velocity for heating cases.

With only a few cases, it is hard to draw definitive conclusions about the general trend, as additional factors such as airflow patterns, room layout, and temperature distribution could influence the results. More data would be needed to confirm whether this trend holds consistently in different heating scenarios. Unlike cooling, where a higher ΔT increases the maximum velocity, heating does not appear to have the same effect.

Correlation between max air velocities and Reynolds number

The maximum velocity has also been plotted against the Re number, which can be seen in Figure D.4

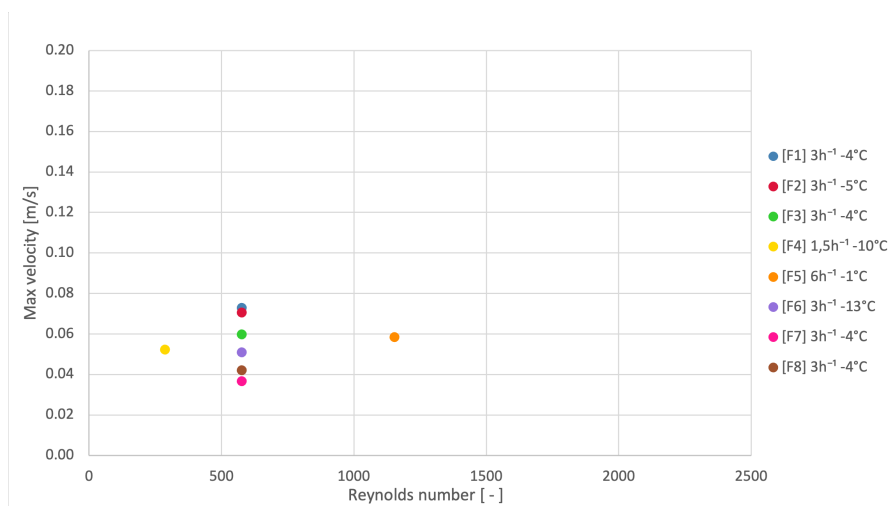


Figure D.4. Re number vs. max velocity for heating cases.

No correlation is found as not enough data points with varying ACH are provided. The velocity might be too low to find any correlation, and further datapoints thereby need to be investigated to draw any meaningful conclusions.

Selection of turbulence model E

Some studies have tried modelling high heat load in a room with DCV. Due to the unstable nature of such a system, this has not been successful with a steady-state model. In this chapter, the aim is to make the model from Zhang [2016] transient, to see how this would affect the results.

E.1 Overview of CFD models from papers

Most studies use a steady-state model when simulating DCV. Only two papers were found that used a transient model. In a study by Mikeska and Fan [2015], transient models are recommended when using CFD models for simulating a space with DCV. The reason they found the transient model to be most accurate was that it accounts for the fluctuation in airflow by using average values among the different time steps. Nocente et al. [2020] also argue that a transient model is preferable, as it can better capture the dynamic behaviour of airflow, maintain numerical stability, and offer more detailed flow visualisations. These advantages support a more thorough analysis of system performance and contribute to the effective evaluation and optimisation of DCV systems.

In Table E.1, the different viscous models used in the literature are shown. Here, it can be seen that most studies use a steady-state model.

Table E.1. Overview of papers with CFD, steady/transient, and viscous model.

Source	Steady/Transient	Turbulence model
[Zhang et al., 2016]	Steady state	RNG k- ϵ
[Chodor and Taradajko, 2013]	Steady state	Realizable k- ϵ
[Kristensen and Jensen, 2015]	Steady state	SST k- ω
[Mikeska and Fan, 2015]	Transient	LES
[Fan et al., 2013]	-	RNG k- ϵ
[Nocente et al., 2020]	Transient	Standard k- ϵ
[Wirowski et al., 2024]	-	Standard k- ϵ
[Zhang, Zhang, Bai and Wen, 2023]	-	Standard k- ϵ
[Peng et al., 2023]	Steady state	SST k- ω
[Zhang, Zhang, Zhang, Xuan and Liu, 2023]	-	Standard k- ϵ
[Zhang et al., 2021]	Steady state	Standard k- ϵ
[Sadeghian et al., 2022]	Steady state	Realizable k- ϵ
[Peng et al., 2023]	Steady state	SST k- ω

E.2 Comparison of turbulence models

Most papers use the Standard $k-\epsilon$, SST $k-\omega$ or RNG $k-\epsilon$. These are tested in the model by Zhang et al. [2016]. The results are compared to experimental results from the same paper. Each measurement point is at the same height in the different positions, and this value is compared to the value at the same height in the CFD model. The deviation between each measurement point and the CFD results with RNG $k-\epsilon$, SST $k-\omega$ and Standard $k-\epsilon$ is compared.

The velocity in the first two measurement lines, A and B, closest to the inlet are shown in Table E.2 and E.3. The average deviation for each turbulence model is found and compared.

Table E.2. Comparison of turbulence models with study by Zhang et al. [2016] at measurement line A.

Height [m]	[Zhang et al., 2016] [m/s]	RNG [m/s]	SST [m/s]	Standard [m/s]
0.1	0.0866	-0.0396	-0.0437	-0.0241
0.7	0.0403	0.0050	-0.0397	0.0164
1.1	0.0356	-0.0366	-0.0018	-0.0171
1.7	0.0320	-0.0029	-0.0054	0.0065
2.3	0.1162	-0.0346	-0.0664	-0.0733
		-0.0218	-0.0314	-0.0183

Table E.3. Comparison of turbulence models with study by Zhang et al. [2016] at measurement line B.

Height [m]	[Zhang et al., 2016] [m/s]	RNG [m/s]	SST [m/s]	Standard [m/s]
0.1	0.0669	-0.0720	-0.0781	-0.0212
0.7	0.0508	-0.0456	-0.0556	-0.0219
1.1	0.0483	-0.0001	-0.0173	-0.0275
1.7	0.0533	0.0296	0.0423	0.0194
2.3	0.1785	-0.0770	-0.0626	-0.0821
		-0.0330	-0.0342	-0.0267

Based on the first two positions, the Standard $k-\epsilon$ turbulence model is the one that fits best with the measurement data. Next, the last two positions, C and D, furthest away from the inlet, are shown in Table E.4 and E.5.

Table E.4. Comparison of turbulence models with study by Zhang et al. [2016] at measurement line C.

Height [m]	[Zhang et al., 2016] [m/s]	RNG [m/s]	SST [m/s]	Standard [m/s]
0.1	0.0504	-0.0796	-0.0439	-0.0377
0.7	0.0720	-0.0290	0.0014	-0.0075
1.1	0.0504	-0.0157	-0.0023	-0.0254
1.7	0.0396	-0.0092	-0.0179	0.0057
2.3	0.1500	-0.0520	-0.0491	-0.1106
		-0.0371	-0.0224	-0.0351

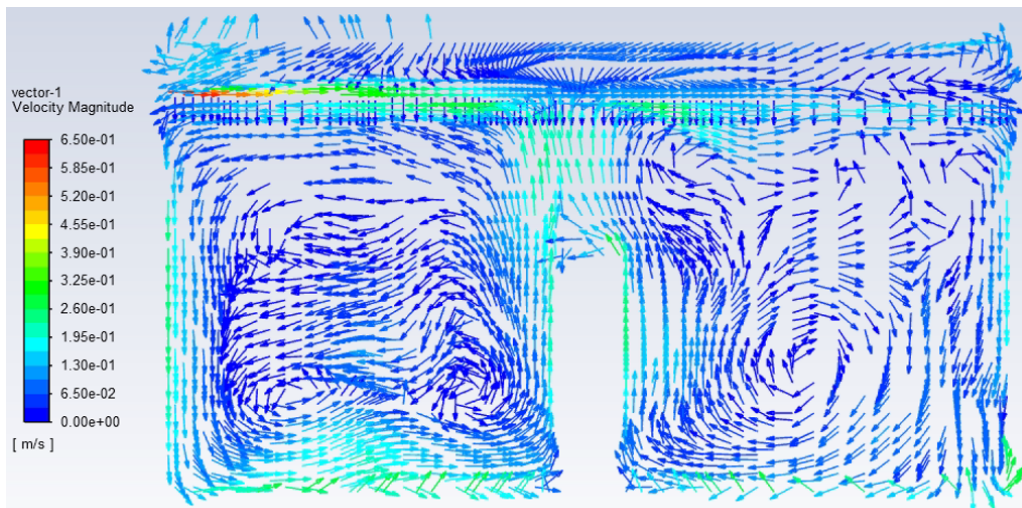
Table E.5. Comparison of turbulence models with study by Zhang et al. [2016] at measurement line D.

Height [m]	[Zhang et al., 2016] [m/s]	RNG [m/s]	SST [m/s]	Standard [m/s]
0.1	0.0449	-0.0728	-0.0767	-0.0433
0.7	0.0474	-0.0309	-0.0029	-0.0665
1.1	0.0389	-0.0258	-0.0169	-0.0461
1.7	0.0474	0.0120	-0.0084	0.0126
2.3	0.0510	-0.1325	-0.0896	-0.1006
		-0.0500	-0.0389	-0.0488

The data from the last two positions show a different result. The SST $k-\omega$ turbulence model fits best with the data. Overall, the different turbulence models show similar results when averaged across all heights and positions, but the Standard $k-\epsilon$ and SST $k-\omega$ turbulence models are the two best.

To determine which model is chosen, a vector velocity plot is made for each of the turbulence models. The model that best suits the theory behind air movement in the room determines the selection of the turbulence model.

The RNG $k-\epsilon$ turbulence model can be found in Figure E.1.

**Figure E.1.** Velocity distribution with a RNG $k-\epsilon$ turbulence model.

This model shows clear circulation in the right part of the room, furthest away from the inlet. This is similar to the airflow seen in other literature. The airflow pattern in the plenum closest to the inlet is however not as expected. The flow does not seem to have the expected flow pattern of an air jet. Next, the $k-\omega$ SST turbulence model can be found in Figure E.2.

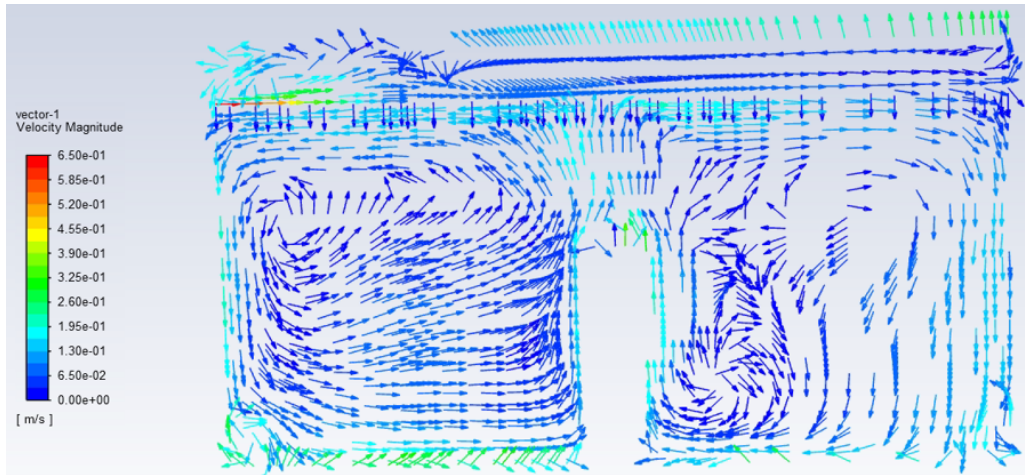


Figure E.2. Velocity distribution with a $K-\omega$ SST turbulence model.

The air movement in this model does not follow the theory. The air movement separated by the central heat source does not show similar tendencies as expected. The airflow patterns on the left and right sides of the figure are very different, which indicates that the turbulence model does not show the expected results. The airflow in the plenum shows a very different pattern compared with the other two models. Lastly, the Standard $k-\epsilon$ turbulence model can be found in Figure E.3.

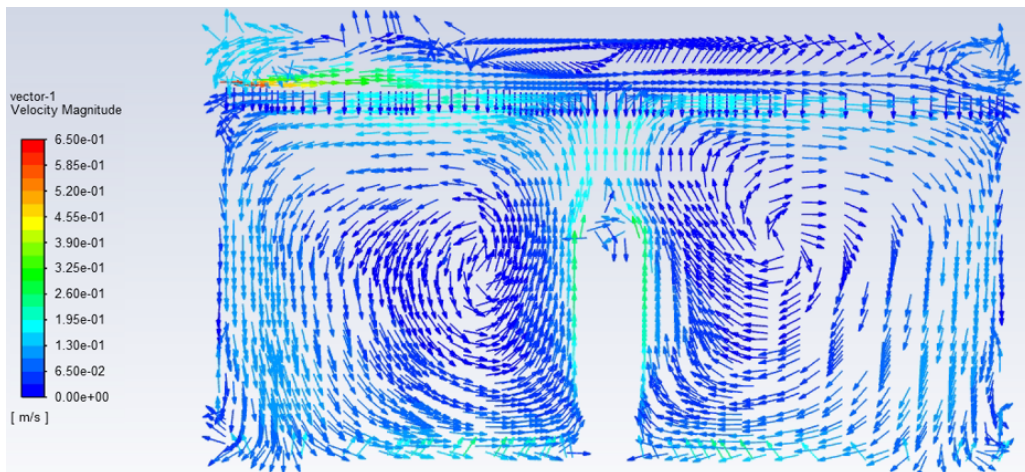


Figure E.3. Velocity distribution with a Standard $k-\epsilon$ turbulence model.

The Standard $k-\epsilon$ is the model that shows the most correct streamlines according to the DCV theory. The model shows clear similarities to those found in smoke experiments. Here, the thermal buoyancy from the occupant is present, and two vortices are present on each side of the centred heat load. This model is also the one that showed the closest relation to the measurement data, and thereby, this turbulence model is the one chosen. Next, the wall treatment of the different turbulence models needs to be investigated.

E.3 Analysis of wall treatment

The way the model is set up increases the surface temperature to account for the radiant heat load. Large gradients are also seen in the results, especially near the walls. This makes wall treatment an important factor to ensure the most reliable results. Therefore, the wall treatment is analysed in this section, where two approaches were tested. Enhanced wall treatment, which offers high accuracy in cases with strong gradients and heat transfer, provided that the mesh near the wall is sufficiently fine, ideally, the y^+ value should be close to 1, but can be as high as 5. However, this method requires more computational resources. In comparison, non-equilibrium wall functions are better suited for complex flows with separation and reattachment. They work well with coarser meshes, where the first cell lies within the logarithmic region with y^+ values between 30 and 300. This makes this method more efficient while still providing good accuracy in challenging flow conditions. [ANSYS, 2023, 2025] In Figure E.4, the y^+ can be seen for the room.

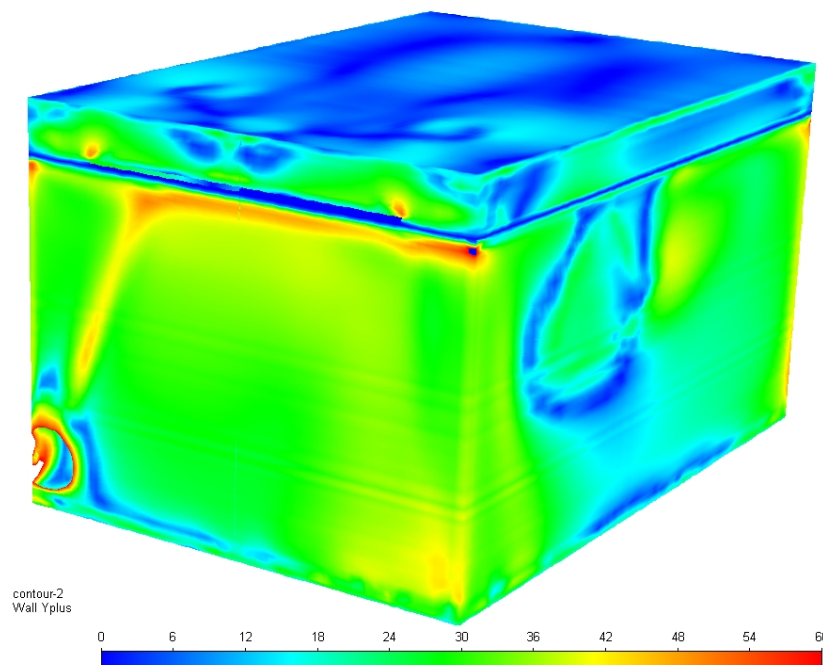


Figure E.4. Visualisation of y^+ on south wall of model.

From the figure, it can be seen that the y^+ values range mostly between 20 and 30 at the boundaries. In Figure E.5 and E.6, the comparison of the enhanced and equilibrium wall treatment is made at two points in the room.

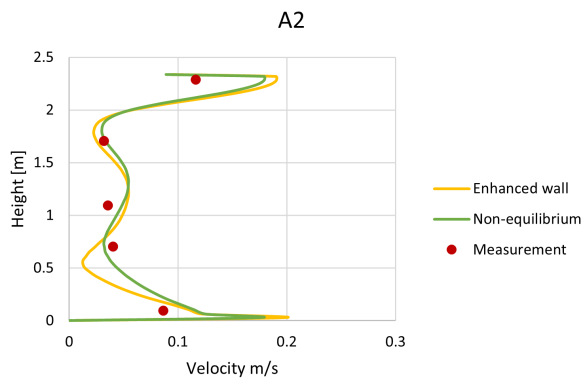


Figure E.5. Wall treatment comparison, location A.

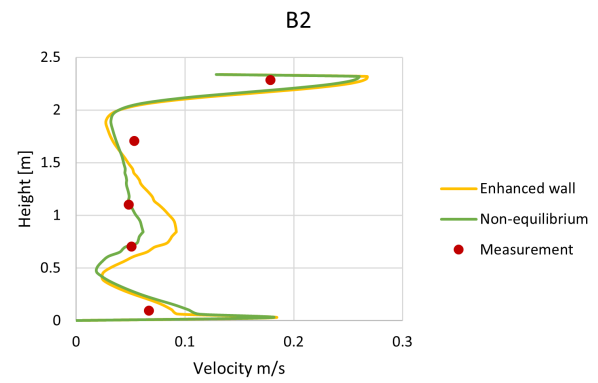


Figure E.6. Wall treatment comparison, location B.

From this investigation, it is chosen to use the Standard $k-\epsilon$ with the non-equilibrium Wall Function in further calculations.

Temperature sections F

Temperature section for case 1.

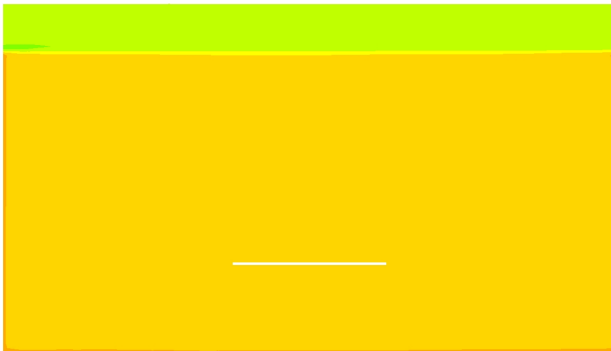


Figure F.1. Middle of room.

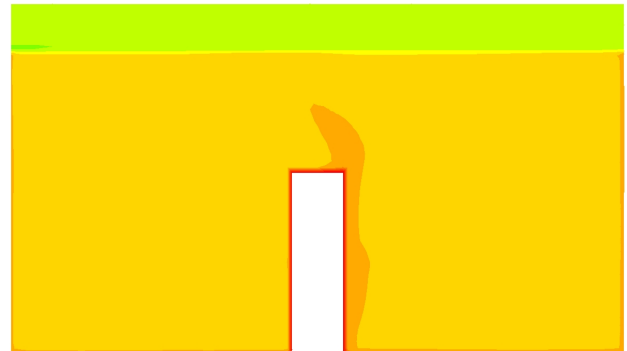


Figure F.2. Through occupant.

Temperature section for case 2.

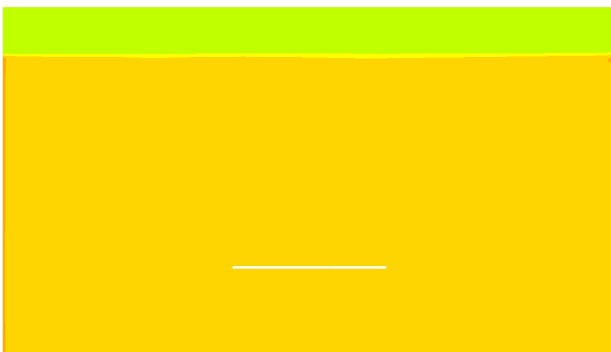


Figure F.3. Middle of room.

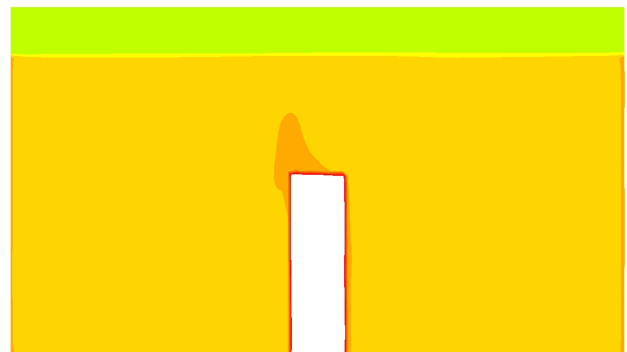


Figure F.4. Through occupant.

Temperature section for case 3.



Figure F.5. Middle of room.

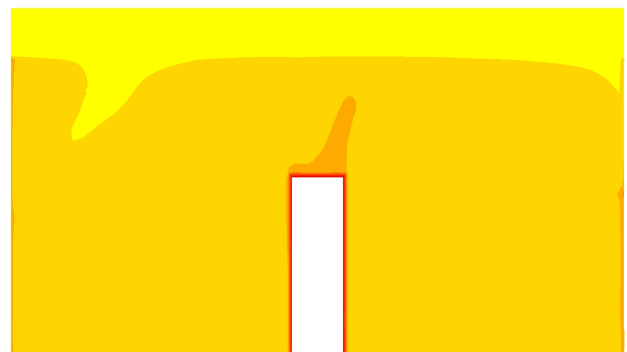


Figure F.6. Through occupant.



Temperature section for case 4.

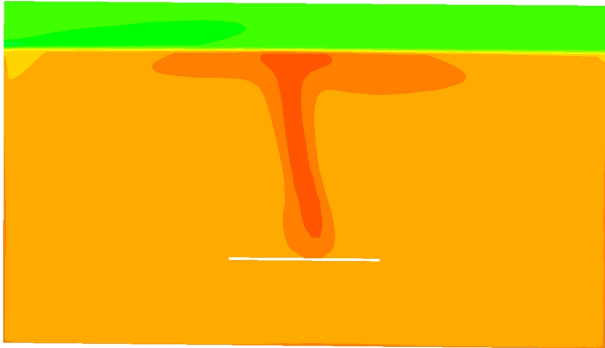


Figure F.7. Middle of room.

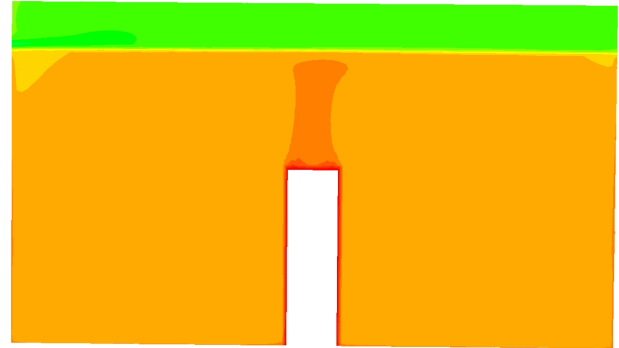


Figure F.8. Through occupant.

Temperature section for case 5.

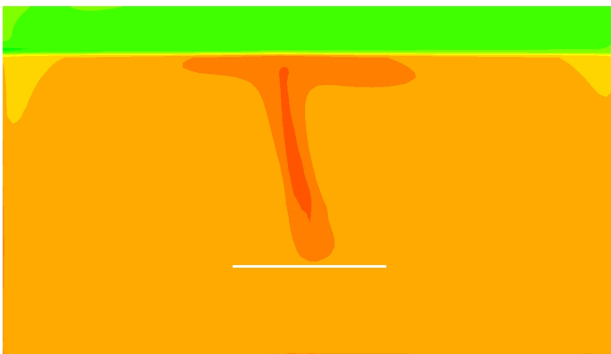


Figure F.9. Middle of room.

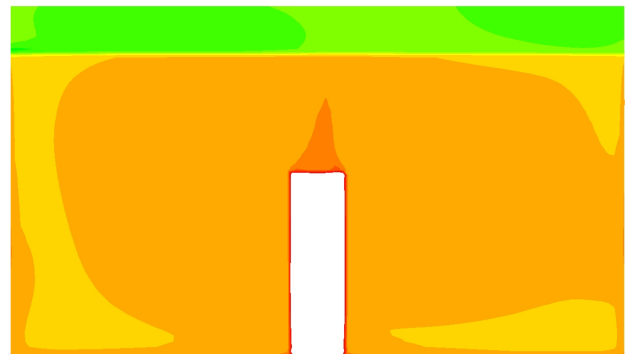


Figure F.10. Through occupant.

Temperature section for case 6.

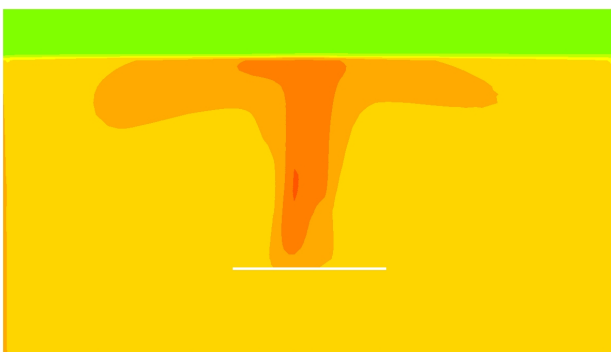


Figure F.11. Middle of room.

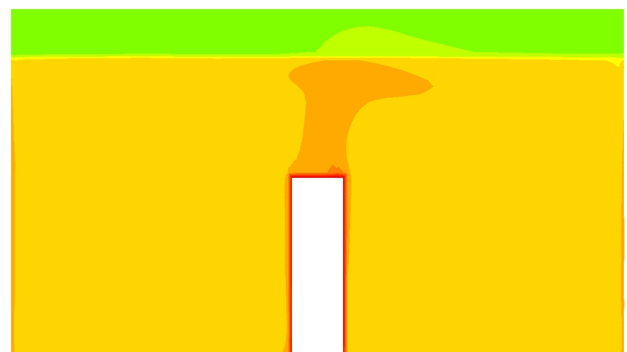


Figure F.12. Through occupant.



Temperature section for case 7.

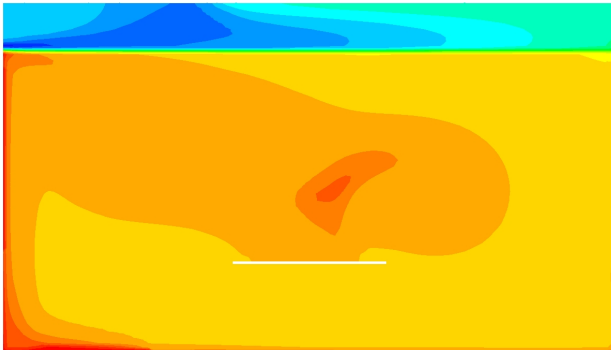


Figure F.13. Middle of room.

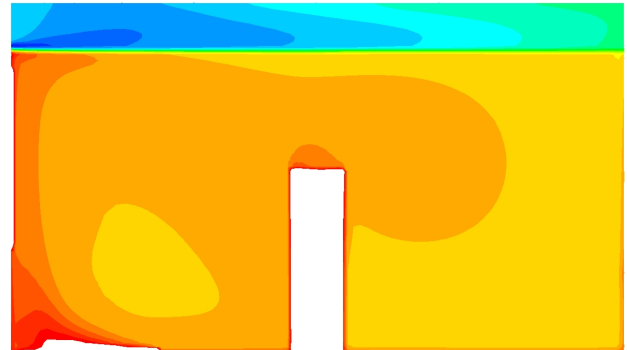


Figure F.14. Through occupant.

Temperature section for case 8.

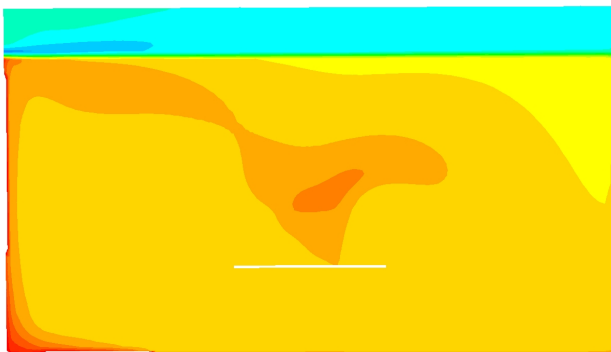


Figure F.15. Middle of room.

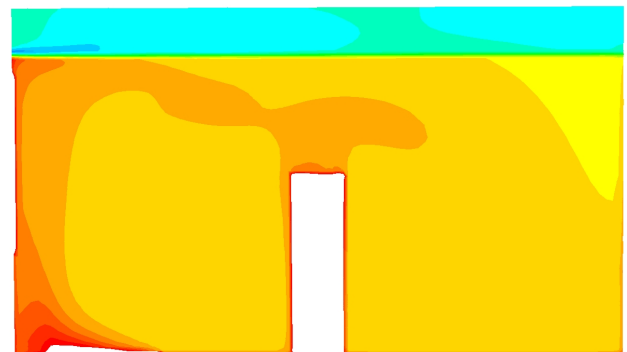


Figure F.16. Through occupant.

Temperature section for case 9.

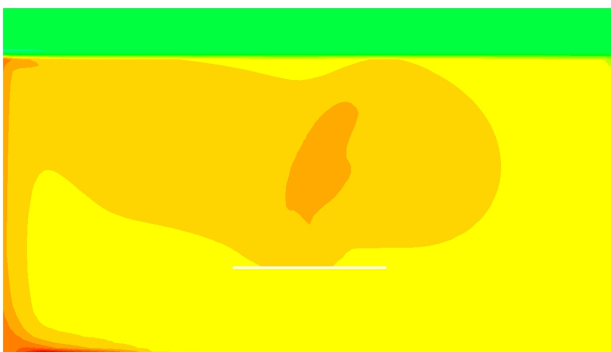


Figure F.17. Middle of room.



Figure F.18. Through occupant.



Temperature section for case 10.

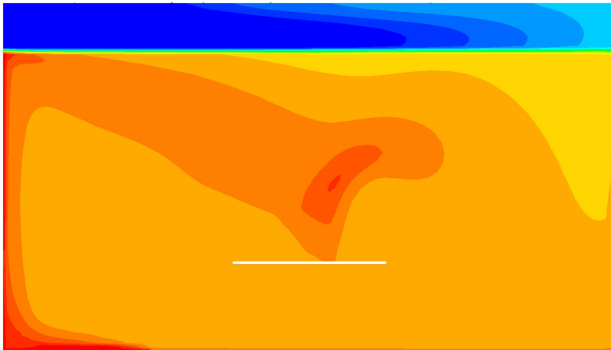


Figure F.19. Middle of room.

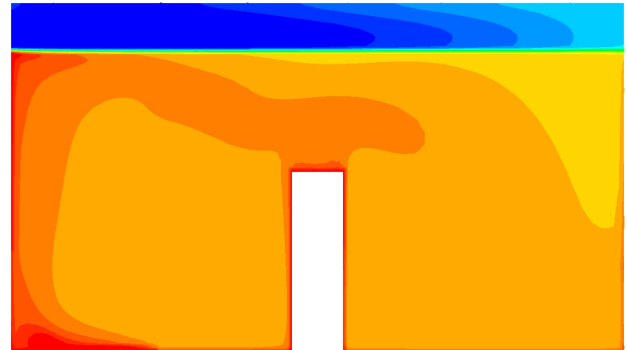


Figure F.20. Through occupant.

Temperature section for case 11.

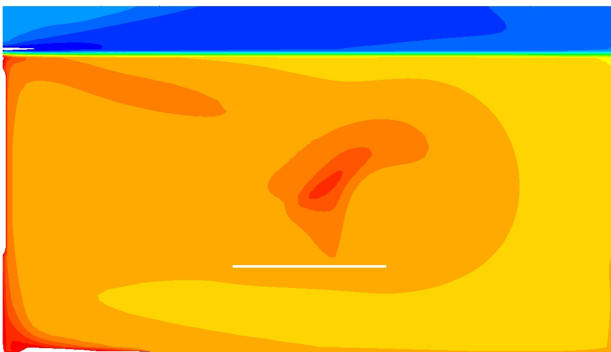


Figure F.21. Middle of room.



Figure F.22. Through occupant.

Temperature section for case 12.

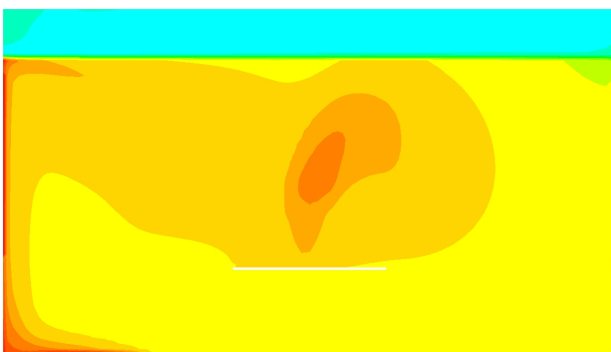


Figure F.23. Middle of room.

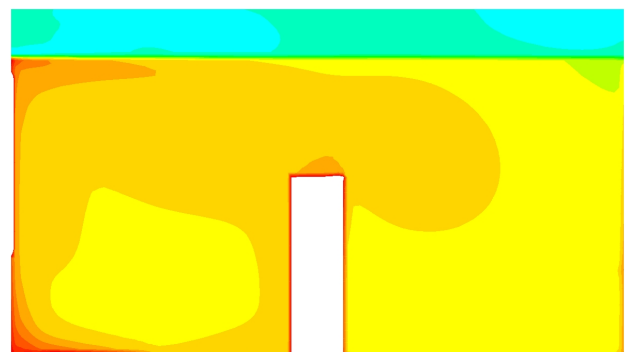


Figure F.24. Through occupant.

Velocity sections G

Velocity section for case 1.

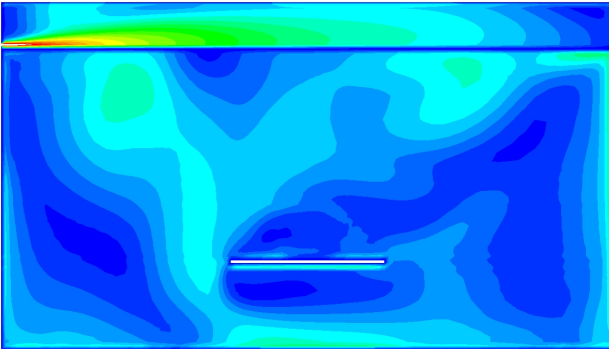


Figure G.1. Middle of room.

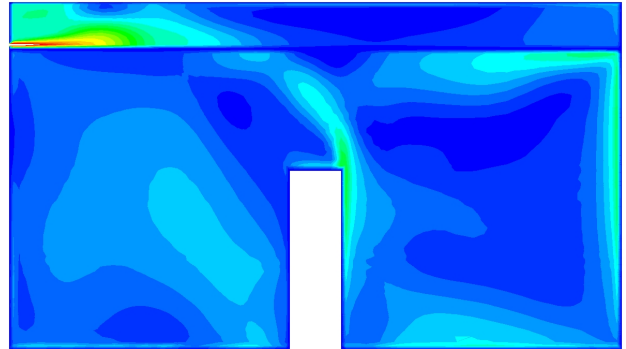


Figure G.2. Through occupant.

Velocity section for case 2.

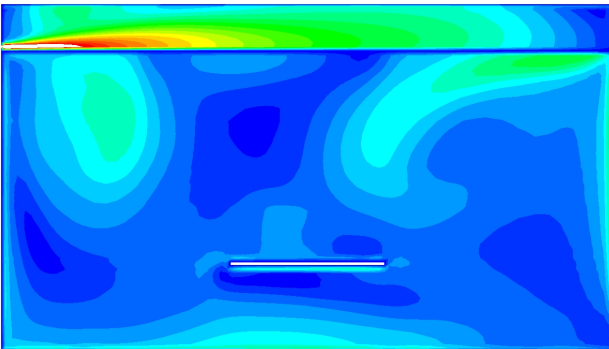


Figure G.3. Middle of room.

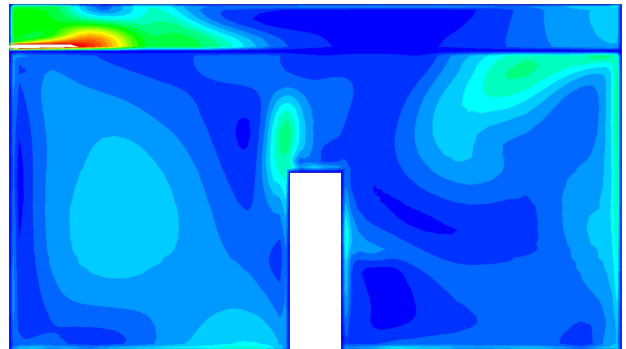


Figure G.4. Through occupant.

Velocity section for case 3.

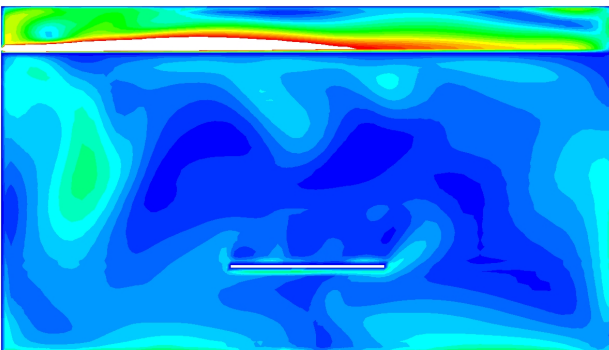


Figure G.5. Middle of room.

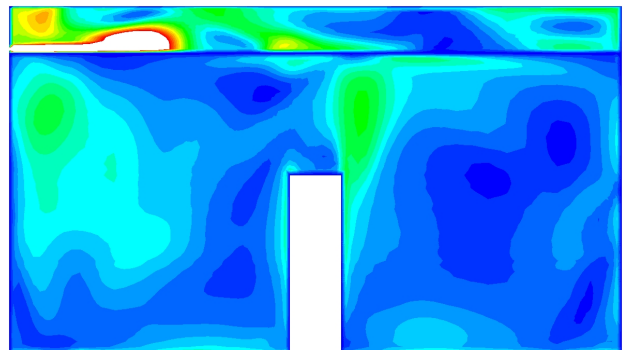
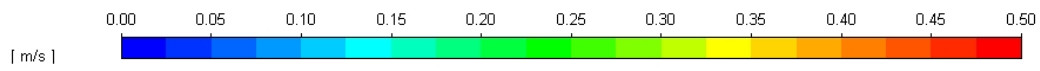


Figure G.6. Through occupant.



Velocity section for case 4.

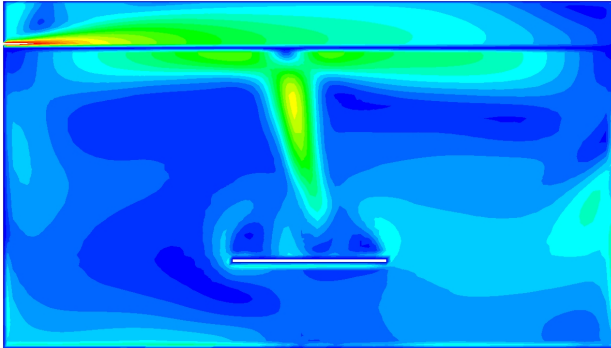


Figure G.7. Middle of room.

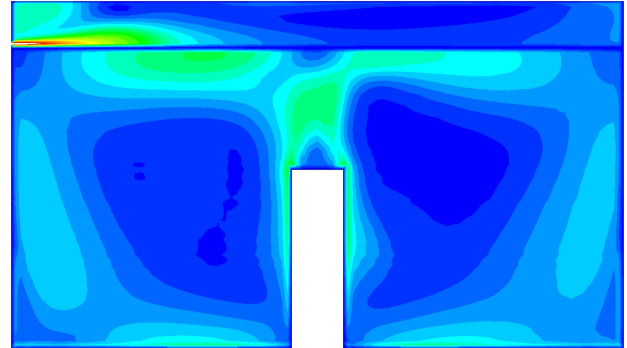


Figure G.8. Through occupant.

Velocity section for case 5.

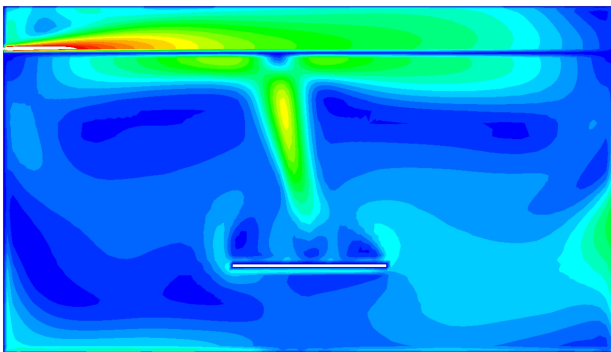


Figure G.9. Middle of room.

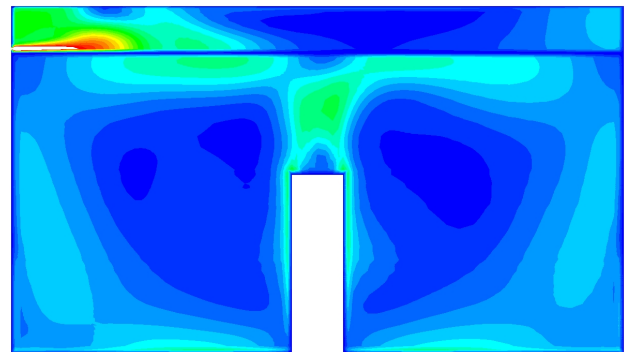


Figure G.10. Through occupant.

Velocity section for case 6.

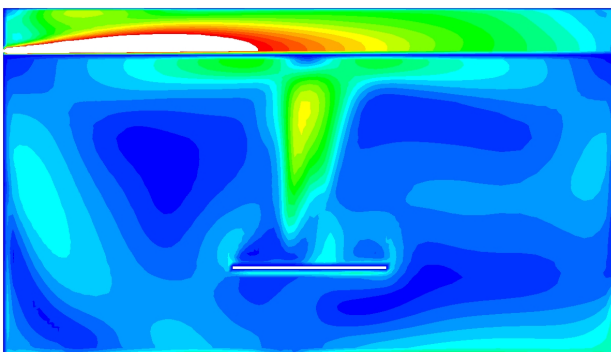


Figure G.11. Middle of room.

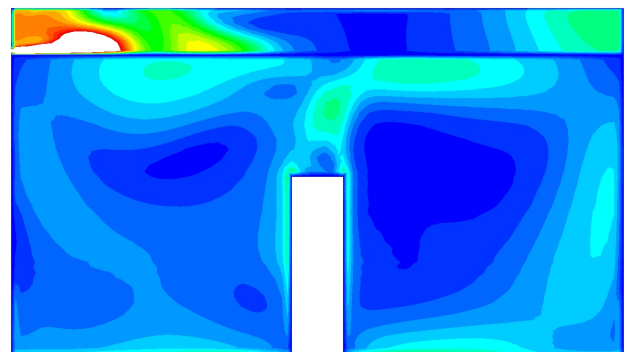
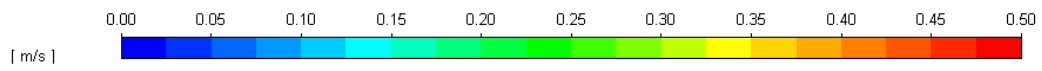


Figure G.12. Through occupant.



Velocity section for case 7.

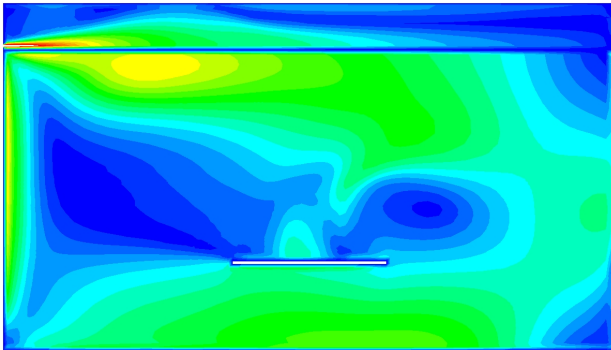


Figure G.13. Middle of room.

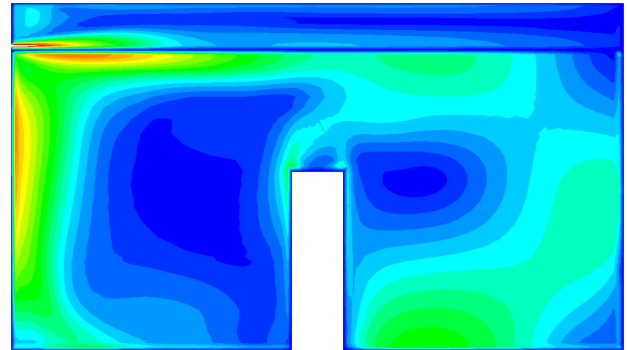


Figure G.14. Through occupant.

Velocity section for case 8.

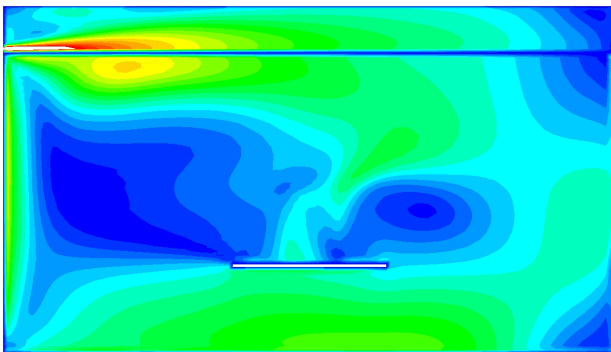


Figure G.15. Middle of room.

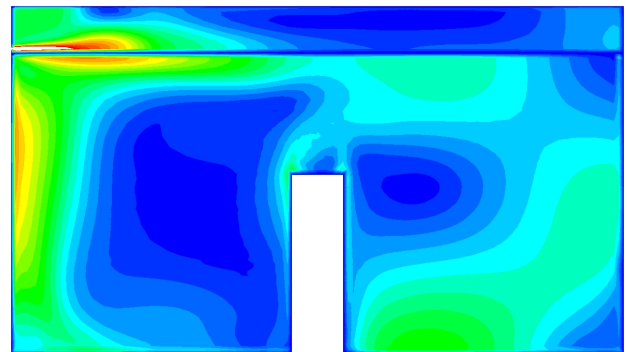


Figure G.16. Through occupant.

Velocity section for case 9.

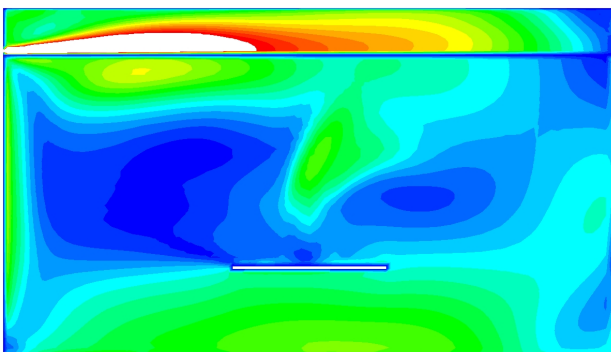


Figure G.17. Middle of room.

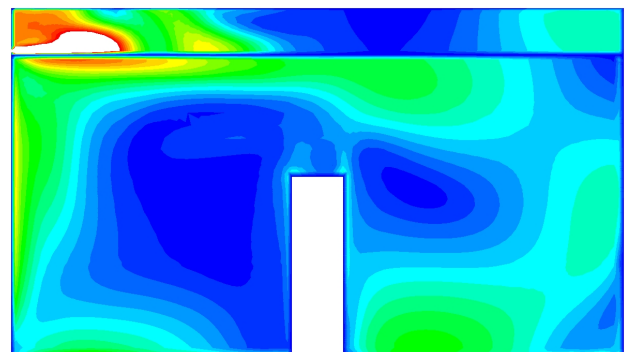
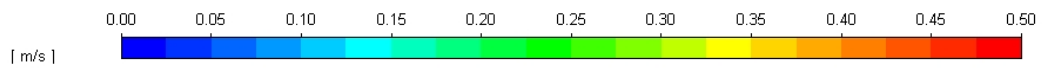


Figure G.18. Through occupant.



Velocity section for case 10.

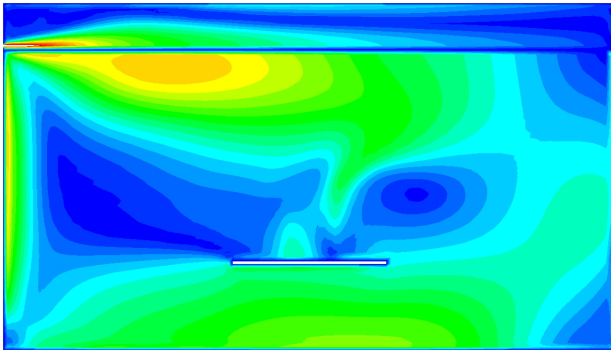


Figure G.19. Middle of room.

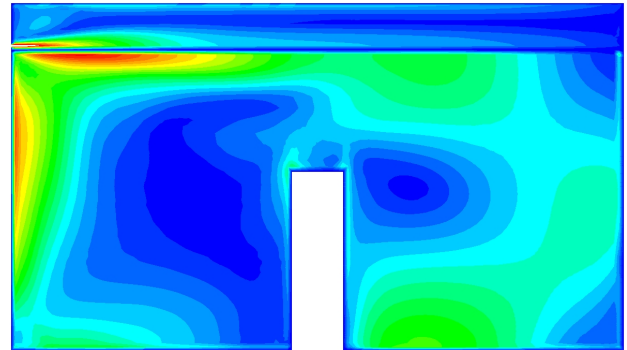


Figure G.20. Through occupant.

Velocity section for case 11.

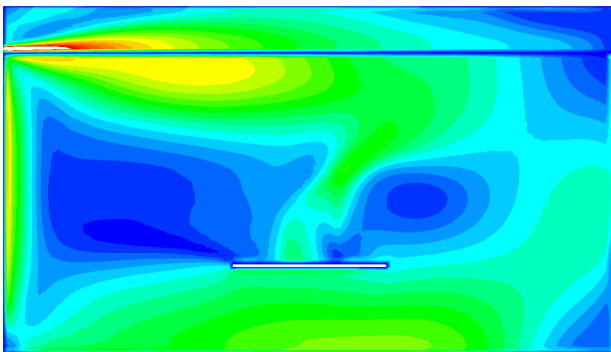


Figure G.21. Middle of room.

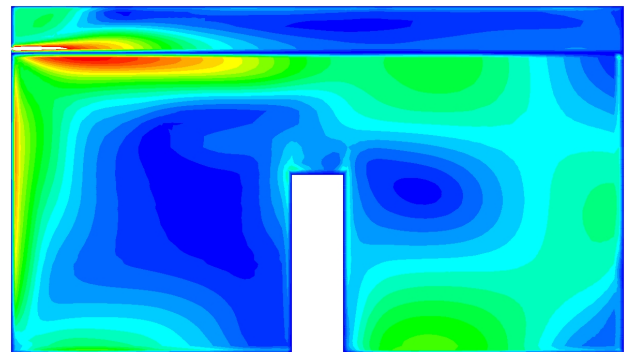


Figure G.22. Through occupant.

Velocity section for case 12.

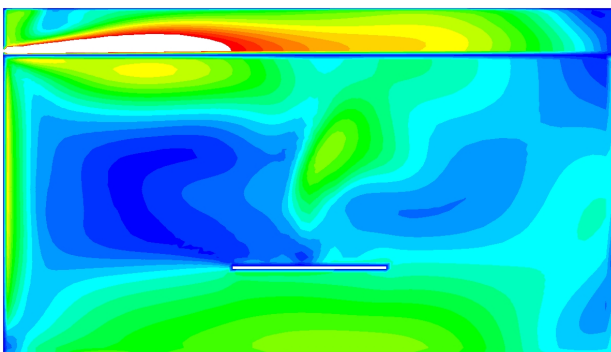


Figure G.23. Middle of room.

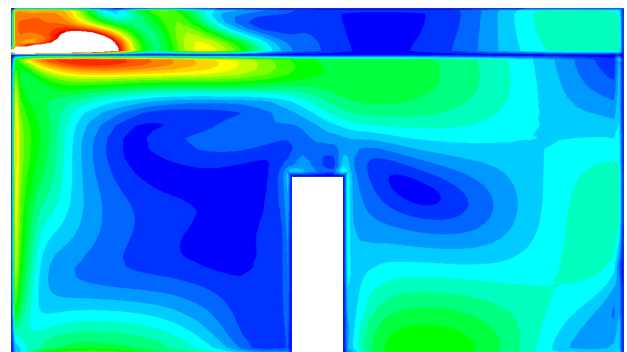


Figure G.24. Through occupant.

Path lines H

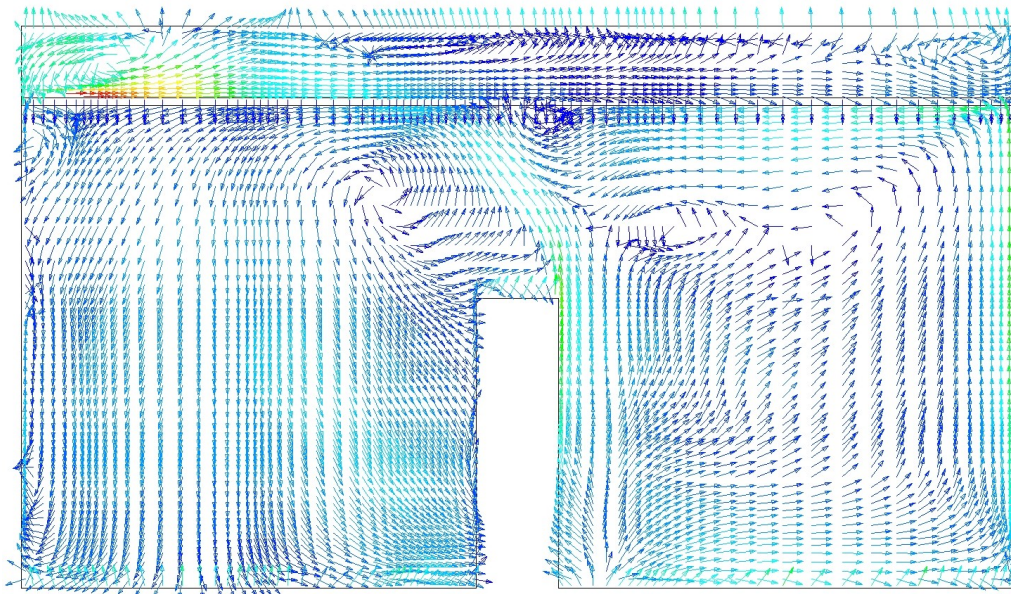


Figure H.1. Path lines through occupant section for case 1.

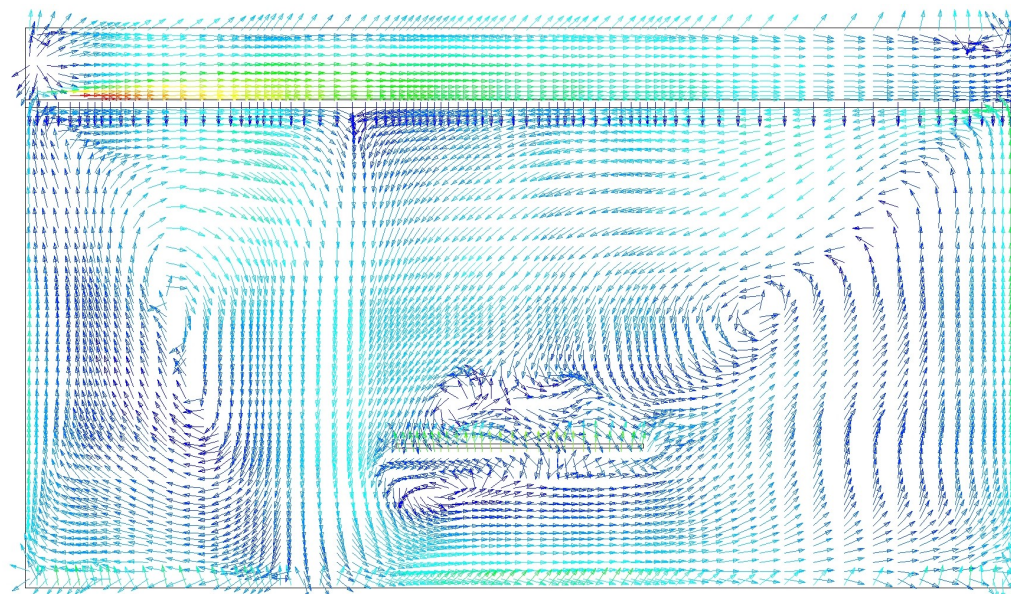
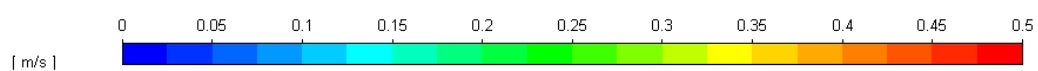


Figure H.2. Path lines through table section for case 1.



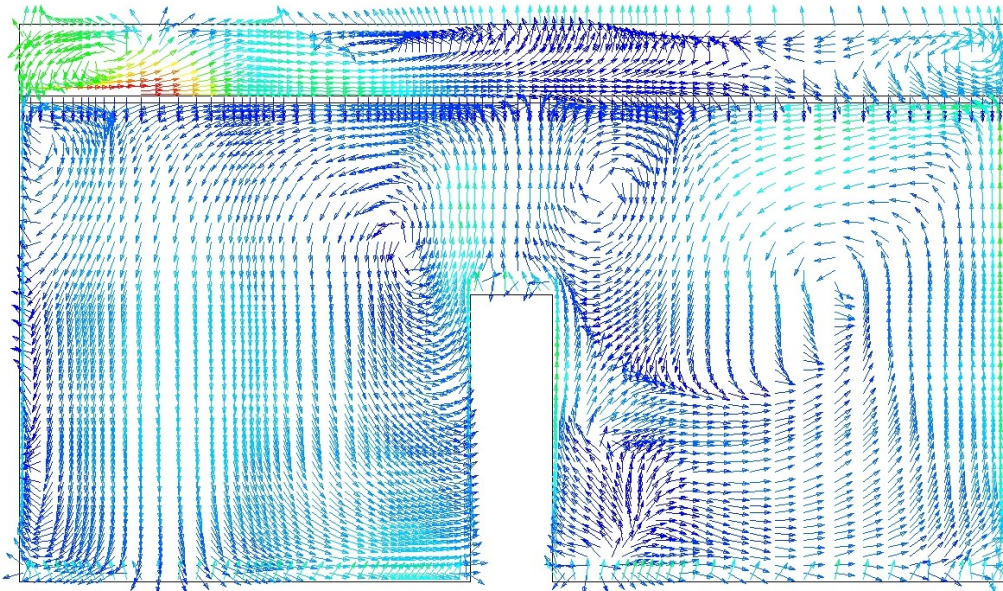


Figure H.3. Path lines through occupant section for case 2.

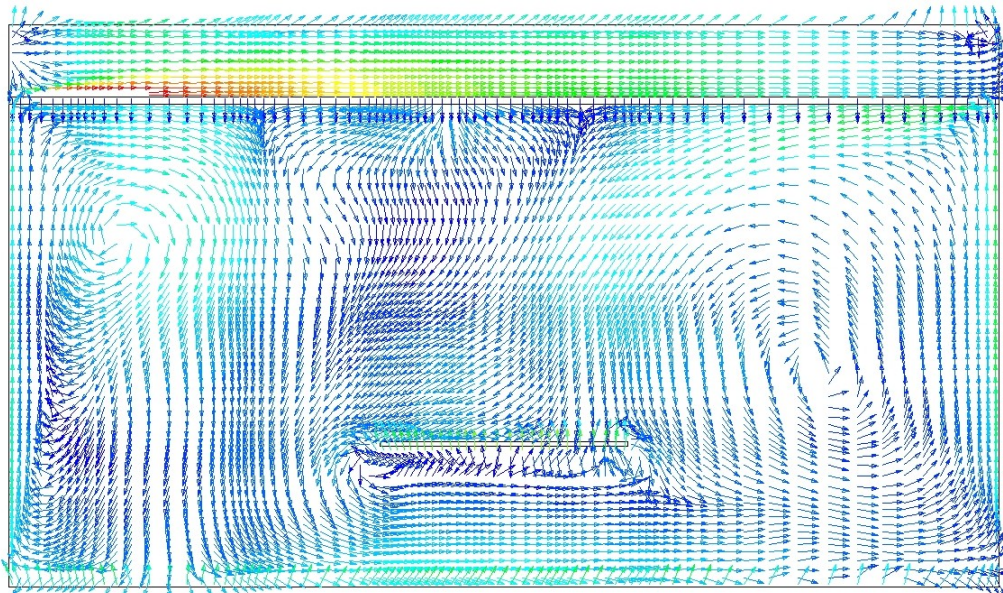


Figure H.4. Path lines through table section for case 2.



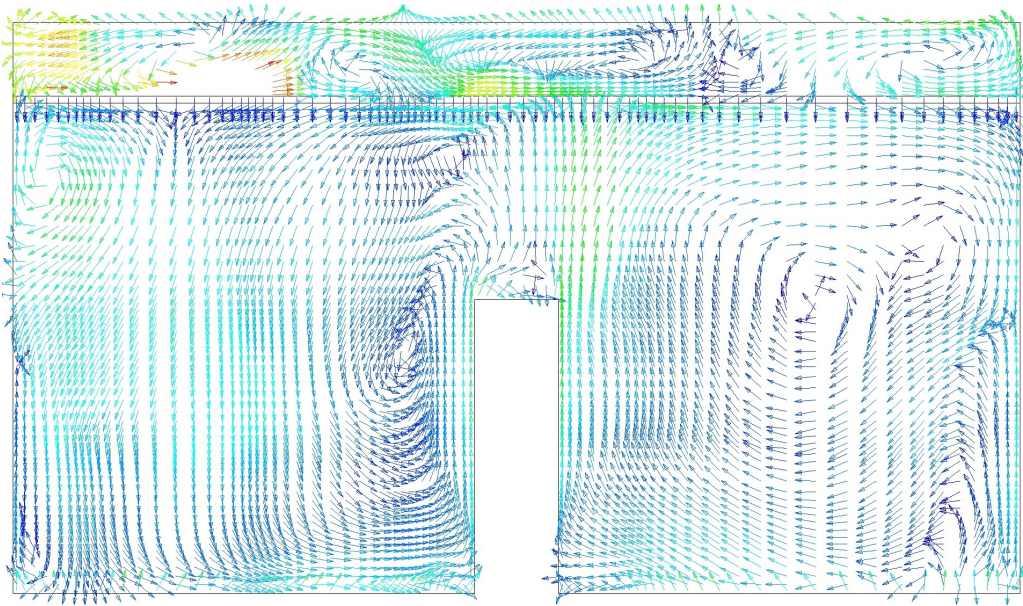


Figure H.5. Path lines through occupant section for case 3.

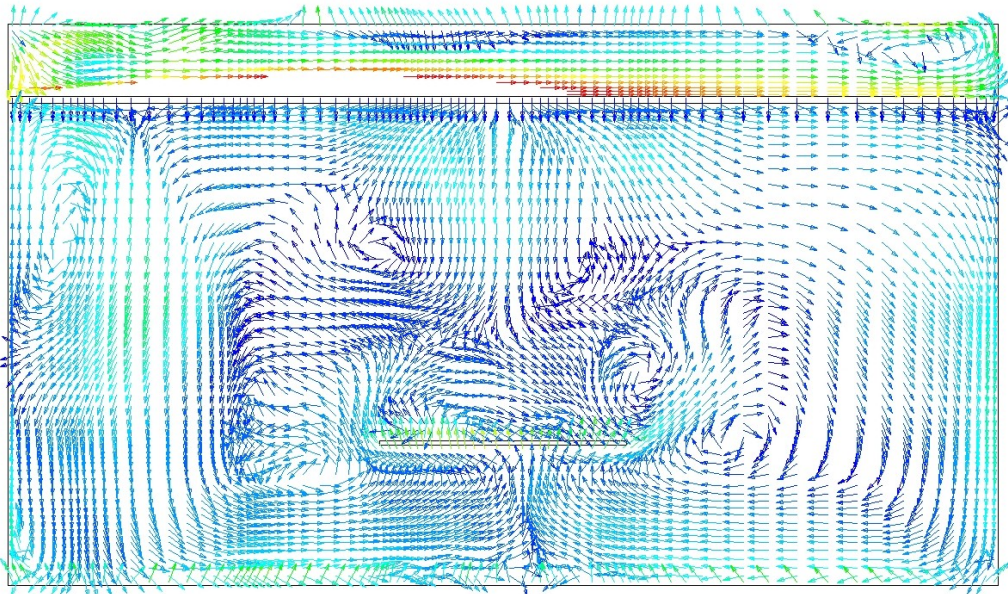
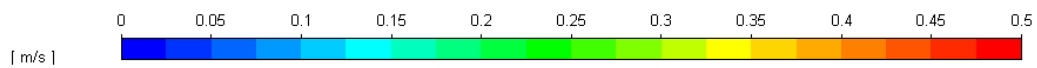


Figure H.6. Path lines through table section for case 3.



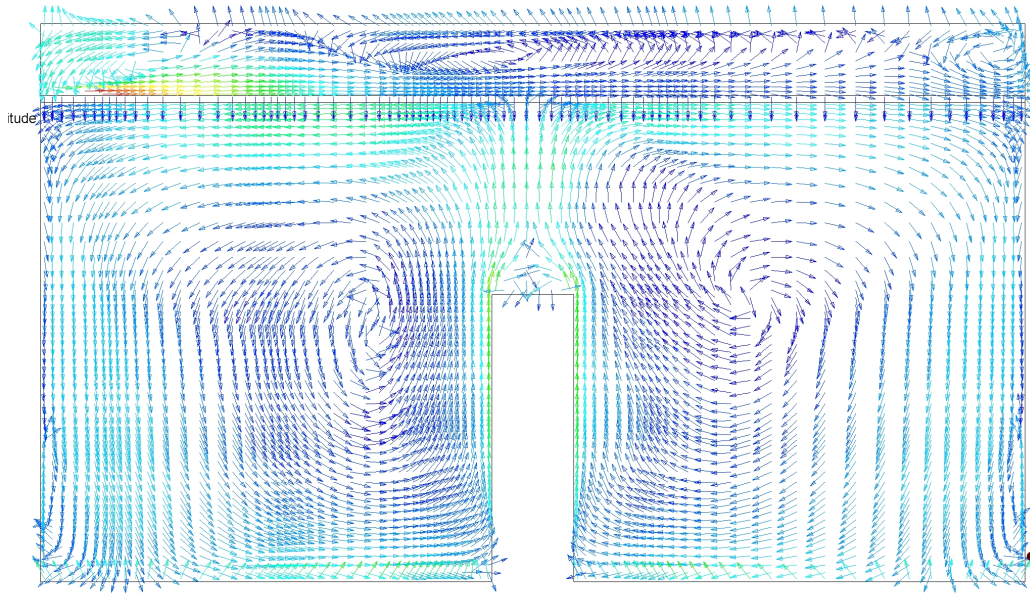


Figure H.7. Path lines through occupant section for case 4.

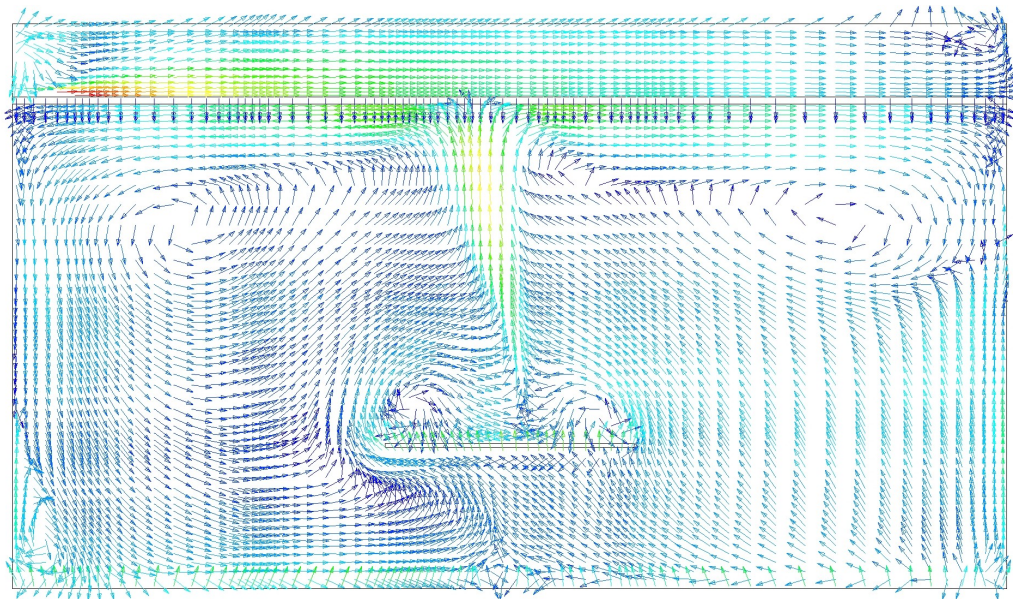
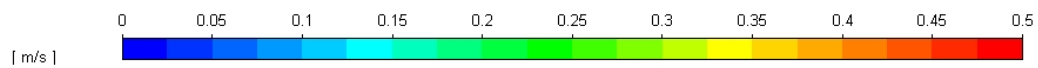


Figure H.8. Path lines through table section for case 4.



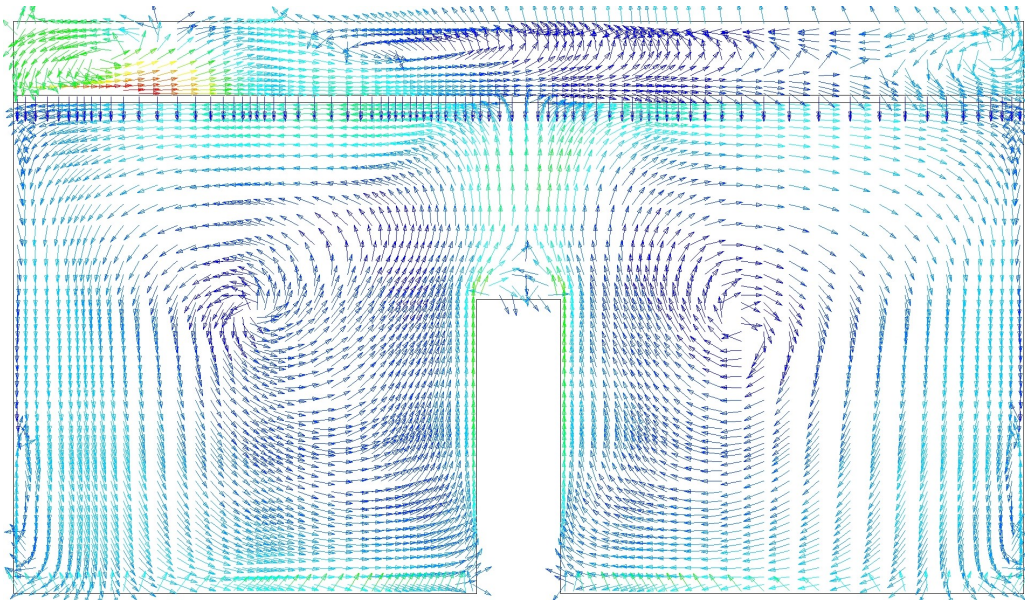


Figure H.9. Path lines through occupant section for case 5.

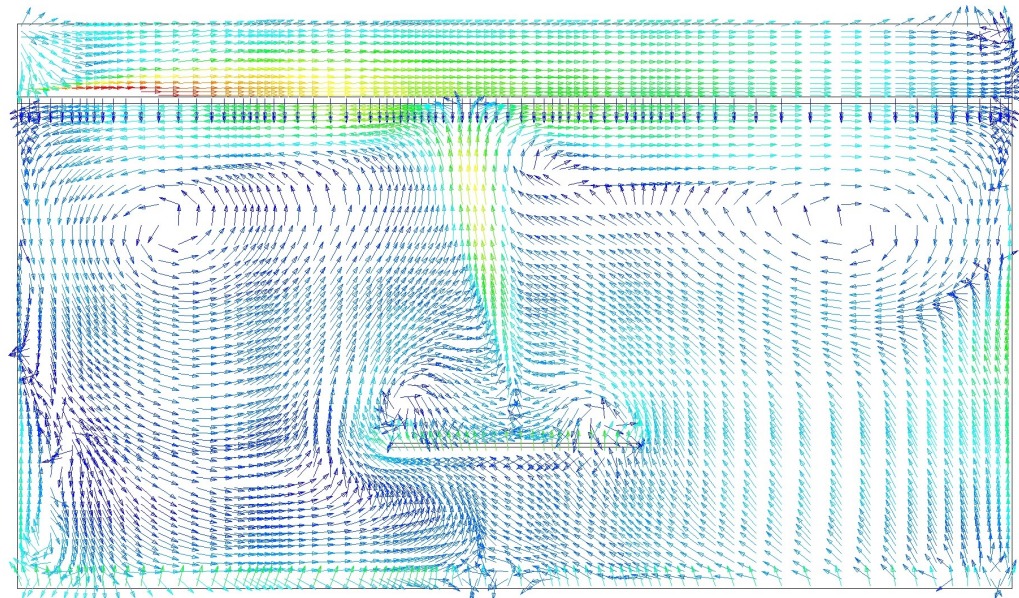


Figure H.10. Path lines through table section for case 5.



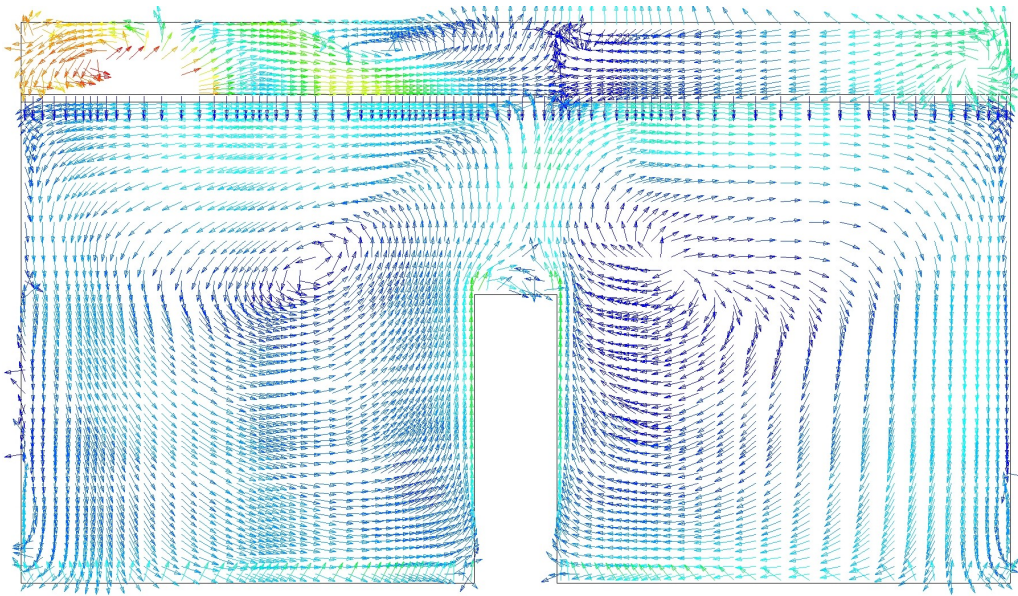


Figure H.11. Path lines through occupant section for case 6.

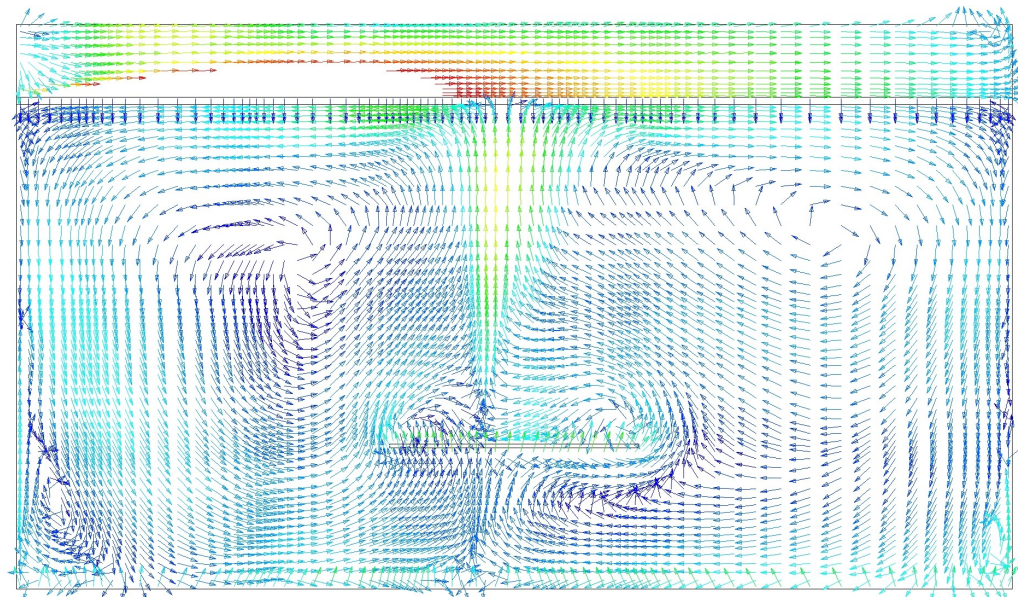
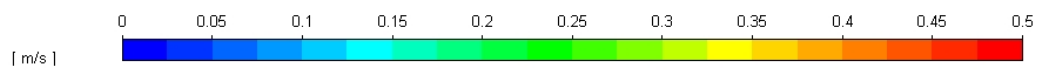


Figure H.12. Path lines through table section for case 6.



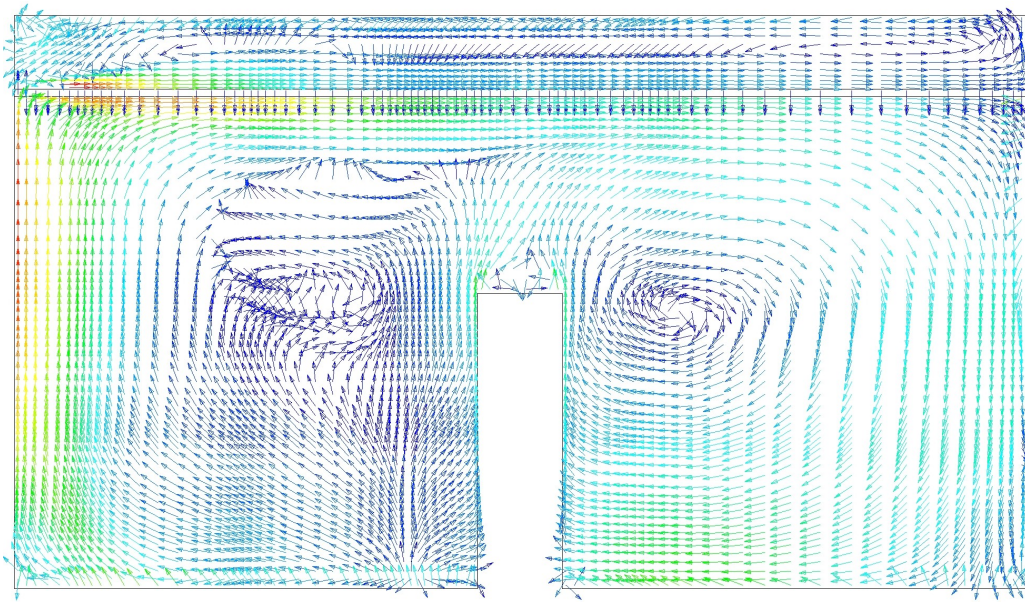


Figure H.13. Path lines through occupant section for case 7.

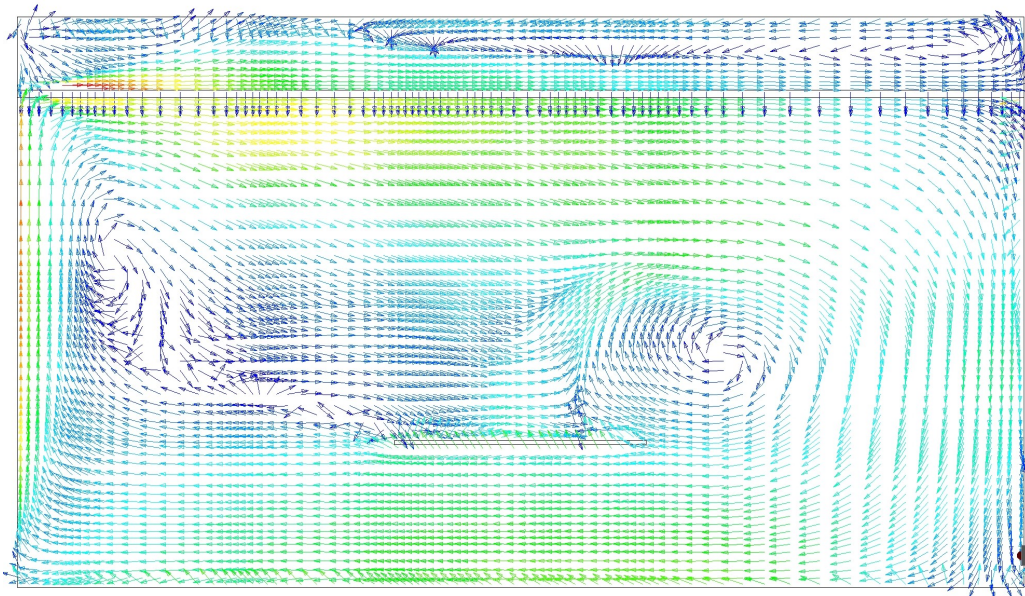
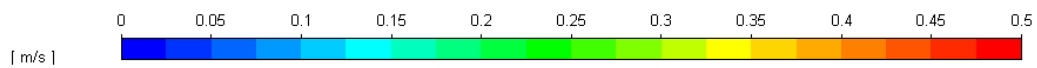


Figure H.14. Path lines through table section for case 7.



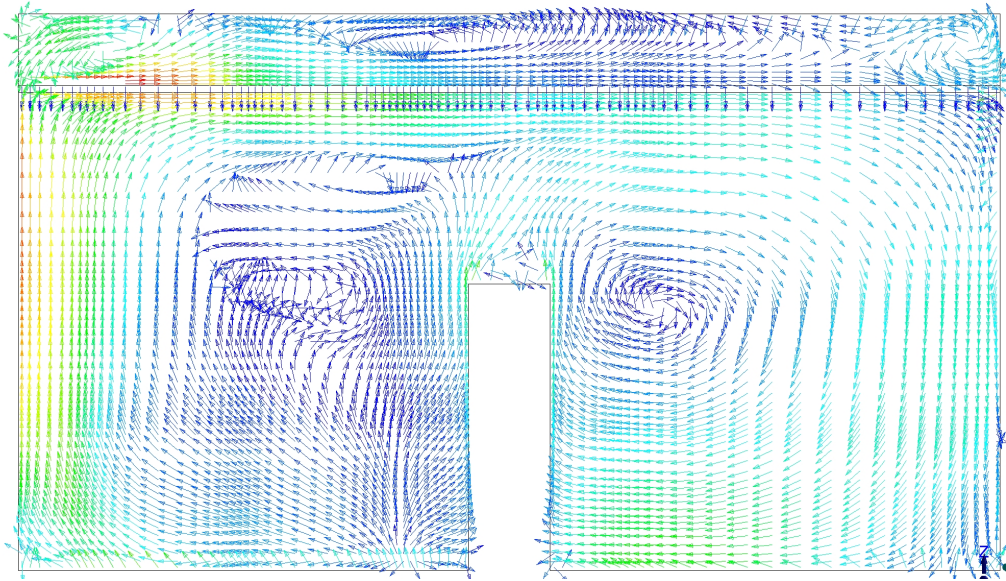


Figure H.15. Path lines through occupant section for case 8.

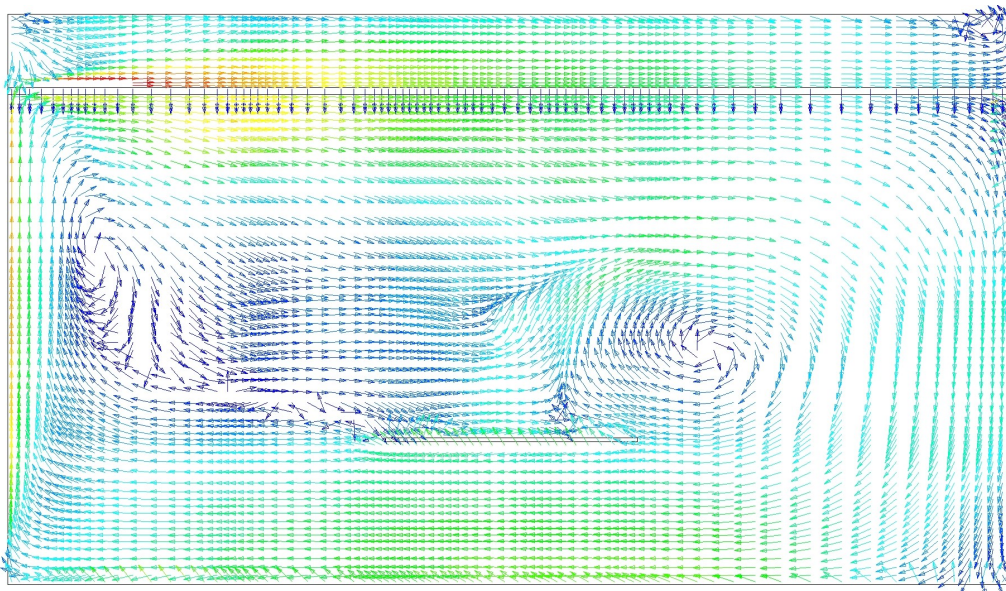


Figure H.16. Path lines through table section for case 8.



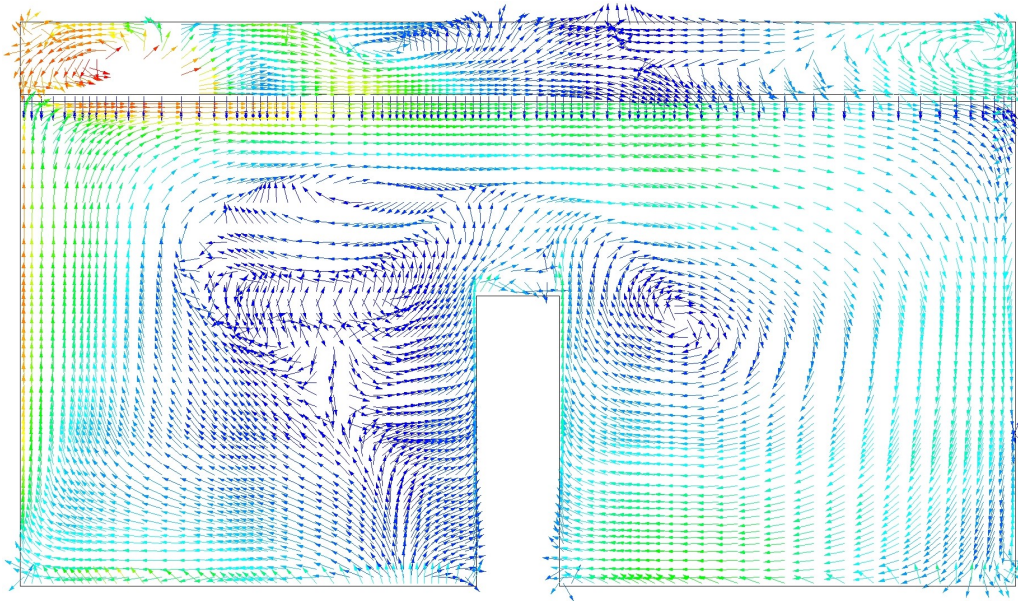


Figure H.17. Path lines through occupant section for case 9.

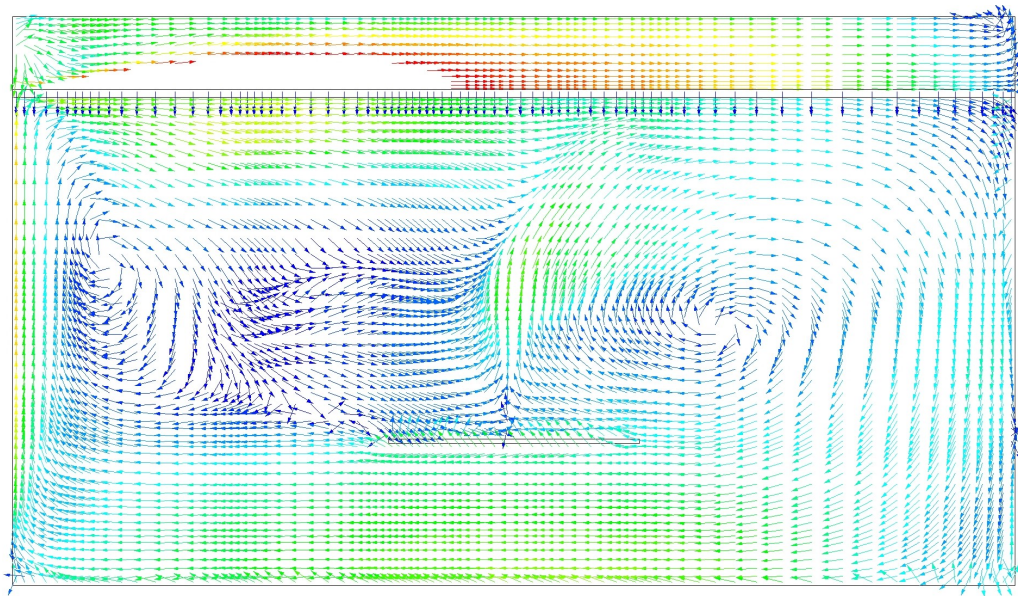
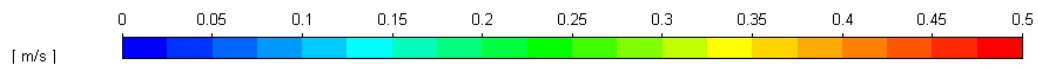


Figure H.18. Path lines through table section for case 9.



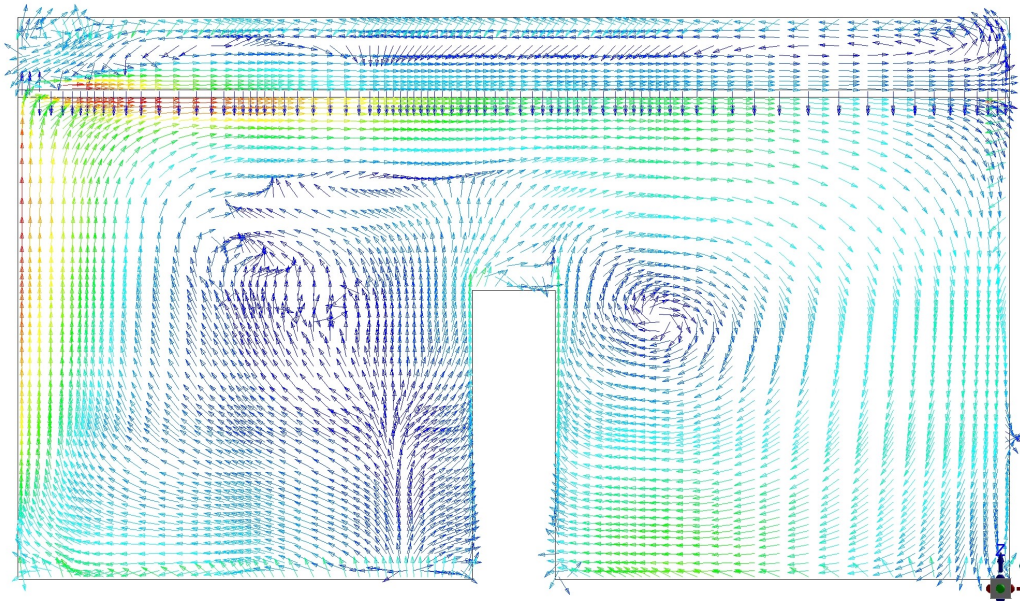


Figure H.19. Path lines through occupant section for case 10.

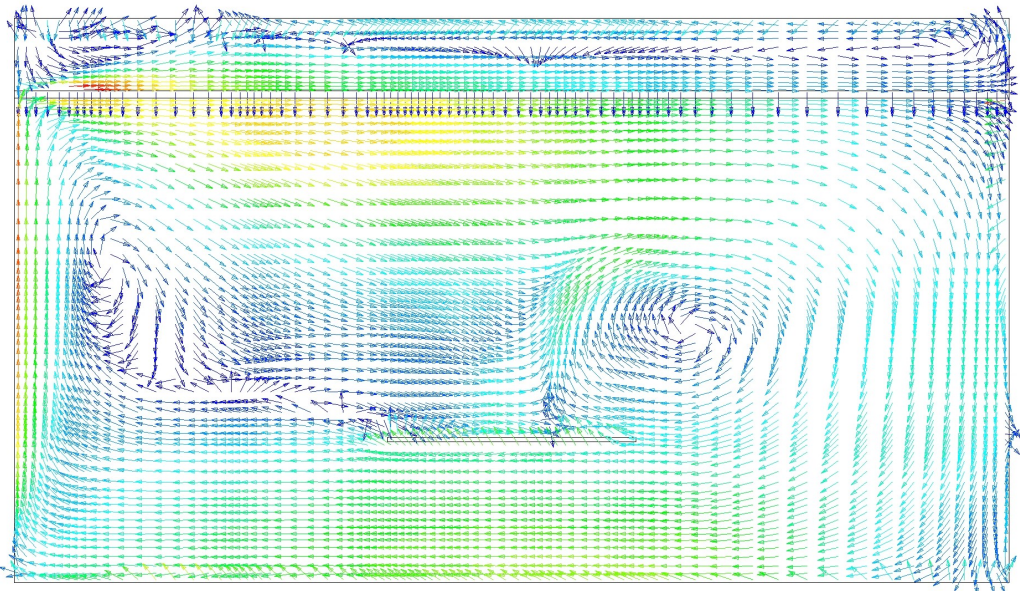
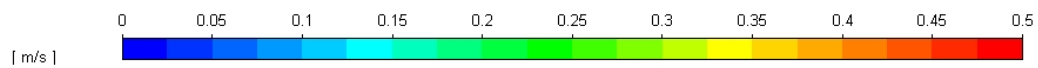


Figure H.20. Path lines through table section for case 10.



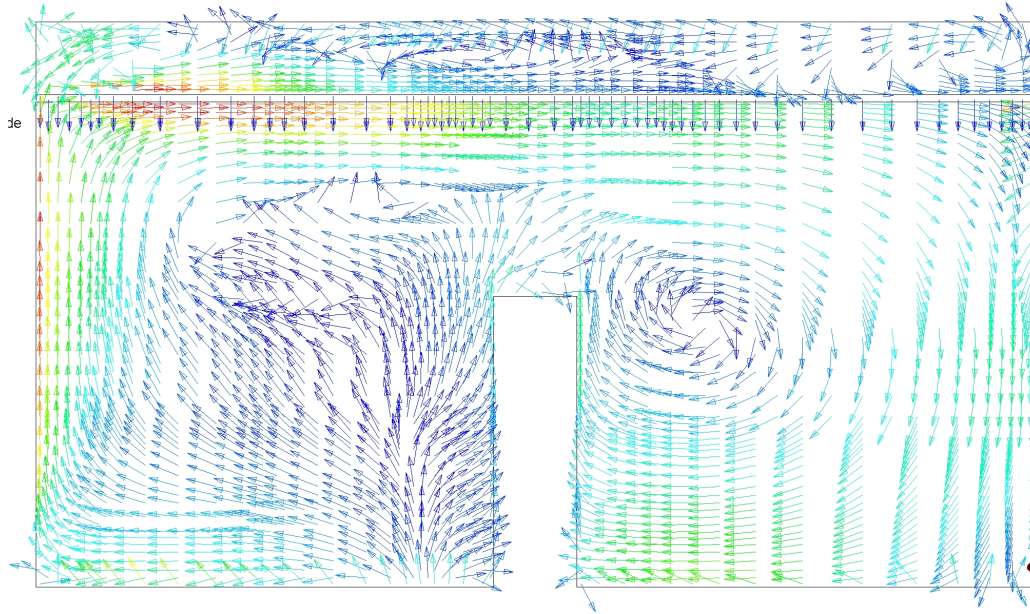


Figure H.21. Path lines through occupant section for case 11.

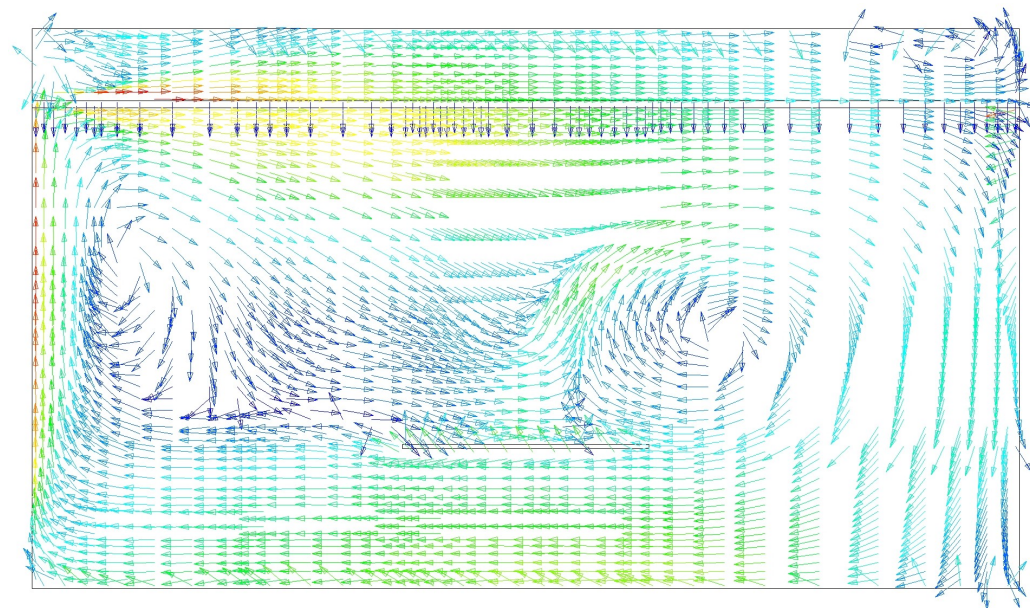


Figure H.22. Path lines through table section for case 11.



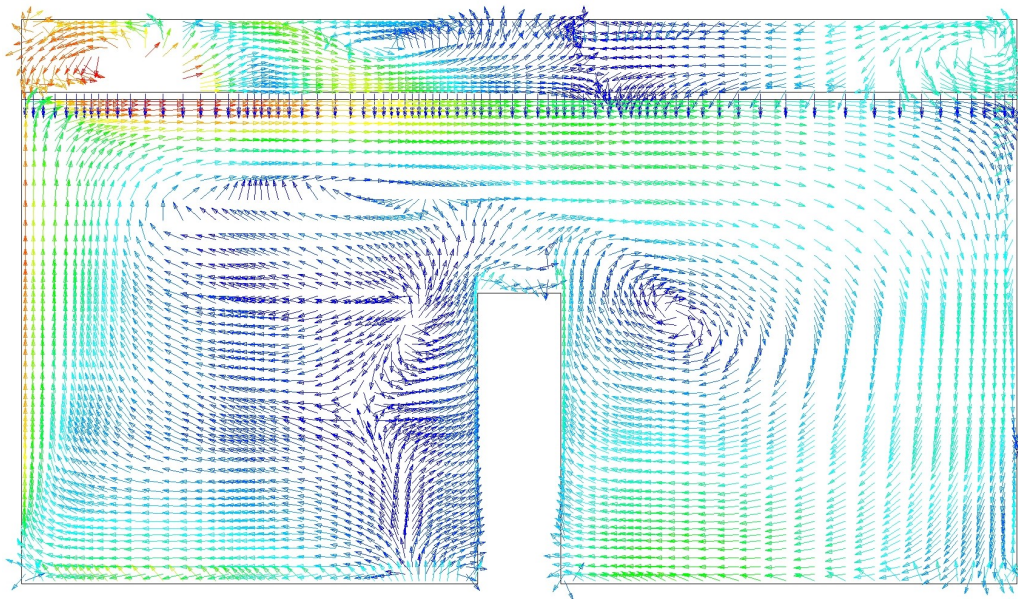


Figure H.23. Path lines through occupant section for case 12.

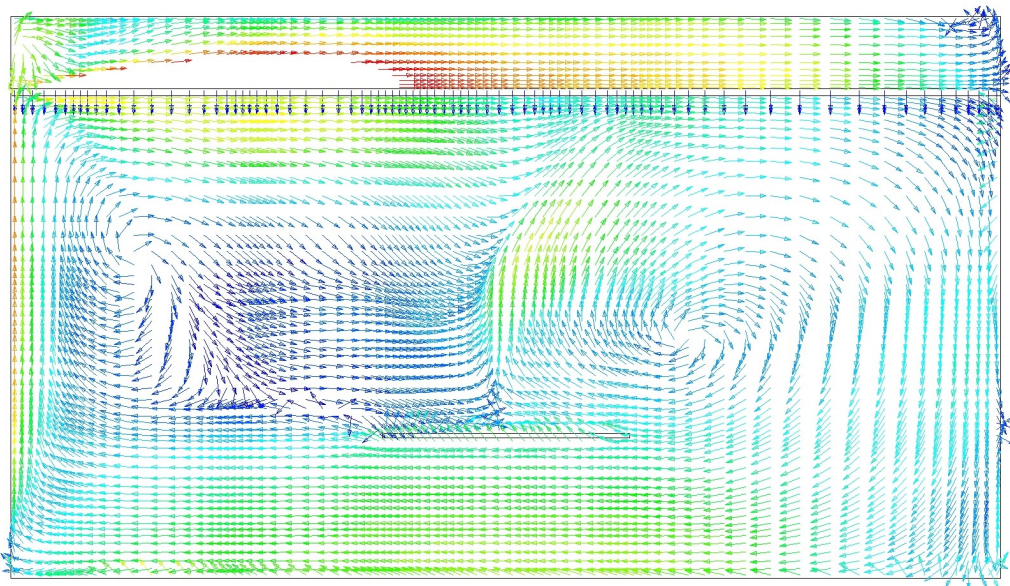
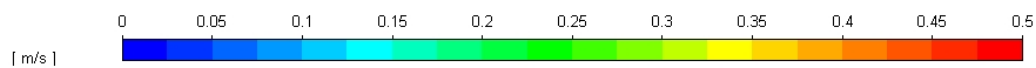


Figure H.24. Path lines through table section for case 12.



Selection of reference points for design chart development I

I.1 Velocity analysis

From the CFD simulations, it is possible to find the maximum velocity point in the room. This was investigated at first, but the results were not representative of the draught the person will experience. Therefore, reference points close to the occupant were examined to give an indication of the draught risk. To select a measuring point for the reference velocity, u_{draught} , four lines next to the heat sources are examined.

All lines are positioned 20 cm away from the occupants, as this distance is significantly affected by the buoyancy of the occupants. This distance also represents the region where a person would experience draught. Both the right and left sides of the occupant are examined. This is also crucial due to one side being closer to the inlet and the exhaust. This results in four different lines, which can be seen in Figure I.1.

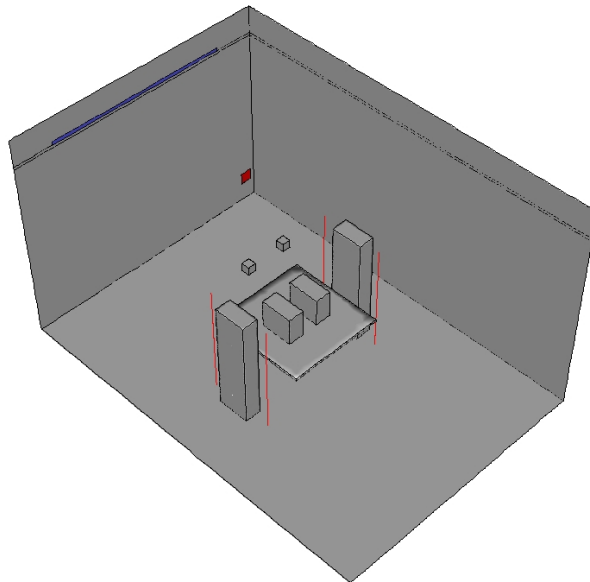


Figure I.1. Placement of measurement lines for the analysis (marked in red).

In the figure above, the manikin in the foreground is person 1, and the other is person 2. The lines positioned closest to the inlet/exhaust are marked as East and West. The velocity profile for cases 2, 5 and 11, showing the four lines adjacent to the occupant, is illustrated in Figure I.2, I.3 and I.4.

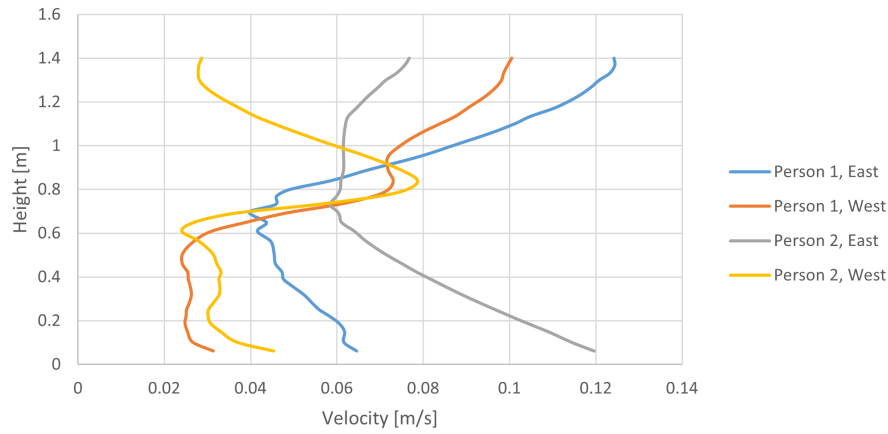


Figure I.2. Line analysis of case 2 with 200 W heat load.

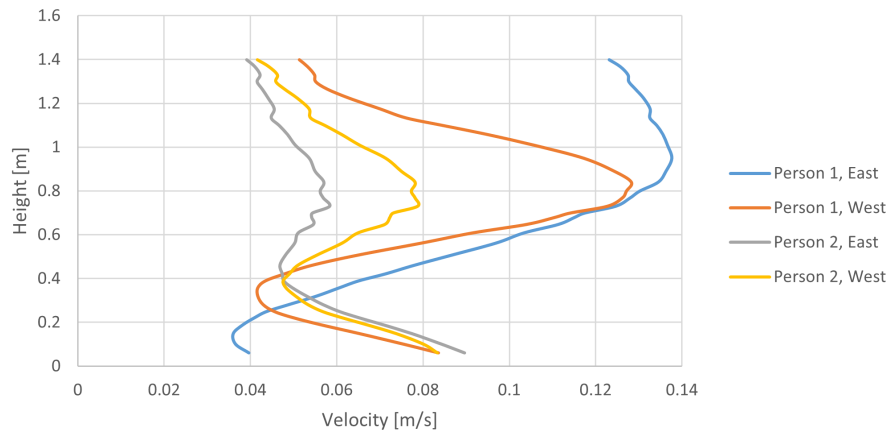


Figure I.3. Line analysis of case 5 with 430 W heat load.

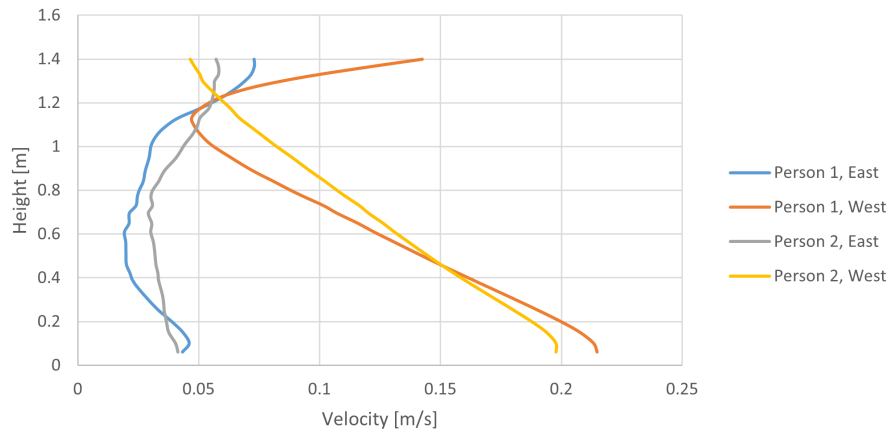


Figure I.4. Line analysis of case 11 with 1,430 W heat load.

From the three figures, it can be seen that the point of maximum velocity is very dependent on the case configuration. Both heat load and distribution have an impact on the results. Based on the graphs, it can be concluded that cases with solar radiation on the surface lead to different results compared with only heat from people. This will likely be due to different flow patterns.

For case 2 with a heat load of 200 W, high velocities are observed both at the floor and head height. Case 5, with a heat load of 430 W, exhibits another velocity distribution, with the highest velocities located at a height of approximately 1 m. In case 11, with a heat load of 1,430 W, a different pattern is observed. Here, the Western orientation of the occupant experience high velocities near the floor level and the Eastern part of the occupant experience significantly lower velocities.

I.2 Point selection

Based on the analysis, it has not been possible to select one representative point for the maximum velocity. Thereby, two points have been chosen, and the maximum value between these points is used for the calculation in the design chart development. The highest velocities often occur near person 1 around the floor. Both the East and West sides appear to experience high velocities depending on the heat load configuration. Based on the charts, it is observed that the East line for person 1 has high velocities, placed higher in the room for most cases. Thereby, the point at 1.1 m is chosen to be representative. The West side of person 1 is also chosen as a representative point. In this case, a high velocity is observed near the floor in case 7 with a high heat load. Thereby the person 1, West side, is chosen at a height of 0.1 m.

The placement of the two points compared to the two occupants can be seen in Figure I.5.

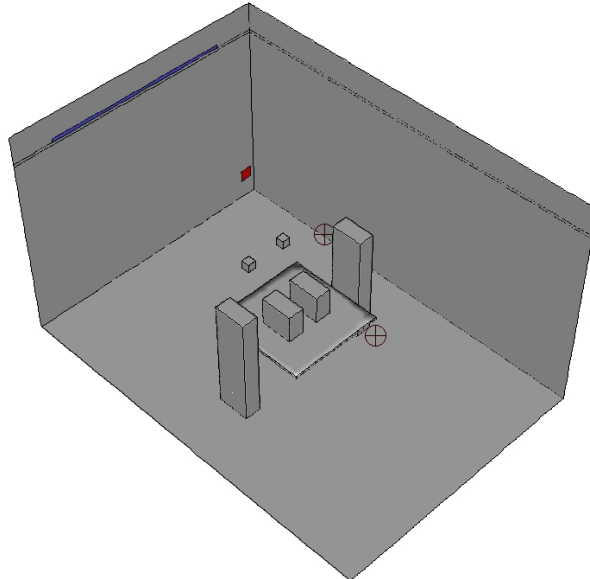


Figure I.5. Point placement marked with a circle with a cross. The inlet and exhaust are shown on the left side.

Based on this chapter, it can be concluded that the placement of the u_{draught} reference point is of great importance. In this study, the point is selected close to the occupants due to their experience of draught. The maximum velocity is observed at two critical points.

Investigation of residuals J

To determine the optimal conditions for the model calculation, one model is run with different sizes of the monitored residuals. Residuals represent the difference between the calculated values and the expected values. Reducing the residuals helps improve the accuracy of a numerical solution, ensuring that the model converges effectively. All residuals, except for the energy residual, were set to 0.001 in the first calculation and 0.0001 in the second. The energy residual was in the first calculation set to $1 \cdot 10^{-6}$ and $1 \cdot 10^{-8}$ in the second.

Total heat transfer and mass flow rate

The total heat transfer and mass flow rate in the two models are investigated to ensure that the energy balance in the model is correct and to verify mass conservation within the model. In Table J.1, these values are seen, and the difference that the total heat transfer makes of the heat load in the model is calculated.

Table J.1. Comparison of residuals: Coarse and Fine.

	Coarse residuals	Fine residuals
Total heat transfer rate (W)	-0.040	-0.001
Difference in heat transfer	0.009	0.000
Mass flow rate (kg/s)	$1.39 \cdot 10^{-17}$	$4.16 \cdot 10^{-17}$

All values are very small, indicating that both models demonstrate a high degree of accuracy in maintaining energy balance and mass conservation. This suggests that the differences between the coarse and fine residuals are negligible, and neither model exhibits significant errors related to heat transfer or mass flux.

Average temperatures

The average temperatures in the three parts of the room were compared to better understand the accuracy of the models. This can be seen in Table J.2.

Table J.2. Temperature values coarse residuals. **Table J.3.** Temperature values fine residuals.

Temperature	[°C]
Plenum	17.57
Ceiling	18.65
Room	21.88

Temperature	[°C]
Plenum	17.70
Ceiling	19.04
Room	21.94

The largest difference was seen in the average temperature in the ceiling, where the difference was 2% in the other parts of the model, the difference between using the coarse and fine residuals is less than 1%. Because the focus of the project is inside the room, these differences are acceptable.

Temperature gradients

The temperature gradients were also investigated and compared. This was done in the four lines A, B, C and D. This comparison can be seen in Figure J.1 to J.4

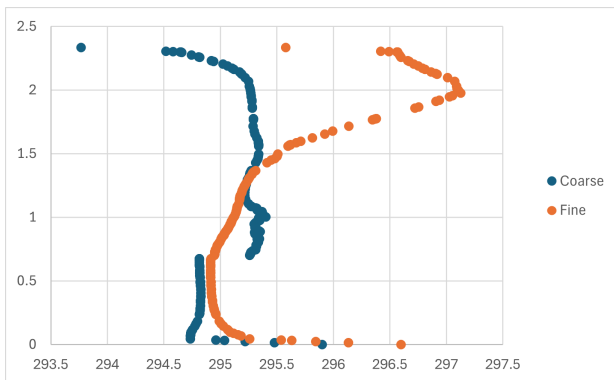


Figure J.1. Comparison of temperature in line A.

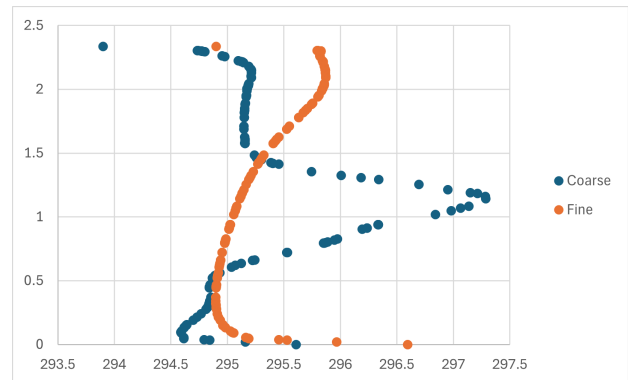


Figure J.2. Comparison of temperature in line B.

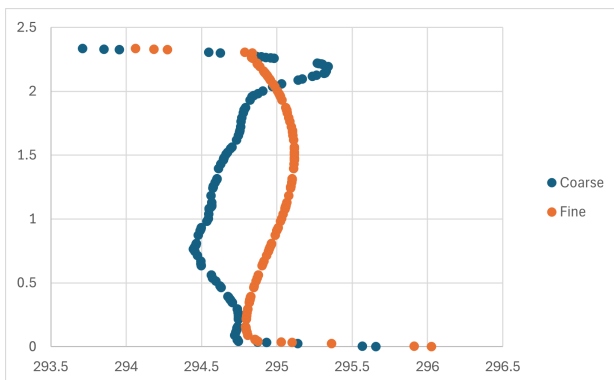


Figure J.3. Comparison of temperature in line C.

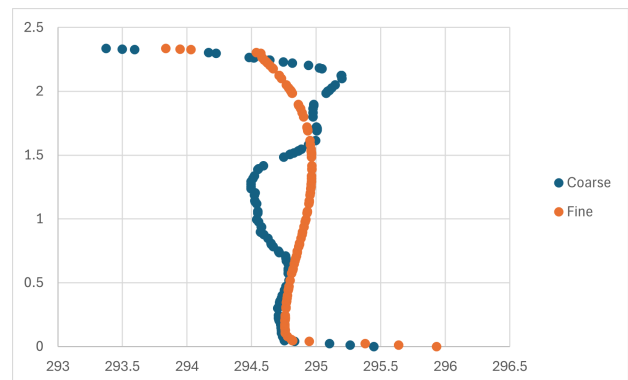


Figure J.4. Comparison of temperature in line D.

Some differences are seen between the models, and in Figure J.1 at height 0.7 m, a jump in the results is seen for the coarse mesh. This could indicate that the models are not fully converged.

Velocity profile

The velocity profile was investigated similarly to the temperature gradient, in the four lines A, B, C and D. The velocity profiles are seen in Figure J.5 to J.8.

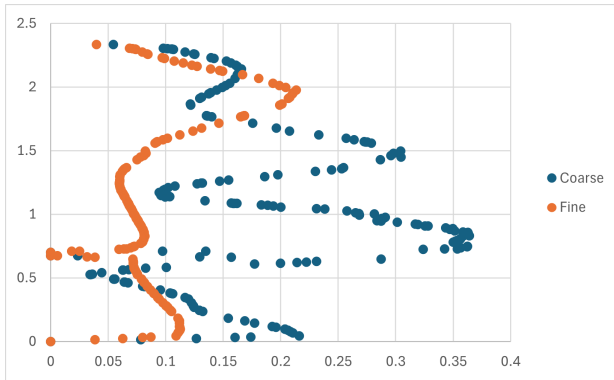


Figure J.5. Comparison of velocity in line A.

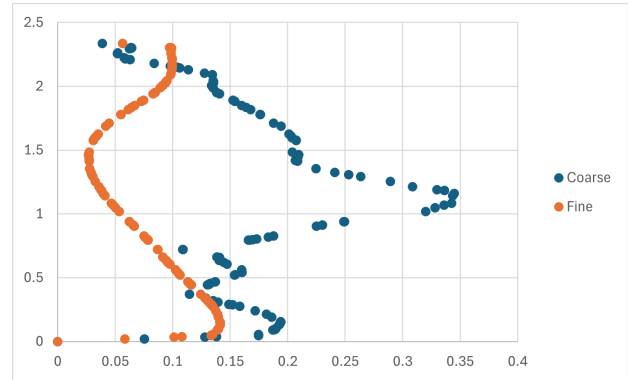


Figure J.6. Comparison of velocity in line B.

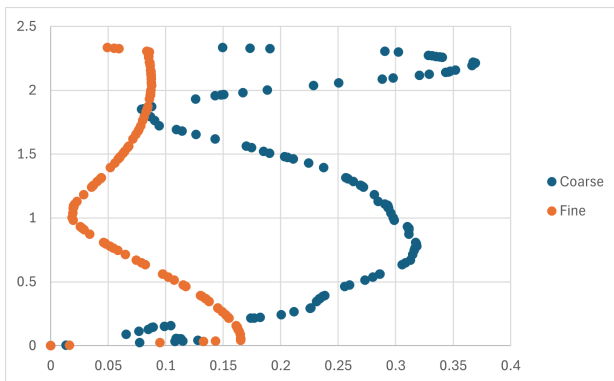


Figure J.7. Comparison of velocity in line C.

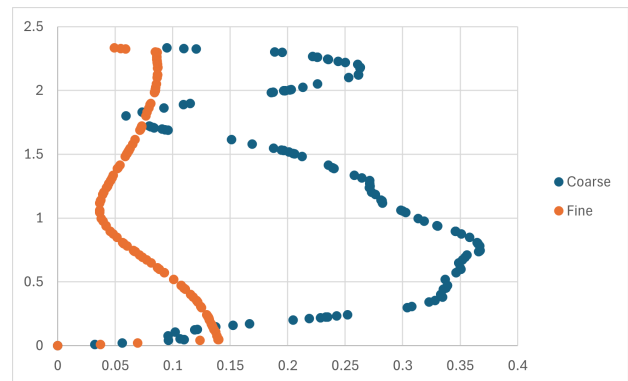


Figure J.8. Comparison of velocity in line D.

For the velocity, big differences are seen when using the coarser residuals, the velocity is very uneven. It is chosen to use the fine residuals in the further investigations, and monitor the residuals to determine if further refinement is necessary in some models.

Mesh independency of model 2 K

K.1 Mesh

For Model 2, the mesh was created based on the number of cells reported in other studies. In the study by Zhang [2016], a model with 741,831 cells is used, and by Vilsbøll [2014], the model used consists of 617,400 cells. Therefore, this has been the basis of the new model, and finer meshes have been created to check if independence is met in the model. Information about the mesh made can be found in Table K.1.

Table K.1. Mesh information.

Model	Number of		Occupants	Element size of [m]			
	Nodes	Elements		PC	Lamp	Exhaust	Main cell
Mesh 1	341,367	1,263,145	0.020	0.015	0.010	0.050	0.060
Mesh 2	426,711	1,719,442	0.015	0.010	0.010	0.040	0.060
Mesh 3	845,897	3,193,032	0.015	0.010	0.010	0.040	0.035

To check the quality of the mesh, the skewness and aspect ratio have been investigated for the different meshes. These values can be found in Table K.2 and K.3.

Table K.2. Aspect ratio for different meshes.

	Mesh 1	Mesh 2	Mesh 3
Min	1.04	1.04	1.00
Max	15.51	15.29	13.20
Average	2.12	2.06	1.91
Standard deviation	1.03	0.93	0.58

Table K.3. Skewness for different meshes.

Mesh 1	Mesh 2	Mesh 3
$5.60 \cdot 10^{-10}$	$5.60 \cdot 10^{-10}$	$5.68 \cdot 10^{-10}$
0.94	0.94	0.90
0.22	0.22	0.21
0.15	0.15	0.14

The maximum skewness is higher than the recommendations, but when further investigated, it is seen that only a few elements have this skewness, and their placement is at the corners of the room. Therefore, this is not further improved.

K.2 Independency

The model was tested using various mesh densities. The number of nodes and elements was doubled until independence was met, as seen in Table K.1. To determine if independence was met, different parameters were compared. It should be noted that the scaled residuals for mesh 3 were further refined in the calculations.

Total heat transfer

The total heat transfer was not compared between models, but it was calculated how big of an error the total heat transfer was in relation to the heat load in the model. The heat load used in the model was 430 W, in Table K.4, the calculation can be seen.

Table K.4. Total heat transfer and error for different mesh types.

Mesh type	Total heat transfer [W]	Error [%]
Mesh 1	-0.0038	0.0009
Mesh 2	-0.0008	0.0002
Mesh 3	-0.0013	0.0003

These errors were a very small part of the heat load in all the models, which indicates a high degree of accuracy in maintaining energy balance. The total heat transfer was therefore found to be acceptable in all models.

Mass flow rate

The mass flow rate was also investigated for the models with different meshes. These values can be found in Table K.5.

Table K.5. Mass flow rate for different mesh types.

Mesh type	Mass flow rate [kg/s]
Mesh 1	$-2.78 \cdot 10^{-17}$
Mesh 2	$-4.16 \cdot 10^{-17}$
Mesh 3	$-2.78 \cdot 10^{-17}$

As these values are close to zero across all mesh types, the model demonstrates acceptable mass conservation independent of the mesh.

Temperature

The average temperatures for the different parts of the room are compared, and the differences are calculated. This comparison can be seen in Table K.6.

Table K.6. Temperature values and differences for various mesh types.

	Mesh 1 [°C]	Mesh 2 [°C]	Difference [%]	Mesh 3 [°C]	Difference [%]
Temp. plenum	17.70	17.70	0.00	17.68	0.14
Temp. ceiling	19.02	19.04	0.08	18.93	0.57
Temp. room	22.01	21.94	0.30	21.82	0.57

The difference is smaller between Mesh 1 and Mesh 2. However, in general, the difference is very small between all models. This could indicate that independence has been reached in all models.

The temperature gradients are also compared in the four locations inside the room. This comparisons can be found in Figure K.1

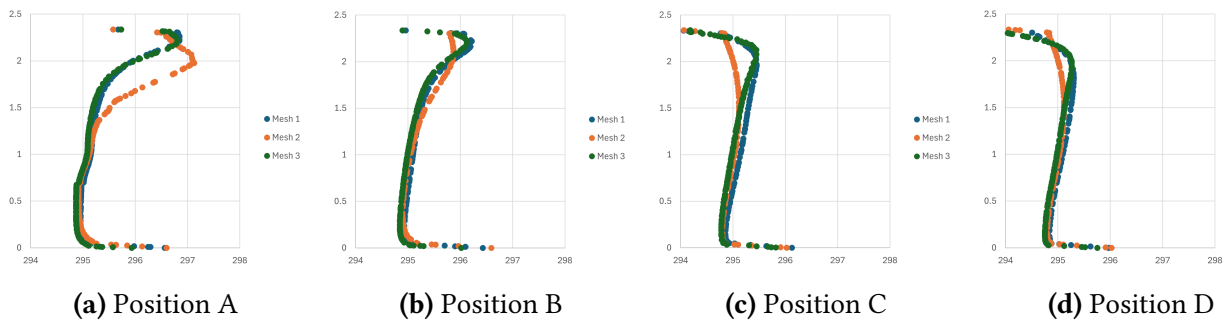


Figure K.1. Temperature profiles at positions A, B, C, and D for mesh independence study.

The temperature gradient is very similar between all mesh types, especially Mesh 1 and Mesh 3. This could be due to the refinement of the monitored residuals in Mesh 3, which has ensured that the results with this mesh are more converged than the results with Mesh 2.

Velocity

In Figure K.2, a comparison of the velocity profile is made in the same four positions A-D.

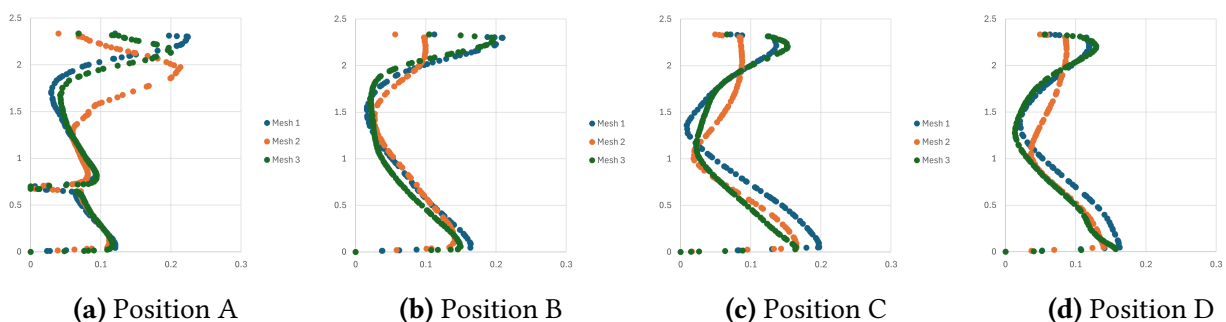


Figure K.2. Velocity gradients at positions A, B, C, and D for mesh independence study.

Again, it is seen that the results from Mesh 1 and Mesh 3 deviate less. These velocity profiles are very similar and only differ a bit in the two profiles further away from the occupants and the inlet. Since only two points are chosen when the design chart is developed, the difference in velocity at these points is compared. This can be seen in Table K.7.

Table K.7. Comparison of east and west points for different mesh types.

	Mesh 1 [°C]	Mesh 3 [°C]	Difference [%]
East point	0.12	0.07	6.24
West point	0.12	0.1	2.60

From these results, it is seen that the difference between the results from Mesh 1 and Mesh 3 differs by a couple of percentage points. The path lines from the model with Mesh 1 and Mesh 2 can be seen in Figure K.3 and K.4.

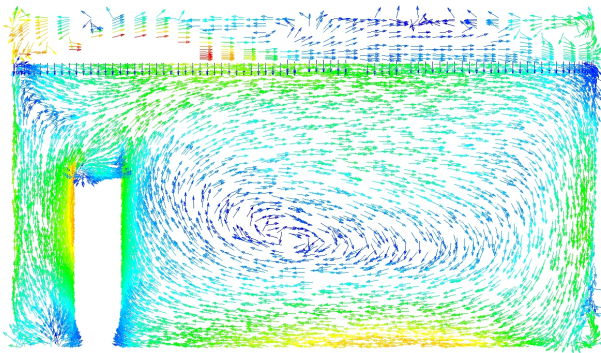


Figure K.3. Path lines for Mesh 1.

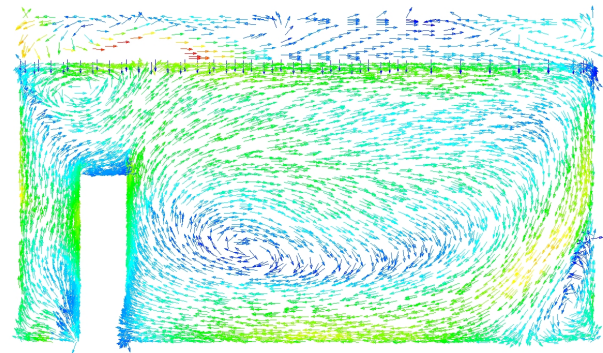
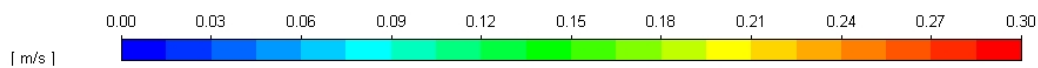


Figure K.4. Path lines for Mesh 3.



In the further analysis, it is based on this analysis, chosen to simulate with Mesh 1. Since the results do not change much between this and the more dense mesh.

Mesh independency of model 3 L

Model 3 was the model with a higher room height. Because this model has other geometrical dimensions, the mesh was not made directly based on models from the literature. The model was instead made with the same element sizes as used for Model 2 in Appendix K. Mesh information can be found in Table L.1.

Table L.1. Mesh information.

Model	Number of		Occupants	Element size of [m]			
	Nodes	Elements		PC	Lamp	Exhaust	Main cell
Mesh 1	285,483	1,199,052	0.020	0.015	0.010	0.05	0.080
Mesh 2	468,702	2,040,826	0.015	0.010	0.010	0.04	0.060

To check the quality of the mesh, the skewness and aspect ratio have been investigated for the different meshes. These values can be found in Table L.2 and L.3 for Model 3.

Table L.2. Aspect ratio for different meshes.

	Mesh 1	Mesh 2
Min	1.01	1.01
Max	20.69	15.81
Average	2.18	1.99
Standard deviation	1.21	0.78

Table L.3. Skewness for different meshes.

	Mesh 1	Mesh 2
Min	$4.97 \cdot 10^{-1}$	$5.01 \cdot 10^{-1}$
Max	0.96	0.96
Average	0.25	0.23
Standard deviation	0.17	0.15

The maximum skewness is higher than the recommendations, but when investigated, it is seen that only a few elements have this skewness, and their placement is at the corners of the room, outside the area of interest.

L.1 Mesh independency

The model is tested with different meshes to determine if and when mesh independence is reached. To determine this, different parameters were compared.

Total heat transfer

The analysis does not compare total heat transfer across different meshes. Instead, it focuses on how much the total heat transfer contributes to the overall heat load in the model. The heat load in the mode is 430 W, in table Table L.4 results of the calculation are seen.

Table L.4. Total heat transfer and error for different mesh types.

Mesh type	Total heat transfer [W]	Error [%]
Mesh 1	-0.0032	0.0007
Mesh 2	0.0010	0.0002

These errors make up only a small part of the heat load in the model, which indicates a high level of accuracy in maintaining energy balance. The total heat transfer is therefore found to be acceptable in all models.

Mass flow rate

The mass flow rate was also investigated for the models with different meshes. These values can be found in Table L.5.

Table L.5. Mass flow rate for different mesh types.

Mesh type	Mass flow rate [kg/s]
Medium mesh	0
Fine mesh	$-1.39 \cdot 10^{-17}$

These values are zero or close to zero for all mesh types, indicating that the model achieves acceptable mass conservation regardless of mesh configuration.

Temperature

The average temperatures for the different parts of the room are compared, and the differences are calculated to see how much this changes with the refinement of the mesh. This comparison can be seen in Table L.6.

Table L.6. Temperature values and differences for various mesh types.

	Mesh 1 [°C]	Mesh 2 [°C]	Difference [%]
Temp. plenum	21.04	21.13	0.42
Temp. ceiling	21.30	21.39	0.43
Temp. room	21.98	22.11	0.56

The differences are all less than 1%, which supports that the model with mesh 1 should be independent. To further examine the temperature, the gradient in four lines inside the room is also compared. These comparisons can be found in Figure L.1.

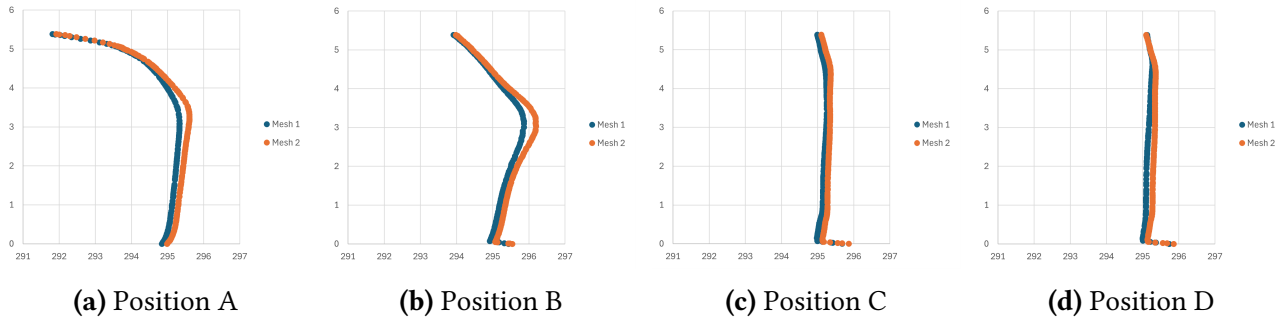


Figure L.1. Temperature profiles at positions A, B, C, and D for mesh independence study.

The temperature gradient is very similar between both meshes, in all positions.

Velocity

In Figure L.2, the same analysis in four lines inside the room has been made, but for the velocity profiles.

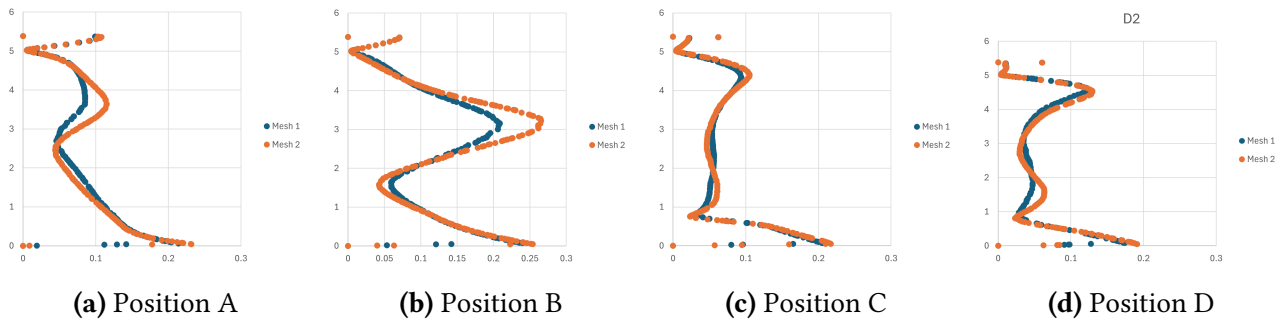


Figure L.2. Velocity gradients at positions A, B, C, and D for mesh independence study.

These results are also very similar, especially in the OCZ. Since only two points are chosen when the design chart is developed, the difference in velocity at these points is also compared. This can be seen in Table L.7, because these values are small, a minor difference makes a big impact, therefore, the difference has been calculated in relation to the inlet velocity.

Table L.7. Comparison of east and west points for different mesh types.

	Mesh 1 [°C]	Mesh 2 [°C]	Difference [%]
East point	0.07	0.04	3.79
West point	0.08	0.07	1.24

From these results, it is seen that the difference between the results is within a couple of percentage points. However, when looking at the values, these are very small and would not make a big difference in the further analysis.

It is also chosen to compare the path lines for the two meshes. This is seen in Figure L.3 and Figure L.4.

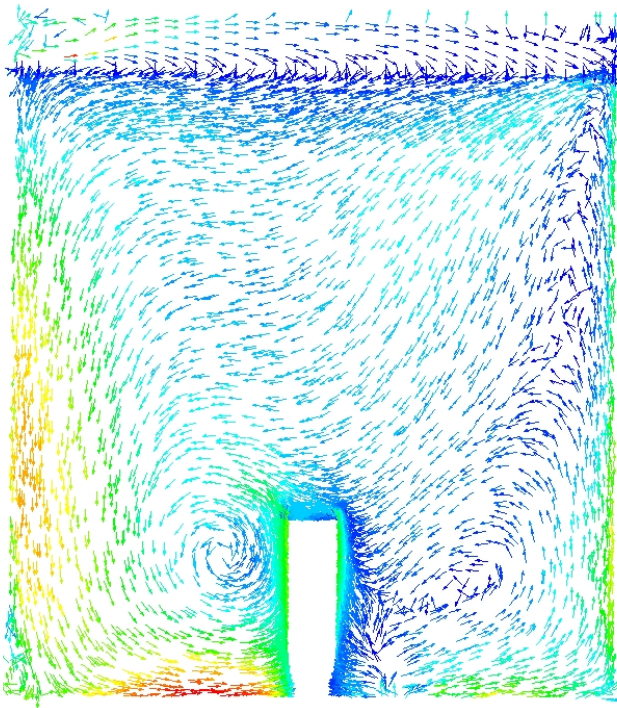


Figure L.3. Path lines for Mesh 1.

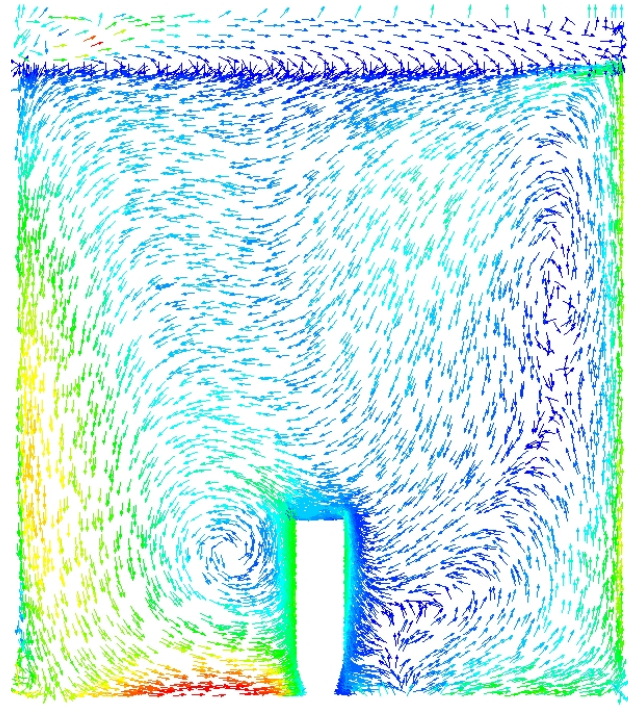
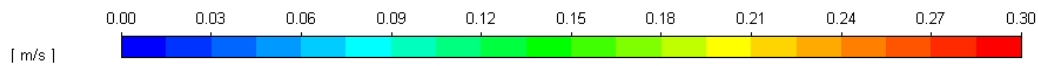


Figure L.4. Path lines for Mesh 2.



The path lines inside the room are almost identical. Based on this and the other parameters which has been compared, it is chosen to use Mesh 1 for further simulations.

Mesh independency of model 4 M

Model 4 is the room with double the length and heat load compared to Model 1. The model was made with the same element sizes as those used in Model 2 in Appendix K. Mesh information can be found in Table M.1.

Table M.1. Mesh information.

Model	Number of		Occupants	Element size of [m]			
	Nodes	Elements		PC	Lamp	Exhaust	Main cell
Mesh 1	487,196	1,938,235	0.020	0.015	0.010	0.05	0.080
Mesh 2	1,128,079	4,414,983	0.015	0.010	0.010	0.04	0.045

To check the quality of the mesh, the skewness and aspect ratio have been investigated for the different meshes. These values can be found in Table M.2 and M.3 for Model 4.

Table M.2. Aspect ratio for different meshes.

	Mesh 1	Mesh 2
Min	1.02	1.00
Max	20.71	17.02
Average	2.17	1.95
Standard deviation	1.23	0.64

Table M.3. Skewness for different meshes.

	Mesh 1	Mesh 2
Min	$4.39 \cdot 10^{-1}$	$5.86 \cdot 10^{-1}$
Max	0.96	0.92
Average	0.23	0.21
Standard deviation	0.15	0.14

The maximum skewness is higher than the recommendations, but when investigated, it is seen that only a few elements have this skewness, and their placement is at the corners of the room, outside the area of interest.

M.1 Mesh independency

The model is tested with different meshes to determine if and when mesh independence is reached. To determine this, different parameters were compared.

Total heat transfer

The analysis does not compare total heat transfer across different meshes. Instead, it focuses on how much the total heat transfer contributes to the overall heat load in the model. The heat load in the mode is 430 W, in table Table M.4 results of the calculation are seen.

Table M.4. Total heat transfer and error for different mesh types.

Mesh type	Total heat transfer [W]	Error [%]
Mesh 1	0.0024	0.0003
Mesh 2	-0.0019	0.0002

These errors make up only a small part of the heat load in the model, which indicates a high level of accuracy in maintaining energy balance. The total heat transfer is therefore found to be acceptable in all models.

Mass flow rate

The mass flow rate was also investigated for the models with different meshes. These values can be found in Table M.5.

Table M.5. Mass flow rate for different mesh types.

Mesh type	Mass flow rate [kg/s]
Medium mesh	$1.11 \cdot 10^{-16}$
Fine mesh	0

These values are zero or close to zero for all mesh types, indicating that the model achieves acceptable mass conservation regardless of mesh configuration.

Temperature

The average temperatures for the different parts of the room are compared, and the differences are calculated to see how much this changes with the refinement of the mesh. This comparison can be seen in Table M.6.

Table M.6. Temperature values and differences for various mesh types.

	Mesh 1 [°C]	Mesh 2 [°C]	Difference [%]
Temp. plenum	11.86	11.88	0.16
Temp. ceiling	13.11	13.14	0.16
Temp. room	16.01	15.93	0.53

The differences are all less than 1%, which supports that the model with mesh 1 should be independent. To further examine the temperature, the gradient in four lines inside the room is also compared. These comparisons can be found in Figure M.1.

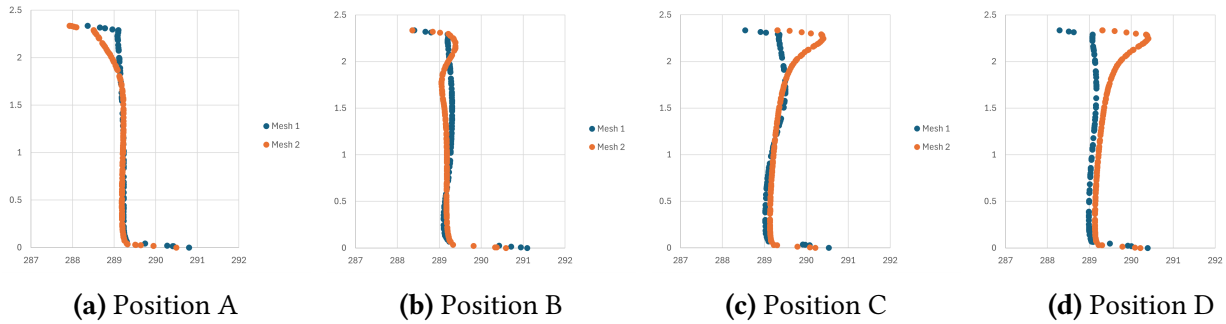


Figure M.1. Temperature profiles at positions A, B, C, and D for mesh independence study.

The temperature gradient is very similar between both meshes, in all positions. However at the ceiling some difference occur between the two meshes.

Velocity

In Figure M.2, the same analysis in four lines inside the room has been made, but for the velocity profiles.

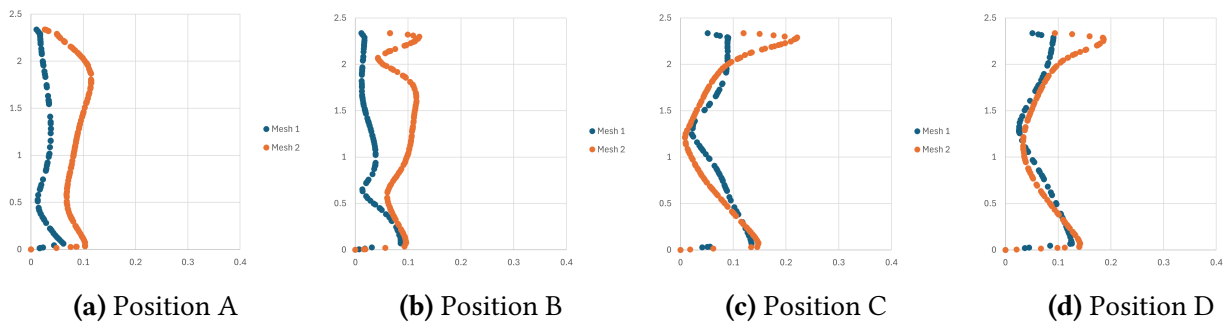


Figure M.2. Velocity gradients at positions A, B, C, and D for mesh independence study.

These velocity profiles are different, and mesh independency does not seem to have occurred, however, due to time restrains, it has not been possible to run a finer mesh. It is unclear whether the observed difference is due to an insufficiently fine mesh or the higher residuals in the coarser mesh; both are possible reasons.

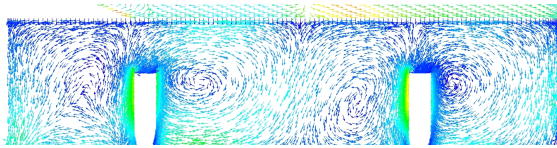
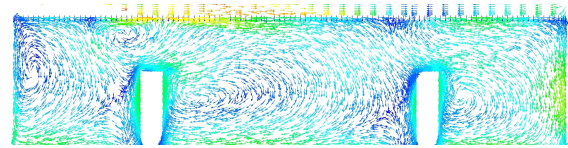
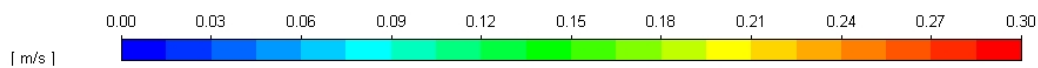
The velocities at the two reference points used in the design charts have also been compared, this can be seen in Table M.7. Due to these values being small, even minor differences can have a significant impact. Therefore, the difference has been calculated in relation to the inlet velocity.

Table M.7. Comparison of east and west points for different mesh types.

	Mesh 1 [°C]	Mesh 2 [°C]	Difference [%]
East point	0.06	0.03	1.96
West point	0.03	0.09	4.36

From these results, it is seen that the difference between the results is within a couple of percentage points.

It is also chosen to compare the path lines for the two meshes. This is seen in Figure M.3 and Figure M.4.

**Figure M.3.** Path lines for Mesh 1.**Figure M.4.** Path lines for Mesh 2.

These pathlines are very different, and independence is not met in this model. However, Mesh 1 is used for further analysis to provide indicative data, though the results should be interpreted with caution, as they cannot be considered fully reliable.

Design charts results N

In this chapter, all the design charts made based on the CFD simulations are presented. This includes both the ones simulated for the heat load intensity and the design charts for studying the room geometry. The theory used for the development is described in the main report and includes the procedure found in Appendix O.

N.1 Design charts for heat load intensity

In this section, the design charts for the four different heat load intensities are presented. These can be seen on Figure N.1 to N.4. The points on each graph indicate the CFD simulation used to calculate the design graph. Some graphs have points that are not shown due to the range of the plot.

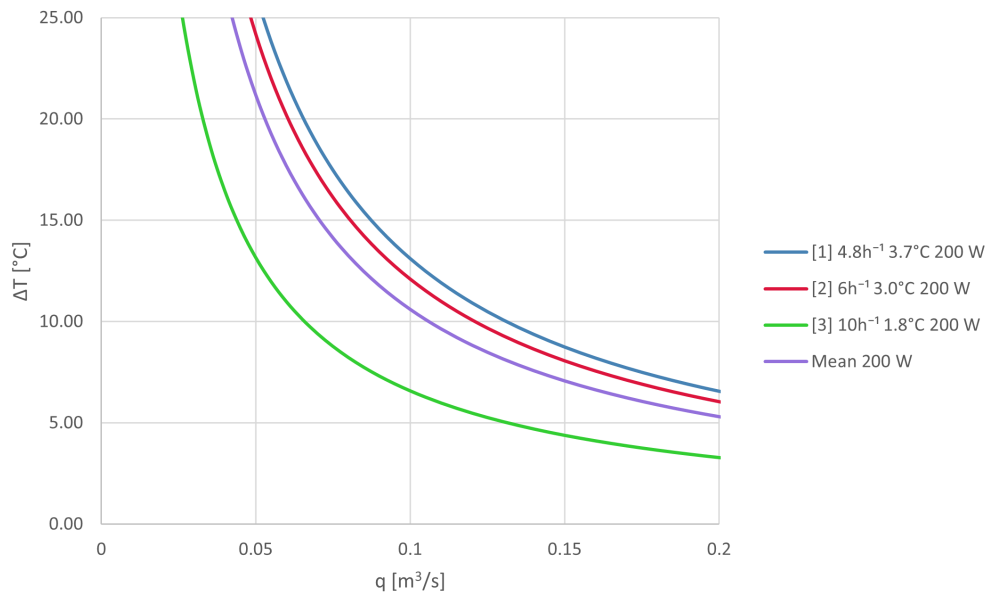


Figure N.1. Design chart heat load of 200 W.

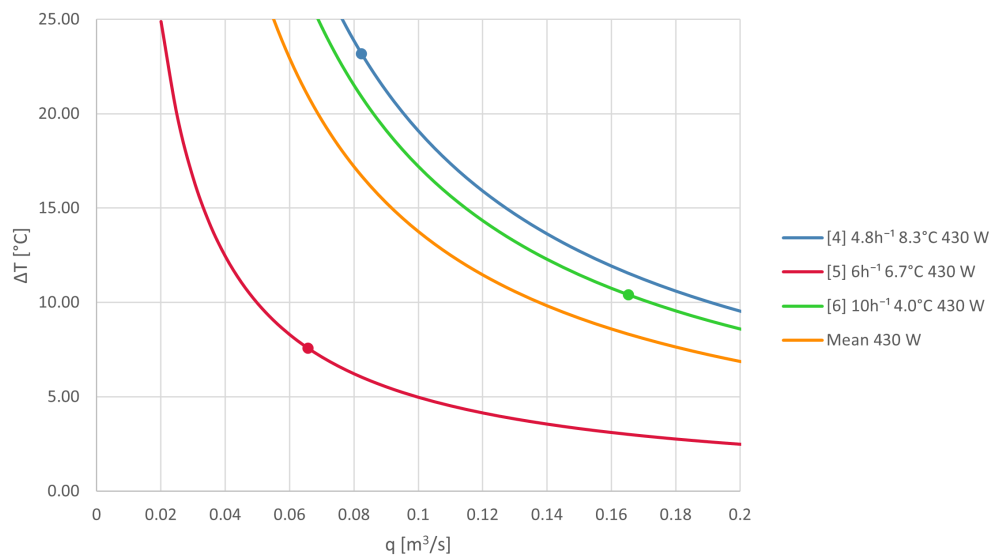


Figure N.2. Design chart heat load of 430 W.

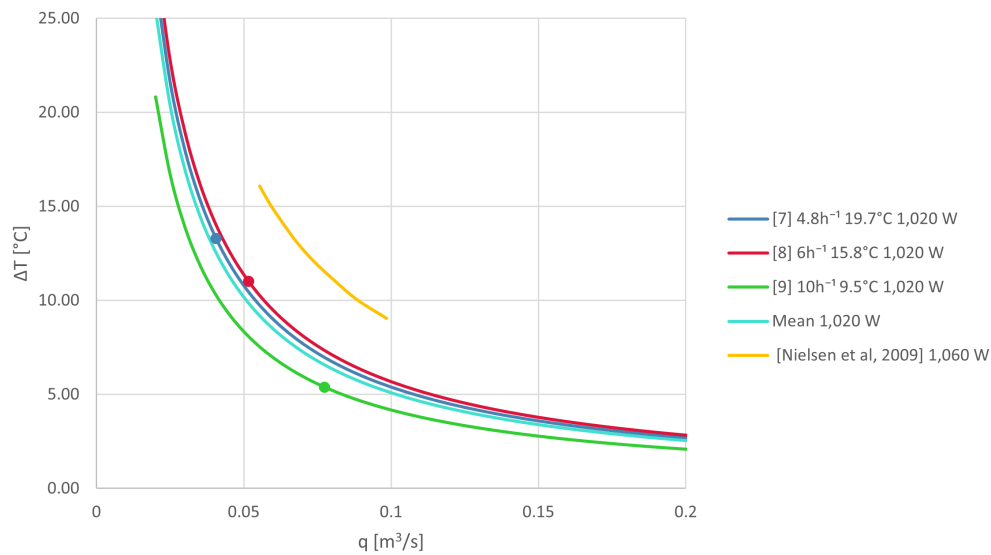


Figure N.3. Design chart heat load of 1,020 W. Include data from Nielsen and Jakubowska [2009].

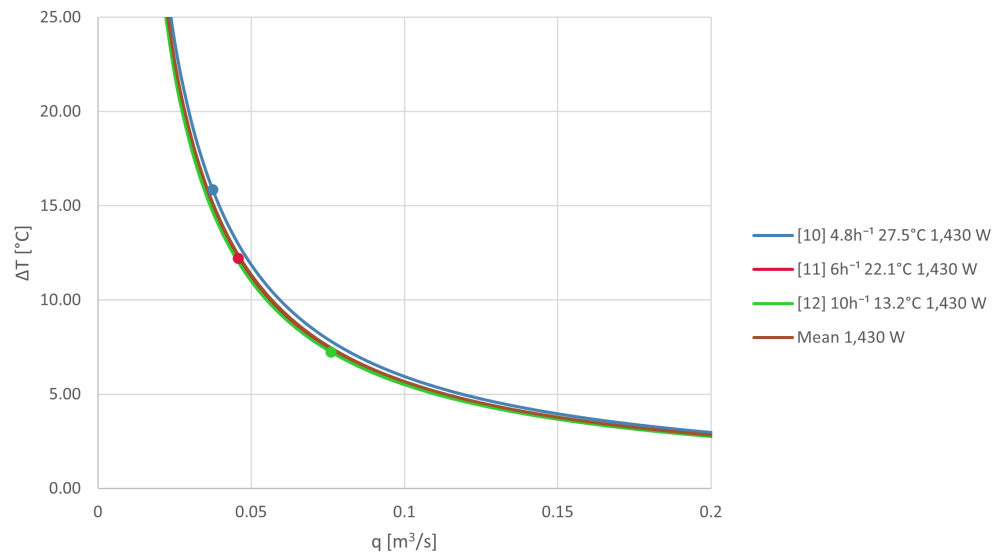


Figure N.4. Design chart heat load of 1430 W.

When creating the design chart, the graph for the cases with ACH of 10 h^{-1} is placed below the other graphs, except in the heat load case of 430 W. On the other hand, the design curve for cases with an ACH of 4.8 h^{-1} is located highest for heat loads of 200, 430 and 1,430 W.

Now, the heat load intensity has been investigated, showing a tendency of better cooling performance at lower heat loads. It is now relevant to examine the distribution of the heat load.

N.2 Design charts for heat load distribution

To investigate the influence of heat load distribution on a DCV system, two configurations with identical heat loads of 430 W are analyzed. In one case, the heat source is centrally located, while in the other, it is positioned along one side of the room. The design chart comparison between these two scenarios can be seen in Figure N.5.

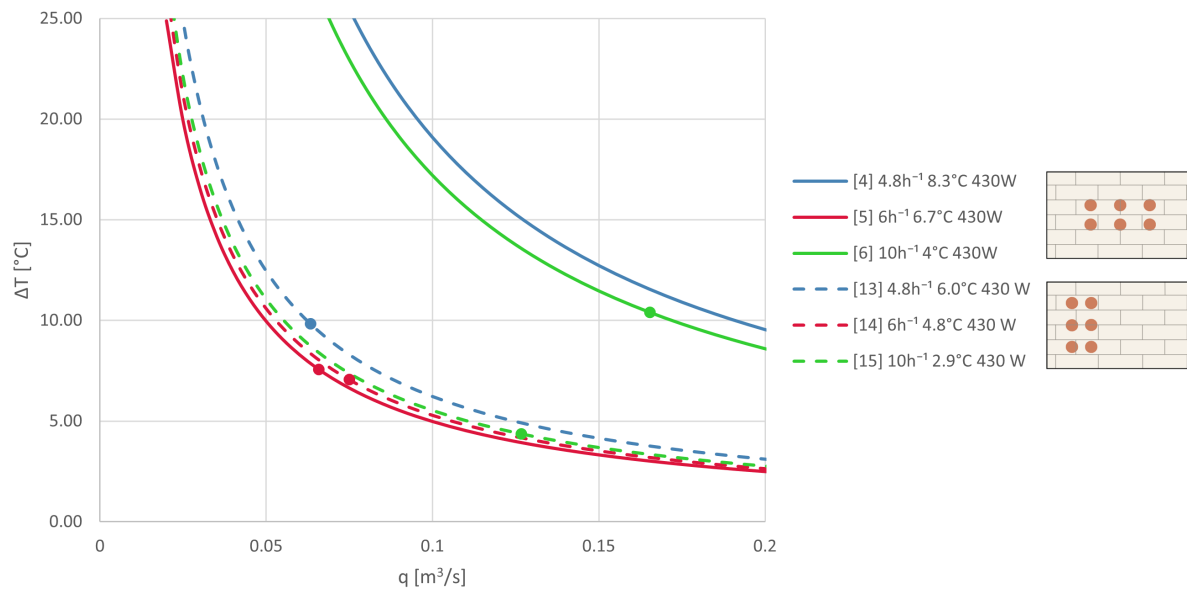


Figure N.5. Centred vs. one side heat load distribution. The dashed line represents the one-sided heat load.

Based on the figure, it can be concluded that a system with a centred/uniform distribution has a higher cooling capacity than a one-sided heat load distribution. This is in line with the literature review.

N.3 Design charts for room geometry

Lastly, the room geometry and its influence on the DCV performance are examined. This is done by analysing a room with increased height and a room with increased length. This investigation will indicate these specific changes and their impact on system performance.

N.3.1 Room height

The design graphs for the high room can be found in Figure N.6.

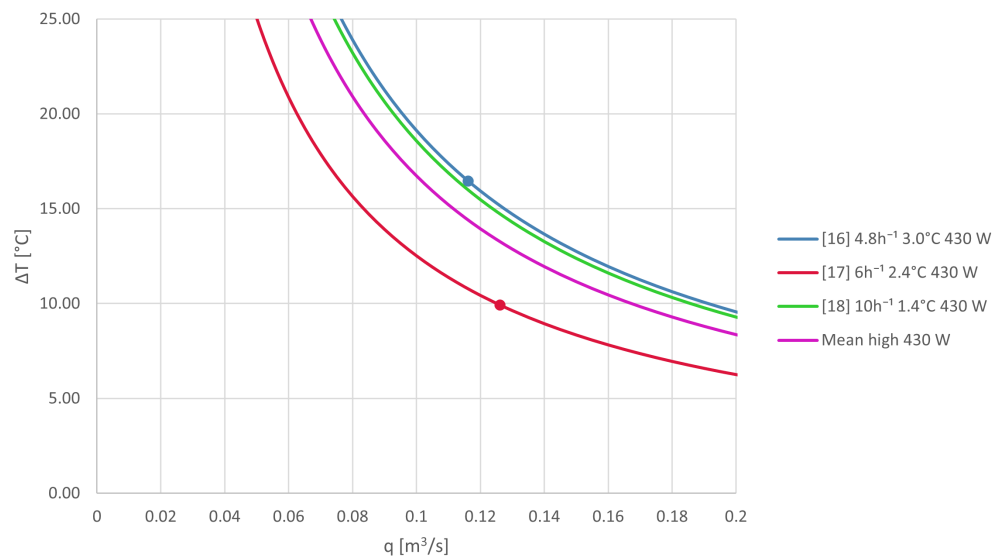


Figure N.6. Design chart for a high room with a heat load of 430 W.

N.3.2 Room length

The design graphs for the long room can be found in Figure N.7.

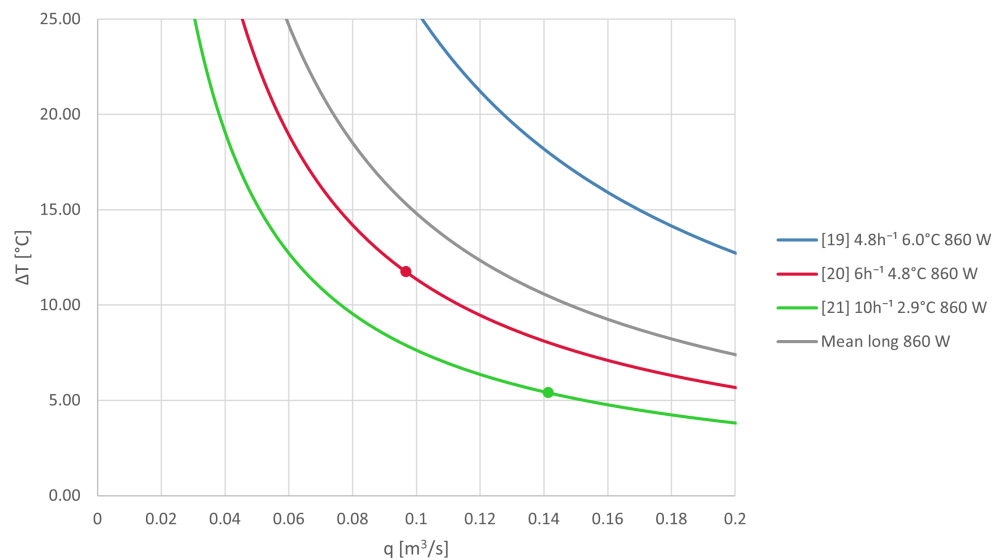


Figure N.7. Design chart for a long room with a heat load of 860 W.

Design chart development O

This appendix describes the method of how the design charts used in this thesis are developed. The main principles of the design, charts and assumptions are presented. The theory used is mainly based on the paper of Nielsen [2007]. The two Excel files used for the calculations are in Section A.3.

O.1 Principle and assumptions

The Ar number has to be determined, this is done with Equation O.1.

$$Ar = \frac{H \cdot g \cdot (T_a - T_i)}{T_a \cdot u_i^2} \quad (\text{O.1})$$

Where,

H	Characteristic height	[m]
g	Gravitational acceleration	[m/s ²]
T_a	Average room temperature	[K]
T_i	Inlet temperature	[K]
u_0	Supply velocity	[m]

In the formula for Ar, the characteristic height used is the height of the room without the plenum, and the gravitational acceleration used is 9.82 m/s².

The supply velocity is not directly known, but can be calculated based on the flow rate and the area of the suspended ceiling. The formula is shown in Equation O.2.

$$u_i = \frac{q}{A_i} \quad (\text{O.2})$$

Where,

q	Air flow rate	[m ³ /s]
A_i	Area of suspended ceiling	[m ²]

The simulation results are all based on the same base room geometry, although the room length and height are varied in some simulations. The geometry and total area can be seen in Table O.1.

Table O.1. Room geometry.

Symbol	Dimensions		Unit
Height	2.335	5.385	m
Length	4.8	9.6	m
Width	3.3		m

Furthermore, it is necessary to determine some draught rate limits both for velocity and air flow rate. These are used in the calculation of the design chart and the total DR. The values can be found in Table O.2.

Table O.2. Parameters used for draught rate calculation.

Symbol	Value	Unit
u_{\max}	0.15	m/s
q_{\min}	0.02	m ³ /s
t_u	40	%

O.2 Calculation method

The design chart will be constructed by finding a design variable and using this to make the chart.

First, the proportionality factor, b , has to be defined. This value relates the airflow to a maximum acceptable velocity in the OCZ.

$$b = \frac{u_{draught} \cdot A}{q_0} \quad (O.3)$$

Where,

b	Proportionality factor	[–]
$u_{draught}$	Maximum velocity in reference point	[m/s]
A	Area	[m ²]
q_0	Air flow rate	[m ³ /s]

$u_{draught}$ is based on the maximum value from the points found in Appendix I. Next, the limiting airflow rate based on the maximum acceptable velocity in the OCZ is determined. This value is found in Table O.2.

$$q_{lim} = \frac{u_{draught} \cdot A}{b} \quad (O.4)$$

After the maximum air flow rate is determined, the maximum allowable temperature difference can also be estimated. This is done by using Equation O.5.

$$\Delta T = \frac{q_{lim}^2}{\frac{\Delta T}{q_0^2}} \quad (O.5)$$

Now, it is possible to calculate a design variable used for the chart development.

$$a = q_{lim} \cdot \Delta T \quad (O.6)$$

This design variable is divided by various air flows to get the corresponding ΔT to each of these.

An example of a design chart developed using this method can be found in Figure O.1. Here, the results from the simulations with 200 W are used. The other design charts that were developed can be seen in Appendix N.

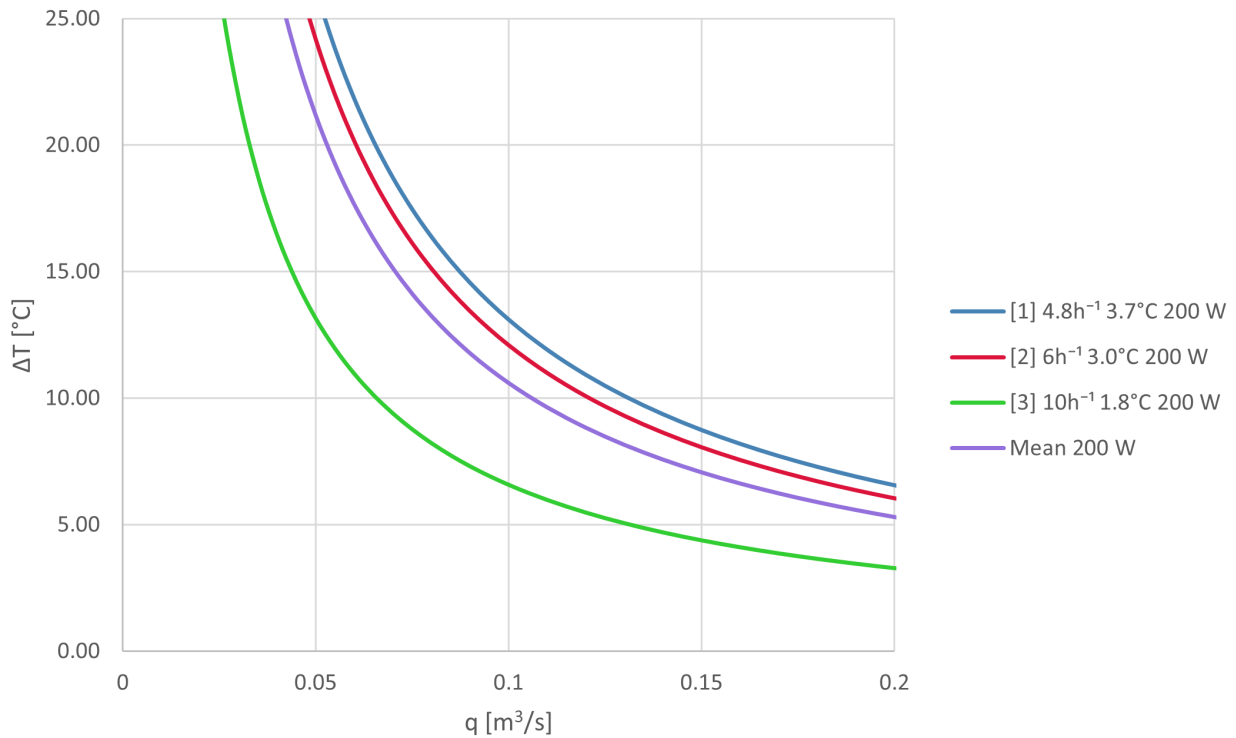


Figure O.1. Design chart heat load of 200 W.

Configuration tool outline P

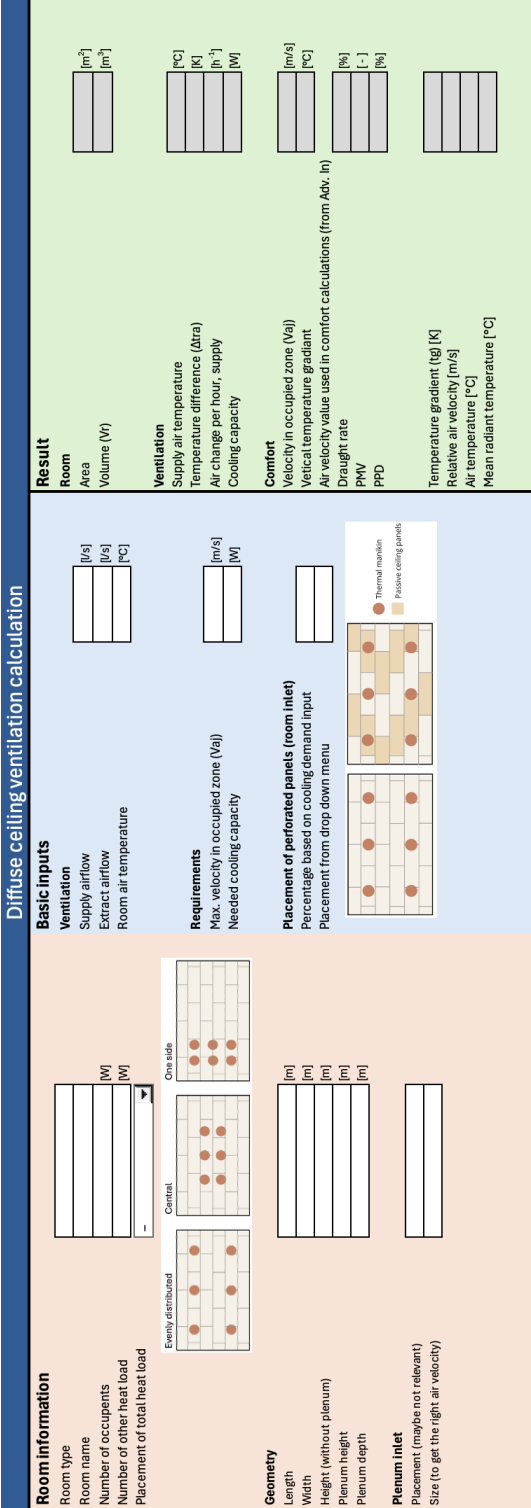


Figure P.1. Outline of the configuration tool.